HARRIS

SOLAR CONCENTRATOR ADVANCED DEVELOPMENT PROGRAM TASK 1 FINAL REPORT

PREPARED BY:

HARRIS CORPORATION
GOVERNMENT AEROSPACE SYSTEMS DIVISION
P.O. BOX 94000
MELBOURNE, FLORIDA 32902

PREPARED FOR:

NATIONAL AERONAUTICS AND SPACE ADMINISTRATION
LEWIS RESEARCH CENTER
21000 BROOKPARK ROAD
CLEVELAND, OHIO 44135

JUNE 1986

NASA LEWIS RESEARCH ORDER

CONTRACT NAS 3-24670

1. Report No.	2. Government Accession No.	3. Recipient's Catalog No.
CR-179489		

4. Title and Subtitle	5. Report Date
Solar Concentrator Advanced Development Program Task 1 Final Report	June 1986
	6. Performing Organization Code
7. Author(s)	8. Performing Organization Report No.
Harris Corporation	None
	10. Work Unit No.
9. Performing Organization Name and Address	11. Contract or Grant No.
Harris Corporation Government Aerospace Systems Division P.O. Box 94000 Melbourne, Florida 32902	NAS 3-24670
	13. Type of Report and Period Covered
12. Sponsoring Agency Name and Address	Contractor Report
National Aeronautics and Space Administration Lewis Research Center 21000 Brookpark Road Cleveland, Ohio 44135	14. Sponsoring Agency Code

15. Supplementary Notes

Project Manager, Robert E. Hyland, Project Engineer, NASA Lewis Research Center, Cleveland, Ohio

16. Abstract

Solar dynamic power generation has been selected by NASA to provide power for the Space Station. Solar dynamic concentrator technology has been demonstrated for terrestrial applications but has not been developed for space applications. The object of the Solar Concentrator Advanced Development program is to develop the technology of solar concentrators which would be used on the Space Station. The first task of this program was to develop conceptual concentrator designs and perform trade-off studies and to develop materials data base and perform material selection. Three unique concentrator concepts; Truss Hex, Spline Radial Panel and Domed Fresnel, were developed and evaluated against weighted trade criteria. The Truss Hex concept was recommended for the Space Station. Materials data base development demonstrated that several material systems are capable of withstanding extended periods of atomic oxygen exposure without undesirable performance degradation. Descriptions of the conceptual designs and materials test data are included.

17. Key Words (Suggested by Author(s))	18. Distribution Statement
Solar dynamic Concentrator Atomic Oxygen Space structures	Unclassified - Unlimited

19. Security Classif. (of this report)	20. Security Classif. (of this page)	21. No. of pages	22. Price*
Unclassified	Unclassified	209	

*For sale by the National Technical Information Service, Springfield, Virginia 22161

1.0 FOREWORD

This report summarizes the work accomplished under NASA Contract NAS 3-24670, "Solar Concentractor Advanced Development, Task 1". The program is sponsored by the NASA Lewis Research Center (LeRC). Robert Hyland is the NASA Project Manager. John E. White is the Program Manager at the Government Aerospace Systems Division of the Harris Corporation. The technical task leader is Philip J. Henderson.

The program is divided into three tasks which address the following:

1. Conceptual Designs, Materials, and Special Tooling and Testing
2. Mechanical Design of Test Concentrator
3. Fabrication and Testing of Concentrator

Task 1 provides the conceptual design and materials testing data base for the concentrator to be designed and tested in Tasks 2 and 3.

2.0 TABLE OF CONTENTS

TABLE OF CONTENTS (Continued)

LIST OF APPENDICES

LIST OF ILLUSTRATIONS

LIST OF ILLUSTRATIONS (Continued)

LIST OF ILLUSTRATIONS (Continued)

LIST OF ILLUSTRATIONS (Continued)

LIST OF ILLUSTRATIONS (Continued)

LIST OF ILLUSTRATIONS (Continued)

LIST OF ILLUSTRATIONS (Continued)

LIST OF ILLUSTRATIONS (Continued)

LIST OF TABLES

LIST OF TABLES (Continued)

3.0 SUMMARY

The objective of the Solar Concentrator Advanced Development (SCAD) Program is to develop the technology of solar concentrators which would be incorporated in a solar, thermodynamic power generation system for use on the Space Station. The program is divided into three tasks:

1. Conceptual designs, materials and special tooling and testing
2. Mechanical design of test concentrator
3. Fabrication and testing of concentrator

The SCAD Program period of performance was proposed as 42 months. Task 1 was authorized 30 September 1985 and the expected period of performance was 6 months. A delay in the Task 1 final presentation at LeRC resulted in an extension of Task 1. The final presentation was held 16 April 1986. This final report completes Task 1.

The objective of Task 1 was: 1) to develop conceptual designs for concentrators with potential application to the Space Station, 2) to select and recommend a concept based on a trade comparison, 3) to perform materials testing providing a data based for concept selection and subsequent design, and 4) to identify the special tooling and testing requirements of the recommended concept. Task 1 was subdivided into three subtasks. The scope of the subtasks is summarized below.

Subtask 1 - Conceptual Designs and Trade Studies

Conceptual designs are developed for solar concentrators which are capable of being mounted to the Space Station. The concentrators are sized to support either an organic Rankine cycle (ORC) or a closed Brayton cycle (CBC) power system with an electric output of 25 kW. The conceptual designs are compared by trade studies to determine an optimum design for each of the two power systems. The trades consider complexity, reliability, cost, deployment versus erection, on-orbit maintainability, and other parameters which might affect performance and suitability for the space system application. The results of the trade studies and the recommended design concepts for both the ORC and CBC power system applications are submitted to NASA for approval.

Subtask 2 - Material Selection

Materials which might be applied to the concentrator designs are selected and tested to evaluate the mechanical, physical, and optical properties for suggested lifetimes of approximately 10 years. The materials under evaluation include those selected for structural components, reflective coatings, protective coatings, and refractive lenses.

Subtask 3 - Identification of Tooling and Test Requirements

A plan is formulated for testing the solar concentrator to demonstrate or verify the operational performance. Also, any special tooling

or facilities which will be necessary for fabrication, assembly, and test are identified.

Three concentrators were selected for design development and trade comparison based on the results of the trade study conducted during the Space Station Work Package 4 Phase B Program (reference 1). The three concentrator options are:

- Truss Hex
- Splined Radial Panel
- Domed Fresnel

These concentrators are described briefly below. The conceptual designs developed during the program are described in detail in Section 6.0.

Truss Hex

The Truss Hex concentrator consists of an array of flat hexagonal structural modules supporting spherical mirror facets that approximate a paraboloidal surface, Figure 3.0-1. The hexagonal modules are an open truss frame which provide support, dimensional location and packaging for the mirror surface elements, facets. The facets reflect the incident solar rays to the paraboloidal focus and into a receiver cavity. The hexagonal modules are connected with a series of hinge and latches which permit the structure to fold into a stack of flat panels for launch, Figure 3.0-2.

Splined Radial Panel

The Splined Radial Panel (SRP) concentrator is a self-deploying, lightweight, small stowed volume structure, Figure 3.0-3. The concentrator consists of a semirigid reflective surface and a Harris developed Deployed Truss Structure (DTS). The reflective surface is composed of thin, reflective, graphite/epoxy panels which are drawn into a splined parabolic curve using a flexible cord and tie shaping technique. The flat panels fold accordian style, stowing inside the DTS stowed envelope. The SRP stowed package is remarkably small, Figure 3.0-4. The SRP concentrator is deployed completely without assistance by a single motor housed in the cylindrical hub.

Domed Fresnel

The Domed Fresnel concentrator refracts the incoming rays into the receiver cavity using a transparent lens with integral Fresnel prisms, Figure 3.0-5. The lens surface is supported by the DTS. The concentrator's domed surface is approximated by an assemblage of flat prismatic panels shaped by the cord and tie technology Harris used on the Tracking and Data Relay Satellite System's deployable RF antennas. The Domed Fresnel concentrator stows into a small cylindrical envelope with the lens panels accordian folded, interleaved and packaged between the stowed DTS rib segments, Figure 3.0-6. This concentrator is remotely and automatically deployed by the DTS.

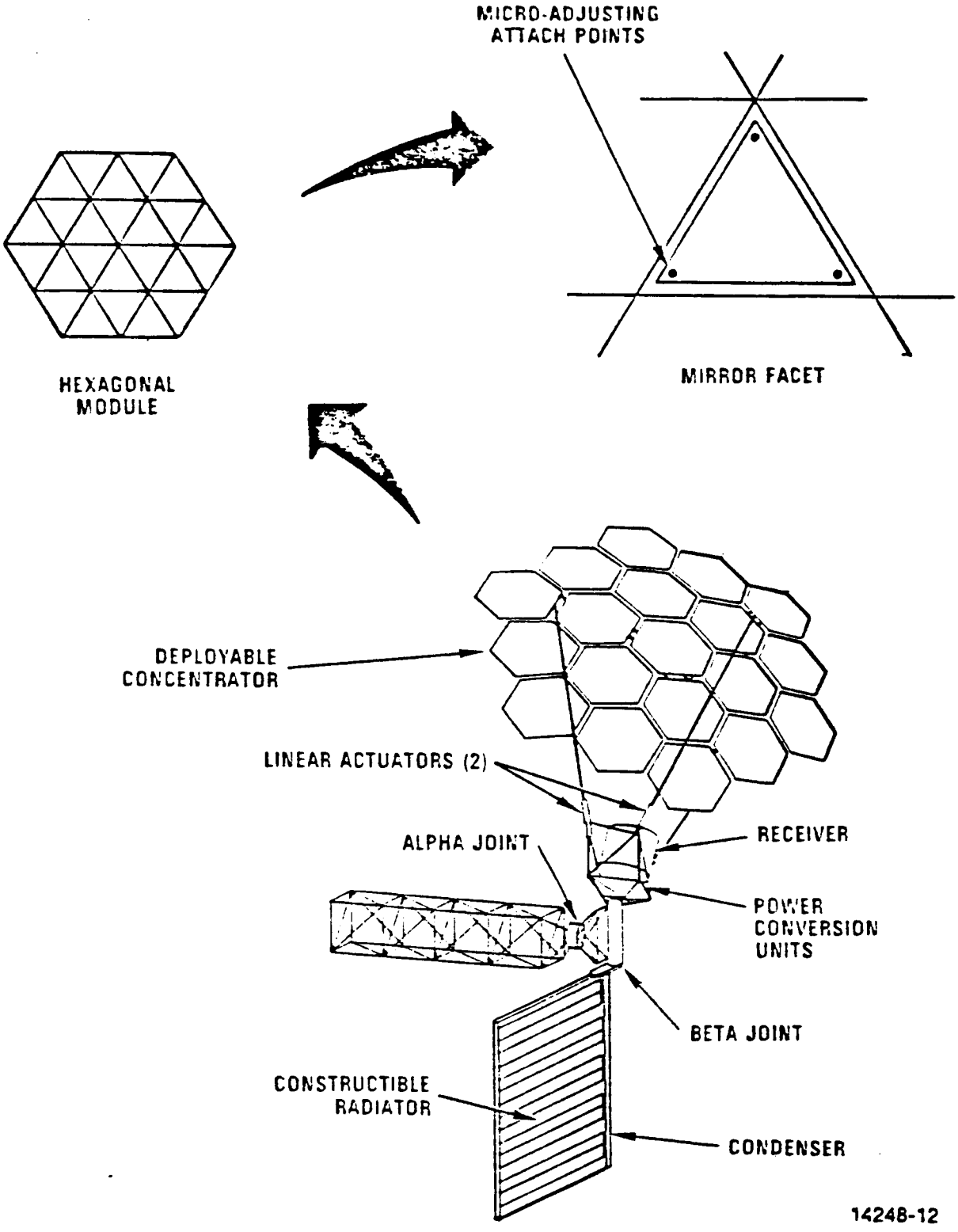

Figure 3.0-1. Truss Hex Concentrator Applied to the Space Station Offers Excellent Producibility and Maintainability.

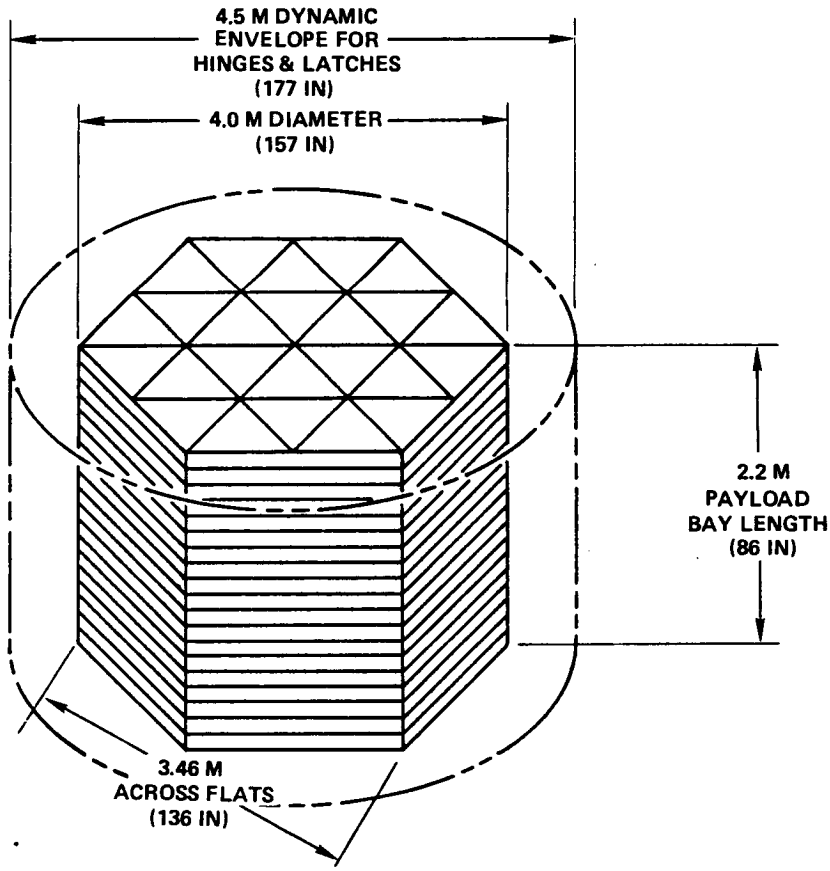

Figure 3.0-2. The Truss Hex Concentrator Folds into a Stack for Compact Packaging.

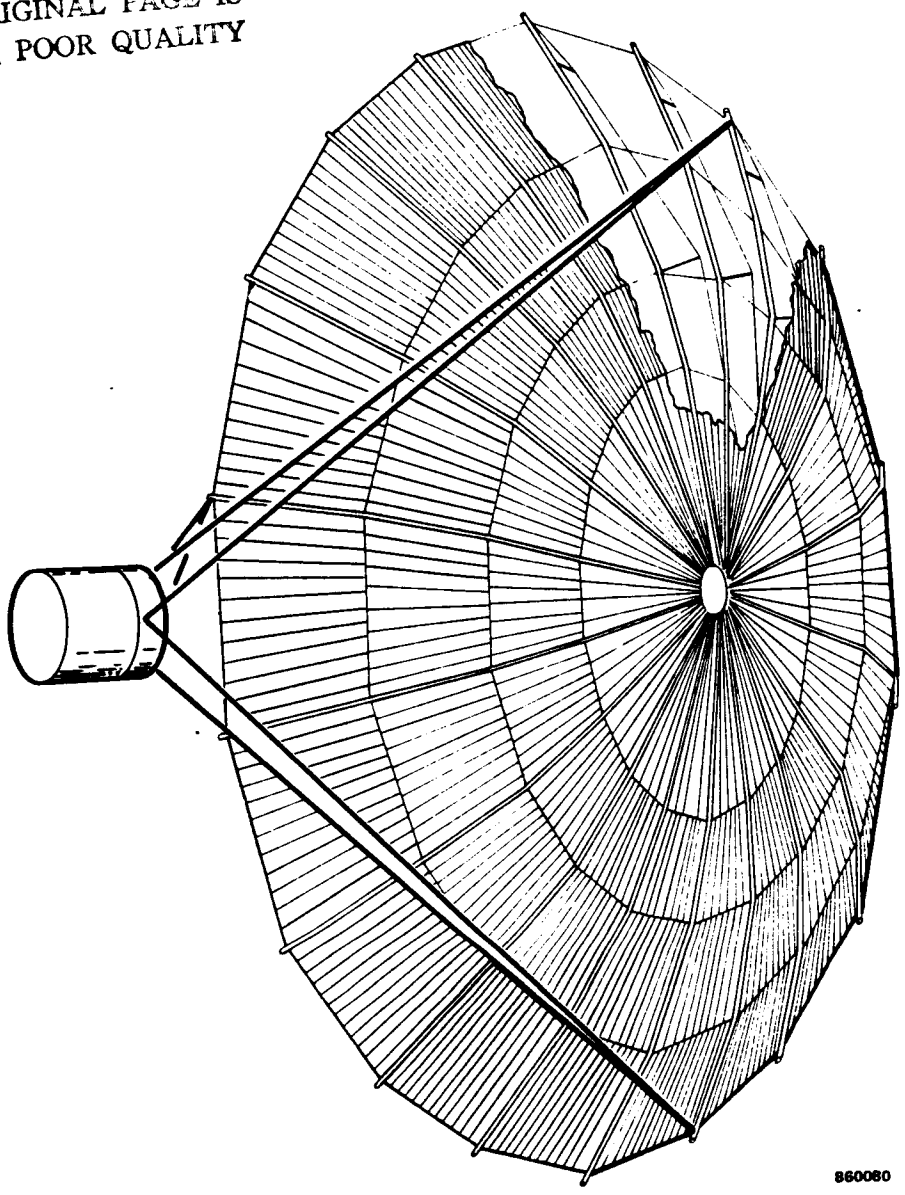

Figure 3.0-3. Lightweight Splined Radial Panel Concentrator Uses Thin Reflective Panels to Approximate Parabolic Contour.

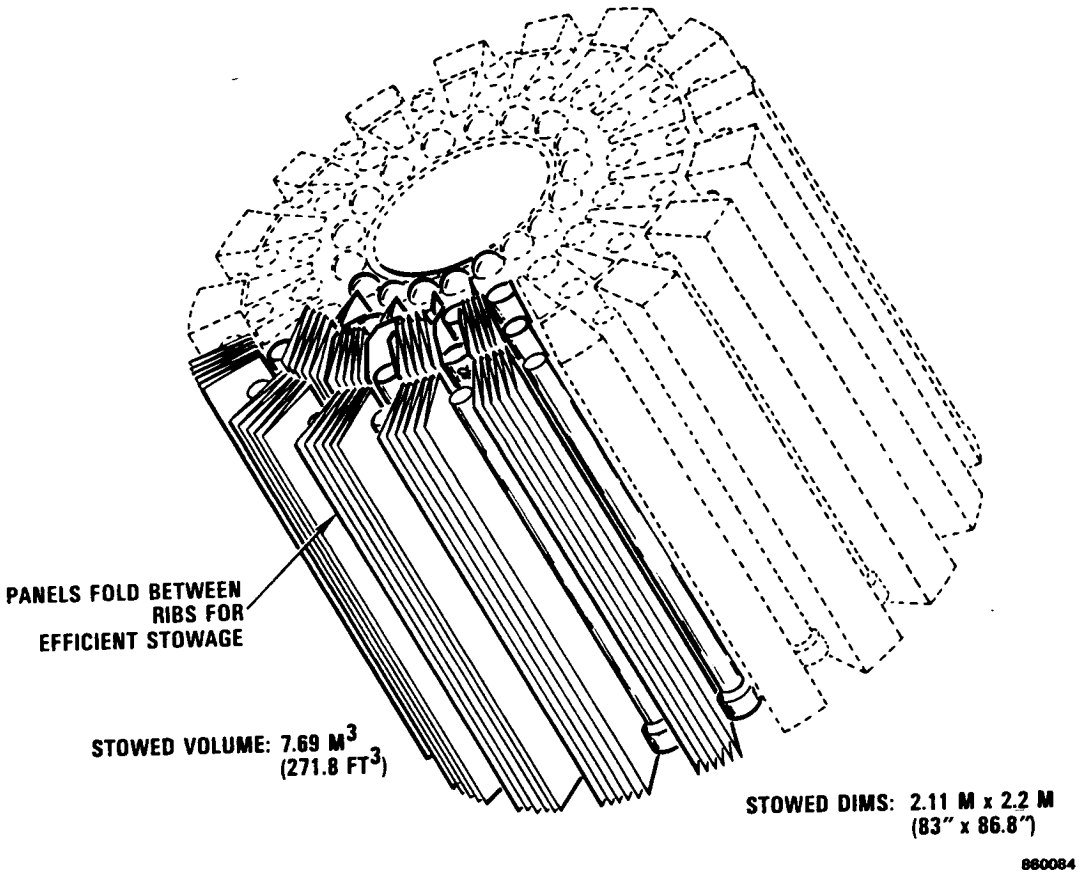

Figure 3.0-4. Splined Radial Panel Concentrator's Strongest Design Feature is the Extremely Efficient Stowed Package.

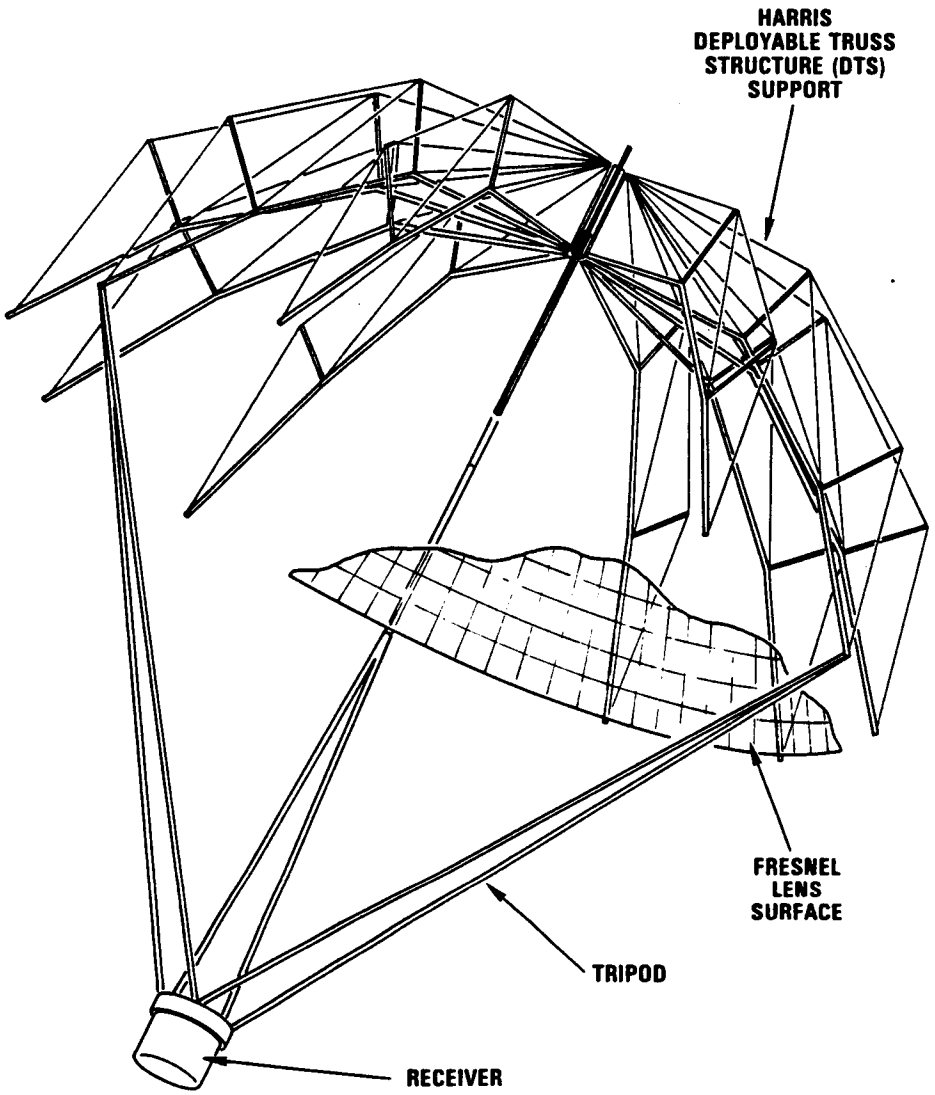

Figure 3.0-5. The Domed Fresnel Concentrator Combines Harris Deployable Space Structure and ENTECH Fresnel Optic Technologies.

DOMED FRESNEL CONCENTRATOR STOWED GORE AND RIB PAIR (END VIEW)

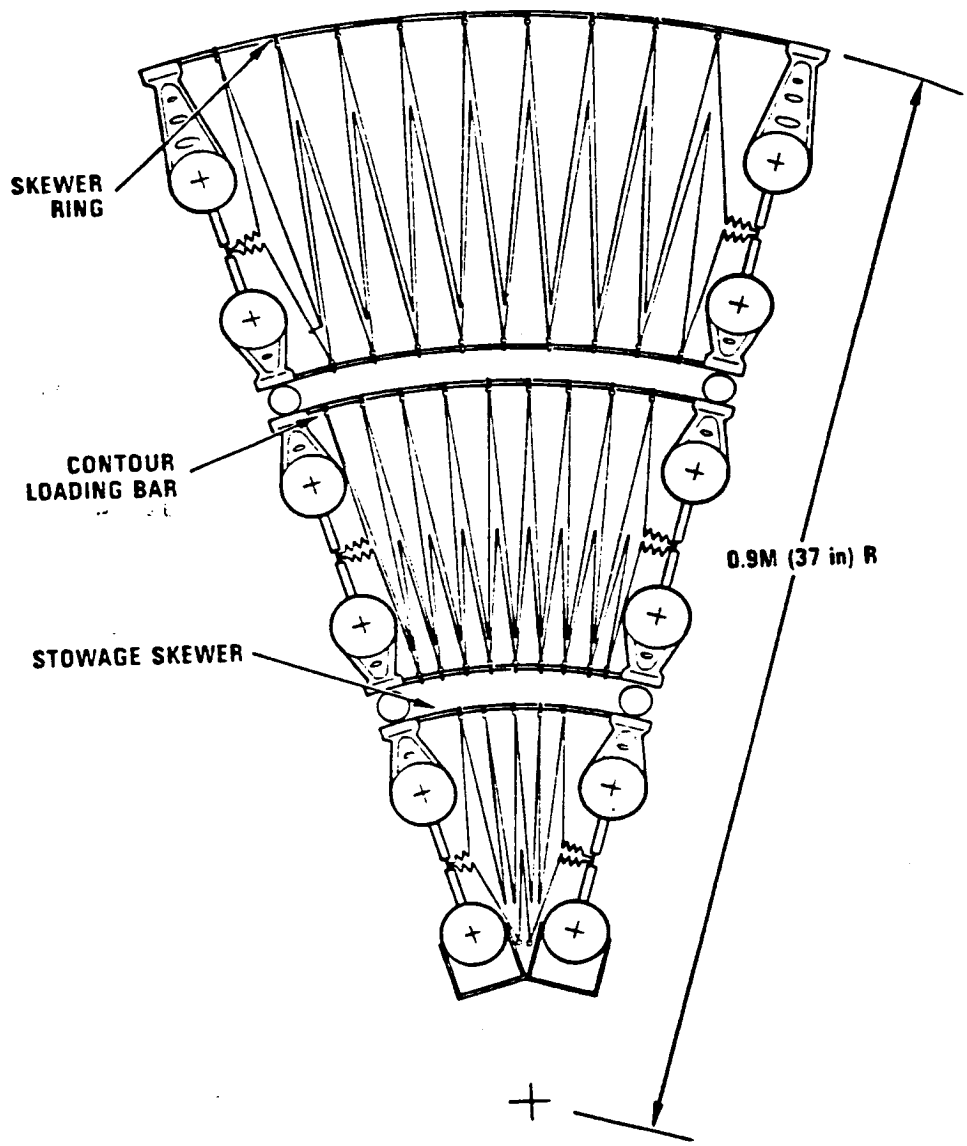

Figure 3.0-6. Accordian Folded Lens Surface Panels are Interleaved for Maximum Volume use.

The primary thrust of the material selection effort, Subtask 2, was to demonstrate the ability of selected reflective mirror concepts and refractive lens materials to withstand degradation due to atomic oxygen impringement. A number of tests were conducted to document the durability of various materials in the low earth orbit (LEO) environment. Simulated oxygen exposure testing indicates that aluminum and silver surface reflectors can be adequately protected with several materials including silica, magnesium flouride, and indium tin oxide. Sample data are summarized in Tables 3.0-1 through 3.0-2 for various exposure times. Sixteen asher hours approximate the atomic oxygen fluence experienced by a ram facing surface during one year in LEO. Additional testing was performed to document the effects of micrometeoroid impacts and thermal cycling on sample integrity. Based on NASA micrometeoroid fluence models and debris data, conservative estimates shown that less than .002 percent of the concentrator surface will be damaged as a result of high velocity impacts. Thermal cycling tests indicate that composite substrate materials suffer no adverse effects as a result of continuous temperature fluctuations.

Table 3.0-1. Reflectance of Aluminum Samples Following Atomic Oxygen Exposure

				Reflectance*			
Substrate	R	P	Asher Hours	Start Total	Start Specular	Finish Total	Finish Specular
Glass	Al	SiOx	634	0.912	0.891	0.904	0.879
Glass	Al	SiOx/MgF_2	634	0.906	0.882	0.859	0.834
Glass	Al	ITO	225	0.858	0.850	0.852	0.844
Glass	Al	ITO/MgF_2	225	0.854	0.847	0.822	0.815
GFRP	Al	SiOx	180	0.875	0.868	0.858	0.851
GFRP	Al	MgF_2	180	0.945	0.925	0.940	0.910
GFRP	Al	RTV655	151	0.935	0.905	0.850	0.805

*Measured over 200 NM to 2500 NM

R - Reflective Surface
P - Protective Surface
RTV655 - GE Silicone
GFRP - Graphite Fiber Reinforced Epoxy

Table 3.0-2. Reflectance Data for Silver Samples Following Atomic Oxygen Exposure

Substrate	R	P	Asher Hours	Reflectance* Start Total	Start Specular	Finish Total	Finish Specular
Glass	Ag	SiOx	634	0.978	0.972	0.958	0.937
Glass	Ag	$SiOx/MgF_2$	634	0.978	0.970	0.943	0.927
Glass	Ag	ITO	225	0.905	0.899	0.914	0.908
Glass	Ag	ITO/MgF_2	225	0.932	0.925	0.909	0.902
GFRP	Ag	$SiOx/MgF_2$	180	0.955	0.940	0.930	0.915
GFRP	Ag	SiOx	180	0.975	0.945	0.945	0.910
GFRP	Ag	MgF_2	180	0.955	0.930	0.955	0.925
GFRP	Ag	RTV655	151	0.965	0.940	0.905	0.840

*Measured over 200 NM to 2500 NM

R - Reflective Surface
P - Protective Surface
RTV655 - GE Silicone
GFRP - Graphite Fiber Reinforced Epoxy

Materials tested for Fresnel lens applications showed severe degradation at lower exposure times than did the reflective samples. Sample data are illustrated in Table 3.0-3 for several polymeric materials including; silicones, fluoropolymers, and acrylic and polycarbonate lens materials. The decrease in specular transmittance and mass loss associated with long term monoatomic oxygen exposure experienced by these materials increases the risk associated with the implementation of a Fresnel concentrator. Although the Fresnel concept is very attractive from several viewpoints, more experiments are necessary to develop and demonstrate materials for LEO durable lenses.

The trade comparison evaluated the three concentrator concepts against 16 weighted criteria including: optical performance, packaging efficiency, maintainability, design complexity, development risk and other criteria. The Truss Hex concept was ranked highest by the trade comparison and is recommended as the concept which best support the Space Station mission. The Splined Radial Panel and the Domed Fresnel concepts were ranked nearly equal and were judged to be sound concepts with unique features better suited for other applications. The trade comparison is discussed in detail in Section 8.0.

Table 3.0-3. Transmission Data for Fresnel Materials Following Atomic Oxygen Exposure

Material	Asher Hours	Start Total*	Start Specular*	Finish Total*	Finish Specular*
SILICONES					
RTV615	214	0.910	0.845	0.830	0.640
RTV655	214	0.910	0.850	0.840	0.635
RTV670	214	0.880	0.810	0.840	0.725
DC 93-500	214	0.890	0.780	0.830	0.650
FLUOROPOLYMERS					
ETFE	151	0.891	0.830	0.933	0.492
PFA	151	0.926	0.867	0.948	0.553
FEP (A)	151	0.937	0.900	0.952	0.602
KEL-F	168	0.918	0.885	0.947	0.430
OTHER ORGANICS					
LEXAN PC	117	0.825	0.825	0.842	0.728
UVA-11 Acrylic	21.5	0.845	0.838	0.872	0.393

*Transmittance Values measured over 200 NM to 2500 NM

The manufacturing flow and a preliminary test plan were developed for the Truss Hex concentrator. Special tooling and test requirements were defined. The manufacturing flow, Figure 3.0-7, is described in Section 9.1. The demonstration test plan, Figure 3.0-8, is described in Section 9.2.

The conclusions drawn as a result of Task 1 are summarized in Figure 3.0-9. Harris recommends the Truss Hex concentrator for Space Station and recommends further development of the technology by continuing with Tasks 2 and 3 of the SCAD program.

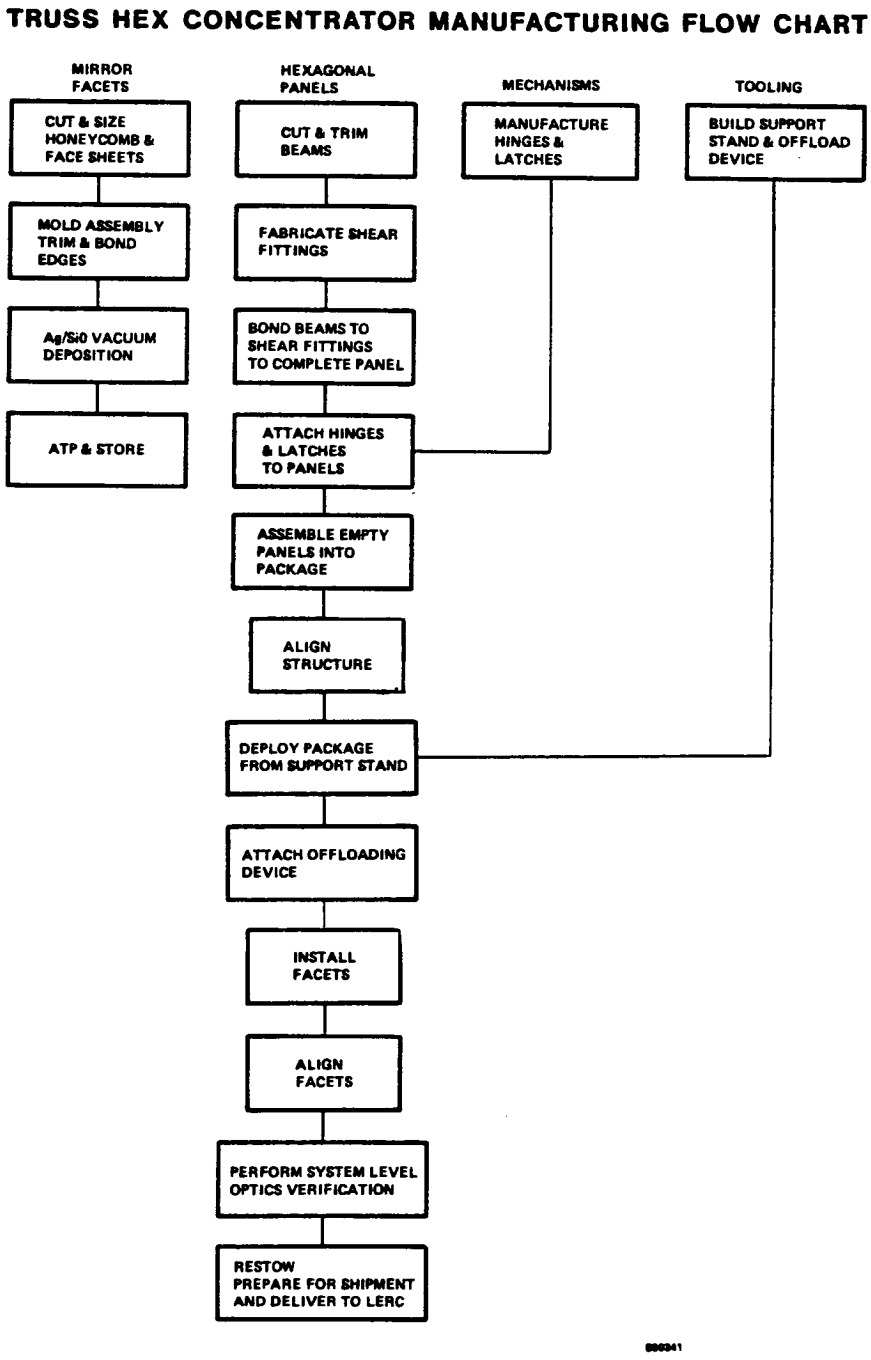

Figure 3.0-7. The Truss Hex Manufacturing Flow Depicts Major Fabrication and Assembly Operations.

PRELIMINARY OPTICAL TEST PLAN

OBJECTIVE	DEMONSTRATE BY
• DETERMINE SPECULAR REFLECTANCE OF COATINGS	• REFLECTANCE TESTS PERFORMED BY DEPOSITION VENDOR
• PERFORM DETAILED FIRST ARTICLE FACET CHARACTERIZATION (EACH MOLD)	• LASER SCAN
• PROVIDE LOW COST ACCEPTANCE TEST FOR EACH FACET	• GO-NO/GO AUTOFOCUS TEST
• PERFORM OPTICAL FACET ALIGNMENT AT ASSEMBLY LEVEL	• USE TRANSLATING VERTICAL LASER BEAM TO AIM FACETS AT PRE-DETERMINED CYLINDRICAL GRID POINTS
• DETERMINE GLOBAL CHARACTERISTICS - OPTICAL BORESIGHT - EFFECTIVE SLOPE ERROR - FOCAL LENGTH	• TRANSLATING VERTICAL LASER BEAM WITH DIGITIZED PHOTOSENSING SCAN IN THE APERTURE PLANE
• ASSESS EFFECTS OF 1 g DISTORTIONS	• PERFORM ABOVE WITH & WITHOUT COUNTER WEIGHTS
• DEMONSTRATE DEPLOYMENT REPEATABILITY	• APERTURE PLANE SCANS WITH INTERVENING STOW/DEPLOY
• CHARACTERIZE RECEIVER OPTICS	• MAINTAIN CORRESPONDENCE DATA FOR LASER BEAM LOCATION & INTERCEPT LOCATION AT APERTURE PLANE. DEFINE VECTOR INPUTS FOR OPTICAL ANALYSIS TO PREDICT FLUX

Figure 3.0-8. Preliminary Optical Test Plan Meets Concentrator Demonstration Test Objectives.

CONCLUSIONS/RECOMMENDATIONS

- TRUSS HEX SOLAR CONCENTRATOR IS SELECTED AND RECOMMENDED AS THE BEST DESIGN FOR THE SPACE STATION APPLICATION
- DOMED FRESNEL AND SPLINED RADIAL PANEL CONCENTRATORS ARE SOUND CONCEPTS
- MATERIAL INVESTIGATIONS HAVE DEMONSTRATED A 10+ YEAR SERVICE LIFE ON SMALL REFLECTIVE SURFACE SAMPLES
- ADEQUATE REFRACTIVE LENS MATERIAL HAS NOT BEEN FOUND
- FACILITIES AND TEST EQUIPMENT ARE DEFINED FOR MANUFACTURE AND VERIFICATION OF TRUSS HEX CONCENTRATOR

Figure 3.0-9. Key Conclusions Drawn as a Result of Task 1.

4.0 INTRODUCTION

4.1 Background

Solar dynamic concentrator technology has been demonstrated for terrestrial applications on several DOE and NASA programs including: the Advanco Vanguard Concentrator; Fixed Mirror Distributed Focus Collector (E-Systems); 20 kW Parabolic Dish Power System (ENTECH); Innovative Point Focus Solar Concentrator, Domed Point Focus Fresnel Lens Solar Concentrator (ENTECH); JPL Dish Stirling Solar Receiver; JPL Test Bed Concentrators, Solar Thermal Power Systems Project Parabolic Dish System Development; and Acurex Innovative Concentrator Development. However, solar dynamic (SD) technology has not been developed for space applications. The efficiency and deployed area advantages of SD over flight proven photovoltaic power generation for the Space Station were identified on the Phase B program. NASA has utilized the Phase B program to develop system designs and identify technology needs. Parallel, but independent, advanced development programs are used to address the technology issues raised by the Phase B program.

The Space Station Work Package 4, Phase B program identified the need to demonstrate space applied solar dynamic concentrator technology. Therefore, the Phase B program directly preceded and led to the Solar Concentrator Advanced Development (SCAD) program. Several other advanced development programs are particularly important to the SCAD program. Similarly structured programs addressing radiator, receiver and engine technologies are directly related to this program. Especially important is the Boeing receiver advanced development program, Solar Dynamic Heat Receiver Technology (SDHRT), from which the receiver geometries used in the trade studies conducted on this program were derived. Studies to develop atomic oxygen protection for station structure and coating processes for concentrator reflective and protective materials are also of special interest to the SCAD program.

Several previous Harris programs form the foundation for the SCAD program. Harris is the recognized leader in precision space deployable structures with a primary emphasis on RF antennas such as the TDRSS 16 foot diameter Ku band antenna and the Galileo S and X band antenna. Harris recently completed a study on extremely high frequency antennas, Extreme Precision Antenna Reflector (EPAR) program, for NASA LeRC. The recommended EPAR concept is the basis of the Truss Hex concentrator design selected in this study. The SCAD program made extensive use of the Harris Deployable Truss Structure (DTS) developed on internal research and development. The DTS was used as the support structure for two concentrator concepts.

4.2 Objectives and Scope

The SCAD program objective is to develop the technology of solar concentrators which would be incorporated in a solar, thermodynamic power generation system for use on the Space Station. The SCAD program is task ordered. The program scope is divided into three tasks and includes:

1. Concentrator conceptual designs and trade-off studies, material selection, and special tooling and testing identification
2. Concentrator design
3. Concentrator fabrication and test

Task 1, the effort covered by this report, was divided into the three subtasks described below.

Subtask 1 - Conceptual Designs and Trade-off Studies

The Contractor shall look at all potential concepts for concentrators capable of being mounted to the Space Station. These concepts shall include; for reflective type concepts, parabolic, Cassegrainian (double reflection), and trough; and for refractive concepts, the spherical type and the planar type. The conceptual designs shall include design drawings, Level 1. The concentrators shall be of such a size so that it would be comparable to that used for the IOC Space Station (i.e., either for an organic Rankine engine or a Brayton engine).

In addition to these conceptual designs, the Contractor shall conduct a trade-off study in order to determine the optimum design for each of the power systems conducted over the respective temperature ranges. The trade-off study shall take into account as a minimum, the complexity of fabrication, reliability of components, the cost of the concentrator, whether the design is for a deployable concentrator or for an erectable, the ease of in-orbit servicing, and the materials that would be reliable to operate in the orbital environment for at least ten years.

From the results of the trade-off studies and the conceptual designs, the Contractor shall submit his recommendations of the two most promising designs, one to be used with the organic Rankine engine and one to be used with the Brayton engine.

Subtask II - Material Selection

The Contractor shall test or report on testing of materials considered applicable for the concentrator, its support structure and the support structure for the receiver for use onboard the Space Station. The suggested lifetimes for the materials shall be approximately 10 years.

The Contractor shall include the following efforts in the subtask:

1. Assist in establishing component material requirements necessary to meet design objectives including space environment operations.

2. Conduct a materials data review.

3. Provide data on the mechanical, physical, and optical properties of the materials to be considered.

4. Provide a materials selection for: the structural components, the reflective coatings, the protective coatings, and the refractive lens; for, at minimum, the recommended designs. Include with the materials selection, the justifications for those selections.

The Contractor shall identify and recommend the testing necessary to demonstrate and to verify the operation of the solar concentrator that would be fabricated in Task III. In addition, the Contractor shall identify the required test facility that would be required for operation in Task III.

At the conclusion of Task I, the Contractor shall make a presentation on the results attained in subtasks I, II and III to the NASA Project Manager. This presentation shall be made at the LeRC and will be opened to any interested Space Station participating contractors or interested persons.

4.3 Program Approach

The SCAD concentrator conceptual development began by reducing the number of concepts based on the results of the Phase B program. The three concepts considered in the SCAD study offered a unique approach and potential to satisfy the Space Station mission. Independent design teams were established for each concept. The teams developed the designs in parallel supported by the material development effort. At the conclusion of the design effort, the concepts were evaluated against criteria established at the beginning of the program. The results of the trade comparison were the basis of the concept selection.

4.4 Reserach Relevance

Several items reported herein are relevant and significant to researchers in solar dynamic, optic, material engineering, and space structure technologies. These items are:

1. Use of an offset optical configuration to achieve low gimbal mass and moments of inertia

2. Use of triangular, spherical mirror elements to approximate the parabolic contour

3. Use of flat, hexagonal, open trusses to position and support mirror elements

4. Use of hinges and latches to efficiently package a concentrator and provide reliable deployment

5. Identification and testing of materials that survive atomic oxygen exposure

6. Development of two sound concentrator concepts which provide decreased stowed volume and mass at increased cost and development risk

4.5 Report Format

This document has been prepared in accordance with NASA LeRC Technical Writing Standards for Contractor Reports, LHB 2230.1. The design requirements established for the trade comparison are discussed in Section 5.0. The conceptual designs developed on the program are described in Section 6.0. Section 7.0 presents the results of the material development effort. The trade comparison is presented in Section 8.0. Manufacturing and test plans are described in Section 9.0. Conclusions and recommendations are given in Section 10.0. Appendix A describes the DTS deployment sequence and Appendix B contains additional material testing data.

5.0 DESIGN REQUIREMENTS AND GOALS

Specific system design requirements are essential to any engineering program. System design requirements and goals were established on the Solar Concentrator Advanced Development (SCAD) program for Task 1 to provide a common basis and guidelines for the development of different conceptual designs and for the trade comparison of the concepts. The objective in generating the requirements list was to address all known and expected requirements independent of having specific or final figures regarding the requirement. Typical flight hardware requirements were included with the SCAD specific requirements.

Table 5.0-1 presents the design requirements and goals used on the Task 1 program. The requirements were derived from several sources as given in Table 5.0-2. Unknown requirements which were not perceived to be discriminators in the trade comparison were not assigned values.

Table 5.0-1. SCAD System Design Requirements

PARAMETER	ORGANIC RANKINE CYCLE (ORC)	CLOSED BRAYTON CYCLE (CBC)
Power System Output	25 kWe continuous	25 kWe continuous
Power Cycle Efficiency, Receiver to Bus	18 percent	22 percent
Receiver Aperture Diameter	0.46M (18 in)	0.33M (13 in)
Maximum Aperture Heat Flux	TBD	TBD
Concentrator Surface Area	TBD: 195 M^2 (16 m dia)	TBD: 159 M^2 (14 m dia)
Power System Pointing Error Budget	0.3 degrees (TBD)	0.1 degrees (TBD)
Concentrator Pointing Error Budget	0.075 degrees (TBD)	0.025 degrees (TBD)
Receiver Flux, Maximum	TBD: 30 W/CM^2 on Receiver Wall	TBD

Table 5.0-1. SCAD System Design Requirements (Continued)

PARAMETER	REQUIREMENT
Solar Constant	1371 W/M^2 +3.2% (Use 1323 W/M^2 for sizing)
Eclipse Factor (AKA: Exposure Factor, Solar Multiple)	0.618 (sunlit fraction of 460 kM orbit)
Shading Factors	• Assume no blockage for offset reflector sizing • Lens support structure blockage = TBD
Intercept Factors	95% Minimum (97% Design Goal) (At worst case operational T/E, Mfg uncertainties, etc.)
Concentrator Losses	• Surface Specular Reflectance (Reflector): TBD EOL = 0.90 estimated • Surface Specular Transmittance (Lens): TBD
Configuration	• Compatible with IOC Space Station • Adaptable to center fed or offset (except lens)
Weight	• Minimize, 360 kg (792 lbs) design goal
Moments of Inertia	• Minimize
Deployed Stiffness	• Maximize ($\geq$1 Hz)
Stowed Packaging	• Minimum volume • Multiple system payload in NSTS • Support by cradle/pallet/canister
Deployment Scheme	• Goal of fully automated concentrator deployment • Receiver and masts erected or deployable • Manual override desirable for concentrator
Disposal	• Plan required • Restow and return desirable
Maintainability	• Goal of partial replacement of surface
Design Life	• 10 years (with maintenance as required)

Table 5.0-1. SCAD System Design Requirements (Continued)

PARAMETER	REQUIREMENT
Environments:	
• Launch Loads	• TBD: JSC 07700 (NSTS Loads and I/F's)
• Ground Handling	• Size for 1.5 G (Counterbalance if required)
• Acoustics	• JSC 07700, ISD 2-19001
• Fracture Control	• JSC 19649
• Stress Corrosion	• MSFC-522
• Outgassing	• NASA-SPR-022A
• Thermal	• JSC 07700, Vol XIV, Rev H
• Vibration	• JSC 07700, ICD 2-19001

Table 5.0-2. Source of System Design Requirements

PARAMETER	SOURCE
Power System Output	Task Order #1
Power Cycle Efficiency, Receiver to Bus	Current Phase B Documents
Receiver Aperture Diameter	Boeing Receiver Advanced Development Proposal Baselines
Maximum Aperture Spillage Heat Flux	None
Concentrator Surface Area	Harris Phase B Program
Power System Pointing Error Budget	Current Phase B Documents
Concentrator Pointing Error Budget	Harris Allocation
Receiver Flux, Maximum	Sundstrand Phase B Program
Solar Constant	Physical Constant

Table 5.0-2. Source of System Design Requirements (Continued)

PARAMETER	SOURCE
Eclipse Factor	Derived from Orbital Altitude
Shading Factor	Determined by Design
Intercept Factor	Harris Allocation
Concentrator Losses	Harris Allocation
Configuration	Task Order #1
Design Life	Task Order #1
Weight, Moments of Inertia, Deployed Stiffness, Stowed Packaging, Deployment Scheme, Disposal, Maintainability	Harris Determined Design Goal
Environments	Past Experience on Flight Programs

6.0 SOLAR CONCENTRATOR CONCEPTUAL DESIGNS

The primary goal of Task 1 was to develop conceptual designs for several different types of solar concentrators to a level of detail where meaningful trade comparisons could be done. Three generic designs were selected during the proposal process as most likely to fulfill the system requirements: the Truss Hex, the Splined Radial Panel, and the Domed Fresnel. These conceptual designs are described in Sections 6.1 through 6.3. Other generic designs were eliminated earlier during a Phase B trade study (reference 1). However, some consideration was given to both Planar Fresnel and Parabolic Trough concepts early in this study. The Planar Fresnel was previously compared (unfavorably) to the Domed Fresnel by the Dome inventor, Mark O'Neill, and was eliminated on the basis of that work (reference 2). This comparison is presented in Section 6.4. Insufficient information existed for a meaningful evaluation of the parabolic trough and no conceptual design was developed.

Each of the three concentrator concepts covered by this study was developed in a different configuration. Some conceptual design had already been done on the Truss Hex in an offset configuration for a Space Station Phase B study. Development of the offset configuration was continued in the present study. The Spline Radial Panel was developed as a symmetric (center fed) concentrator in a Harris IR&D project. This configuration was developed further in the present study for application to Space Station requirements. An offset Radial Spline Panel design is also feasible, but not necessary for the trade comparison, and therefore, not considered here. The Domed Fresnel is a shaped lens which is unique from the two reflectors. The Domed Fresnel baseline concept was sized for an ORC system because there was some uncertainty about obtaining the required geometric concentration ratio for the CBC system. Later evaluations showed that the Domed Fresnel can also meet CBC requirements if the receiver design is optimized for the lens based system. Both of the reflector concentrators were sized for CBC systems, and therefore, are also applicable to the less demanding requirements of an ORC system.

6.1 Truss Hex Concentrator

6.1.1 Concept Description - Truss Hex

The Truss Hex solar concentrator (see Figure 6.1-1) consists of an array of hexagonal structural modules that approximate a paraboloidal surface. Each hex module is subdivided into equilateral triangular cavities. As shown in Figure 6.1-2, individually adjustable and replaceable mirror facets are mounted inside the triangular openings. The hex modules are connected with a series of hinges and latches which permit the structure to fold into a stack of hexagonal panels. The deployment can be fully automated by the addition of drive motors at the hinges, or the panels may be latched or bolted together one-by-one without folding.

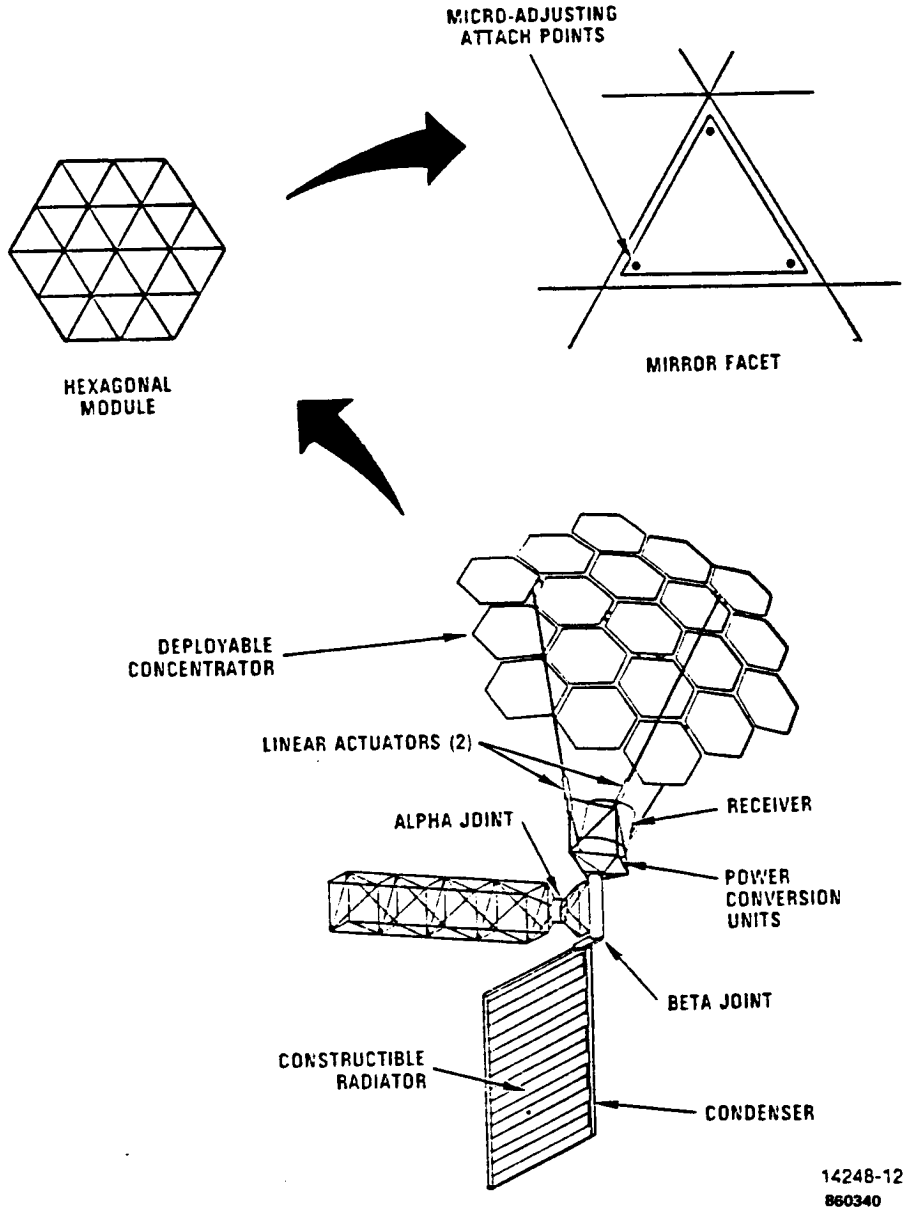

Figure 6.1-1. The Truss Hex Solar Concentrator, Shown Attached to the Space Station, Offers a Modular Structural Design with Triangular Mirror Facets Mounted Inside the Open Bays of the Flat, Hexagonal Panels.

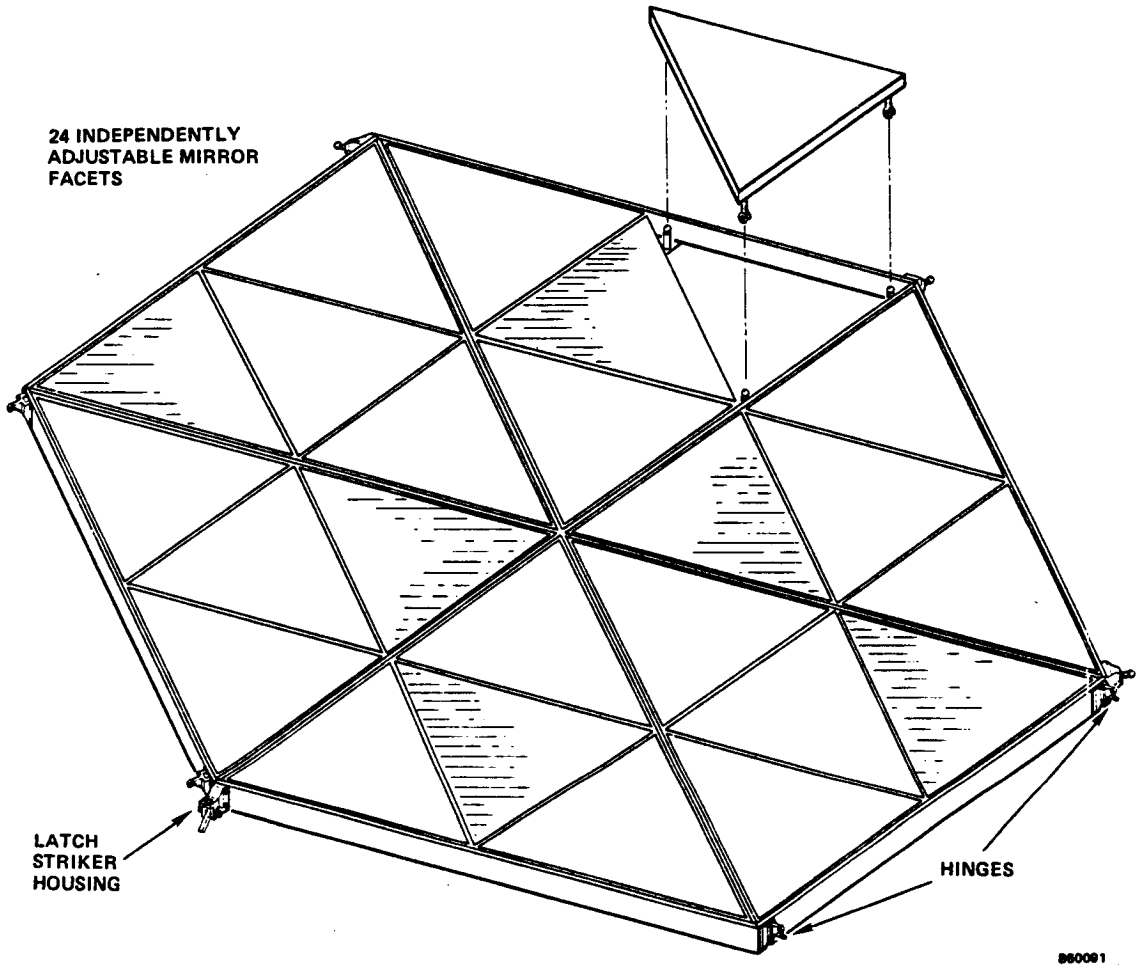

Figure 6.1-2. Individually Adjustable and Removable Mirror Facets Permit Flux Tailoring and Maintenance of the Truss Hex Surface.

The Truss Hex is self-supporting structurally. It attaches to the receiver with support struts to form the Power Generation Subsystem (PGS) module. The overall size of the concentrator is determined by the minimum projected area requirement common to all concentrator designs, plus allowances for gaps and shading. For a 25 kWe power output, the deployed diameter is 17 to 18 m (about 60 ft). Since the maximum hex module diameter that will stow in the Shuttle payload bay is around 4 m (14 ft), a minimum number of maximum size hexes may be set (around 19 to 24 for 25 kWe, according to system conversion efficiencies). Fractional hexes can be produced by leaving out facets or by adding partial hexes of eight mirror facets as shown in Figure 6.1-3. However, the baseline design for the Truss Hex has only complete hex panels. The stowed configuration is a stack of hex panels, 2 to 3 meters tall (7 to 10 ft), determined by the thickness and number of hexagonal structural modules.

6.1.2 Conceptual Design Details - Truss Hex

The projected concentrator collection area is determined by:

1. Solar constant of 1.323 kW/m^2,
2. Exposure time fraction of 0.62 (sunlit fraction of orbit),
3. Illumination fraction of 0.95 (reflected energy minus shading),
4. Surface specular reflectance of 0.92,
5. Intercept factor of 0.97 (energy fraction at the plane of the receiver opening which enters the receiver),
6. Conversion efficiency of 22% for CBC and 18% for ORC Power Conversion Units (PCU) and Power Management and Distribution (PMAD) systems,
7. Required electrical output of the PCU of 25 kWe.

Using these factors, the projected reflective area required to deliver 25 kWe from a CBC system is 160 m^2 (1720 ft^2), or 195 m^2 (2099 ft^2) for an ORC system.

The Truss Hex concentrator configuration for this conceptual design is an offset Newtonian reflector. The concentrator surface is part of the larger parent paraboloid as shown in Figure 6.1-4. The receiver is tilted to an optimum orientation for circumferential distribution of heat flux on the receiver cavity wall.

The size of an individual hex module (see Figure 6.1-5) is constrained by several parameters. Foremost is the size of the Shuttle payload bay with a dynamic envelope of 4.57 m (15 ft) for cargo. The dynamic envelope sets the size of the largest theoretical hexagon that can be carried into space. The theoretical maximum size is reduced by contingency allowances for intrusions by keel fittings and other hardware at different sections of the payload bay, joint allowances for the hex-to-hex attachments, and the distortion associated with mapping any regular polygon onto a compound-curved surface. After accounting for these factors, the resulting design is an array

TRUSS HEX CONCENTRATOR PARTIAL PANEL MODULES

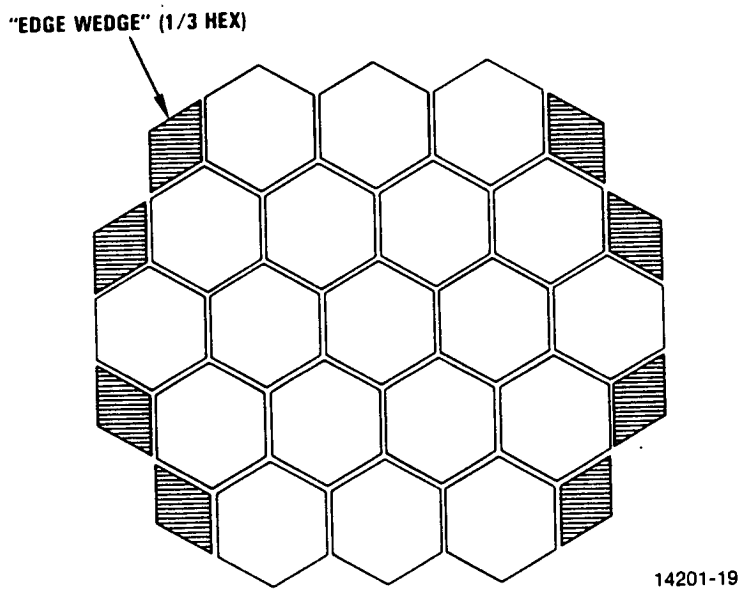

Figure 6.1-3. Partial Panels may be Added to the Truss Hex Concentrator for Fine Tuning the Power Output or Smoothing Flux Patterns in the Receiver.

OFFSET NEWTONIAN COLLECTOR GEOMETRY

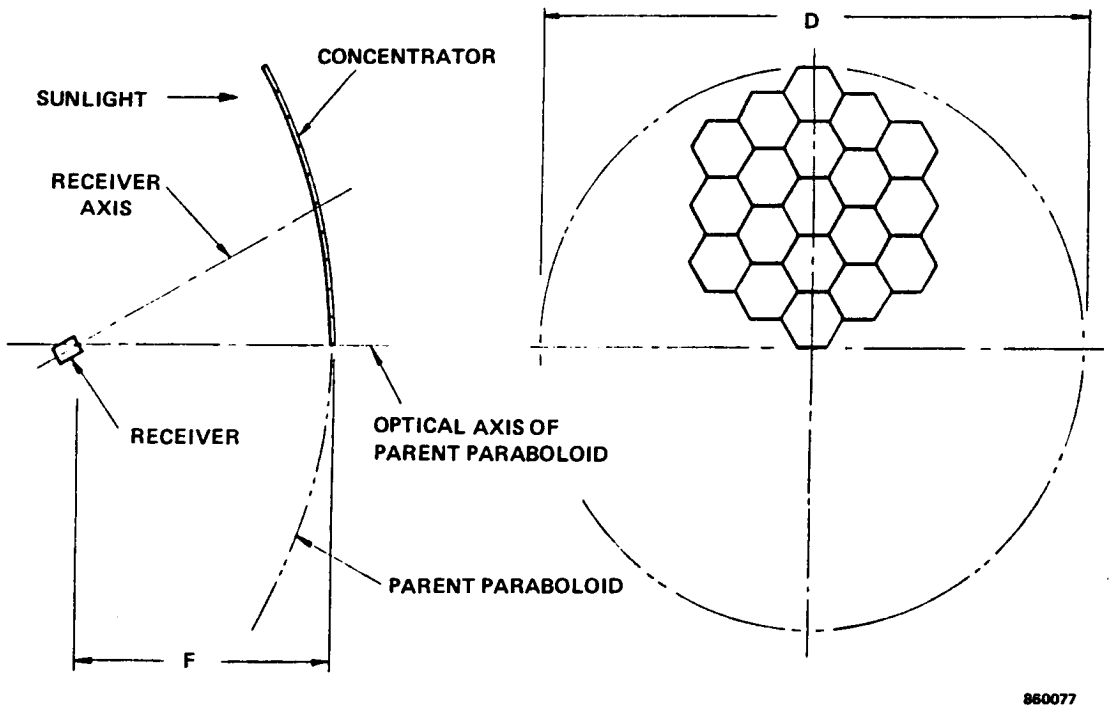

Figure 6.1-4. The Truss Hex Concentrator Baseline Design is Applied to an Offset Newtonian Reflector Geometry; the Current Solar Dynamic Power System Configuration for the Space Station.

TRUSS HEX CONCENTRATOR STOWED ENVELOPE

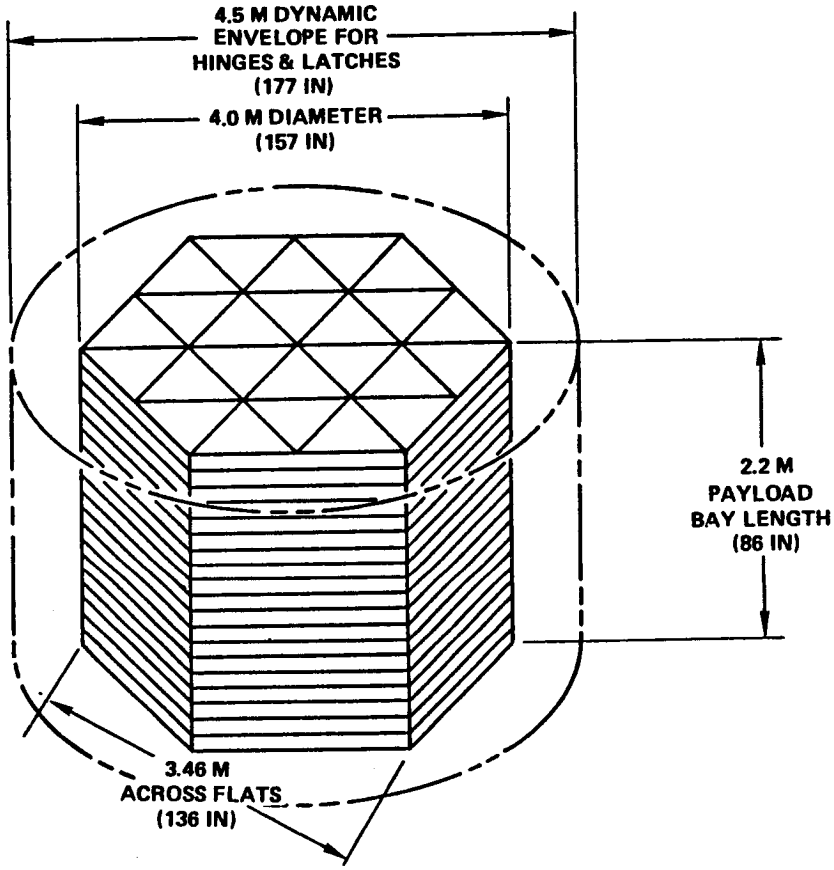

- SUPPORTED BY CRADLE OR PALLET, OR CANTILEVERED FROM FIRST PANEL

860062

Figure 6.1-5. The 19 panel (CBC system) Truss Hex Concentrator Fits Well Inside the Shuttle Payload Dynamic Envelope. Latches, Hinges and Support Pallets, not shown, were Considered.

of replicated hex modules that are approximately 4.00 m (13.1 ft) from point to point.

Geometric evaluation of the array of hex panels leads to a nominal reflective surface area fraction of 0.98, and a ratio of projected area to surface area of approximately 0.82. These design parameters combined with the hex panel sizing and projected area requirements previously discussed result in selection of 19 panels for a 25 kWe CBC system and 24 panels for an ORC system.

Parametric studies of hex mapping indicate an approximately linear relationship between joint allowance, parent paraboloid size and the largest regular hexagon size. Several mapping techniques have been tried to define hex spatial positions, maximum regular hex size, and minimum out-of-plane mismatches between regular hex edges. The resulting geometry of a Truss Hex concentrator sized to support a 25 kWe CBC system is shown in Figure 6.1-6. Gaps between the panels vary from 5 to 35 cm (2 to 14 in).

The Truss Hex packages for launch as a stack of hex panels. The primary variable in stowage volume is stack height, which corresponds to the longitudinal axis of the payload bay. For practical reasons, some space should be left between panels to allow them to stack on discrete contact points and avoid minor interferences that might otherwise develop. The nominal stack height for a 19 panel concentrator using 100 mm deep panels and 16 mm spacers is approximately 2.2 m (86 in). Larger numbers of panels and/or increases in the depth of individual panels would have a linear effect on the total stack height.

One key advantage of the Truss Hex is its structural simplicity. A rear view of an assembled panel is shown in Figure 6.1-7. The basic structural element is a common beam fabricated with HMS graphite fiber reinforced epoxy (GFRP) composite (see Figure 6.1-8). The beams are joined at the nodal points by bonding to shear/support fittings (see Figure 6.1-9). These fittings are either injection-molded out of a fiber-filled advanced resin system, or fabricated from a GFRP layup like the beam elements. Discrete reinforcement of the structure for increased strength or stiffness is accomplished with bonded doublers made of GFRP layups added to the beams or by titanium doublers around fitting attachment points. These structural enhancements would fit inside the edge of the top flange of the beam, without violating the mirror facet envelope.

A wide range of deployment options is available for the Truss Hex concentrator as illustrated in Figure 6.1-10. There are essentially four basic ways of deploying the hex modules: unfolding manually, unfolding automatically, erecting manually, or erecting automatically.

The baseline Truss Hex design as an unfolding deployment where the panels are stowed for launch in a stack, connected by a series of hinges and latches. The panels are deployed by sequentially unfolding the stack as shown

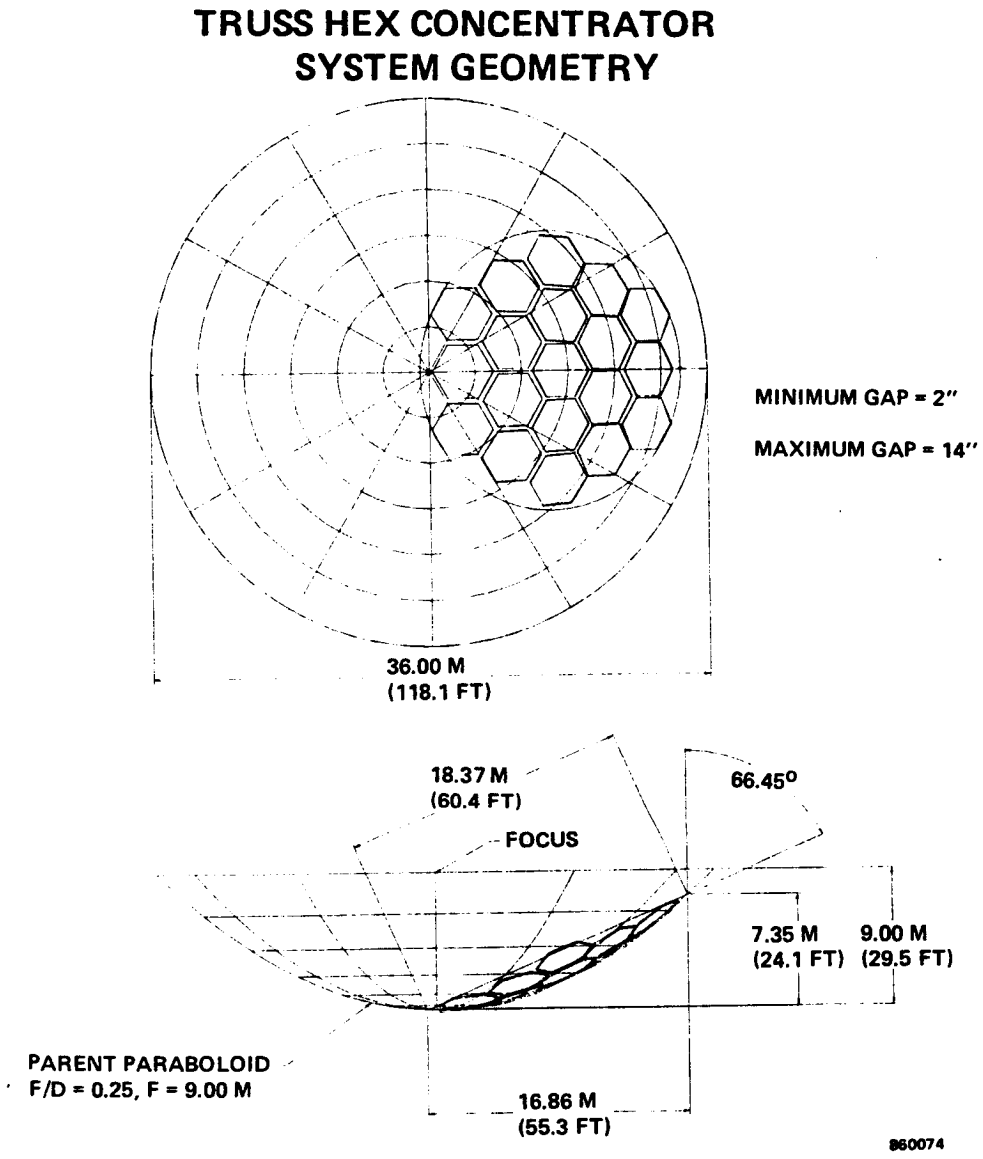

Figure 6.1-6. The 19 panels of the 25 kWe, CBC System, Truss Hex Concentrator are Mapped onto the Parent Paraboloid by Minimizing the Gaps between Replicated, Regular Hexagonal Panels.

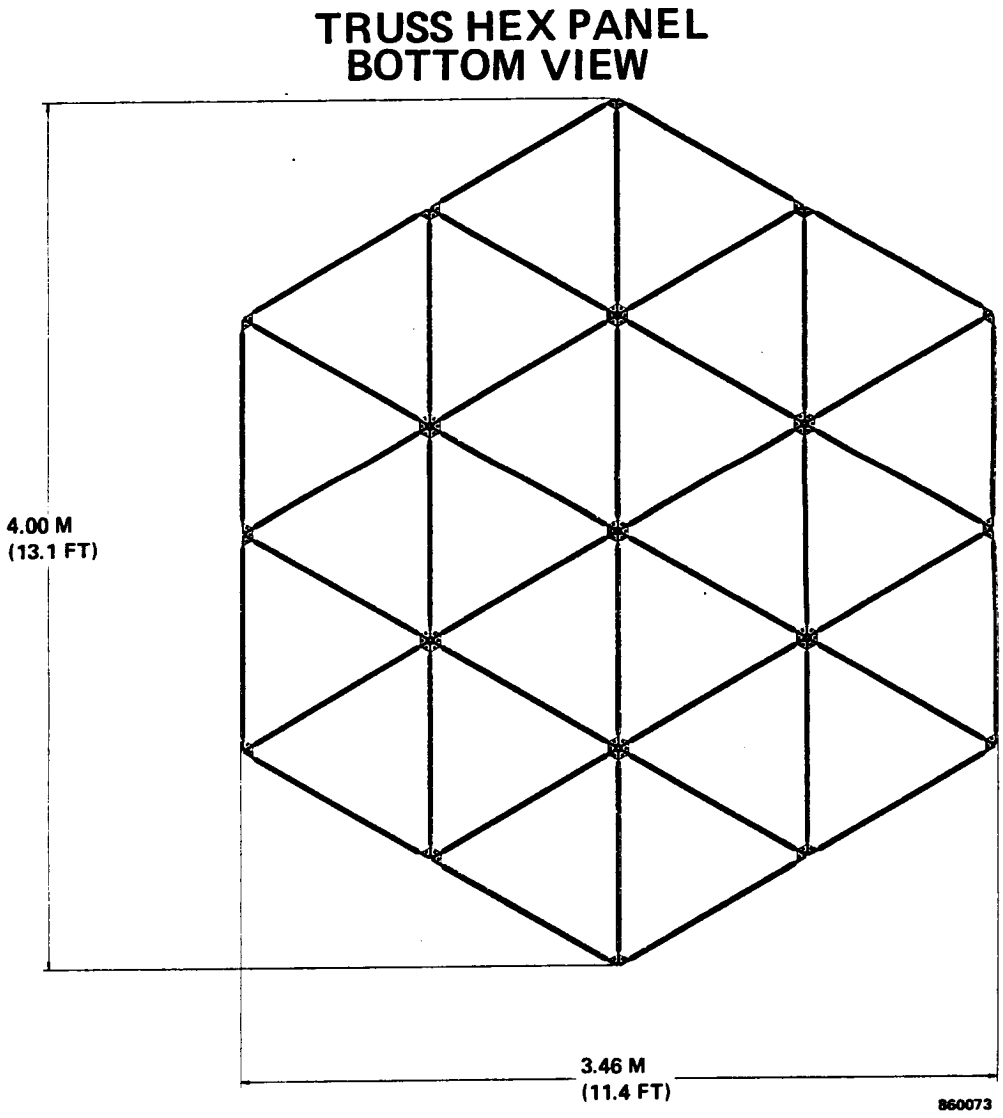

Figure 6.1-7. The Truss Hex Panel Structure (shown from the rear) Appears Simple even in this Detailed, Scale Drawing, because it is Assembled from a Small Number of Common Parts.

TRUSS HEX CONCENTRATOR BEAM DESIGN

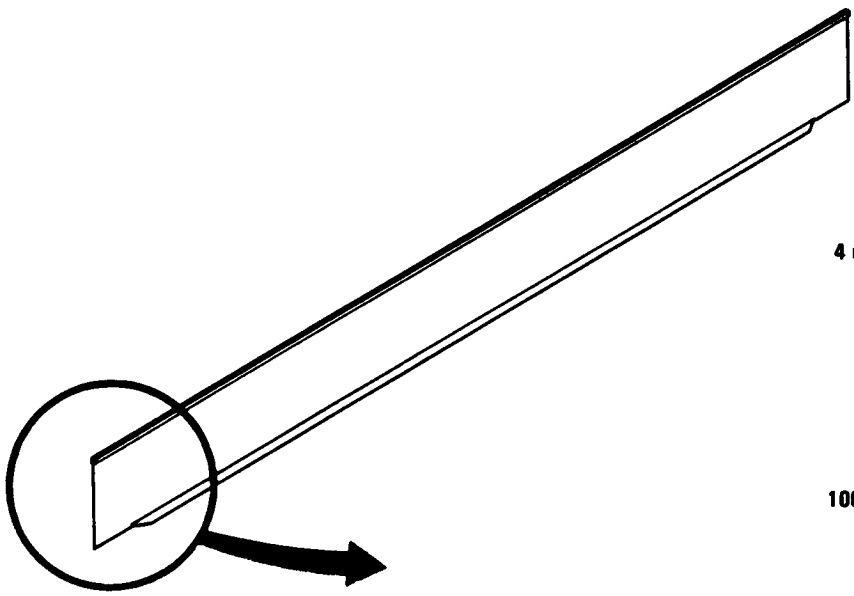

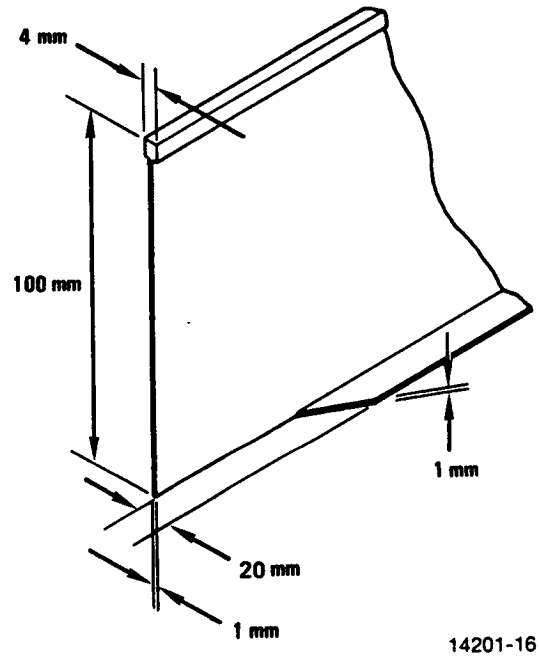

14201-16

- GRAPHITE/EPOXY COMPOSITE
- EI = 25.0 x 10^9 Nmm^2 (8.712 x 10^6 LB IN)^2

  |CTE| = 0.9 x 10^{-6} m/m^{o}c (0.5 x 10^{-6} IN/IN^{o}F)

Figure 6.1-8. The Structural Members of the Panel Provide Adequate Stiffness with Minimum Shading of the Mirrors. Local Reinforcement is Possible Without Changing the Mirror Dimensions.

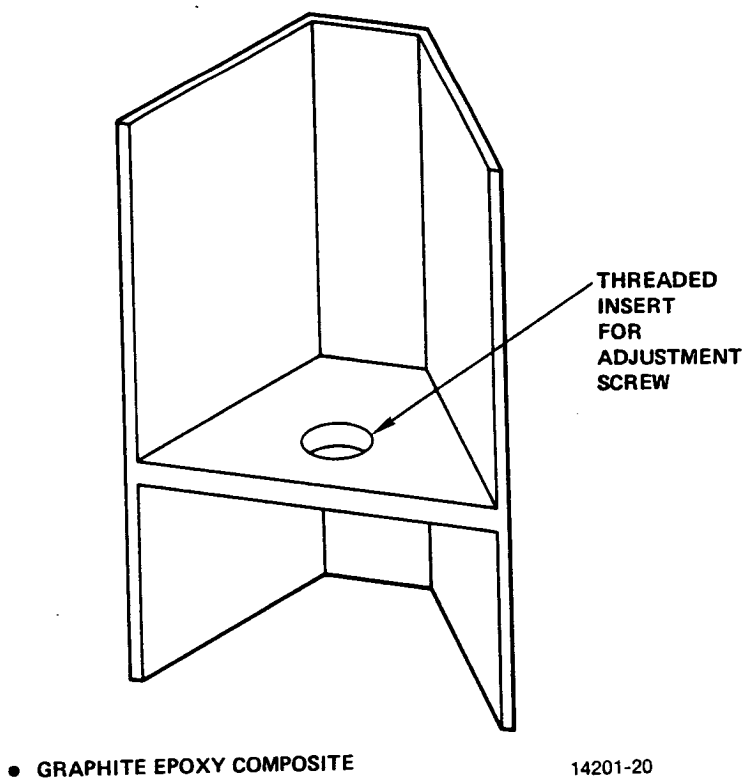

Figure 6.1-9. The Shear/Support Fitting Ties Beams Together at Their Intersections and Provides a Mounting Point for Mirror Facets.

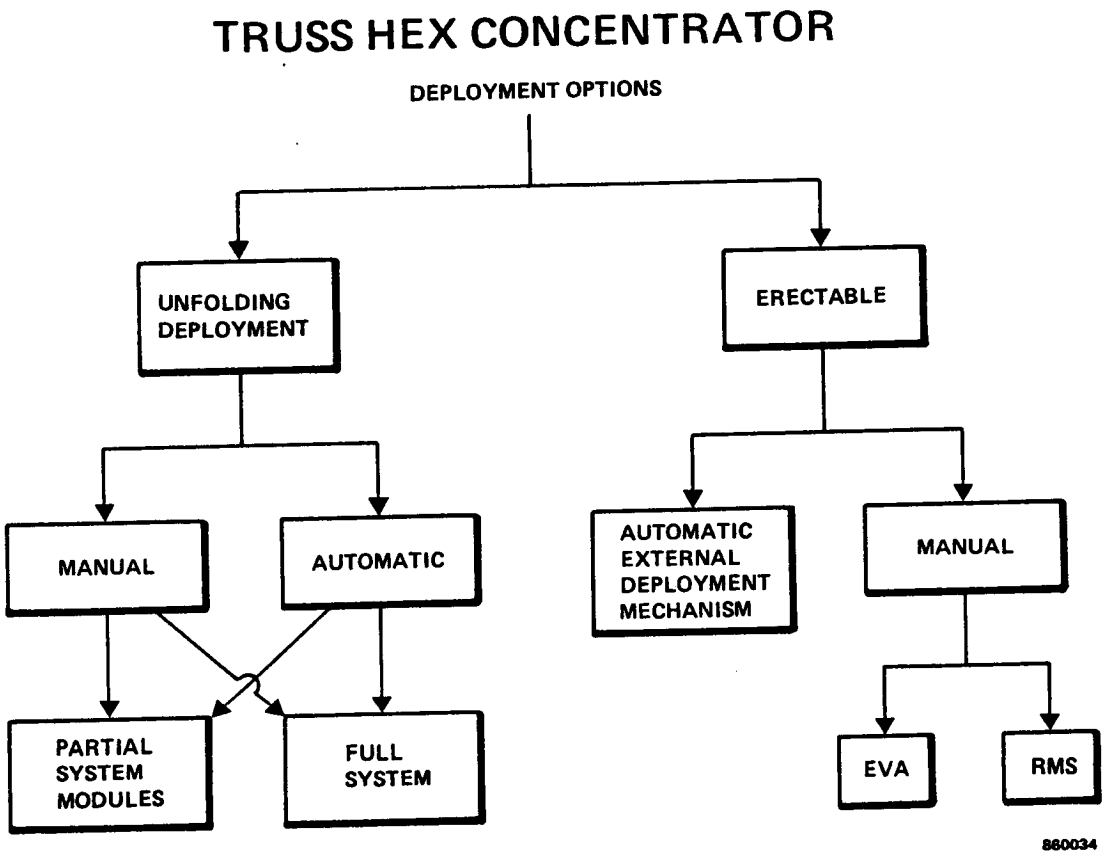

Figure 6.1-10. The Truss Hex Concentrator is an Extremely Flexible Concept Suited to Manual Assembly or Fully Automated Remote Deployment at the Other Extreme.

in Figure 6.1-11. This deployment can be done manually by the astronauts or can be fully automated for remote deployment. In either case, the full stack of panels (19 for a 25 kWe CBC system) is deployable with appropriate design consideration for hinge and latch interferences where the stack of panels passes by the adjoining panel edge. Another option is to join no more than seven panels by folding hinges, completing a ring of six panels around a center panel. Additional "partial system modules" of six hinged panels are later attached to the inner ring with latches, and then sequentially unfolded, forming the second ring. Figure 6.1-12 shows an artist's concept of a set of six panels being attached to the inner seven and deployed manually. The remainder of the 19 panel concentrator panels are shown still stowed in the payload bay.

A three-panel model of a manually deployable Truss Hex was fabricated as part of a Harris internal research and development project. The model, shown in Figure 6.1-13, has two sets of hinge joints and one latch, kinematically simulating the first three panels of the stack. The panels are approximately 1 m across the hexagon flat edges.

A variation on the single-fold method is the bi-fold scheme (see Figure 6.1-14), in which two panels are folded out more or less simultaneously, thus keeping the stack on one side of the concentrator as it builds. This deployment method is one solution for avoiding potential deployment interferences mentioned earlier. This approach could be implemented with powered hinges, but would be awkward for manual deployment. The baseline Truss Hex design does not require this type of deployment.

Manual erection of the hex panels is possible during EVA or with the remote manipulator. Hinges would be replaced by latches so that the panels could be joined together one by one. This approach also makes removal or replacement of an individual panel more feasible, although this is not necessary with individually replaceable mirror facets.

The last proposed concept for constructing a hex-based reflector is automatic external deployment. This involves the use of a separate mechanism shown in Figure 6.1-15. The first panel is attached to a rotating, tilting table. A stack of panels is advanced upward until the top panel engages the latches of the panel on the turntable. The assembled panels rotate into the proper position to receive the next panel from the top of the stack. After the first ring of the concentrator is assembled, the stack translates away from the turntable, and the machine proceeds to build the outer ring of hex panels. Since the mechanism is reusable, it is most applicable where large numbers of concentrators will be deployed. The weight and volume of the deployment mechanism is transported to orbit only once, no matter how many concentrators are built; and this weight does not contribute to the reboost mass or control system inertia of the finished concentrators. The mechanism can be developed to any desired level of sophistication, from a simple erection aid helping the astronauts sequence and position the panels, to a fully autonomous concentrator assembler. Although this deployment concept has

TRUSS HEX CONCENTRATOR
SINGLE FOLD DEPLOYMENT METHOD

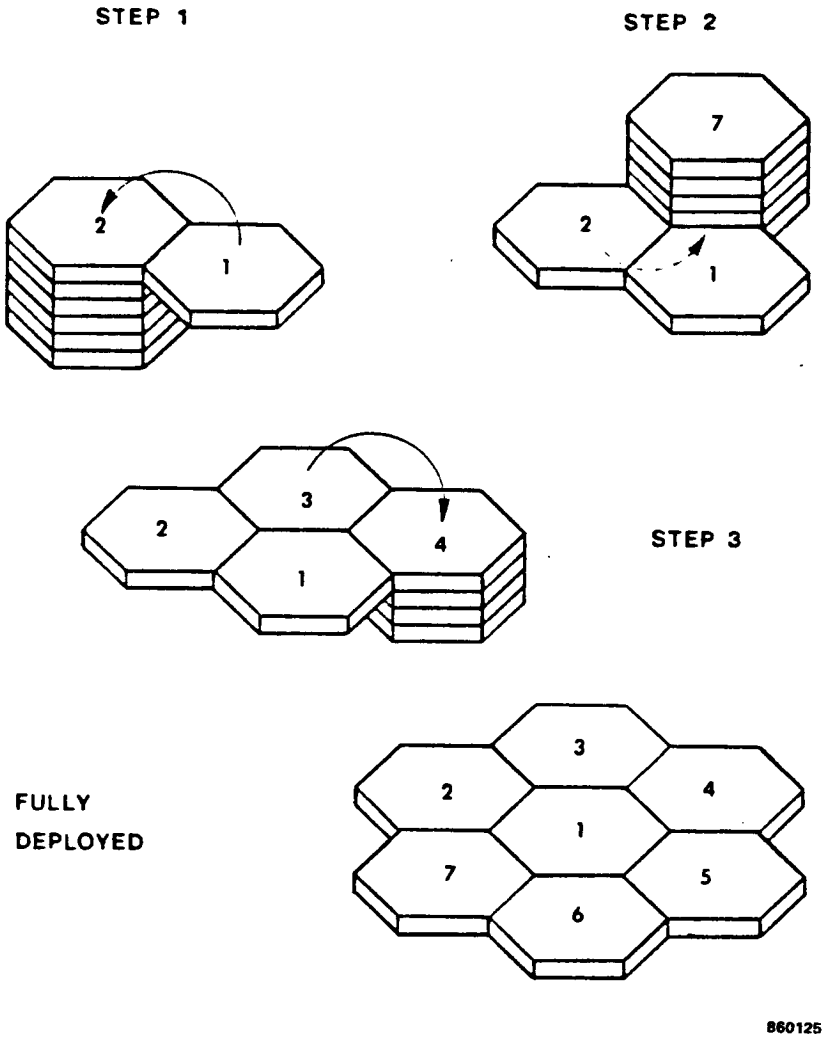

Figure 6.1-11. The Truss Hex Panels are Connected by a Series of Hinges and Latches Which Allow the Panels to Fold into a Stack. Deployment is Sequential, Forming Rings of Panels Around a Center Panel.

TRUSS HEX CONCENTRATOR UNFOLDING DEPLOYMENT

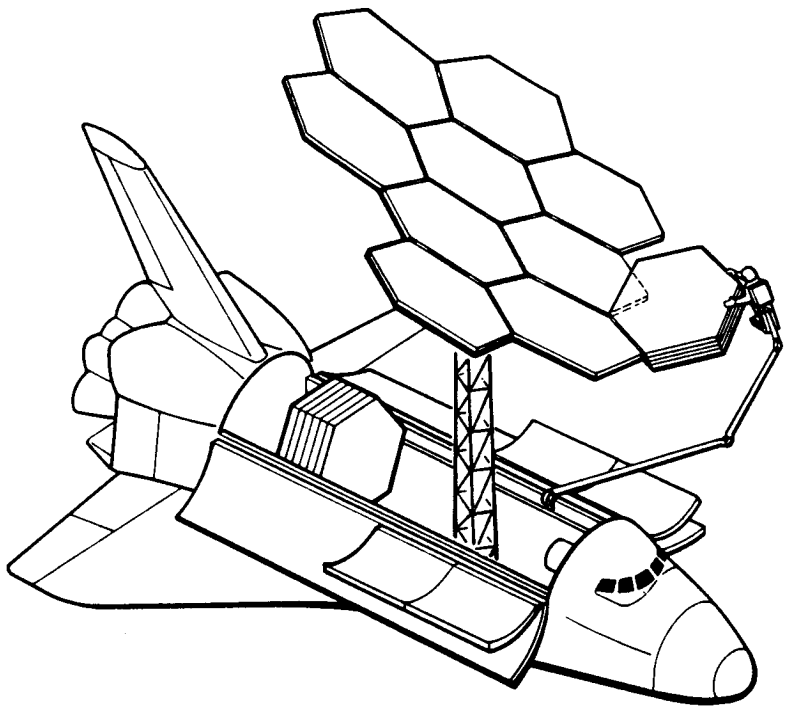

14201-13A

Figure 6.1-12. Manual Unfolding Deployment may be Accomplished with the Astronauts Assistance or using the Remote Manipulator Arm. The First Panel of the Assembly is Temporarily Attached to a Mast or Space Station Structure During the Deployment.

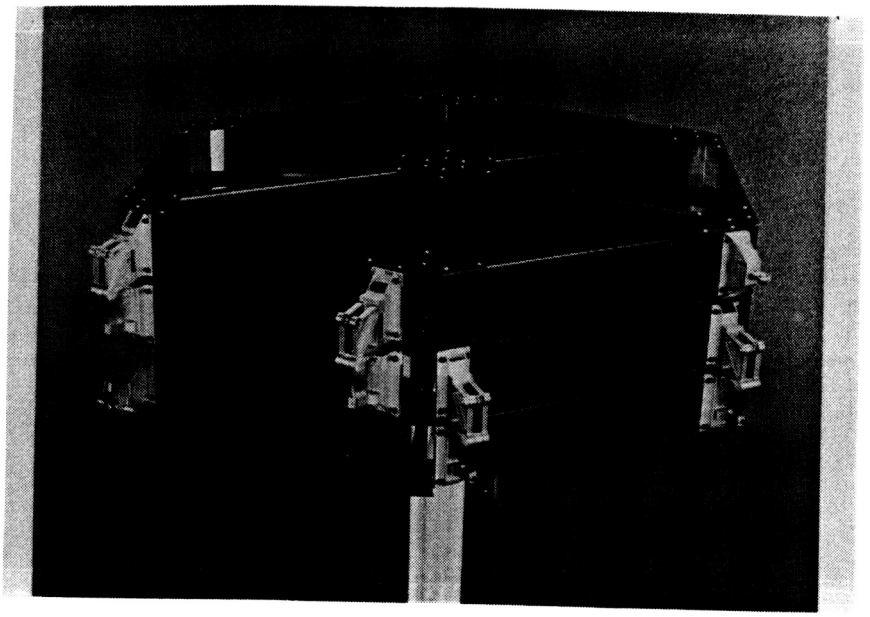

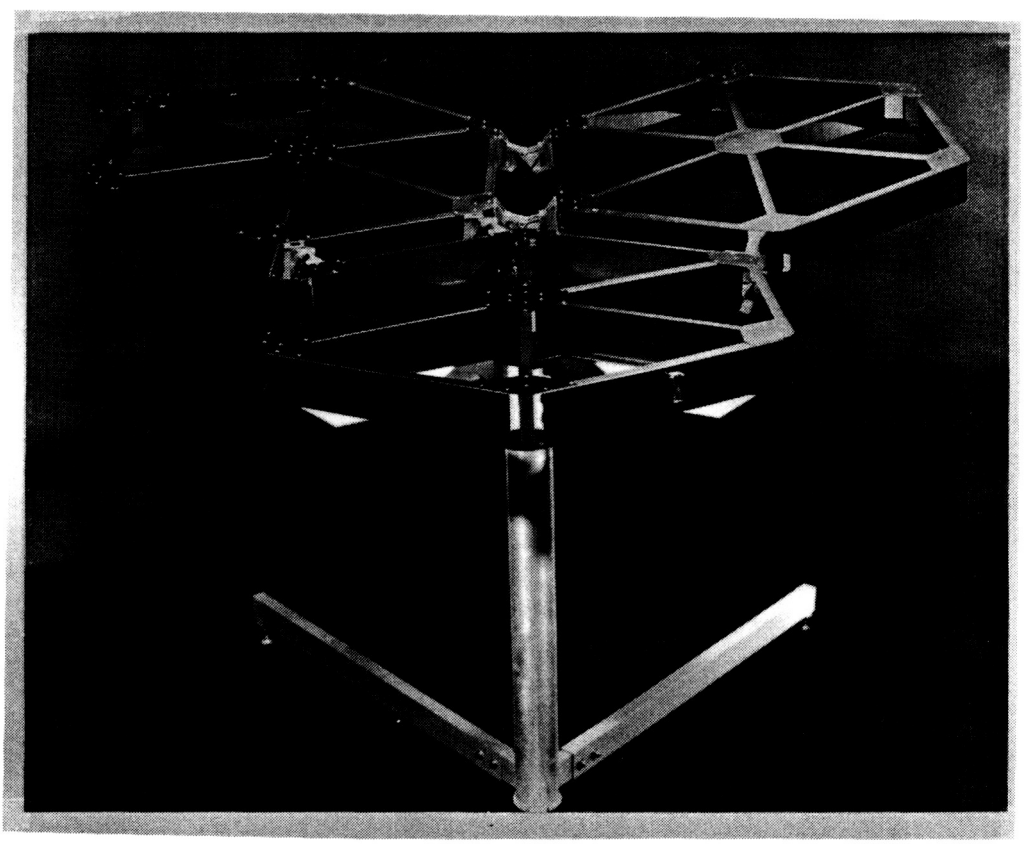

Figure 6.1-13. The Three Panel Model Demonstrates the Deployment and Latch-up Kinematics of the First Three Panels of the Concentrator. The Model Panels are 1/4 Scale from Flat to Flat and the Same Thickness as the Full Size Concentrator.

TRUSS HEX CONCENTRATOR BIFOLD DEPLOYMENT METHOD

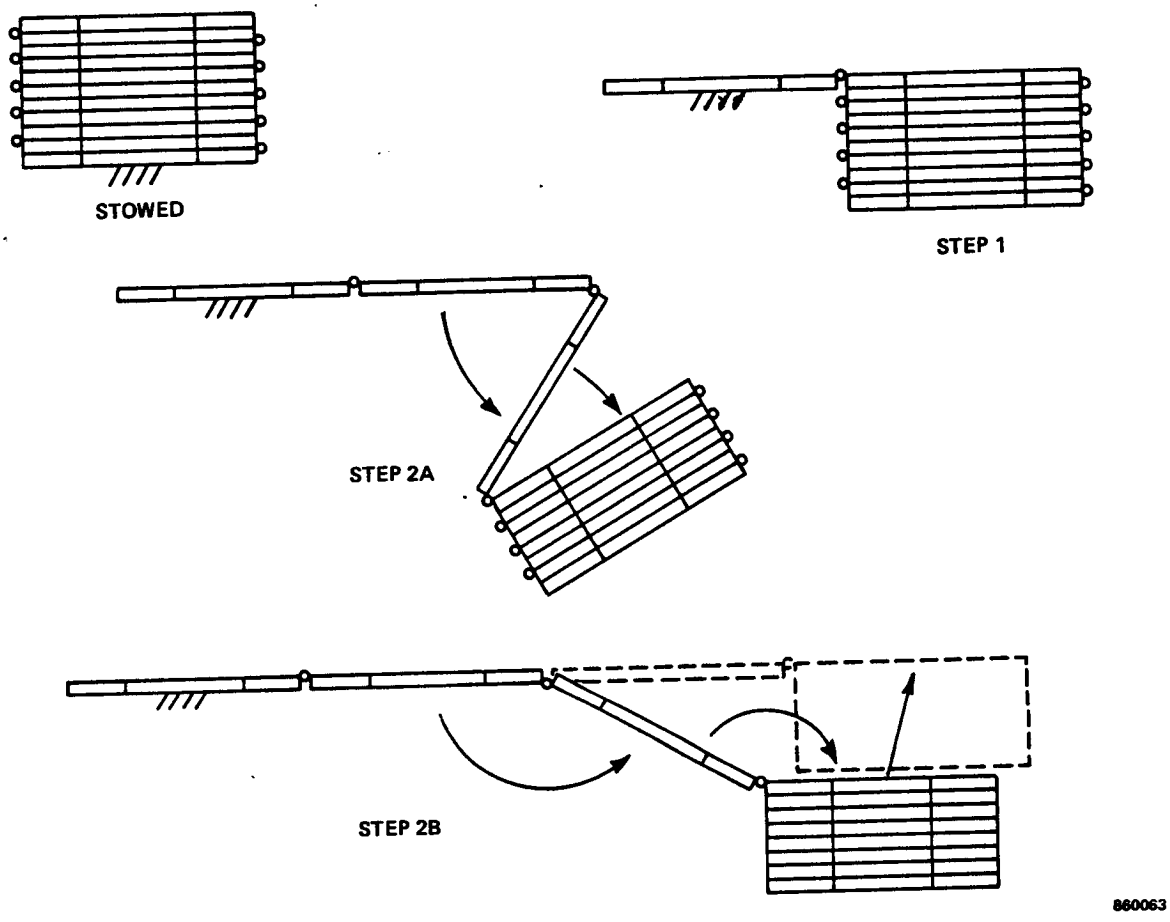

Figure 6.1-14. The Bifold Deployment, Shown Schematically, Avoids Envelope Interferences by Keeping the Stack on One Side of the Concentrator.

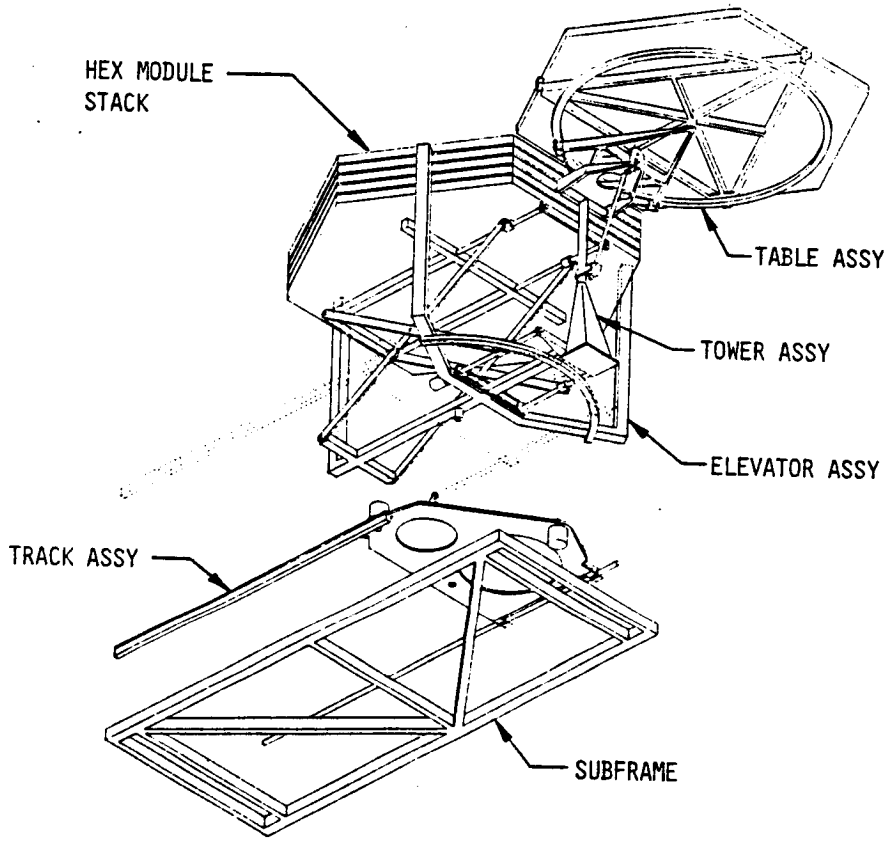

Figure 6.1-15. The External Deployment Mechanism is most Applicable to the Automated Assembly of Large Numbers of Concentrators Where Significant Launch Weight Savings Could be Achieved.

much merit, it was judged to be too complex to pursue within the scope of this study.

The unfolding deployment schemes, selected as best suited for this study, all require hinges and latches. Hinges can be unpowered, as shown in Figure 6.1-16, for manual deployment, or powered, as in Figures 6.1-17, 18 and 19, for remote, automatic deployment. All powered hinges require rather large gear reductions to accommodate one-g deployment verification testing. The size of this reduction is highly dependent on the deployment sequence chosen and the degree of offloading that can be provided compatible with that sequence.

A structural latch based on the NASA docking probe was developed for use on all the deployment schemes (reference 3). A simple latch is illustrated in Figure 6.1-20, showing the basic ball, conical cavity and regenerative cam components. When precision structures are deployed with multiple latches operating at once, slight misalignment might prevent the latches from complete engagement. To ensure the positive latching of more than one latch at a time, a toggle-driven, spring-actuated latch design was developed (see Figures 6.1-21 and 22). As the drive pawl trip enters the drive pawl, the pawl is pushed over-center and the drive spring forces the ball into the conical receptacle. Concepts for retracting latches (see Figures 6.1-23 and 24) were also explored for use in locations where deployment interferences occur.

The optical surface of the Truss Hex is formed from equilateral triangular facets with a spherical surface contour (see Figure 6.1-25). These facets are approximately 1 m (3.3 ft) on a side and 10 mm (3/8 in) thick. The facesheets are made of 1 layer of GFRP with a thickness of 0.1 mm (0.004 in). The core is either polyetherimide honeycomb (such as the General Electric Ultem based core available from Plascore) or a lightweight aluminum with a cell size of 6.3 mm (1/4 in). The reflective surface is vapor-deposited silver with a combination of silicon oxide and magnesium flouride protective coatings.

The deflection limit for the facets was set at 0.5 mm in one-g to keep the gravity induced surface slope error to less than one milliradian of arc (1 mrad/0.057 deg). In space, while sag due to facet weight is not a problem, distortion due to thermal cycling over wide ranges is. Thus, for a facet that is both ground-verifiable and flight-worthy, a material with a high stiffness-to-weight ratio and a low coefficient of thermal expansion (CTE) is needed. Of the materials currently available, GFRP composites are the most cost effective solution.

The mirror facets are attached to the hex module structure near each corner by ball and socket fittings. The ball is mounted on an adjustment screw (see Figure 6.1-26). This arrangement allows individual adjustment of the corners of the facet for flux-tailoring. The facets would be adjusted and locked in place during ground assembly. The ball and socket fittings provide quick release for replacement of individual facets in service. To replace a facet, a tool such as the one illustrated in Figure 6.1-27 may be used to grab

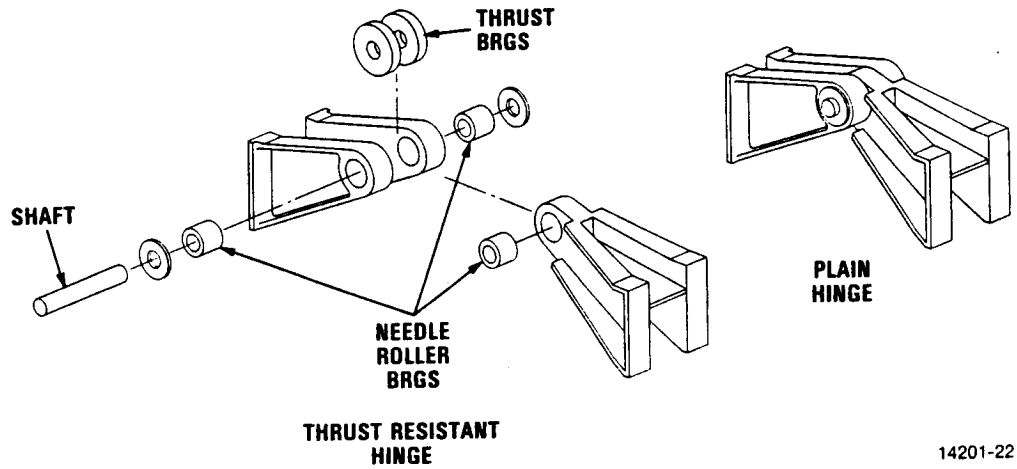

Figure 6.1-16. The Unpowered Hinge Which Joins the Folded Panels is Easily Produced and Extremely Reliable. Individual Spacers or Variations in the Side Plate Dimensions are Required to Account for Irregularities in the Panel-to-Panel Gaps.

TRUSS HEX CONCENTRATOR
POWERED HINGE FOR KINEMATIC MODEL

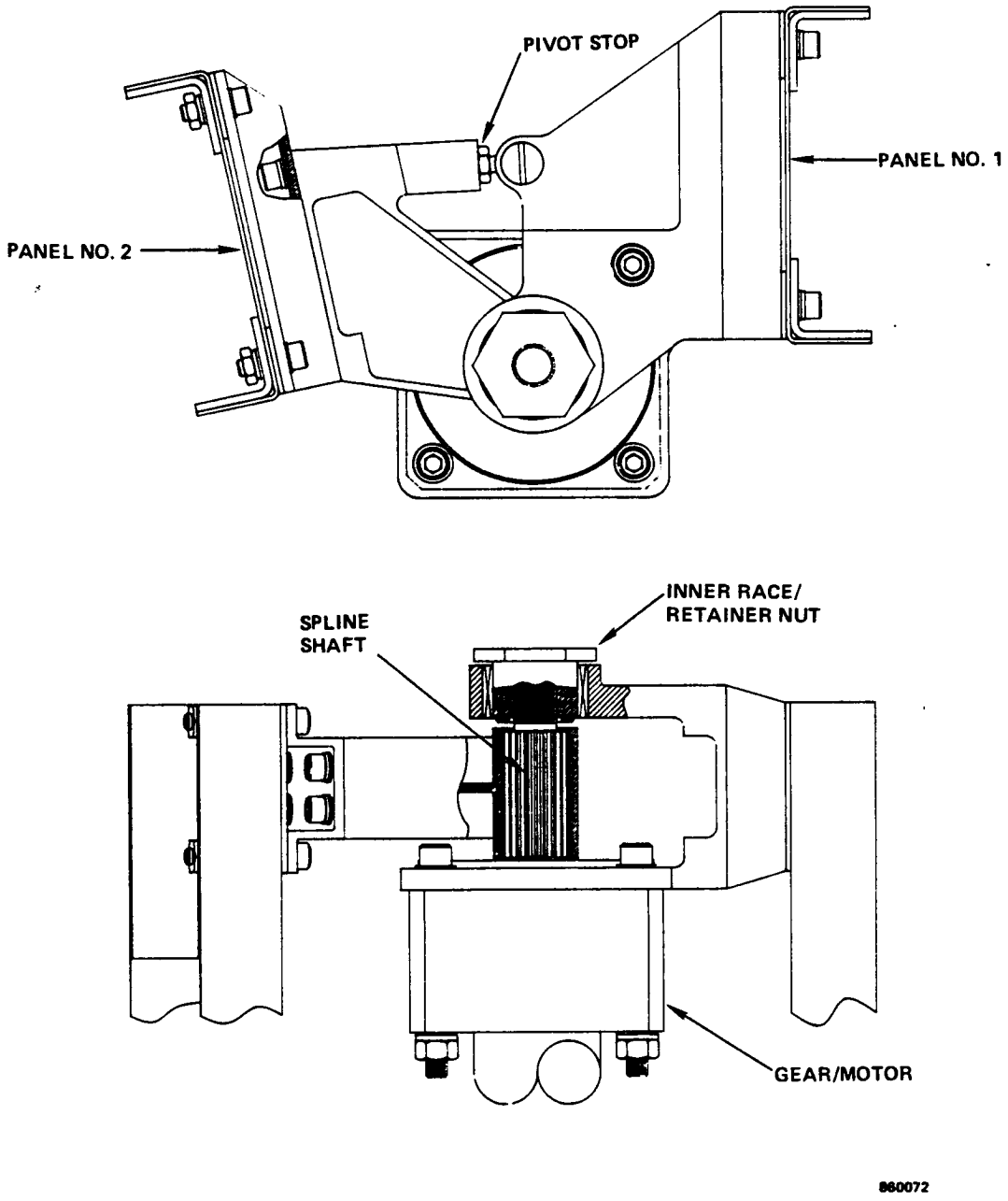

Figure 6.1-17. The Truss Hex Hinges may be Motorized for Automatic, Remote Deployment.

TRUSS HEX CONCENTRATOR
HIGH TORQUE POWERED HINGE - ASSEMBLY

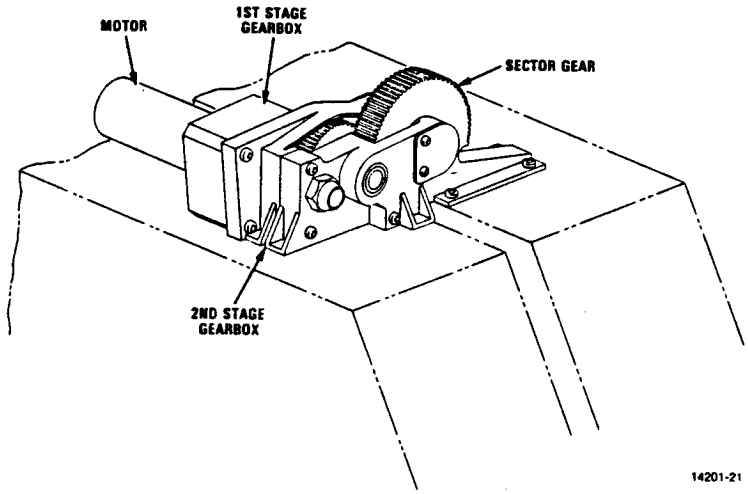

TRUSS HEX CONCENTRATOR
HIGH TORQUE POWERED HINGE (EXPLODED VIEW)

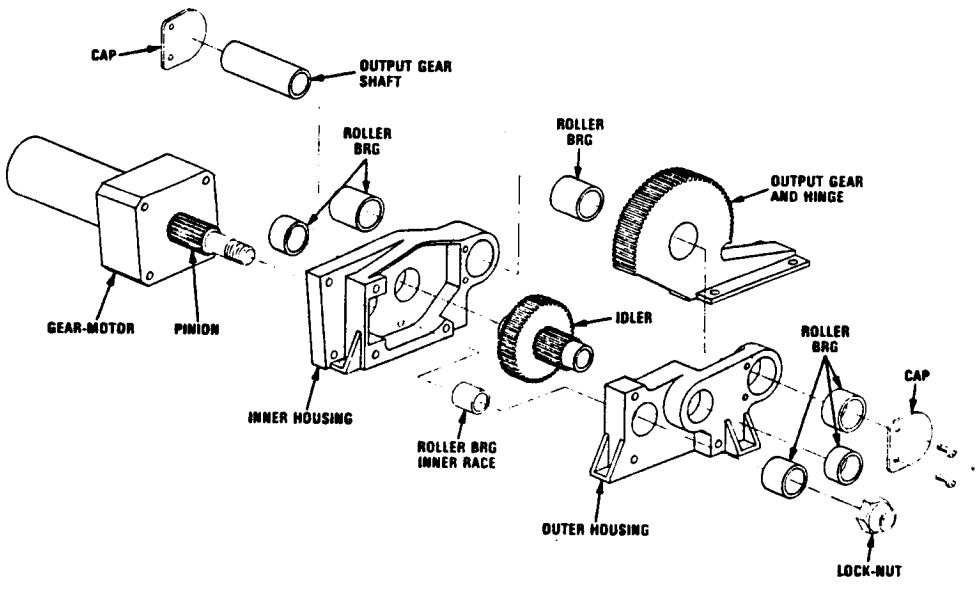

Figure 6.1-18. A Second Concept for Motorized Hinges uses Additional Reduction Gearing to Permit 1-g Deployment Verification Testing.

TRUSS HEX CONCENTRATOR
HELICAL DRIVE SYSTEM

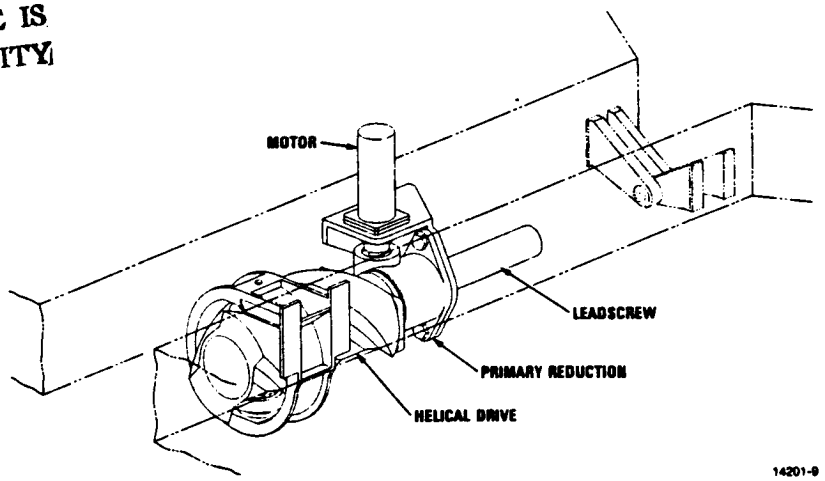

TRUSS HEX CONCENTRATOR
HELICAL DRIVE SYSTEM (EXPLODED VIEW)

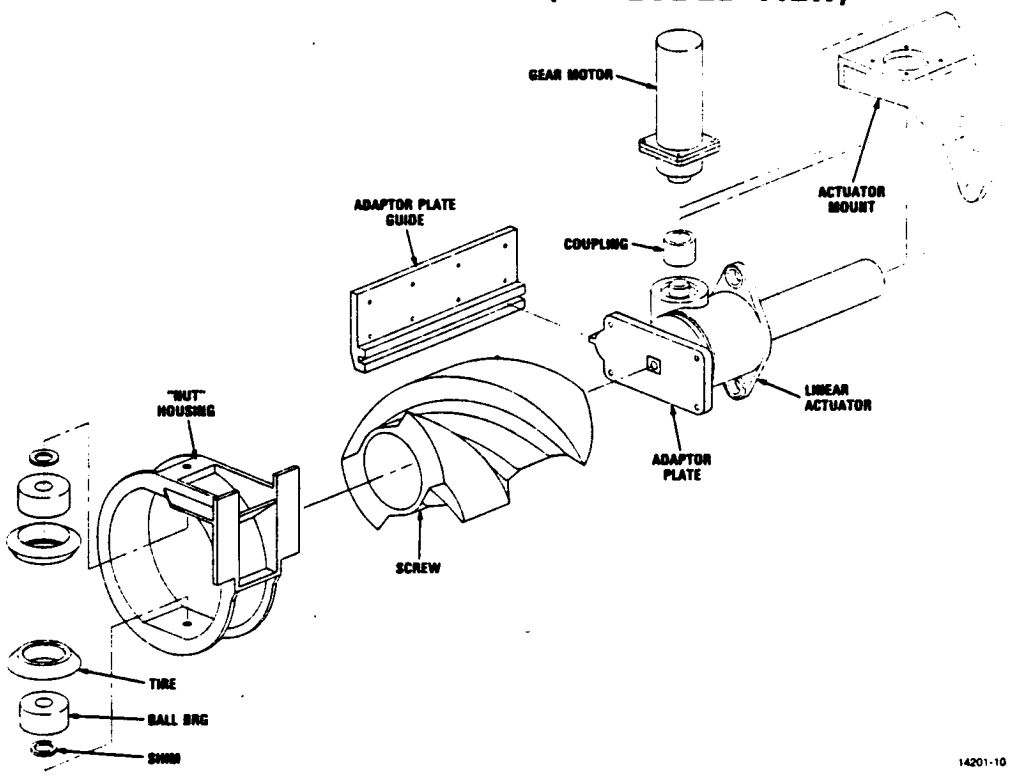

Figure 6.1-19. This Helical Drive for a Motorized Hinge Achieves Tremendous Torque with a Small Motor and Provides Some Unique Packaging Options.

TRUSS HEX CONCENTRATOR PANEL LATCH COMPONENTS

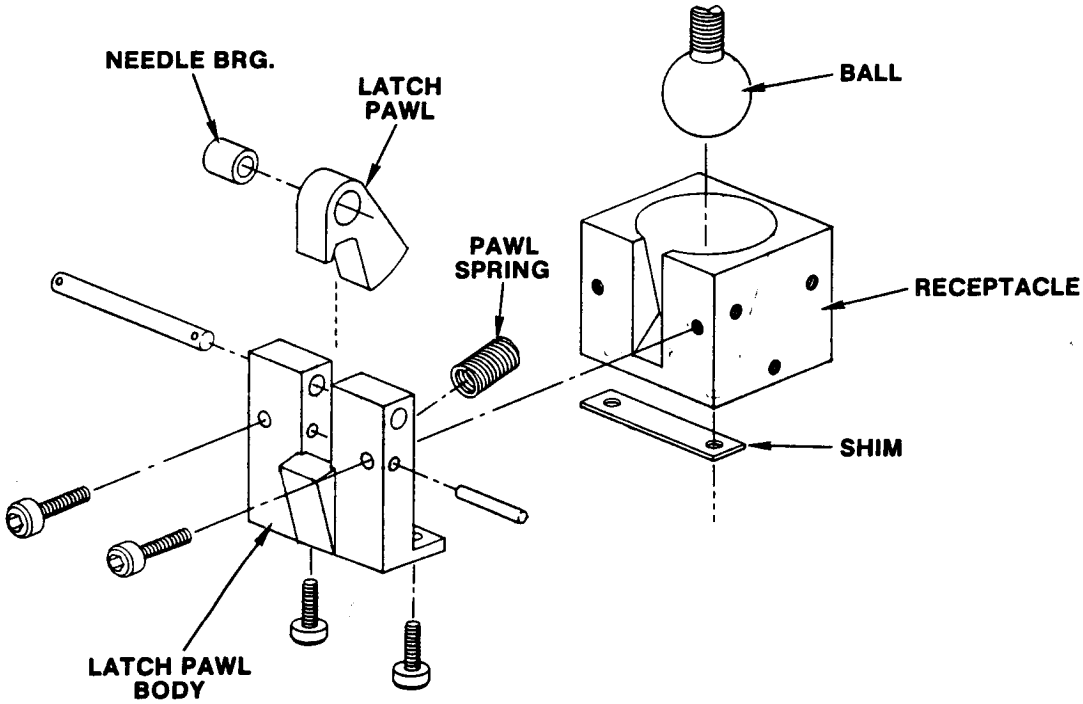

Figure 6.1-20. The Structural Latch Proposed for use Between Truss Hex Panels is Based on the NASA Docking Probe Concept; a Ball is Retained in a Conical Socket by a Regenerative Cam.

TRUSS HEX CONCENTRATOR
POWERED LATCH

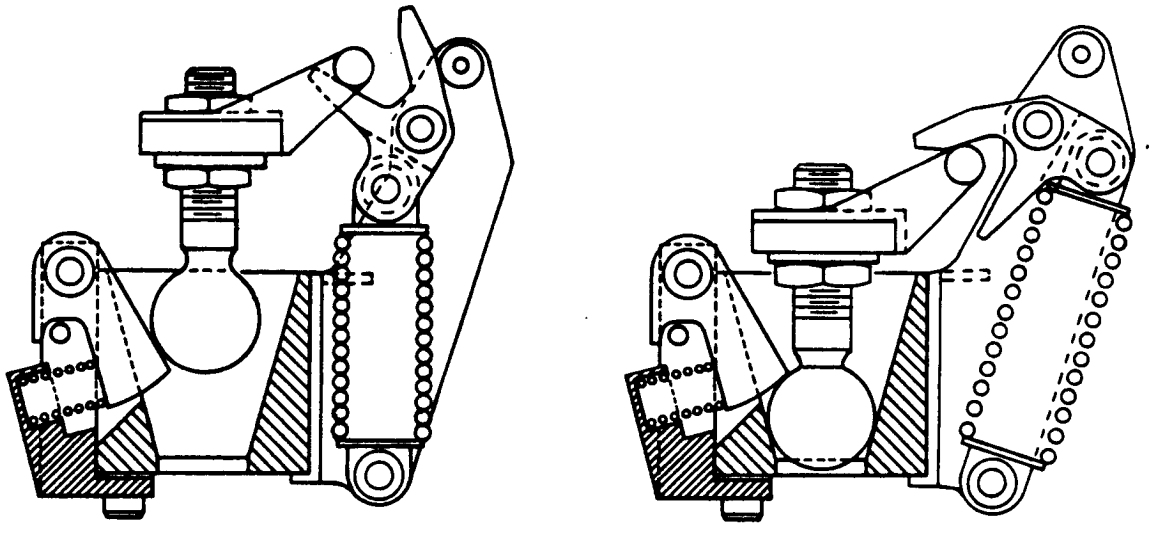

Figure 6.1-21. A Toggle-Driven "Powered Latch" was Developed to Ensure Engagement of Latches where More Than One Interface Must Lock Simultaneously.

TRUSS HEX CONCENTRATORS
POWERED LATCH COMPONENTS

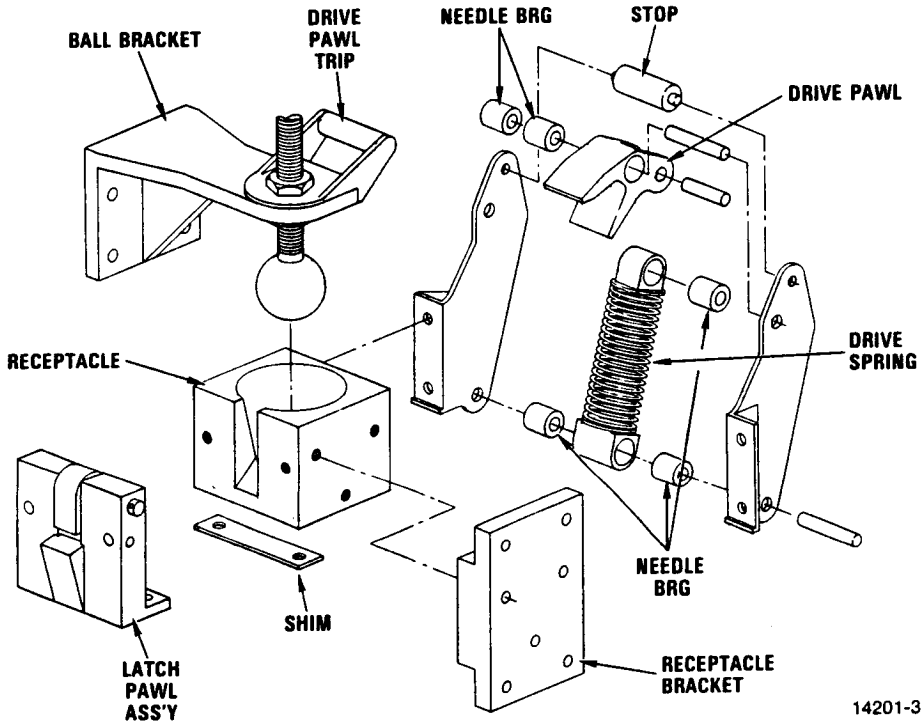

Figure 6.1-22. Exploded View of Powered Latch Shows that Spring and Drive Components may be added to Standard Latch Assembly.

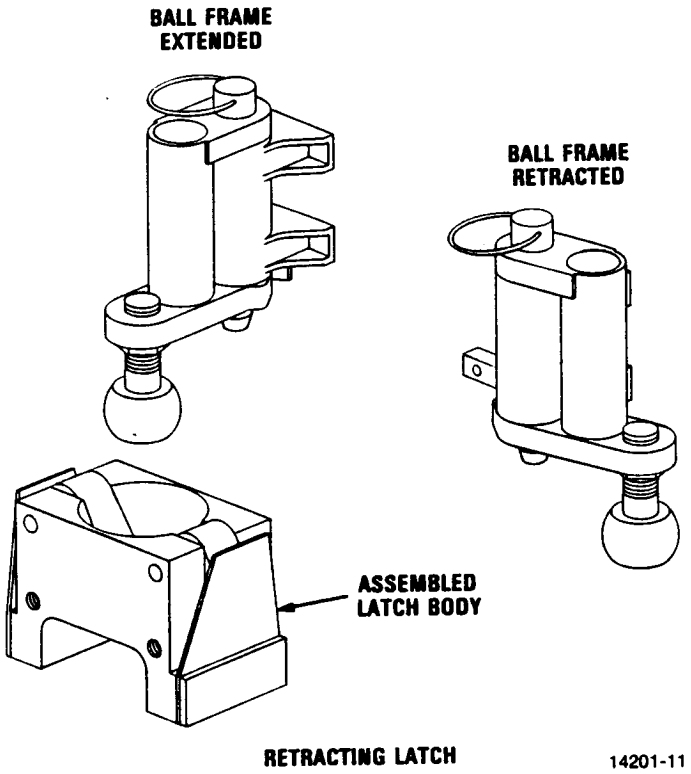

Figure 6.1-23. A Retracting Latch is one Method to Eliminate Potential Interferences During the Deployment of Hex Panels with the Single Fold Method.

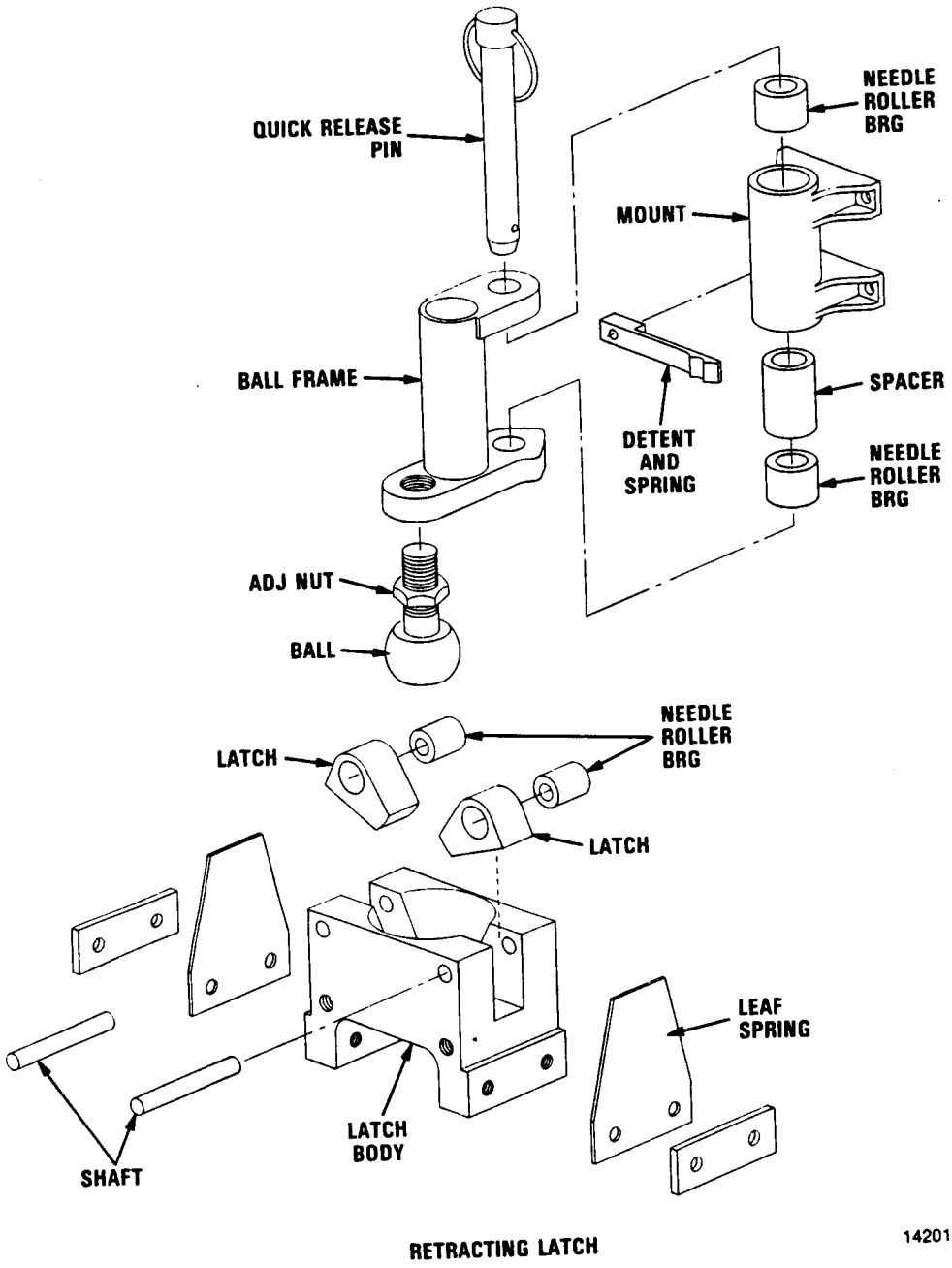

Figure 6.1-24. This Exploded View Shows the Major Components of the Hinged Latch. The Quick-Release Pin Allows On-Orbit Replacement of Individual Hex Panels.

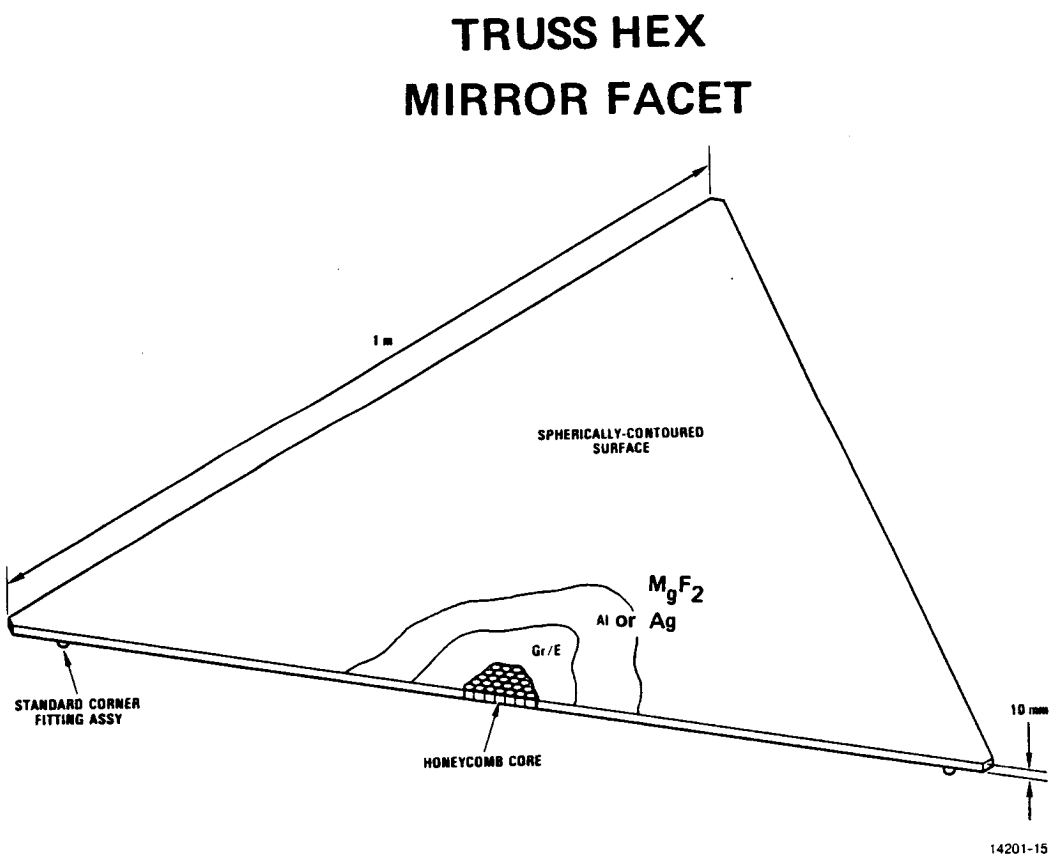

Figure 6.1-25. The Truss Hex Mirror Facets are Fabricated Sandwich Panels with a Spherically Contoured Surface Which Approximates the Local Curvature of the Paraboloid. The Number of Individual Mirror Curvatures is Determined through Analytical Optimization (Probably 6 to 8 for a 19 Panel System).

TRUSS HEX CONCENTRATOR
CORNER ASSEMBLY AND MIRROR ADJUSTMENT

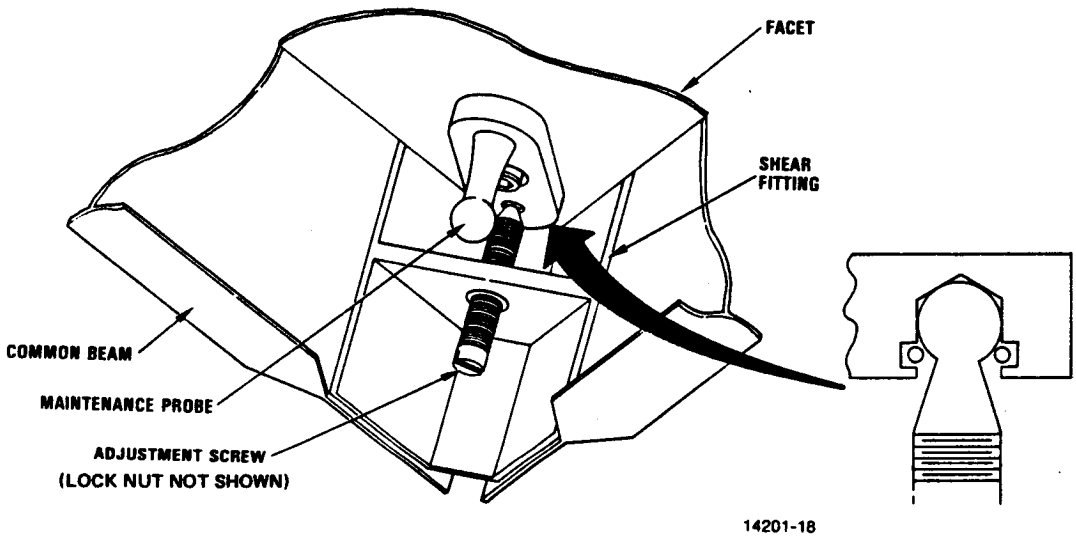

Figure 6.1-26. The Corner Attachment Design Allows Ground Adjustment of Individual Facets for Flux-Tailoring and On-Orbit Replacement of Facets.

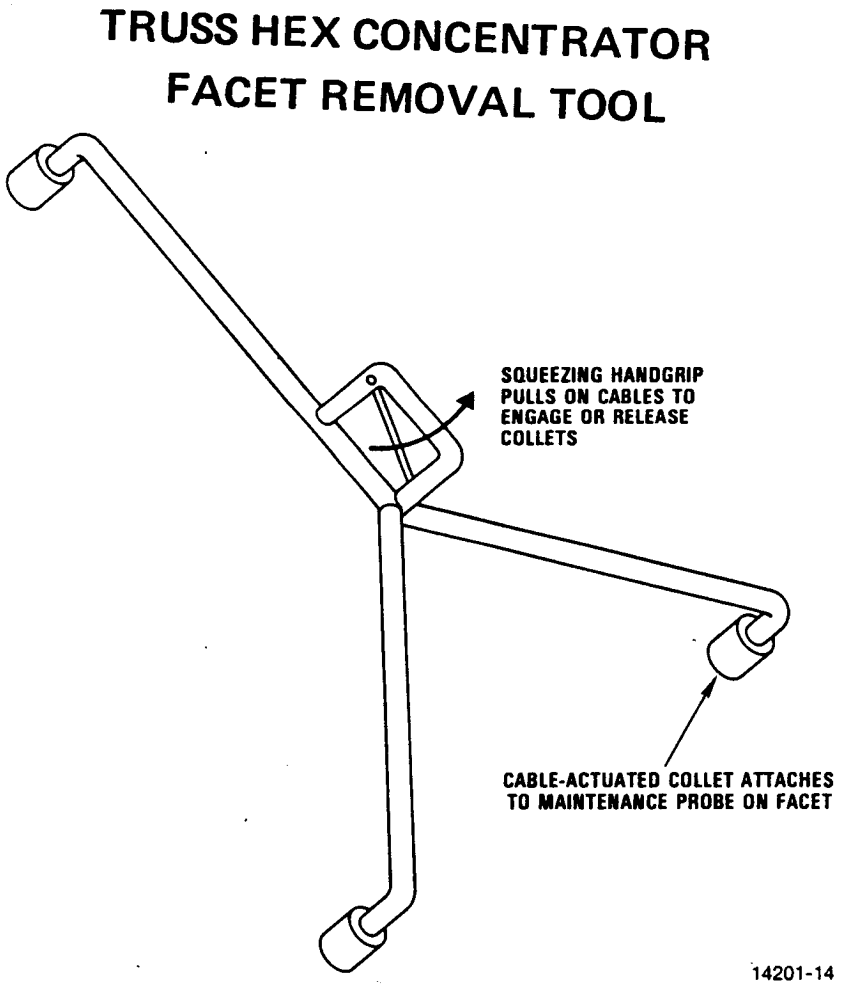

Figure 6.1-27. A Tool such as this may be Used for Handling Facets, Both During Construction of the Concentrator and in Space.

the maintenance probes of the facet and detach the facet from the adjustment screw balls. Reaching through the panel, the astronaut can rotate the facet and pull it back through the open facet cavity. The entire operation may be accomplished from behind the concentrator surface and without facet realignment.

The latest mass summary for the Truss Hex is listed in Table 6.1-1. The current mass estimate exceeds the design goal of 360 kg. Although system mass is an important trade study parameter, the Truss Hex concept is competitive and is volume limited not mass limited.

Table 6.1-1. Truss Hex Mass Summary

Component Set	Avg. Panel kg (lb)	19 Panels kg (lb)	24 Panels kg (lb)
Honeycomb facets	10.9 (24.2)	208 (459)	262 (578)
Beams	9.5 (21.0)	181 (399)	228 (503)
Shear fittings	1.5 (3.3)	29 (64)	36 (79)
Hinges	0.9 (2.0)	17 (37)	22 (49)
Latches	0.4 (0.9)	8 (18)	10 (22)
Totals	23.2 (51.1)	443 (977)	558 (1230)

6.1.3 Analysis Results - Truss Hex

The structural and optical capabilities of the Truss Hex concentrator were characterized on the Phase B program. A finite element model of a 19 panel concentrator was used to perform parametric analyses. The objective of the analyses was to determine the deployed stiffness capability, measured by deployed frequency, and the sensitivity of the concept to various design parameters. This effort was reported under the Space Station Phase B Work Package 4 program (reference 1). The conclusion resulting from the structural analysis was that the Truss Hex concentrator concept is capable of achieving a first fundamental deployed frequency greater than 1.0 Hz.

The Phase B optical analysis was performed using a continuous surface offset concentrator model. Parametric analysis support the conclusion that the offset optical configuration is compatible with proposed receiver designs. The results of these analyses are also reported in reference 1.

The optical performance of the concentrator concepts is the primary analytical performance criteria used in the trade study. The Truss Hex concentrator has a faceted not a continuous surface and incorporation of this design feature in the optical performance predictions was deemed necessary.

The optical analysis of the SCAD program Truss Hex concentrator was performed by Georgia Tech Research Institute (GTRI). The results are summarized in the following paragraphs.

The offset Truss Hex concentrator configuration used in the GTRI analysis included: facets measuring 0.9625 m on a side, focal length of 7.6706 m, 19 panels with 24 spherically curved facets each, and f/D of 0.25 for parent paraboloid. A computer generated plot of the model is given in Figure 6.1-28. The Boeing receiver advanced development proposal reference ORC and CBC geometries, given in Table 6.1-2, were used in the analysis.

Table 6.1-2. Receiver Geometries Used in Optical Analysis

Receiver Dimension	ORC	CBC
Aperture Diameter (m [in.])	0.457 [18]	0.330 [13]
Cavity Length (m [in.])	1.067 [42]	1.016 [40]
Cavity Diameter (m [in.])	1.041 [41]	1.092 [43]

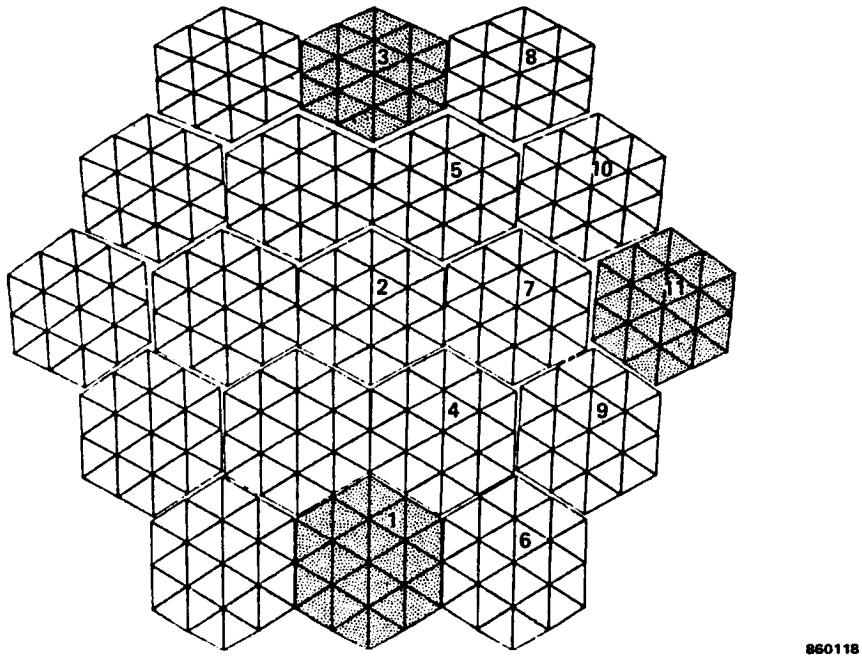

Figure 6.1-28. Computer Plot Depicts Truss Hex Concentrator Geometry Used in GTRI Optical Analysis.

The optical analysis methodology is given in Figure 6.1-29. GTRI placed the centroid of each spherical facet on the paraboloid. It is possible to translate the facet in and out in the radial direction to optimize hex panel depth without changing optical performance. The facet surface normal is oriented to match the paraboloid surface normal. A facet radius which approximates the paraboloid radii is chosen. The facet image is displayed on the aperture plane using a point source. The radius can be optimized to provide the best balance between aberration in the radial and circumferential directions. GTRI constrained the number of facet radii by using the same radius for all facets in a given hex module. Focal plane images for optimized radius facets in hex panels 1, 3, and 11 (see Figure 6.1-28 for panel locations) are given in Figures 6.1-30 to 6.1-32. These images are typical. The Boeing CBC receiver aperture is included on the figures. GTRI concluded that 8 different facet radii, as given by Table 6.1-3, were required.

Table 6.1-3. Facet Spherical Radius Selected for Each Hex Panel

Hex Panel Number (Figure 6.1-28)	Selected Facet Spherical Radius (m)
1	17.50
2	20.00
3	27.25
4	20.00
5	24.00
6	17.50
7	21.00
8	29.00
9	19.00
10	25.50
11	24.00
12-19	By symmetry

Once the model geometry has been finalized, the concentrator is illuminated with a true solar disk source. A gaussian distribution, one sigma slope error; concentrator reflectivity; and a receiver tilt angle are selected. A ray tracing computer program traces the reflected rays to the aperture plane. The aperture plane and receiver cavity side and back walls are segmented into grids. The number of rays traced to a given grid area are counted and compared to the total number of incoming rays to determine the percentage flux collected on the grid area. The ray tracing and collection method are illustrated in Figure 6.1-33. Two hundred thirty one points are traced on each facet for a total of 105,336 rays.

FACETED HEX ANALYSIS METHODOLOGY

- MAP FACETS ONTO PARABOLOID
- CHOOSE FACET GEOMETRY/ORIENTATION
- DISPLAY FACET IMAGES IN APERTURE PLANE USING POINT SOURCE
- ITERATE AS REQUIRED
- PERFORM OPTICS ANALYSIS USING ABOVE GEOMETRY WITH GAUSSIAN DISTRIBUTED 3 MILLIRADIAN SLOPE ERRORS AND SOLAR SOURCE MODEL
- PRELIMINARY RECEIVER GEOMETRIES WERE USED FOR ANALYSIS
- FINAL DESIGN PARAMETERS TO BE ESTABLISHED DURING TASK 2 USING RECEIVER GEOMETRY TO BE SPECIFIED BY NASA

Figure 6.1-29. GTRI Optical Analysis Methodology Includes Optimization of Facet Spherical Radius.

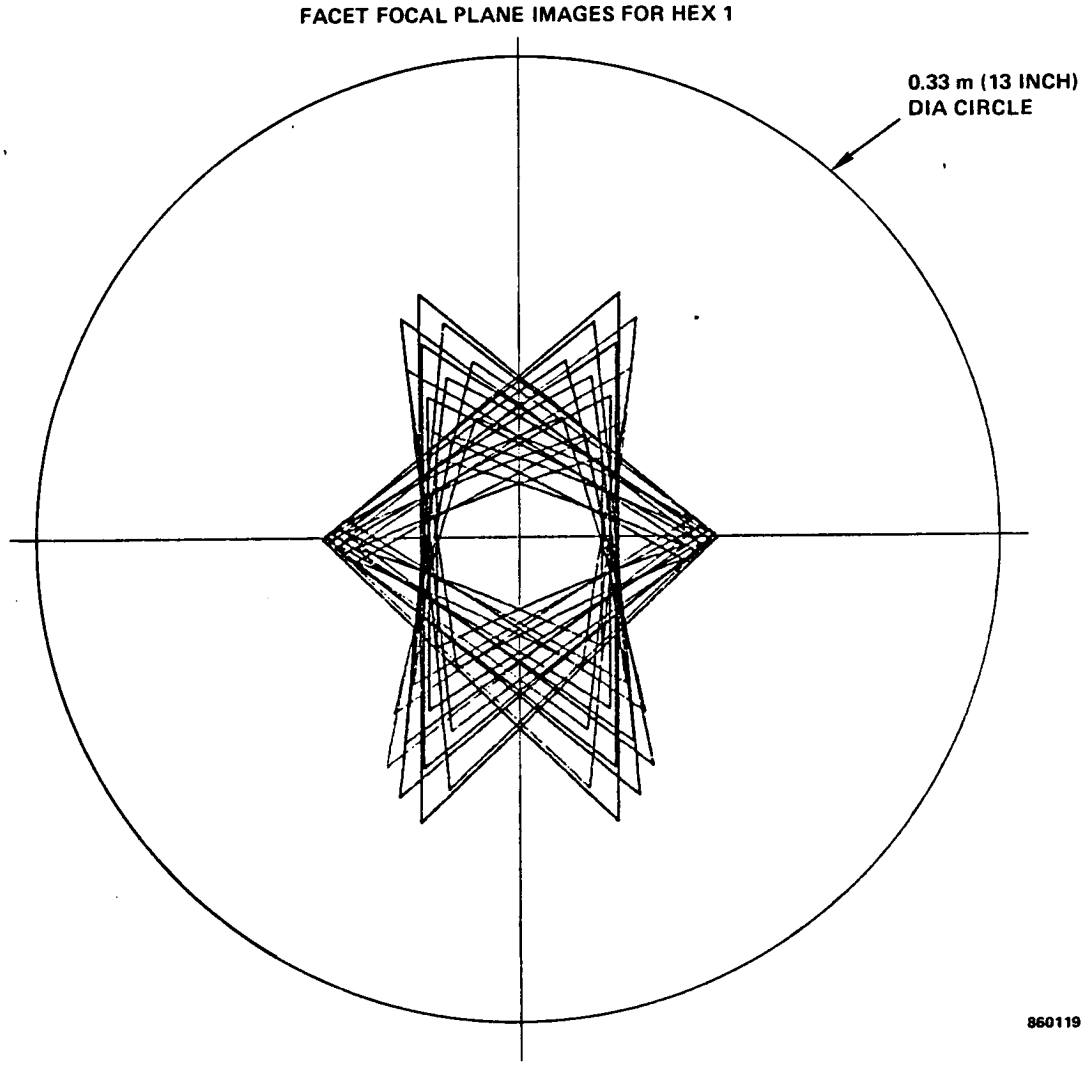

Figure 6.1-30. Facet Focal Plane Images for Hex 1 Depicts Optimum Facet Aspect Ratio.

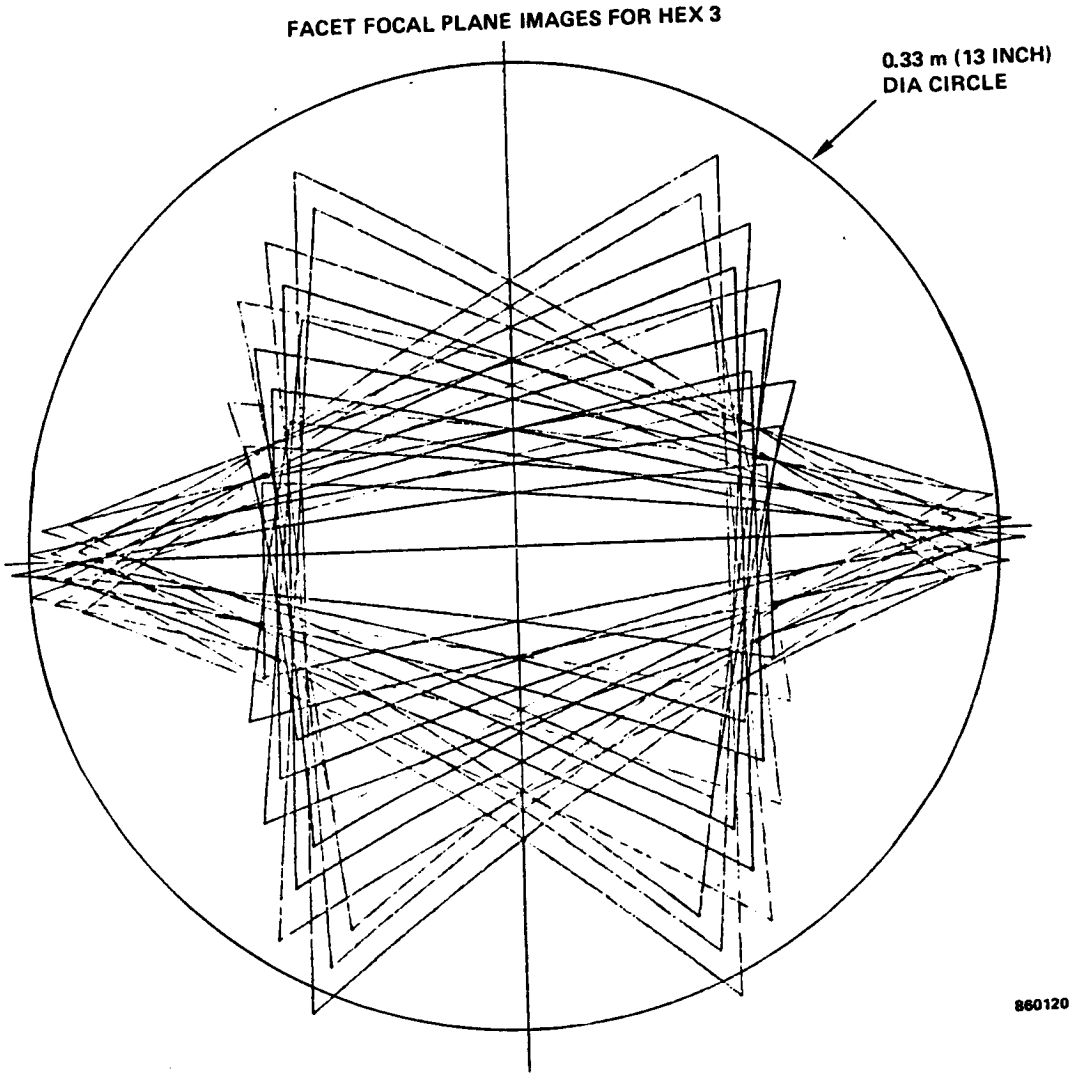

Figure 6.1-31. Facet Focal Plane Images for Hex 3 Depicts Optimum Facet Aspect Ratio.

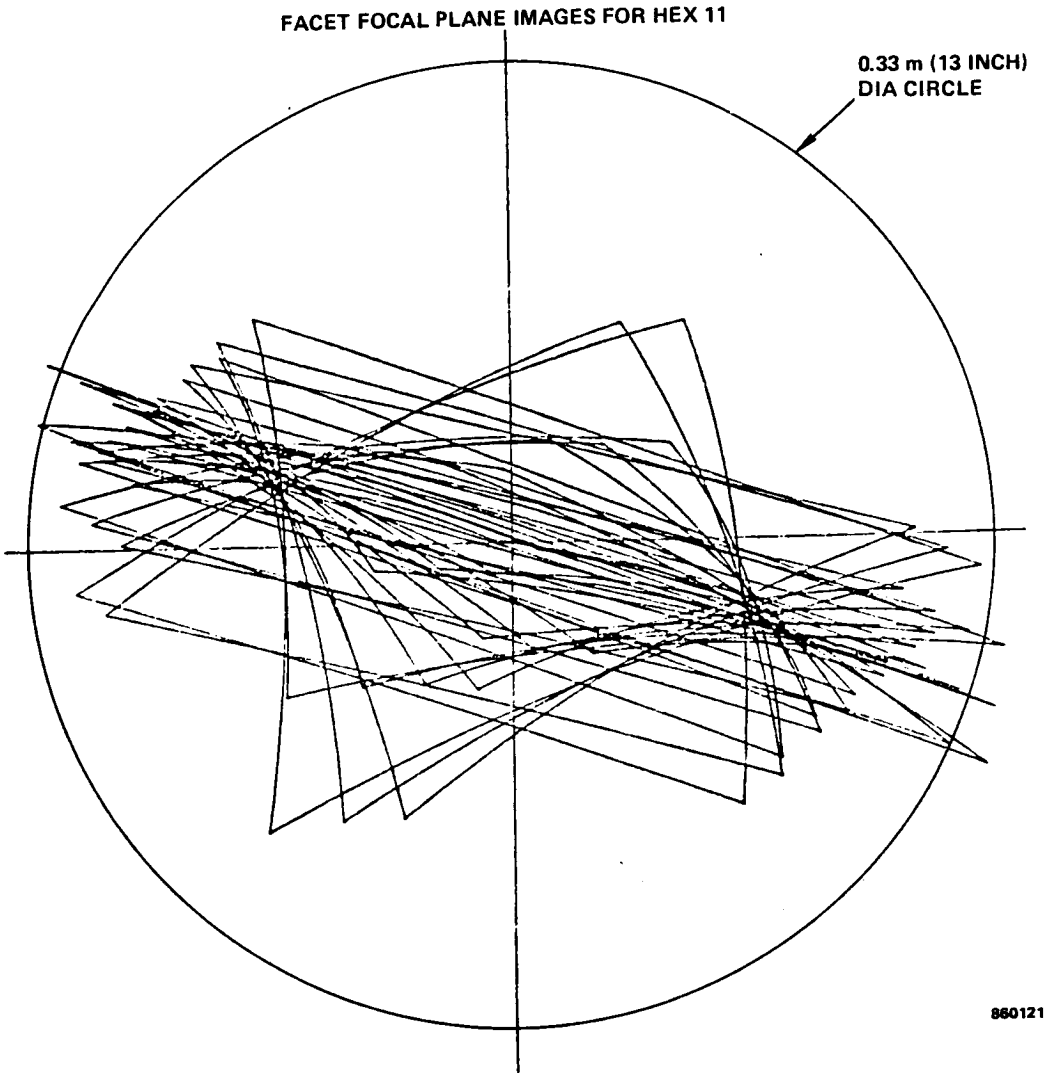

Figure 6.1-32. Facet Focal Plane Images for Hex 11 Depicts Optimum Facet Aspect Ratio.

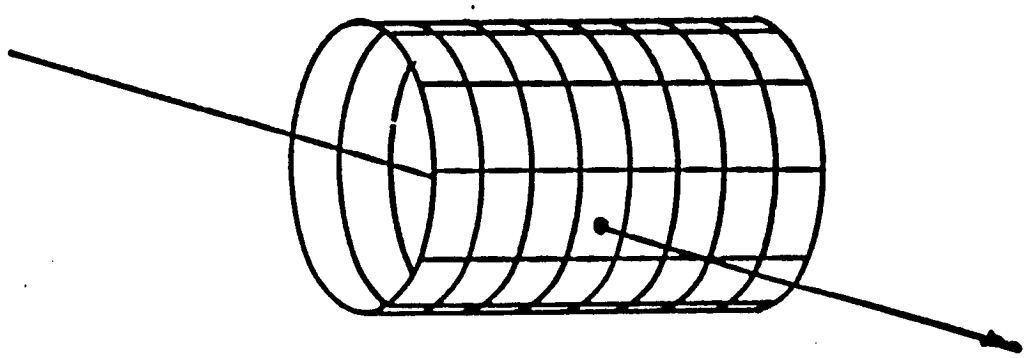

Figure 6.1-33. Each Traced Ray is Collected in Appropriate Grid Area on Receiving Surface.

The input parameters used for the Truss Hex optical analysis were:

- 3 milliradian one sigma slope error
- 0.9 reflectivity
- 1.310 solar constant
- 51° - 54° receiver tilt angle

Typical aperture and cavity side and back wall flux contour plots are given in Figures 6.1-34 to 6.1-36.

The analysis results; intercept factor flux delivered to receiver, and side wall illumination, are tabulated in Table 6.1-4. A complete analysis report was provided by GTRI.

Table 6.1-4. Summary of Truss Hex Optical Analysis Results

Thermodynamic Cycle	Receiver Tilt Angle (degrees)	Intercept Factor	Delivered Flux (kW)	Side Wall Illumination Total Flux / Side Flux
ORC	51	0.99	177.59	0.63
ORC	52	0.99	177.61	0.62
ORC	53	0.99	177.65	0.61
ORC	54	0.99	177.67	0.61
CBC	51	0.94	169.29	0.53
CBC	52	0.94	169.33	0.52
CBC	53	0.94	169.37	0.52
CBC	54	0.94	169.39	0.51

6.1.4 Evaluation of Significant Parameters - Truss Hex

The thrust of the Truss Hex design effort has been toward producibility, flexibility, and maintainability. Subdivision of the optical surface into relatively small facets makes fabrication to optical tolerances much easier. The design of the facets provides sufficient stiffness for 1 g testing allowing facets to be installed and adjusted individually for tailoring of the flux pattern delivered to the receiver. This enhances the compatibility of the design with different conversion cycles.

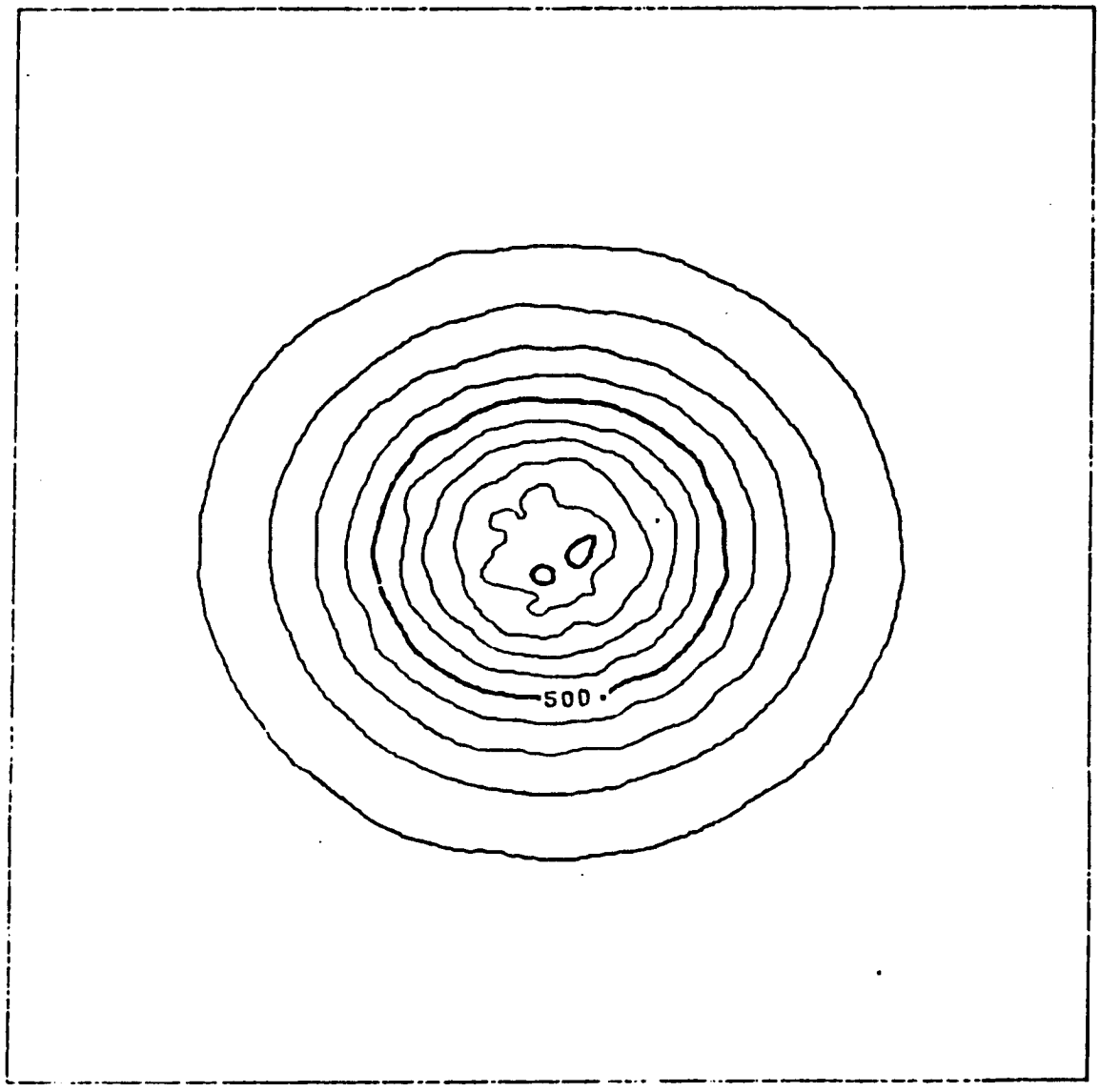

Figure 6.1-34. Aperture Plane Flux Contour Plot for ORC Receiver With 53° Tilt Angle Illustrates Typical Profile.

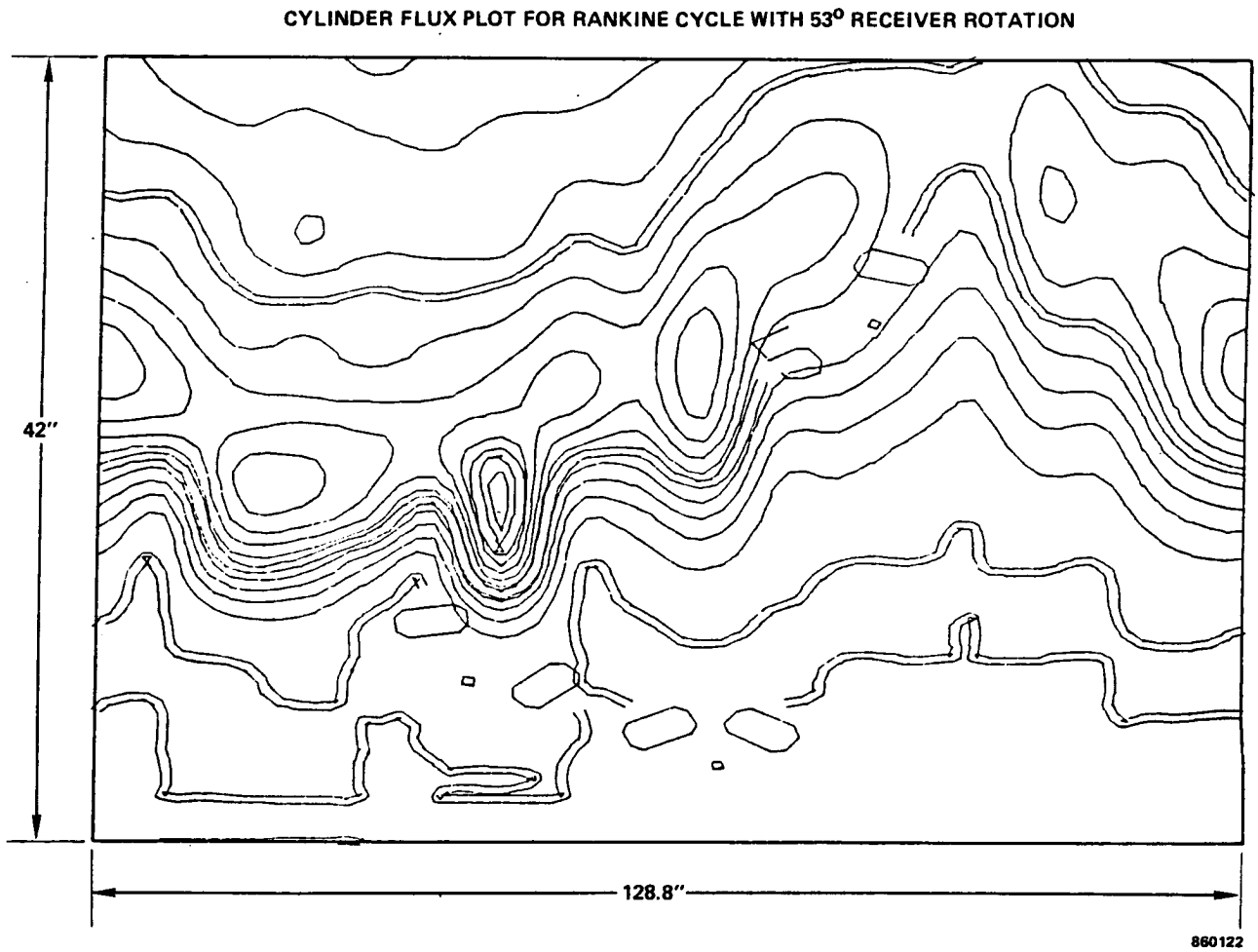

Figure 6.1-35. Cavity Side Wall Flux Contour Plot for ORC Receiver With 53° Tilt Angle Illustrates Typical Profile.

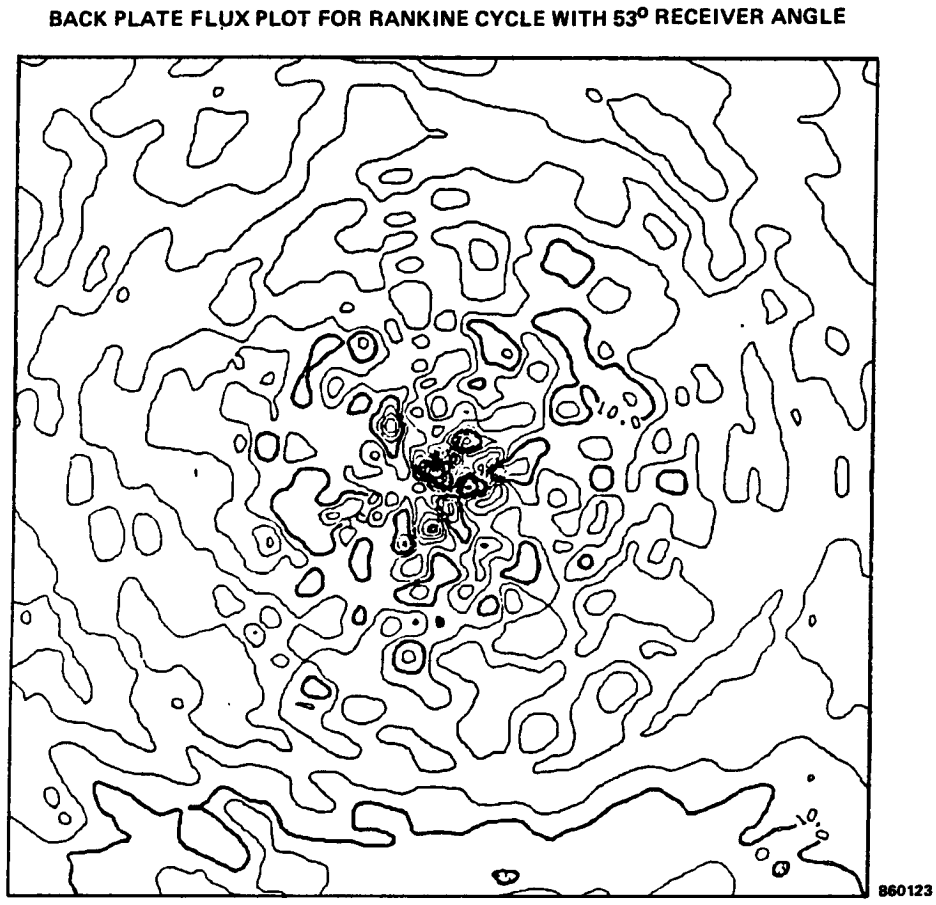

Figure 6.1-36. Cavity Back Wall Flux Contour Plot for ORC Receiver With 53° Tilt Angle Illustrates Typical Profile.

The use of facets also promotes easier on-orbit maintenance of the concentrator, since it allows for smaller line-replaceable units. By discretely replacing facets that have been degraded by the environment, holed by meteoroid impacts, or damaged by low-velocity collisions with equipment; astronauts can maintain a Truss Hex concentrator at essentially beginning of life performance levels. However, the method for determining the performance status of individual mirror elements on-orbit has not been considered.

The next level of modularity is the hexagonal panel that the facets are mounted in. These modules are intended to be common with variation only in the facets and the attachment hardware, located around its edges. Should subsequent analysis mandate the reinforcement of certain elements, the web of the beam can be quintupled in thickness without encroaching on the standard mirror facet envelope. The mounting points for the facets are all common, and the hinges, latches, and other hardware around the outside of the panel are easily accessed for installation, adjustment and maintenance. This suggests that, while restow aboard the shuttle for return to earth and disposal would be straightforward, Truss Hex concentrators may actually be kept in space and maintained indefinitely.

Table 6.1-5 summarizes the significant design parameters and features of the Truss Hex solar concentrator.

Table 6.1-5. Truss Hex Concentrator

Summary of Concept Characteristics

Design Parameter	Parameter Description		
Configuration	Baseline: offset, CBC system Applicable to center fed and ORC configuration		
Deployed Diameter	18.4 m (60 feet)		
Focal Length	8.5 m (28 feet)		
Stowed Package	Stack of hexagonal panels Cylindrical envelope 4.5 m diameter x 2.2 m (177 inch x 86 inch) Volume: 35.0 m^3 (1225 ft^3)		
Mass	Mirror Facets	208	(459)
	Hex Structure	235	(518)
	Total	443 kg	(977 lbs)
Deployed Stiffness	1 - 2 Hz		
Support Structure	19 hexagonal frames joined by precision hinges and latches		

Table 6.1-5. Truss Hex Concentrator (Continued)

Summary of Concept Characteristics

Design Parameter	Parameter Description
Surface Design	456 triangular, spherical mirror facets 24 mirrors per panel Individually adjustable mirrors
Deployment	Extremely flexible - Manual unfolding of partial system modules (EVA) - Fully automated (15-60 min) EVA for attachment of receiver support struts
Maintainability	Mirror facet replacement easy Panel replacement possible Insignificant degradation of surface from impact damage to either structure or surface
Restow and Disposal	Refolding and locking panels easy with manual fold system Automatic restow possible
Complexity	Repeated, simple structure - 19 modules Low parts count Simple, identical latches and hinges
Reliability	Manual deployment Low damage susceptibility Structural simplicity
Scalability/Growth	Size growth by addition of panel modules unlimited Application of adaptive optics possible Robotic assembly feasible
Producibility	Nine facet geometries Identical latches and hinges Modular construction Simple tooling requirements Low parts count Facet materials and manufacturing independent from panel
Receiver Compatibility	Individually adjustable mirrors for flux tailoring with receivers Compatible with current receiver designs

Table 6.1-5. Truss Hex Concentrator (Continued)

Summary of Concept Characteristics

Design Parameter	Parameter Description
Design Maturity	Advanced conceptual design with demonstrated technology 3-panel kinematic model demonstrated Facet demonstration underway Graphite/epoxy construction technology well developed
Development Risk	Optical characteristic determined early No significant technology drivers Low risk

6.2 Splined Radial Panel Concentrator

6.2.1 Concept Description - Splined Radial Panel

The Splined Radial Panel (SRP) solar concentrator is a self-deploying, light weight, small stowed volume structure. The concept, illustrated in Figure 6.2-1, is an extension and application of existing deployable antenna reflector technology.

The SRP design resulted from a Harris IR&D study. Several methods for creating an optically reflective parabolic concentrator using flexible membrane surface materials were conceived and evaluated. Materials such as aluminized polymers were considered most attractive because of their high reflectivity, light weight and very compact folded packages. However, most of the truly flexible (i.e., virtually no out of plane stiffness) surface materials considered were extremely difficult to package, deploy, and shape without incurring surface irregularities and a resulting decrease in optical performance. To overcome these difficulties, various tensioning and shaping schemes were considered along with increasingly heavy membrane films. As film weights increased, a foldable, semirigid composite surface became competitive with the films. In addition, the composite surface is less susceptible to damage and does not require a complex tensioning system. The SRP is the resulting deployable, solid reflector design.

The SRP concentrator consists of two major components; the semirigid reflective surface, and the Deployable Truss Structure (DTS). The reflective surface is composed of thin, low mass graphite/epoxy panels coated with a reflective film such as vapor deposited silver. The semirigid composite panels combine the optical properties of a glass mirror with the stowage capabilities of a flexible membrane-like material. The panels are drawn into a splined parabolic curve in the radial direction using a system of dimensionally stable,

SPLINED RADIAL PANEL CONCENTRATOR

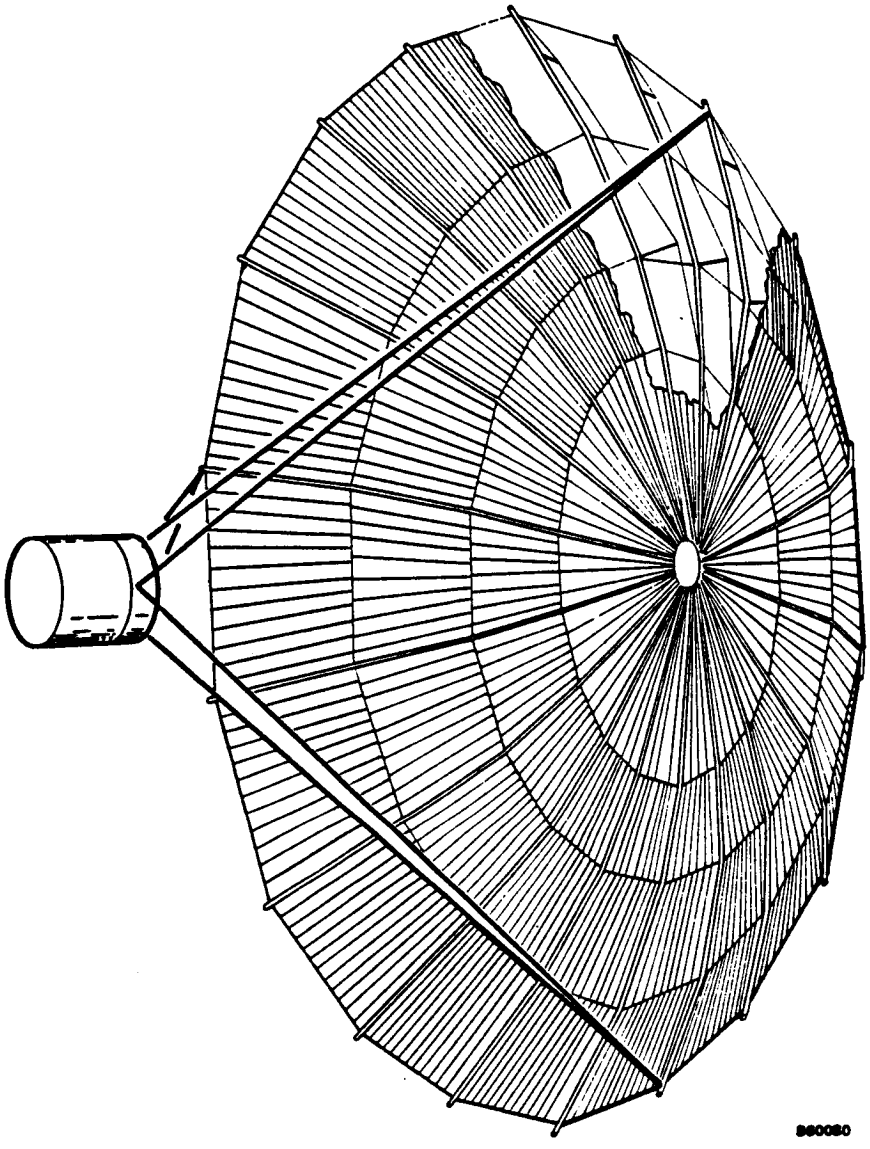

Figure 6.2-1. Splined Radial Panel Concentrator is Self-Deploying, Light Weight and Efficiently Packaged.

but flexible cords and ties similar to the cables and ties used on suspension bridges. A similar surface forming technique has been successfully employed on the deployable Single Access Antennas of the Tracking and Data Relay Satellite (TDRS). In the circumferential direction, the panels remain flat and approximate the paraboloid as a series of straight-line segments. Figure 6.2-2 illustrates how each panel acts as a simply supported beam in bending.

The flexible cords that shape the spline panels are attached between the truss rib members of the DTS which is the precision deployable structural frame supporting the concentrator. As seen in Figures 6.2-3 to 6.2-5, (photographs of a 4.6 m (15 feet) kinematic, antenna model), the unique design of the DTS enables extremely large structures to be folded to a fraction of their deployed size. Thin walled, graphite composite tubes are used as hinged ribs which are deployed to become the compressive truss members. Tension members of the truss ribs are constructed from lightweight graphite tapes or cords. When fully deployed, the structure becomes a system of radial trusses whose depth and size can be varied to meet the needs of a particular application. The structure and surface is completely self deploying by means of a single drive motor and mechanism located in the cylindrical hub. No EVA time is required for deployment, although attachment of the receiver support struts to the tips of the truss is most easily done by EVA. A more complete treatment of the DTS deployment sequence is given in Appendix A.

Like the Truss Hex discussed earlier, the SRP is sized for a 25 kWe CBC system. However, a slightly lower intercept factor (95 percent) and lower surface reflectance (90 percent) were used in a more conservative conceptual design. The resulting projected area is approximately 168 M^2 (1800 ft^2) with a corresponding diameter of 14.6 m (48 feet).

6.2.2 Conceptual Design Details - Splined Radial Panel

The SRP surface design is based on the geometry of the DTS. Top and side views of the reflector in Figures 6.2-6 and 6.2-7 show the spline radial panel surface attached to the DTS rib tubes. The deployable structure consists of 18 radial rib trusses. The main structural rib tubes have four segments joined by three hinges. The two rib tubes closest to the hub are each 10.2 cm (4 inches) in diameter, while the outer segments are reduced to 7.6 cm (3 inches) in diameter. The tubes are GFRP composite with wall thicknesses of 0.5 mm (0.018 inch) and 0.3 mm (0.014 inch), respectively.

The reflective surface is divided circumferentially into 18 gore sections corresponding to the 18 radial ribs. The surface is divided radially into four concentric rings which correspond to the four segments of the rib. This division allows the surface to fold with the ribs for stowed packaging. The maximum allowable width of a spline panel is determined by the optical geometry of the solar image, surface distortion, and desired intercept factor in the receiver aperture (at the focal plane). The allowable panel width is further reduced to next lowest integer number of spline panels which divides the gore width. Other reductions in width are made to accommodate the folding

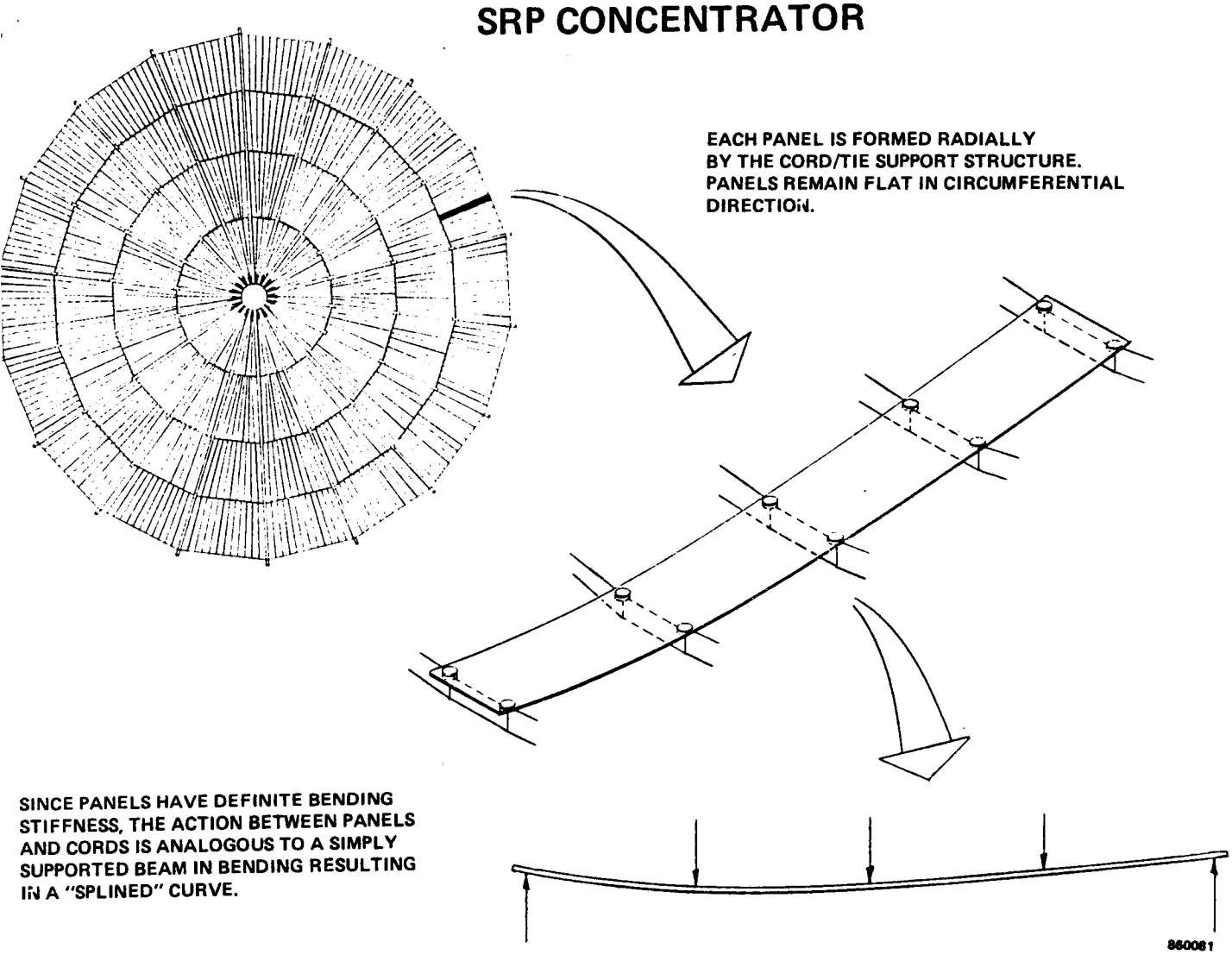

Figure 6.2-2. Spline Panels are put in Bending to Approximate Parabolic Contour.

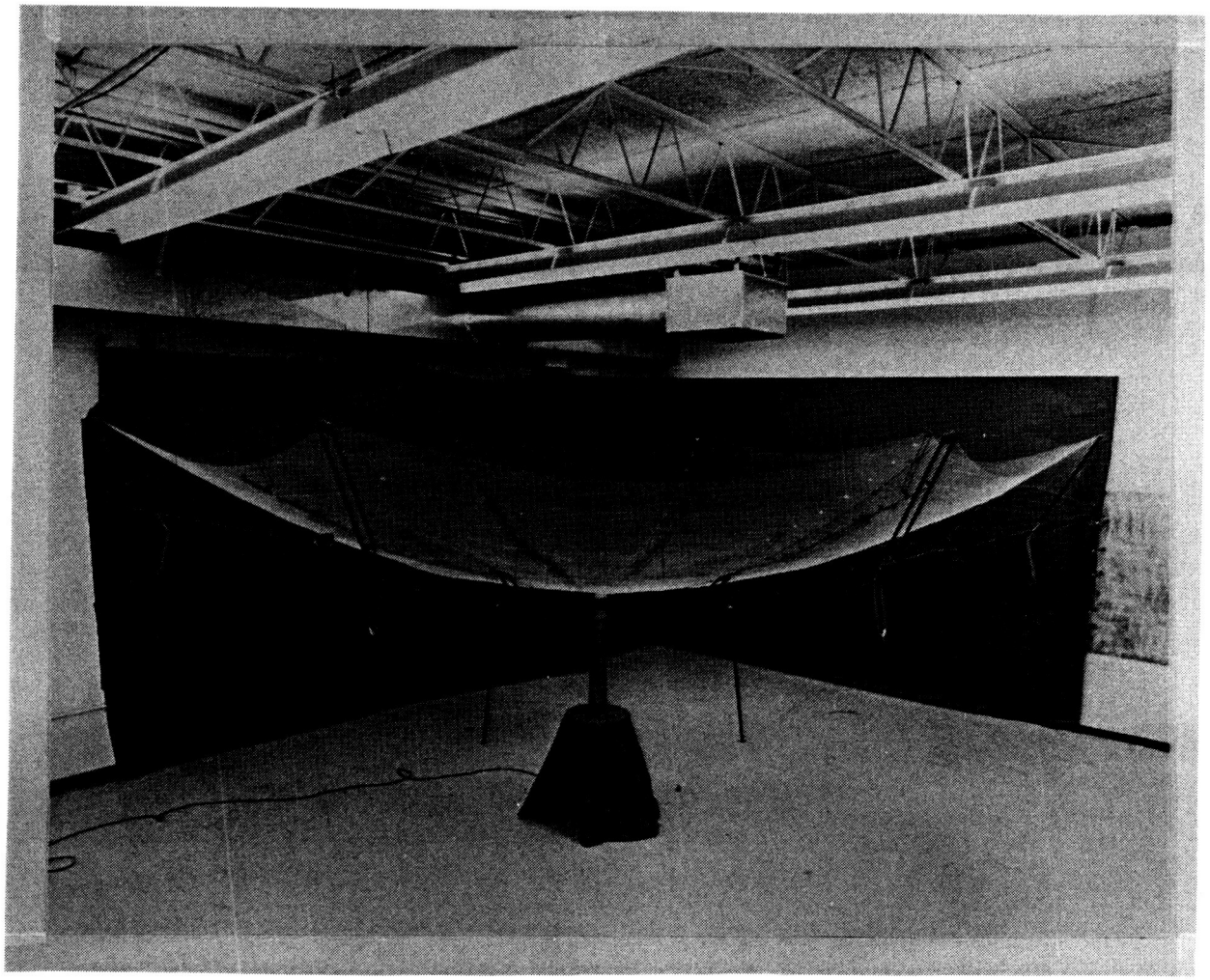

Figure 6.2-3. DTS Kinematic Model, Deployed, Demonstrates High Deployed Stiffness and Surface Accuracy Achievable Using the DTS.

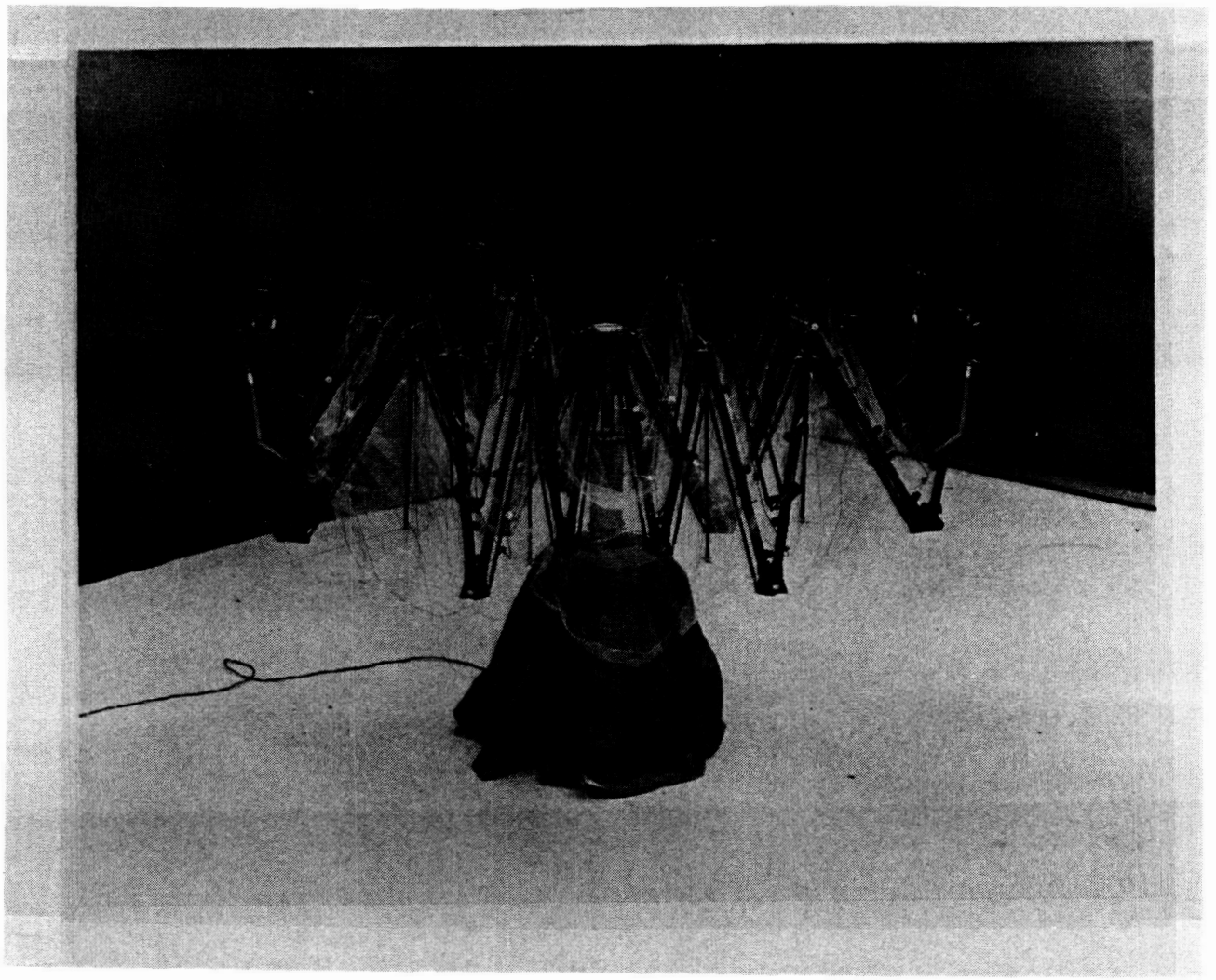

Figure 6.2-4. DTS Kinematic Model, During Deployment, Verified Kinematics of DTS Design.

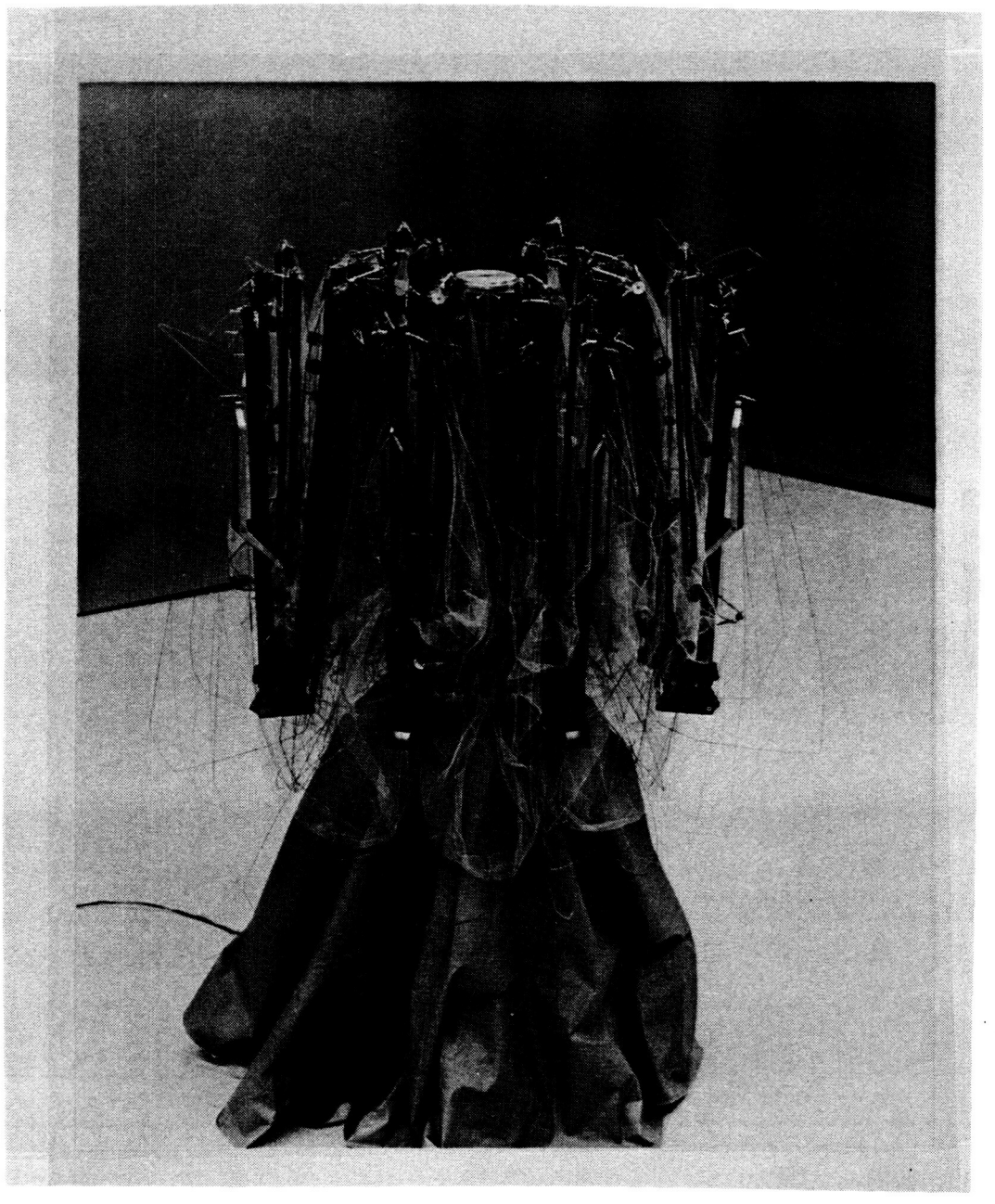

Figure 6.2-5. DTS Kinematic Model, Stowed, Illustrates Very Efficient Packaging Available.

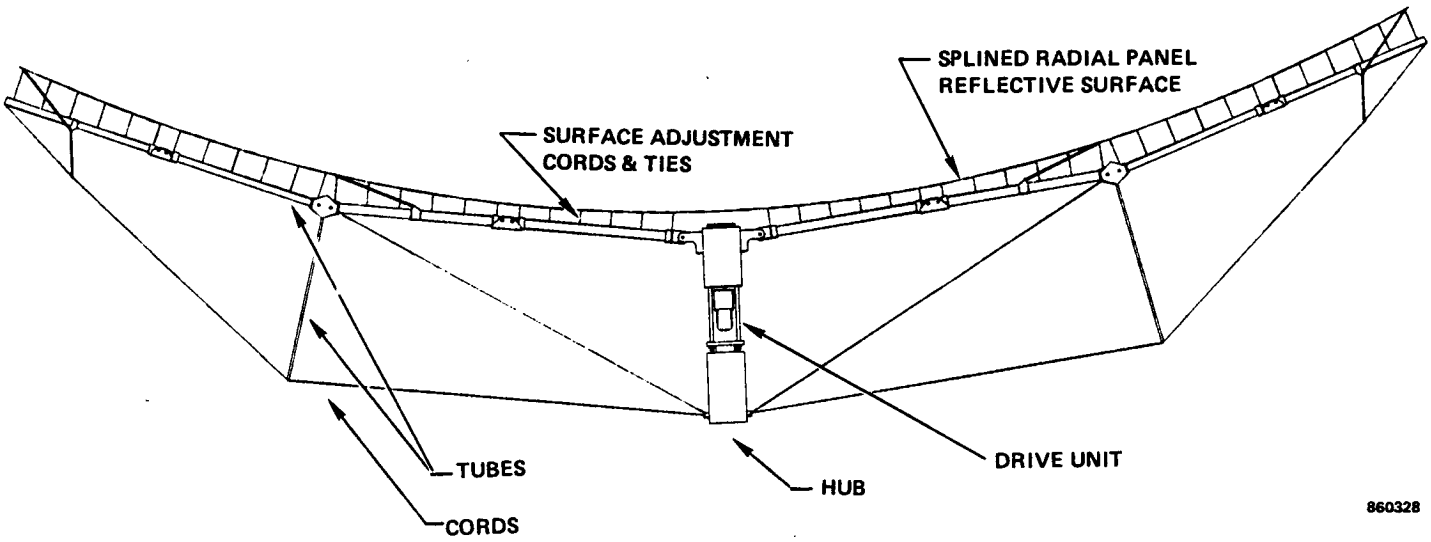

Figure 6.2-6. SRP Surface is Attached to the DTS Support Tubes With Adjustable Catenaries Made of Cords and Ties. Deep Section of DTS (Cross Section Shown) Results in Very Stiff but Light Weight Structure.

SRP CONCENTRATOR
TOP VIEW - DEPLOYED

DIAMETER = 15 m (49 FT)

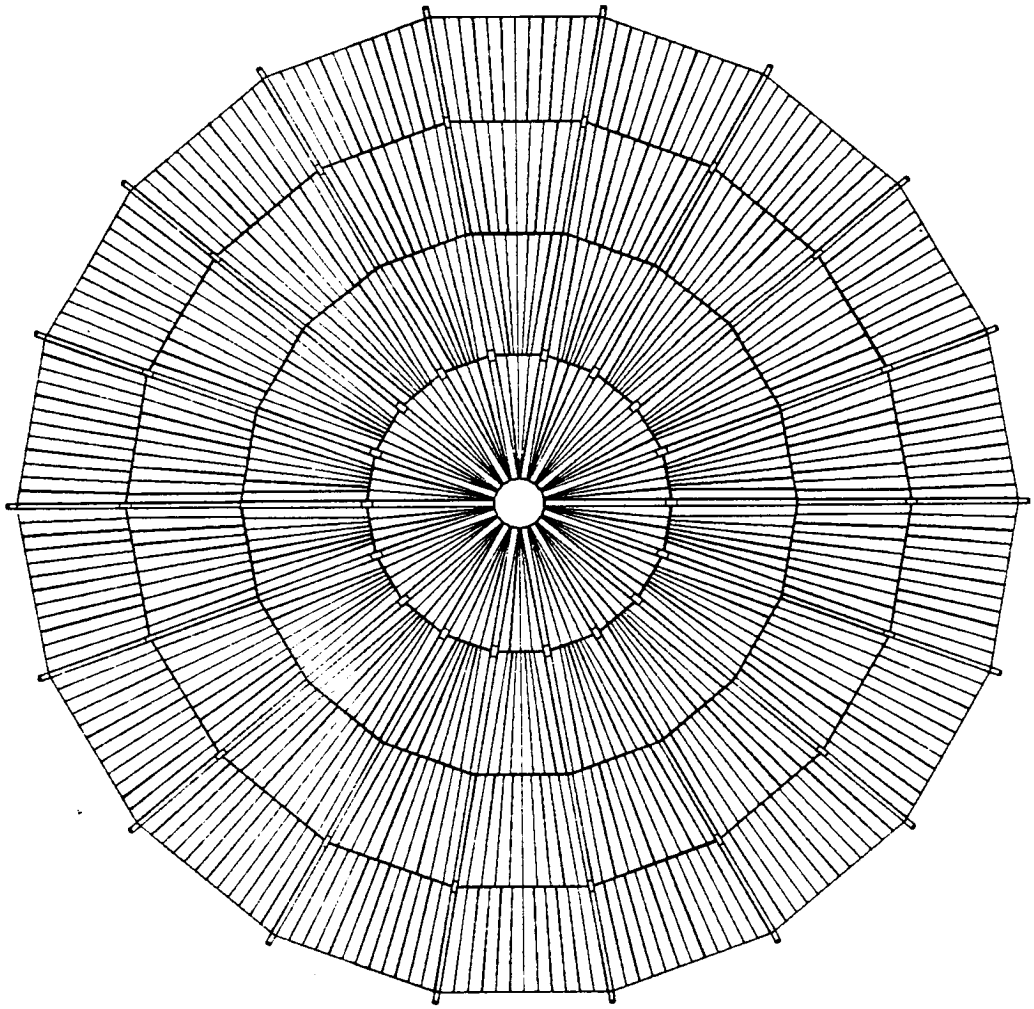

REFLECTIVE SURFACE IS COMPOSED OF
612 MEMBRANE-THIN, RADIAL PANELS

860082

Figure 6.2-7. SRP Reflective Surface Approximates Parabolic Contour by Thin Radial Panels Bent into the Correct Shape.

geometry. Detailed ray tracing analysis is used to verify the final design (see Paragraph 6.2.3). The conceptual design for the 15 m concentrator supporting a CBC system has 12, 10, 8, and 4 panels per ring per gore, respectively, from the rim of the collector to the vertex. The panels are approximately 1.8 m in length with an average width of about 16 cm. Panel-to-panel gaps of 1.25 cm on the ends and 0.65 cm side-to-side give sufficient clearance to fold the surface.

Each panel is attached and shaped at five or six discreet points along both long edges as shown in Figure 6.2-8. Special fasteners hold the spline panels to the cords. As seen in FIgure 6.2-9, the fasteners consist of two parts which are threaded for mating. The lower piece joins the front structural cord with the tensioning drop tie and provides a base for the panel attachment. A circular lip on the top side of the lower piece passes through the panel. The lip is dimensioned to be slightly thicker than the panel so that, when tightened, the upper fastener contacts this surface first, preventing the panel from becoming clamped by the fastener. Mounting holes in the panel are slotted so that small thermally induced changes in length can occur without distorting the reflective surface.

A model was constructed to demonstrate the surface attachment concept (refer to Figure 6.2-10). The GFRP panels are suspended and shaped by cord trusses in the box frame. The panels were not fabricated with optical surfaces and the reflective coating is only an aluminized Kapton tape, but the reflection of the upper corner of the room is clear in the photograph.

The fastener design permits the entire DTS to be assembled and adjusted before the reflective panels are attached. In addition, panels can be removed and replaced on an individual basis, although this would not be feasible on-orbit. Small surface height adjustments can be made by adding or removing shims between the fasteners.

GFRP composite was selected as the best material choice for the spline panels based on stiffness, weight, and coefficient of thermal expansion (CTE). The baseline conceptual design is two layers of bidirectional graphite cloth with a compatible resin system, resulting in properties as described in Table 6.2-1. The front, reflective, side of the layup is made resin-rich resulting in a smooth specular substrate. A silver reflective coating is vapor deposited and covered by a protective coat of magnesium fluoride. The total thickness of the complete panel is about 0.3 mm (0.012 inch).

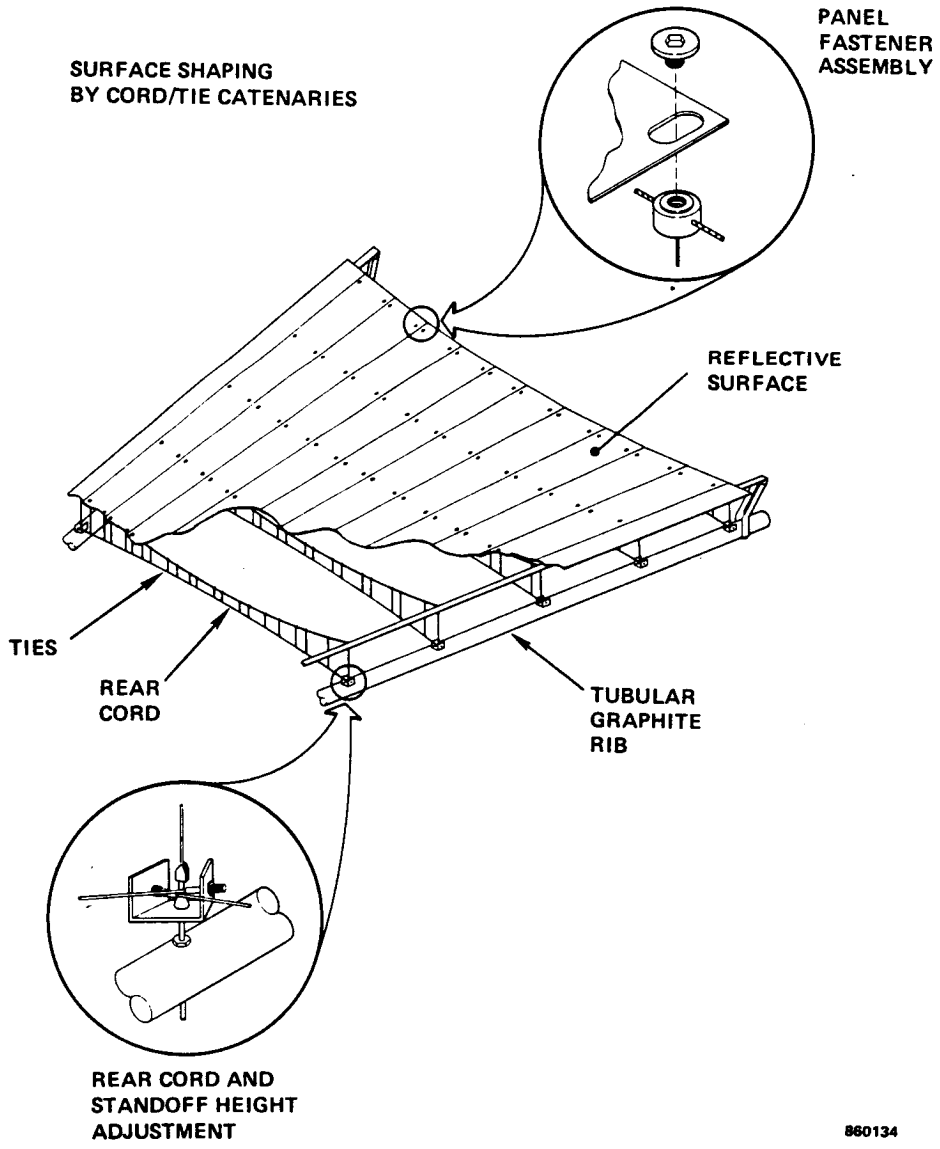

Figure 6.2-8. Radial Panels are Shaped by DTS Catenary Cord and Ties System.

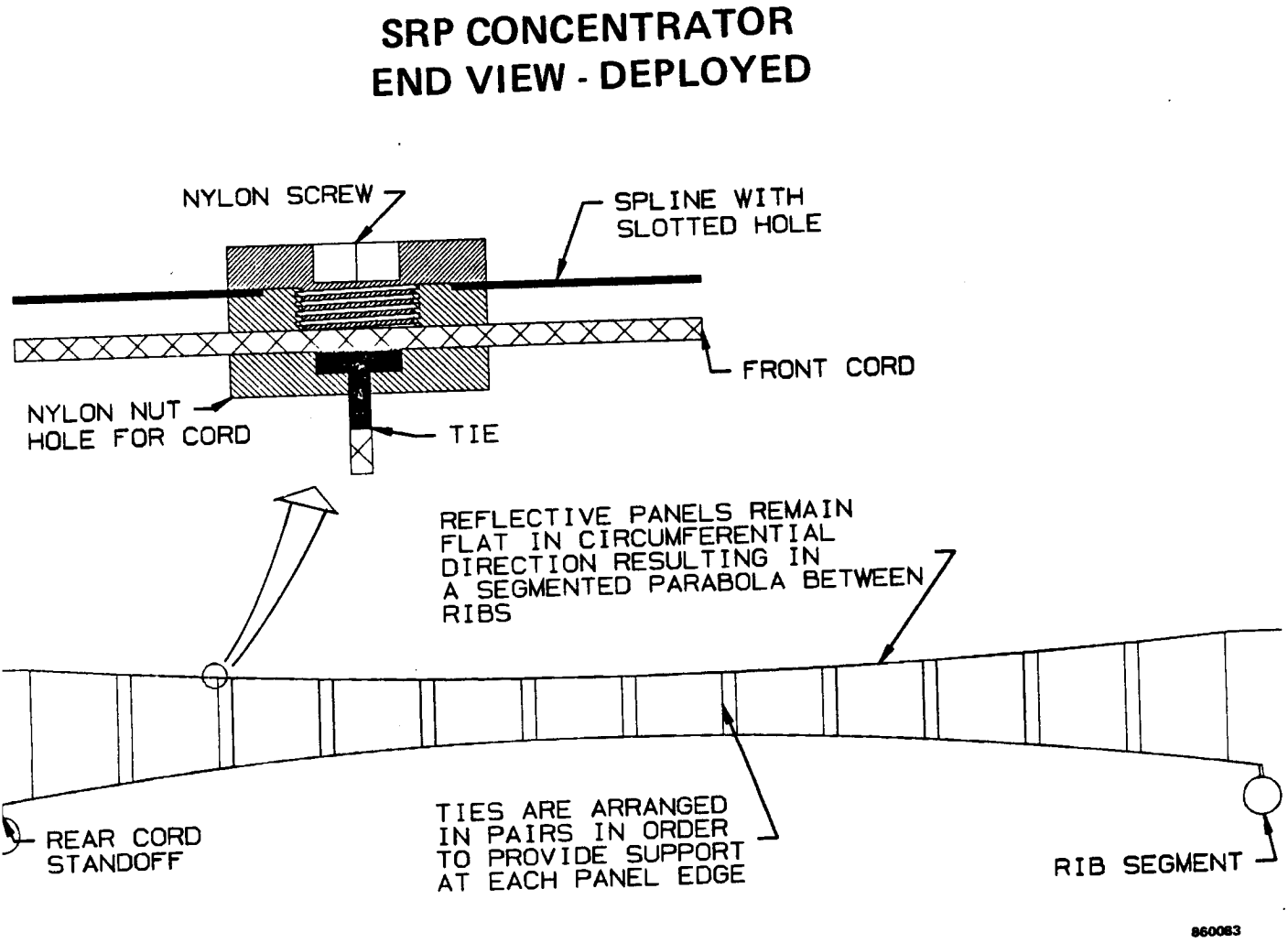

Figure 6.2-9. Panel Attachment Design Provides for Panel Movement During Temperature Excursions Preventing Surface From Inducing Thermal Stresses into DTS.

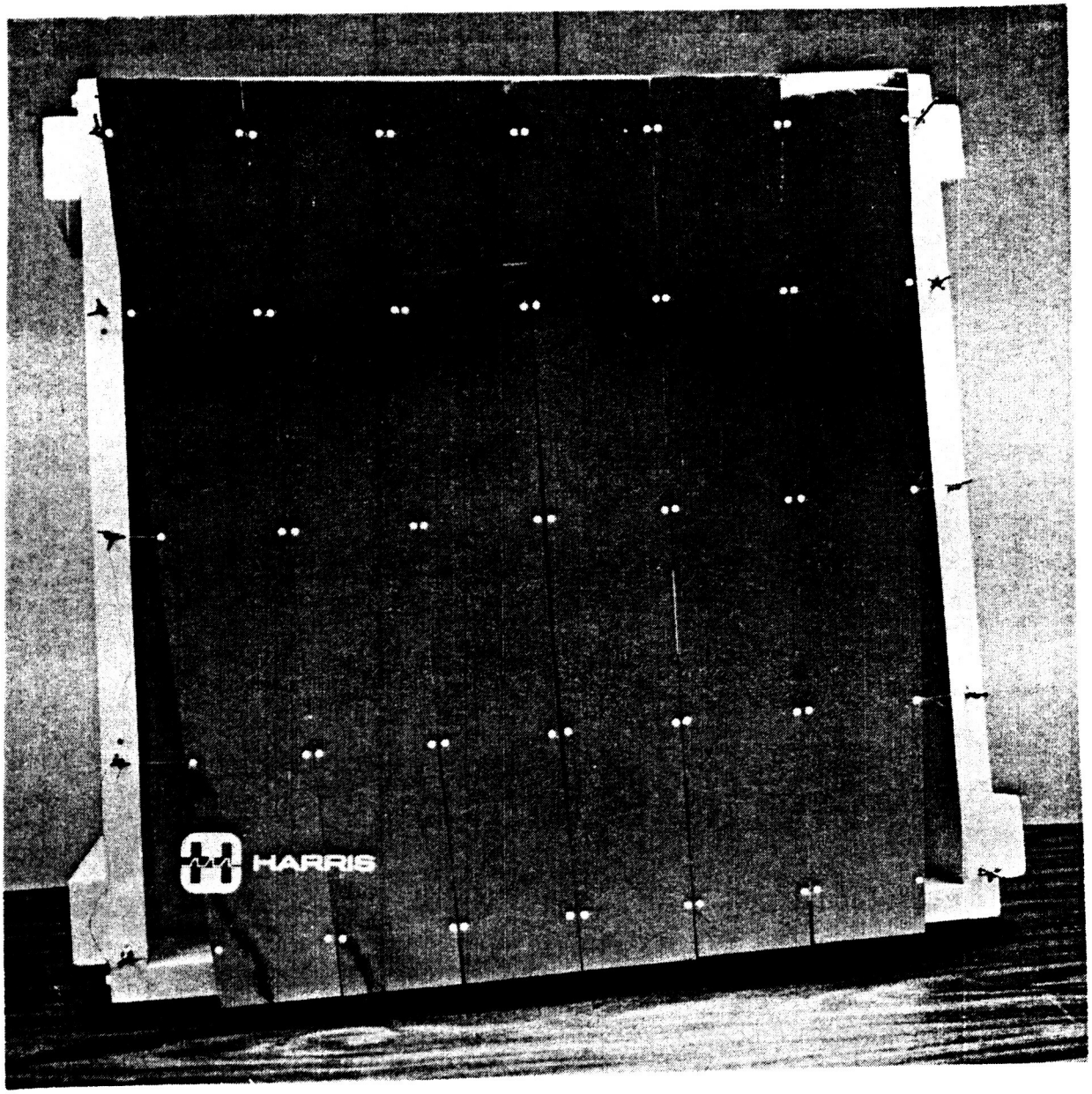

Figure 6.2-10. SRP Surface Attachment Concept was Demonstrated by a Gore Segment Model.

Table 6.2-1. Typical Properties for GFRP Panels

Mechanical - Thermal		
Density		1.4 g/cm^3 (0.05 lb/in^3)
Flexural Modulus		5.52 x 10^{10} N/m^2 (8 x 10^6 psi)
CTE		4 x 10^{-6}/° C (2.2 x 10^{-6}/° F)
No. Graphite Layers	**Thickness**	**Area Factor**
1	0.18 mm (7 mil)	39.7 cm^2/g (2,800 in^2/lb)
2	0.30 mm (12 mil)	23.8 cm^2/g (1600 in^2/lb)
Optical		
Specular Reflectivity	93 percent	
(1000 Å MgF_2 on 3000 Å Ag)		

Some alternate panel designs were considered to reduce surface mass without significant reduction to in-plane stiffness. Surface weight is important not only because of launch weight and system inertia, but because manufacturing processes are complicated by the gravity distortion of the surface. One possible design solution is shown in Figure 6.2-11. In this concept, the panel is reduced to a single thickness of graphite except at the edges where a double layer is needed to maintain stiffness and provide an adequate attachment. A reduction in surface mass of 30 percent is estimated using this approach. Other approaches and additional weight reductions are believed possible.

As a result of modifications incorporated to optimize stowed volume, the panel edges are not perfectly radial and each panel is unique. However, there is symmetry about the centerline of each gore and all gores are identical (for a centerfed concentrator configuration) so that a total of 17 different flat panel geometries are needed.

One of the strongest design features of the SRP concept is its extremely efficient stowed package. Figures 6.2-12, 6.2-13, and 6.2-14 show several views of the 15 meter SRP concentrator packaged for launch. The DTS ribs are folded at the hinges and stow parallel to the hub. Latch/release mechanisms (not shown) at the top and bottom restrain the ribs and surface during launch. When the surface cords and panels are no longer in tension, the panels assume their natural planar geometry and are folded accordian-style between the respective ribs. The enlarged top view of a single gore section shown in Figure 6.2-15 illustrates how compressive stowage restraints attached to each rib segment hold the panels in place. Soft compressible "snubbers"

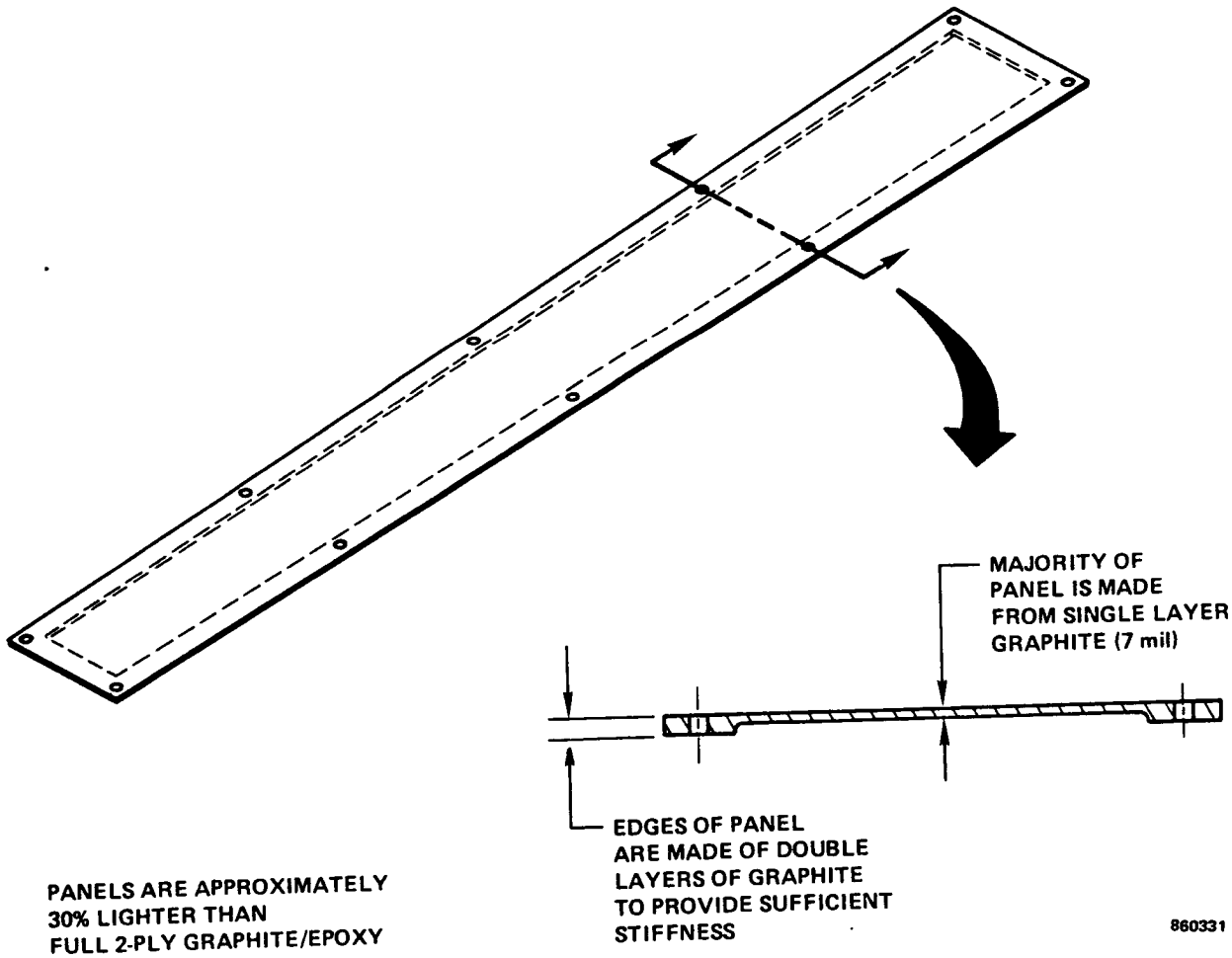

Figure 6.2-11. Candidate Reduced Weight Spline Panel Features Reduced Thickness and Reinforced Edges.

between adjoining panels limit the relative motion of the reflective surfaces and prevent damage to the reflective surface during launch. The packaged 15 meter reflector has a diameter of 2.11 m (83 inches) and a length of 2.2 m (87 inches) for a stowed volume of 7.7 m^3 (272 ft^3). Four, 15 meter deployed diameter SRP reflectors occupy less than 1/3 of the available Shuttle cargo bay as shown in Figure 6.2-16.

One of the unique and useful characteristics of the DTS is the ability to vary stowed dimensions as needed. For instance, by adding additional hinges and rib segments the packaged length may be reduced with a corresponding increase in diameter. In this way, the package may be tailored to meet varying envelope and payload integration constraints.

The SRP concept utilizes demonstrated technologies and manufacturing techniques, except for the demonstration of shaping and control of the solid surface which is an extension of antenna technology. Table 6.2-2 lists the quantities of major components for the 15 meter SRP concentrator.

Table 6.2-2. SRP Concentrator Major Component Quantities

Part Name	Quantity
Reflective panels - 17 different geometries at 36 each	612
Rib sections - 4 geometries at 18 each	72
Locking rib joint	36
Nonlocking rib joint	18
Reflective rib covers - 2 geometries at 36 each	72
Front cord standoff assembly - outer	18
Front cord standoff assembly - inner	18
Rear cord standoff assembly	432
Rib struts	18
Reflective panel fasteners	7776
Deployment drive unit	1
Cord/tie assemblies	432

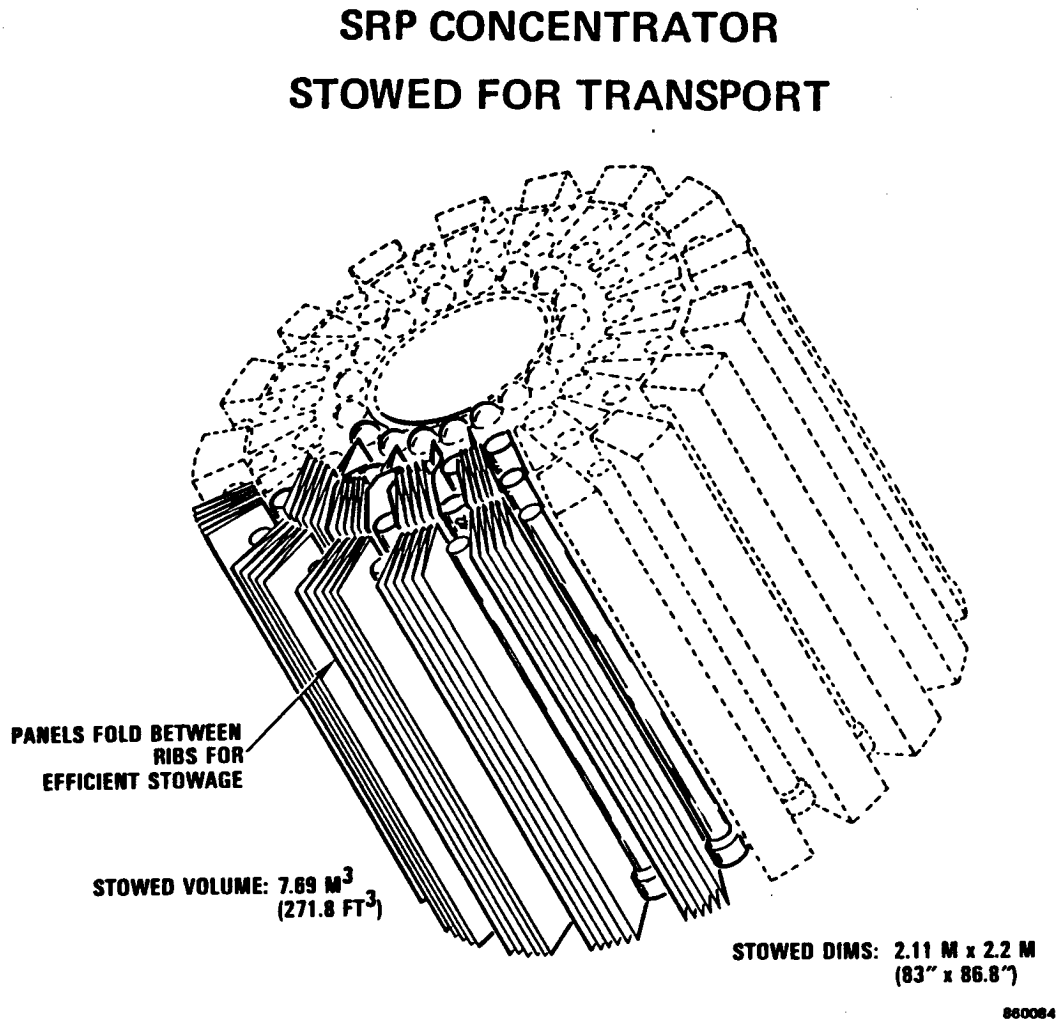

Figure 6.2-12. SRP Concentrator Strongest Design Feature is Extremely Efficient Stowed Package.

SRP SOLAR CONCENTRATOR TOP VIEW - STOWED

DIAMETER = 2.1m (83in)

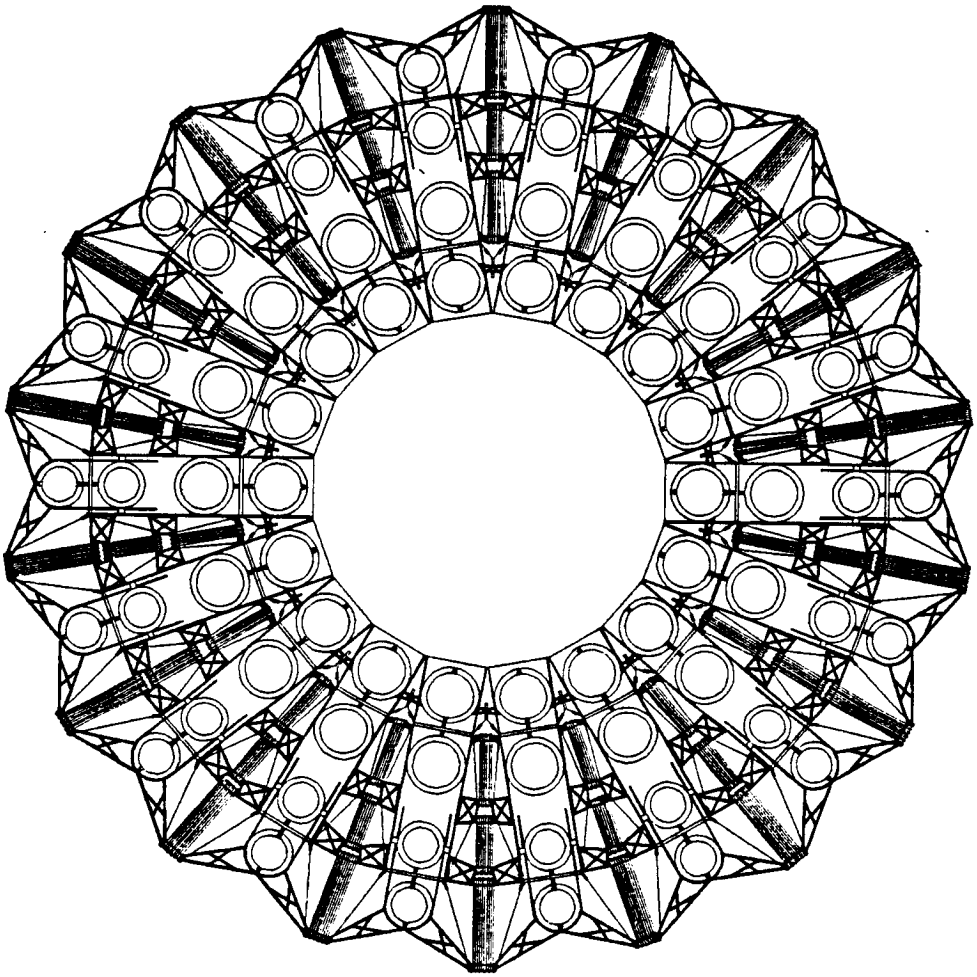

STOWED DIAMETER IS 14% OF DEPLOYED DIAMETER

RELATIVELY SIMPLE SYSTEM OF FOLDING RIBS AND PANELS PROVIDE AN EFFICIENT ORDERLY STOWED PACKAGE

860087

Figure 6.2-13. Flat Radial Panels Enable SRP Surface to Fold Accordian Style Between Stowed DTS Rib Segments.

SRP CONCENTRATOR CROSS SECTION - STOWED

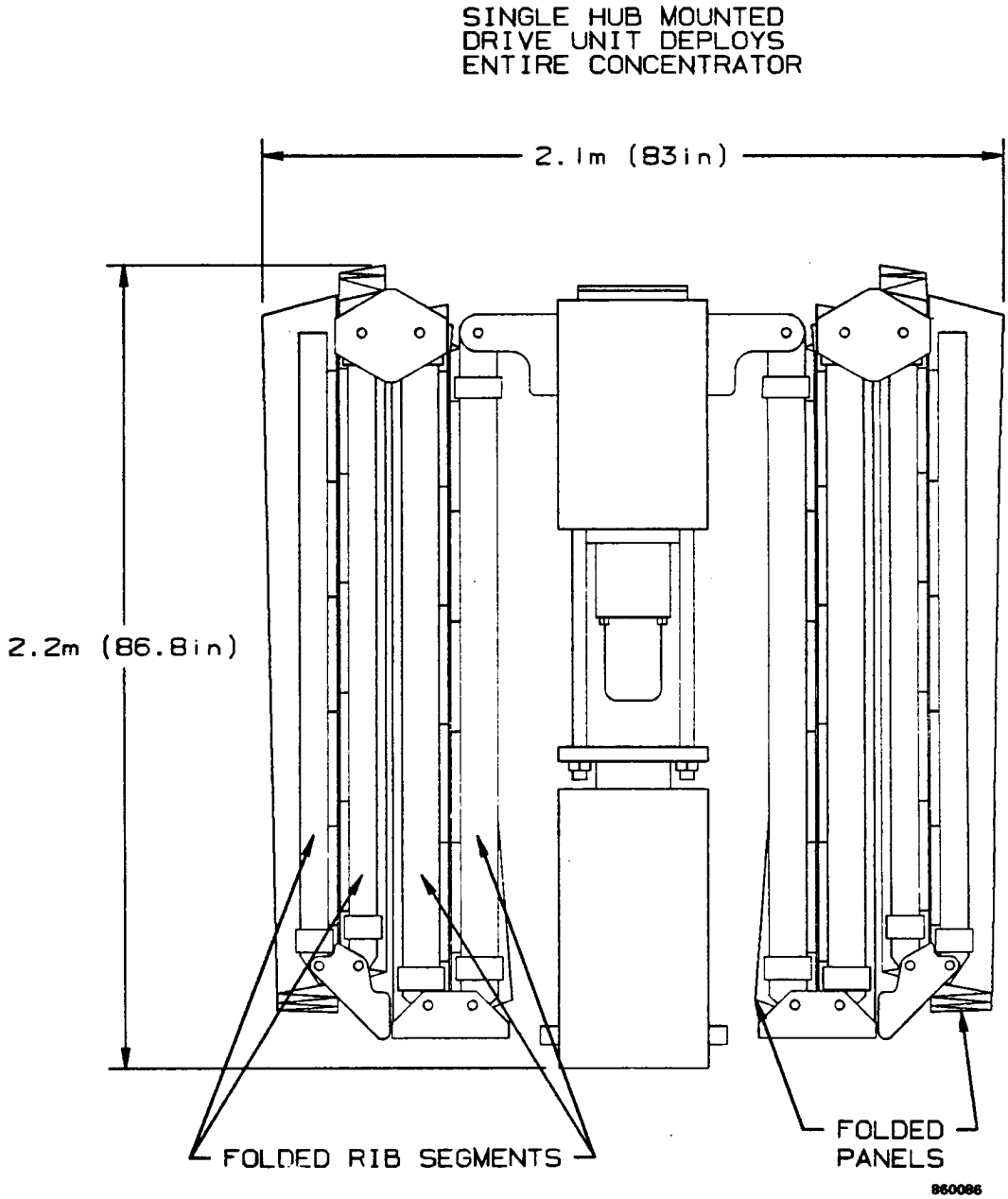

Figure 6.2-14. Stowed SRP Cross Section Illustrates Efficient use of Stowed Volume.

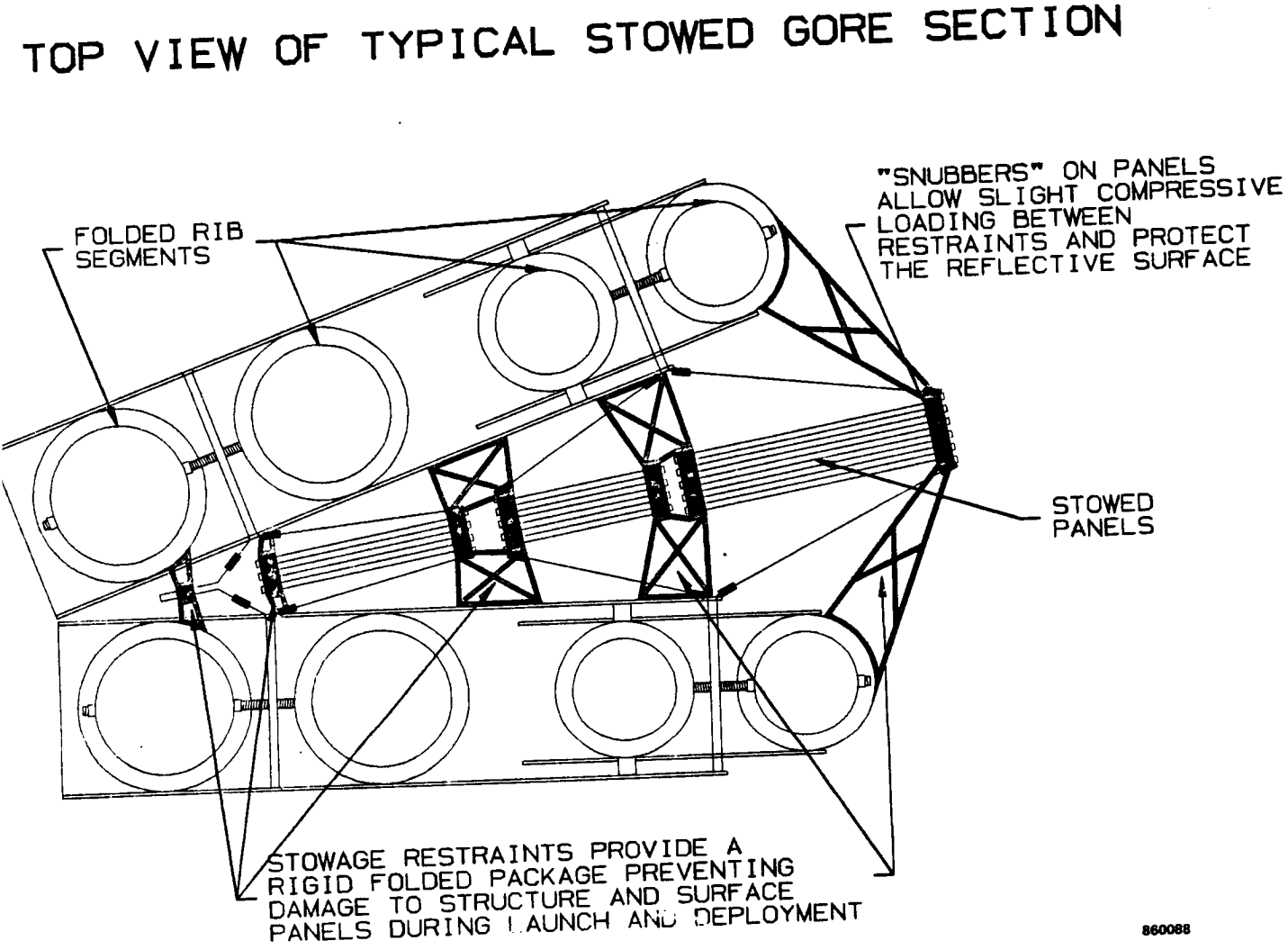

Figure 6.2-15. Compressive Stowed Restraints Hold Panels in Place During Launch.

SIZE OF STOWED SRP CONCENTRATORS RELATIVE TO SHUTTLE CARGO BAY

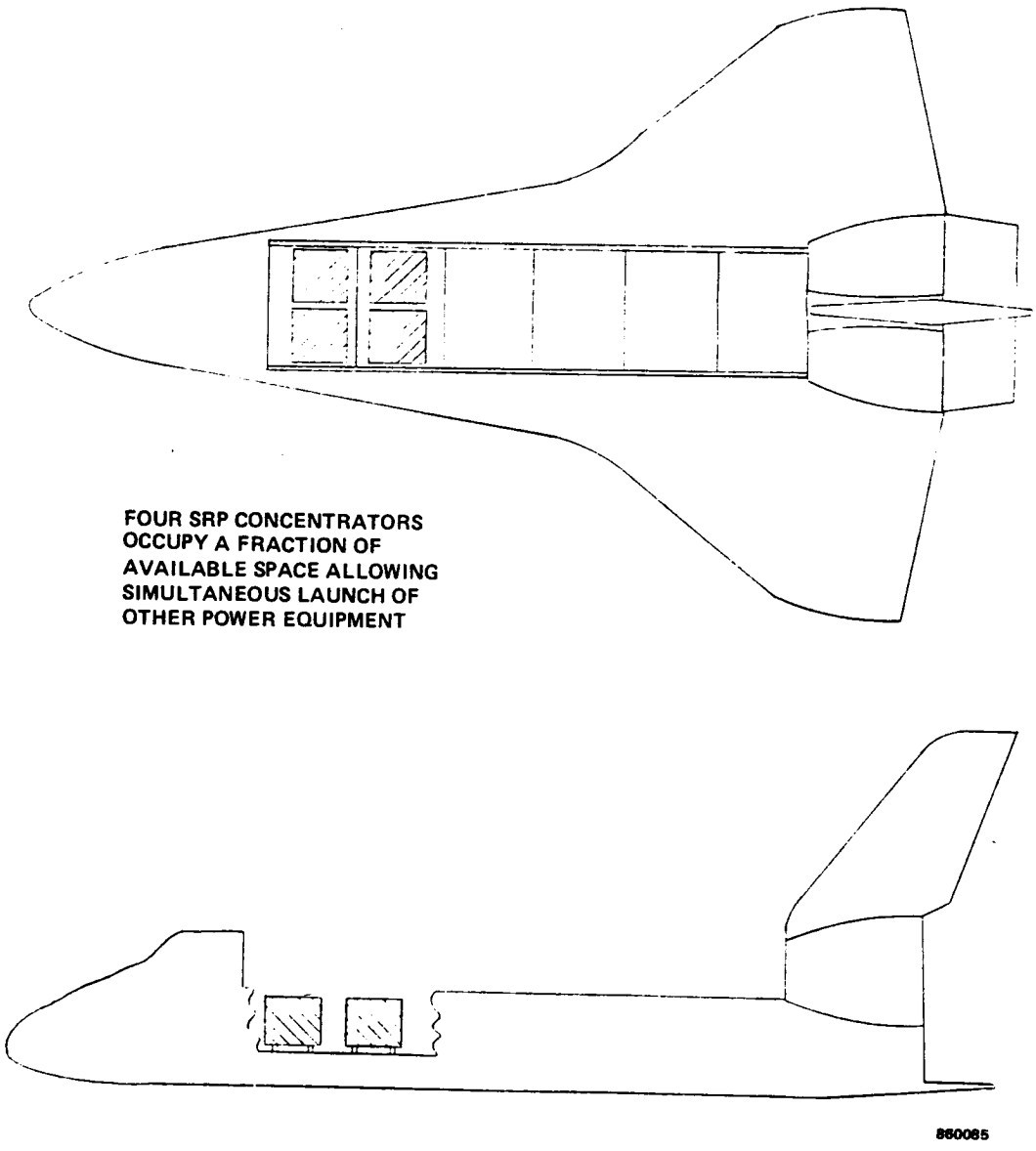

Figure 6.2-16. Two SRP Concentrators can be Packaged in Same Shuttle Bay Volume as one Truss Hex Concentrator.

The efficient structure of the DTS also results in a low mass solar concentrator. Table 6.2-3 gives a breakdown of the estimated mass of concentrator components. The 230 kg total is a conservative estimate falling well within the goals of the study.

Table 6.2-3. Mass of SRP Concentrator Components

Component(s)	Mass kg (lb)
Reflective surface - includes cords and fittings	77 (170)
Ribs - includes joints and standoffs	62 (137)
Vertical struts	14 (30)
Tapes	2 (5)
Hub	16 (35)
Mechanical drive	20 (44)
Structural and panel restraints	23 (50)
Electrical cables	2 (5)
Thermal blankets	14 (30)
Estimated Total	230 (506)

6.2.3 Analysis Results - Splined Radial Panel

The optical performance of the SRP concept was predicted by GTRI. The same ray tracing program used to predict the Truss Hex concentrator performance was used for the SRP concentrator. A symmetric, center fed, optical configuration with a f/D = 0.5 and a 14.6 m diameter was modeled. The optical model of the concept considered each panel to be flat in the circumferential direction and perfectly parabolic in the radial direction. Rays were traced from 33 points on each panel. The Boeing receiver geometries given in Table 6.1-2 were used in the analysis.

The optical model accurately represents a SRP concentrator, without manufacturing errors, in the circumferential direction but only closely approximates the concept in the radial direction. The spline beam bending design approach approximates the paraboloid in the radial direction but the optical model assumes a perfect radial paraboloidal contour. A finite element model of a single typical spline panel was used to determine the amount of error introduced by this approximation. The results show that approximately 2.1 milliradians of slope error, one sigma value, ensue. Surface shaping assembly manufacturing tolerances are a source of systematic slope error. Tie lengths can be controlled to 0.04 cm rms. If a typical panel is 16 cm width and has a 45 cm spacing between tie locations, the resulting one sigma systematic circumferential and radial slope errors are 2.5 and 0.9 milliradians, respectively. The resulting rms manufacturing slope error is 3.26 and 0.9 milliradians in the radial and circumferential directions.

Similarly to the Truss Hex optical analysis, the one sigma slope error and reflectivity are the ray tracking program input parameters. The input parameters used in the SRP optical analysis were:

- 3 milliradian one sigma slope error
- 0.9 reflectivity
- 1.310 solar constant kW/m^2

Note that the 3 milliradian, radial and circumferential, slope error used in the analysis compares well with the manufacturing tolerances identified previously.

The rays are traced from the solar source to the receiver aperture and cavity grid areas. Aperture and cavity side wall flux contour plots are given in Figures 6.2-17 and 6.2-18 for the ORC receiver. The analysis was not performed for the CBC receiver geometry. The results of the analysis are given below.

Intercept Factor	0.996
Flux delivered to Receiver	211 kWth
Side Wall Illumination	0.79
$\frac{\text{Side Wall Flux}}{\text{Total Available Flux}}$	

The structural capability of a DTS with an RF surface has been characterized. The deployed stiffness is primarily dependent on the DTS truss depth, i.e., strut length and number of ribs. Rib tube cross section, number of hinges per rib, hub cross section, and mass also influence DTS deployed stiffness. Depending on design configuration, the DTS is capable of achieving fundamental deployed frequencies ranging from 3.0 to 5.0 Hz.

The Spline Radial Panel concentrator surface is approximately five times heavier than a typical RF surface and represents a significant percentage of the total weight. Although no analysis has been performed to determine the deployed stiffness of the SRP concept, it is believed that a fundamental frequency greater than 1.0 Hz can be achieved.

6.2.4 Evaluation of Significant Parameters - Splined Radial Panel

The SRP concentrator has the lightest weight and smallest stowed package of all the concepts considered. These qualities coupled with its capability for fully automatic deployment qualify it as a strong candidate for a variety of space system applications.

The maintainability of this concept is not as promising as the Truss Hex because individual replacement of spline panels on-orbit is difficult at best. The panels can, however, be replaced in the controlled manufacturing environment. Material sample testing and analysis indicates that insignificant damage will occur to the optical surface as a result of exposure to micrometeoroids and debris. Some system performance degradation

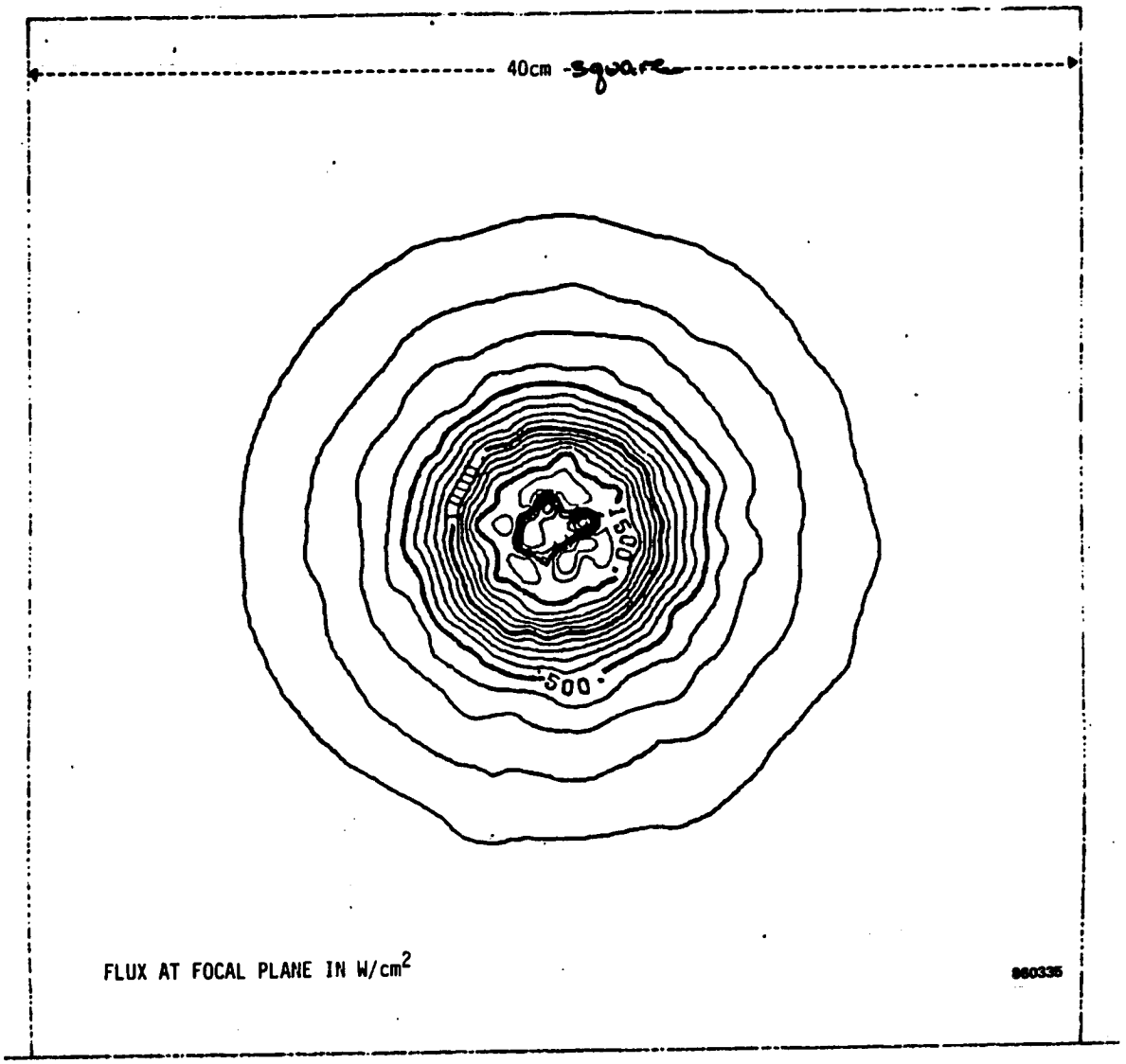

Figure 6.2-17. Aperture Flux Contour Plot for ORC Receiver

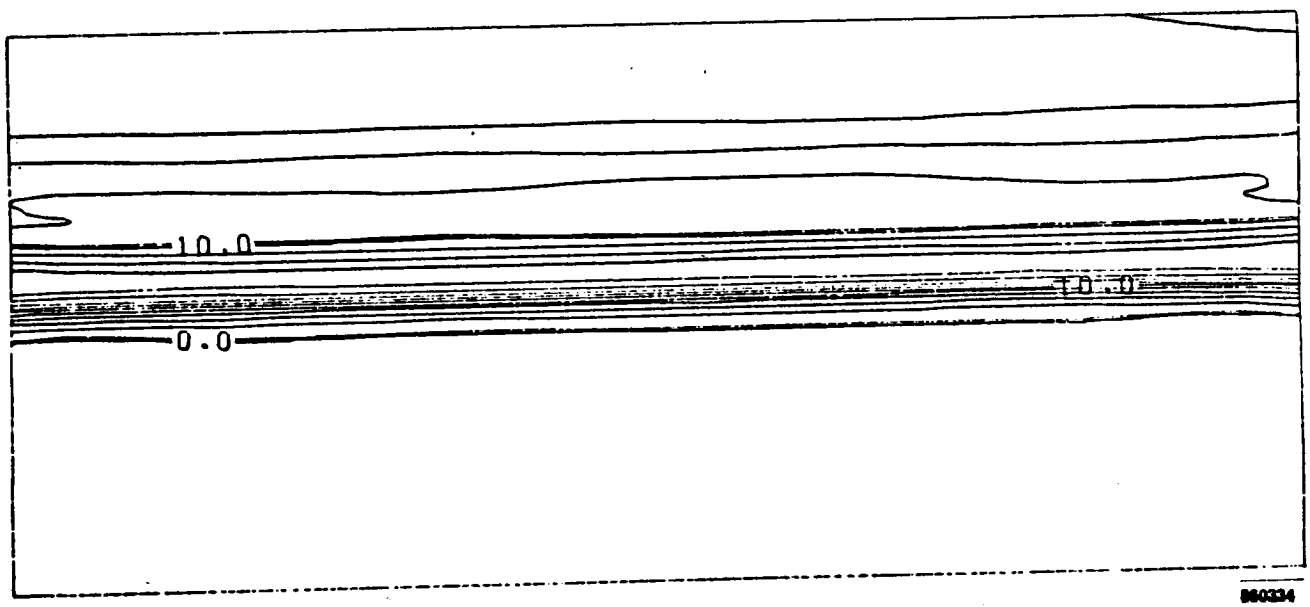

Figure 6.2-18. Cavity Side Wall Flux Contour Plot for ORC Receiver

would occur if a tension member of the DTS was damaged, but the probability of this occurring to the small cord cross section is quite low.

If the concentrator should become damaged or need repair it would need to be returned from orbit. The SRP concentrator can be restowed using the deployment drive mechanism. Although the structural members could be locked in place, the surface panels could not be locked up on-orbit. A containment vessel within the shuttle cargo bay would probably be required for return from orbit.

The SRP concept is more complex than the Truss Hex because of the high parts count associated with the DTS and surface fasteners. An offset concentrator is expected to have a larger number of unique surface panels. Reliability of the deployment drive mechanism has been demonstrated; however, deployment of the SRP surface with a DTS structure has not been demonstrated. Mesh antennas must be thoroughly evaluated to eliminate potential snags, and this application of antenna technology has an undetermined snag potential.

Because the surface weight is a high relative to that of deployable RF antennas, a traveling counterbalance may be required to offload the DTS during deployment. This involves more complex assembly and test tooling than is required for the other concepts. In addition, the surface weight may cause excessive deflection of the surface in 1-G and make optical performance verification difficult.

Table 6.2-4 summarizes the significant design parameters and features of the SRP solar concentrator.

Table 6.2-4. Splined Radial Panel Concentrator

Summary of Concept Characteristics

Design Parameter	Parameter Description		
Configuration	Center fed - supports CBC system Applicable to offset and ORC configuration		
Deployed Diameter	15 m (49 feet)		
Focal Length	7.5 m (25 feet)		
Stowed Package	Cylindrical: 2.1 m diameter x 2.2 m (83 inch x 87 inch) Volume: 7.7 m^3 (270 ft^3)		
Mass	Surface	77	(170)
	Support Structure	153	(337)
	Total	230	(507) lb
Deployed Stiffness	>1 Hz		

Table 6.2-4. Splined Radial Panel Concentrator (Continued)

Summary of Concept Characteristics (Continued)

Design Parameter	Parameter Description
Support Structure	18 rib, 4 segment DTS
Surface Design	612 thin, flat, GFRP, reflective panels 34 panels per gore 18 gores
Deployment	Automatic with redundant drive motor (15 - 30 min) Manual override through drive mechanism only EVA for attachment of receiver support struts
Maintainability	Replacement of splines on ground is possible Replacement of splines on orbit is difficult Insignificant degradation of surface from micrometeoroid/debris damage System degradation from damage to tensioned members - low probability Panel adjustment on orbit is not feasible
Restow and Disposal	Automatic restow of structure possible Surface restow and lockup not possible Requires containment vessel for return
Complexity	High parts count in DTS Repeated assembly - 18 ribs Offset configuration requires large number of unique splines
Reliability	Automatic deployment with single, central mechanism Deployment of surface has undetermined snag potential
Scalability/Growth	Modular growth not possible System design growth potential meets any projected Space Station requirement
Producibility	Flat, graphite/epoxy composite panels produced with conventional methods Structural assembly and surface integration techniques well developed More tooling required than Truss Hex

Table 6.2-4. Splined Radial Panel Concentrator (Continued)

Summary of Concept Characteristics (Continued)

Design Parameter	Parameter Description
Receiver Compatibility	Can be tailored by design Spline panels not easily adjustable after final surface set Compatible with current receiver designs
Design Maturity	Conceptual design with partial demonstration of technology DTS kinematic demonstration at Harris Needs demonstration of surface shaping and surface deployment control
Development Risk	Deployment of solid surface is different from mesh antenna experience Producibility of splines with requisite optical quality has not been demonstrated Optical measurement of complete assembly in 1-G may be difficult due to spline deflections

6.3 Domed Fresnel Lens Concentrator

6.3.1 Concept Description - Domed Fresnel

The Domed Fresnel lens concentrator system, depicted in Figure 6.3-1, is a deployable refractor assembly which concentrates incident solar radiation into a receiver cavity. The sun's rays pass through the transparent lens and are bent by prisms integral in the lens material. This optical configuration naturally locates the receiver, power conversion unit and radiator near the station gimbal axes. The refractor assembly is mounted to the receiver with a six strut tension/compression tripod assembly.

The lens concentrator combines Harris deployable precision space structure and antenna surface shaping technologies with ENTECH's patented Fresnel optics. The Harris Deployable Truss Structure (DTS) supports the Fresnel lens surface. DTS was selected because it is light weight, has a compact folded volume, has high stiffness, and can easily be adapted to surfaces of various degrees of curvature.

The DTS deploys the refractor assembly using a single motor and a set of drive linkage. After the fully automatic deployment of the refractor assembly, the tripod assembly is attached to the receiver during an EVA.

DOMED FRESNEL CONCENTRATOR

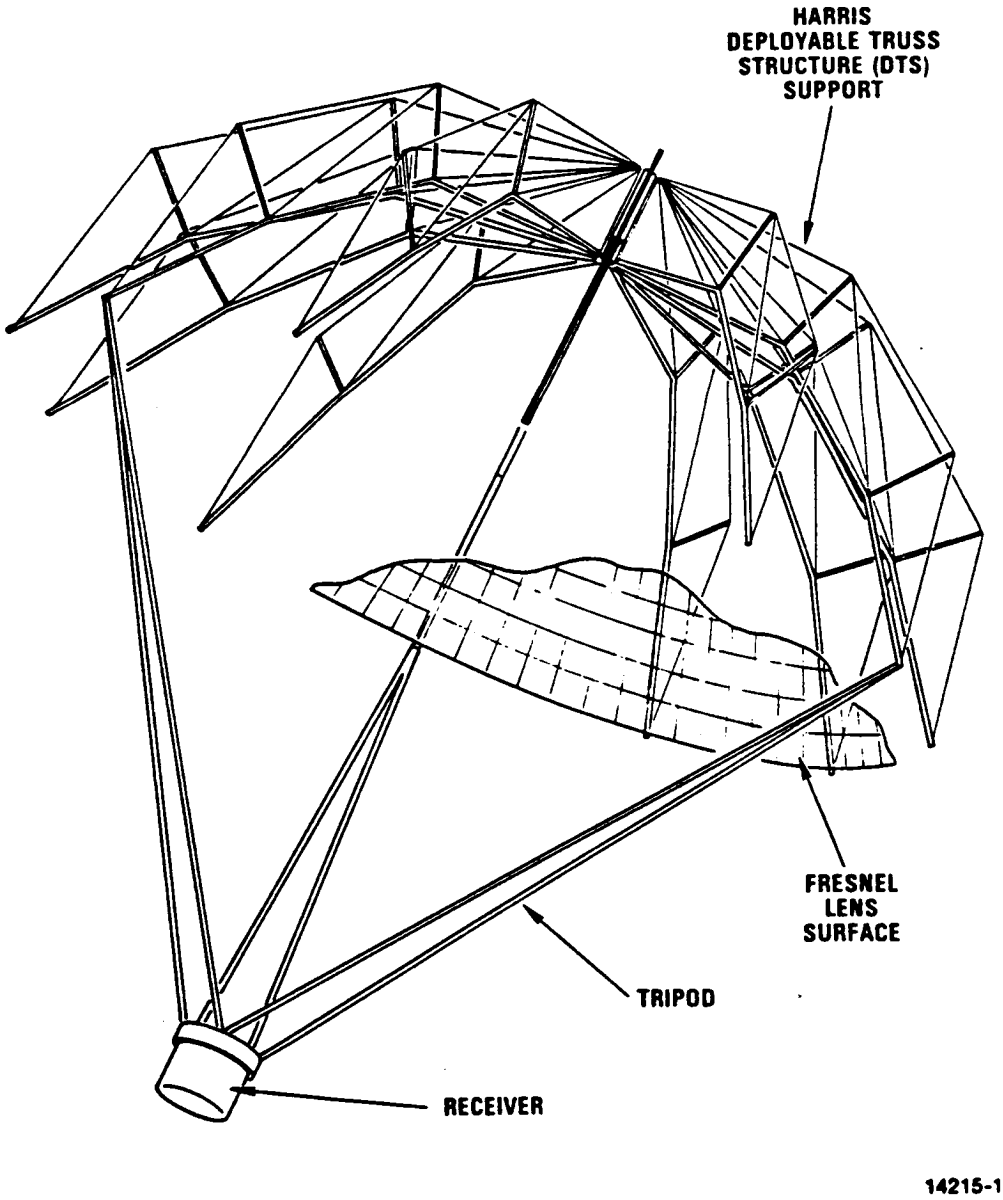

Figure 6.3-1. The Domed Fresnel Concentrator Combines Harris Deployable Precision Space Structure and ENTECH Fresnel Optic Technologies.

The concentrator's domed shaped surface is approximated by an assemblage of flat panels made from a transparent film that has been embossed with refractive prisms. The surface is shaped and supported using technology developed by Harris for use on the Tracking and Data Relay Satellite System's (TDRSS) deployable RF antennas. Since this concentrator concept is sufficiently different and a relatively new technology compared to the traditional parabolic concentrator approach, the following paragraphs have been included to provide a more detailed description of the Fresnel optics.

ENTECH's patented Fresnel lens is transmittance-optimized, error tolerant, and has a short focal length for minimizing the overall concentrator structure. As shown in detailed testing at ENTECH, Sandia National Laboratories, Solar Energy Research Institute, Desert Sunshine environmental testing in Phoenix, Arizona and in Department of Energy demonstration projects, this Fresnel lens concept has outstanding optical performance and unmatched tolerance for environmentally induced slope errors of the optical surface. Compared to a reflective parabolic concentrator, the domed lens can tolerate as much as 200 times the surface slope error with equal image defocusing. This exceptional tolerance to surface radial slope error has led to an advantageous reduction in the complexity of the domed lens surface support and shaping structures.

The high optical and thermal efficiency levels for the lens concentrator a result of the unusual optical design. As shown in Figure 6.3-2, each prism in the lens is configured such that the solar ray incidence angle at the front surface of the prism is equal to the solar ray incidence angle at the back surface of the prism. Prisms configured in this manner are operating in a minimum deviation condition. This minimum deviation prism condition minimizes reflection losses and thereby maximizes transmittance. When each prism is configured in this manner the entire lens offers maximal transmittance. As also shown in Figure 6.3-2, each prism is configured with the prism peaks and valleys. The lens manufacturing process results in sharp valleys, where the lens material is pressed into shape, and rounded peaks, where the lens material must flow into shape. The blunt tips are removed from the optical path and thus no light is lost due to blunt prism tips. In addition to maximal transmittance, the domed lens offers other important optical advantages over conventional Fresnel lens designs including; a smaller solar image, a higher tolerance for prism angle errors due to imperfect manufacture, and a higher tolerance for chromatic aberation (dispersion). Further information and the status of this technology is available in reference 4.

Preliminary sizing, optical analysis, and first order estimates for allowable mispointing and surface errors were provided by ENTECH. The results of this work, discussed fully in subsequent paragraphs, provided sufficient data to allow the selection of a baseline design depicted in Figure 6.3-3. Although the organic Rankine cycle (ORC) was selected as baseline, the domed Fresnel lens concept will support the closed Brayton cycle (CBC) by making appropriate changes in the geometry and optical surface prism specifications.

DOMED FRESNEL CONCENTRATOR SECTION OF LENS SURFACE

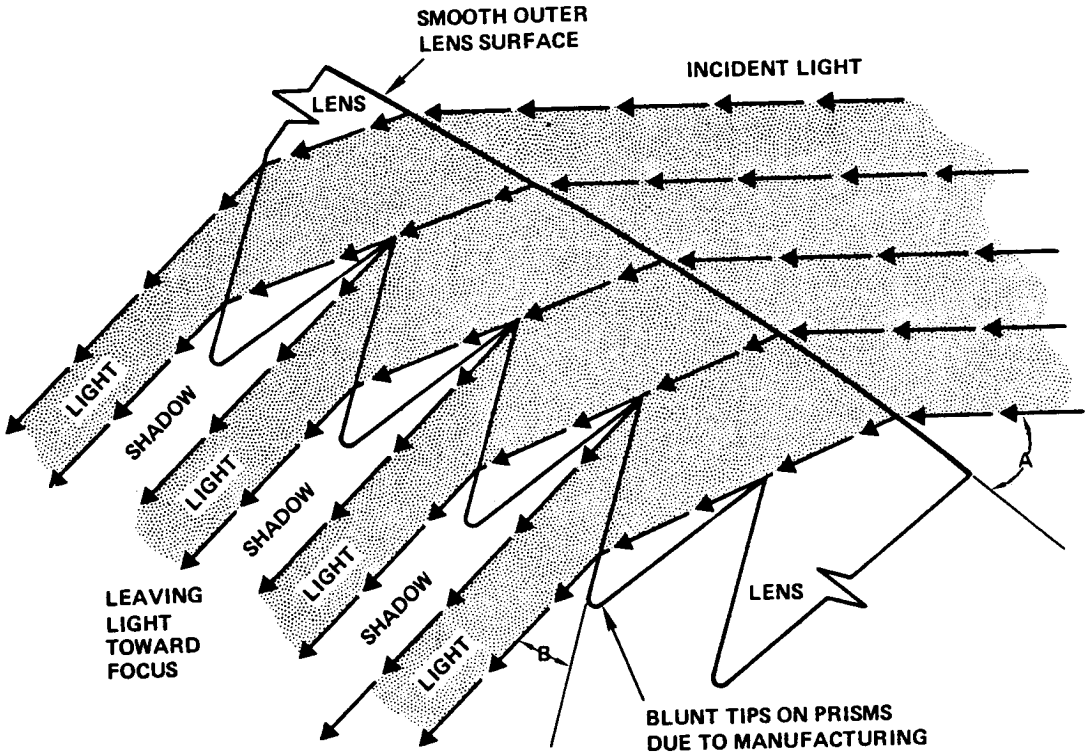

- ANGLE OF INCIDENCE OF INCOMING LIGHT (A) EQUALS ANGLE OF INCIDENCE OF OUTGOING LIGHT (B)
- GEOMETRY OF PRISMS DOES NOT RESULT IN BLOCKAGE
- U. S. PATENT 4069812, MARK O'NEILL, ENTECH, INC. (E-SYSTEMS), 24 JAN 1978

860064

Figure 6.3-2. Typical Prisms in ENTECH's Domed Lens Concentrator Illustrate Equal Incidence/Excidence Ray Angles and Blunt Prism Tip Tolerance.

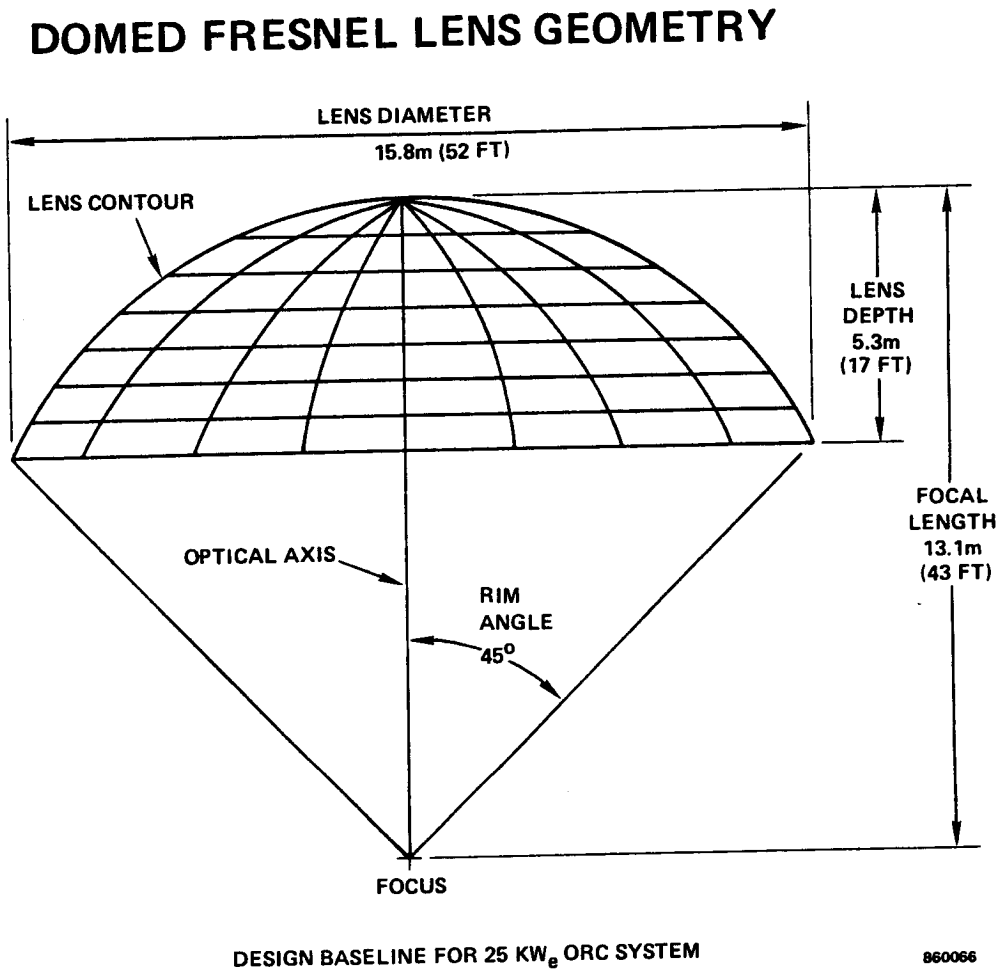

Figure 6.3-3. Baseline Lens Geometry Provides 25 kWe Using an Organic Rankine Cycle.

ENTECH considered both CBC and ORC engine requirements. For the CBC system, with a receiver temperature of 1050° K (1890° F) and a heat sink temperature of 273° K (460° F), the optimal geometric concentration ratio (GRC) is 600. To collect 165.9 kW (CBC efficiency of 22 percent) of heat during the illuminated portion of the orbit, Table 6.3-1 summarizes the concentrator size required for different rim angles and for lenses with and without anti-reflection (AR) coatings. Support structure shading of 5 percent was used as a preliminary estimate. Radiation losses through the receiver aperture were included in the analysis.

Table 6.3-1. CBC System Domed Fresnel Concentrator Sizing

Rim Angle (Degrees)	AR Coating	Optical Efficiency (Percent)	Thermal Efficiency (Percent)	Lens Aperture Area (m^2)	Lens Aperture Diameter (m)
30	No	83	75	172	14.8
45	No	78	70	185	15.3
30	Yes	87	79	164	14.5
45	Yes	83	75	172	14.8

For the ORC system with a receiver temperature of 755° K (1360° F), the optimal GCR is 300. To collect 205.6 kW (ORC efficiency of 18 percent) of heat during the illuminated portion of the orbit, Table 6.3-2 summarizes the required concentrator sizes including the shading and reradiation losses discussed above.

Table 6.3-2. ORC System Domed Fresnel Concentrator Sizing

Rim Angle (Degrees)	AR Coating	Optical Efficiency (Percent)	Thermal Efficiency (Percent)	Lens Aperture Area (m^2)	Lens Aperture Diameter (m)
30	No	88	84	190	15.6
45	No	85	81	197	15.8
30	Yes	93	89	180	15.1
45	Yes	90	86	186	15.4

A 45 degree rim angle was selected as the baseline to minimize the focal length and deployed mass moment of inertia. At this early stage, the feasability of applying anti-reflection coatings to flexible surfaces was unknown. Therefore, the conservative, larger diameter was selected. The 45 degree rim angle, 15.8 m diameter, non-AR coated ORC baseline design was the basis for further design development. The optimum 300 GCR specification

results in a receiver aperture of 0.91 m (36 inches) . The lens depth of 5.3 m (17.4 feet), Figure 6.3-3, is based on a surface material having an average refractive index of 1.41 and represents the optimal contour leading to the minimum slope error sensitivity discussed previously. The mathematical description of the optimum contour as a function of refractive index is available in reference 5.

6.3.2 Conceptual Design Details - Domed Fresnel

A layout of the DTS support structure rib was produced using the optimum lens curvature defined by ENTECH. A five hinge, two strut deployable rib was selected. Attempts to utilize a three hinge, one strut rib were unsuccessful due to the depth of the lens shape. Figure 6.3-4 shows the extreme depth of the lens and how well the DTS support structure adapts to the domed Fresnel geometry. The rib tube diameter is tentatively set at 5 cm.

The three point tripod interface to the receiver mandates the number of ribs selected to support the lens surface be divisible by three. Based on anticipated high surface weights, the one Hz minimum deployed frequency requirement, and the desire to hold the surface span to manageable dimensions, a twelve rib DTS was selected as shown in Figure 6.3-5. A detailed description of the DTS deployment scenario appears in Appendix A. The appendix describes a similar three hinge, one strut structure, but is directly extendable to the DTS design selected for the Domed Fresnel concentrator.

The lens surface is partitioned by the DTS radial ribs into twelve equal sectors or gores. As shown in Figure 6.3-4, the surface above the straight rib tubes is shaped by restraining a tensioned edge strip with adjustable length ties, analagous to a suspension bridge with the edge strip being the catenary cable and the DTS radial tube being the roadway. The gore is further partitioned into equal width rib to rib strips, Figure 6.3-6.

A typical lens strip attachment to the DTS ribs and shaping is depicted in Figure 6.3-7. The typical lens strip is tensioned between the previously mentioned edge strips. The tension force is applied along the strip edge through a lens edge beam. The purpose of the edge beams is to reinforce the thin surface material to prevent tearing and buckling, and to maintain a flat shape at this interface. The lens strip is contoured in the rib to rib direction using catenary dual rear cords and fixed length ties that shape the surface through contour loading bars. The contour loading bars are conceptually designed as lightweight composite thin walled tubes approximately 6 mm in diameter. The loading bars apply the shaping loads uniformly across the lens strip. Both the loading bars and edge beams are straight, stiff, structural members, thus resulting in a surface whose curvature is approximated by flat panels, analogous to a geodesic dome structure. The dual rear cord configuration isolates each lens strip from adjacent strips. This approach simplifies the equalibration of surface finite element models and eases fine tuning of the shape, i.e., making adjustments to a particular rear cord or tie will influence the contour of only one lens strip.

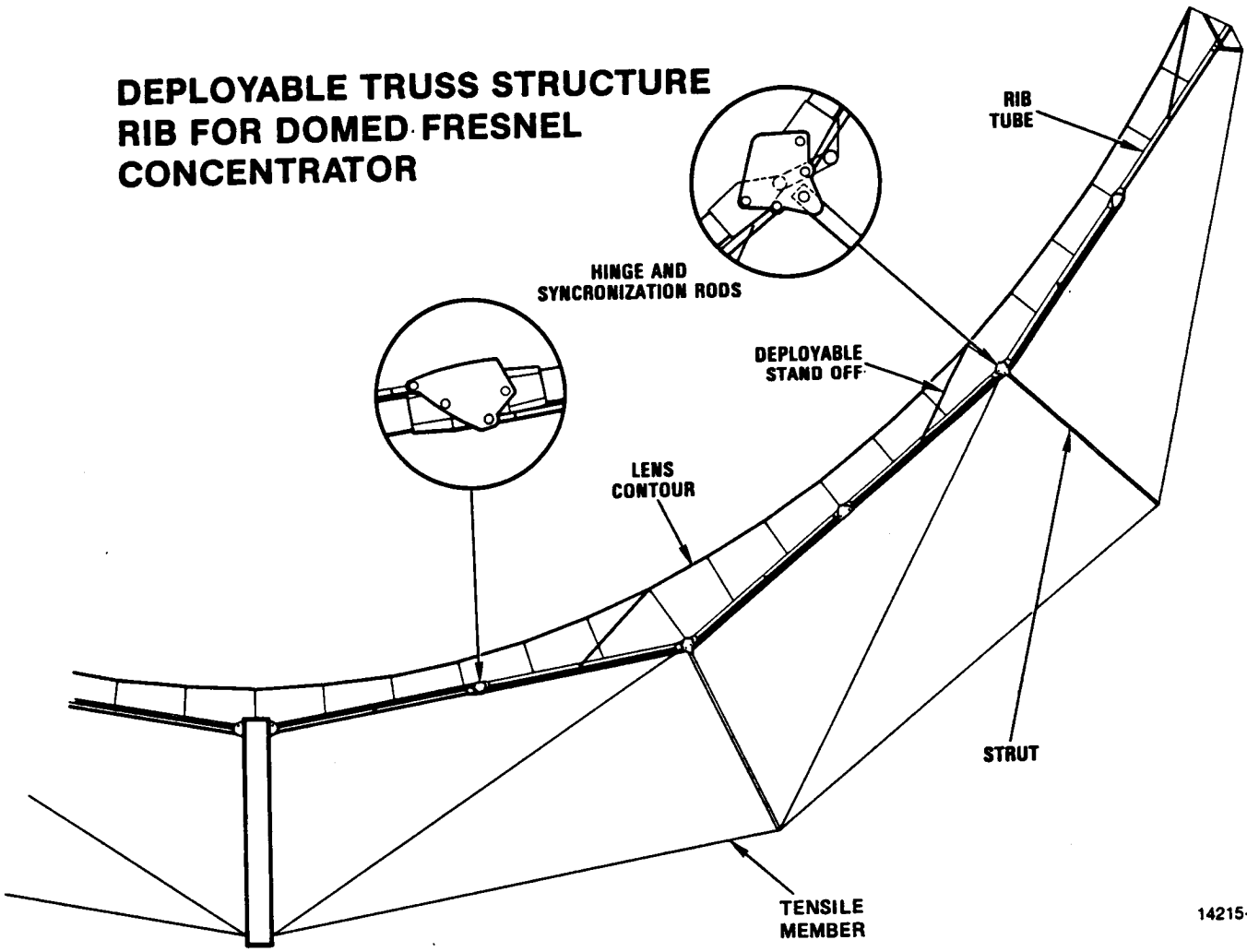

Figure 6.3-4. The DTS Offers Great Flexibility for Matching Even the Very Deeply Curved Surface of the Lens Contour. The Depth of the Truss can be Varied to Enhance Stiffness.

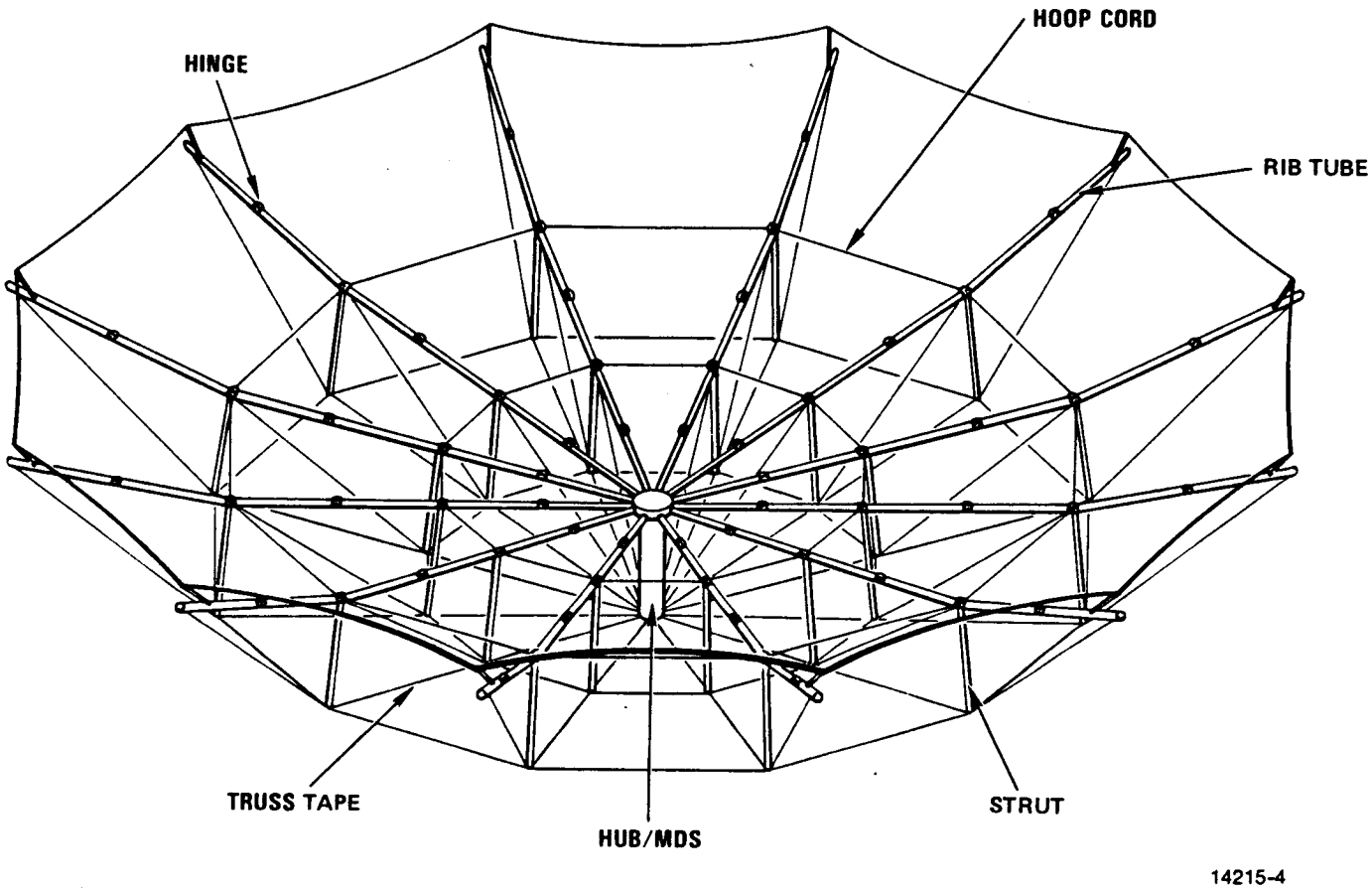

Figure 6.3-5. The 12 Rib DTS Selected to Support the Domed Fresnel Surface Provides Effective Receiver Interface and Manageable Surface Span Dimension.

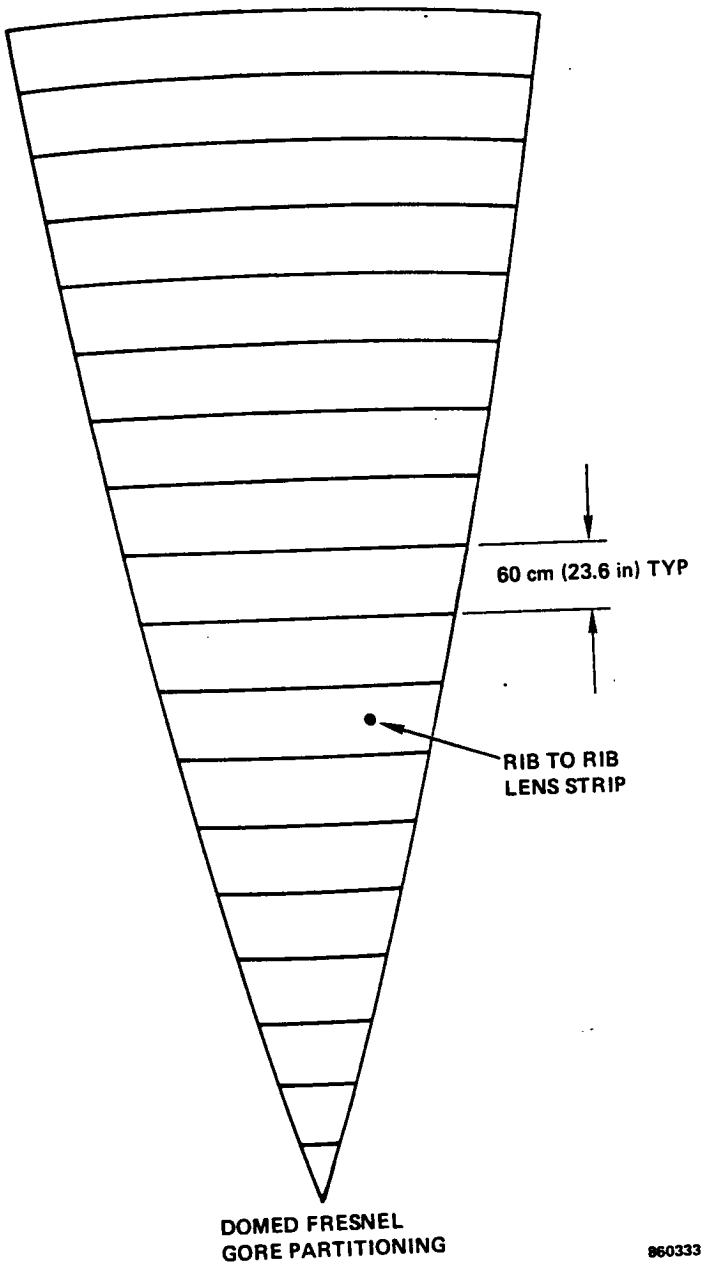

Figure 6.3-6. The 12 Identical Gores are Partitioned into Equal Width Lens Strips.

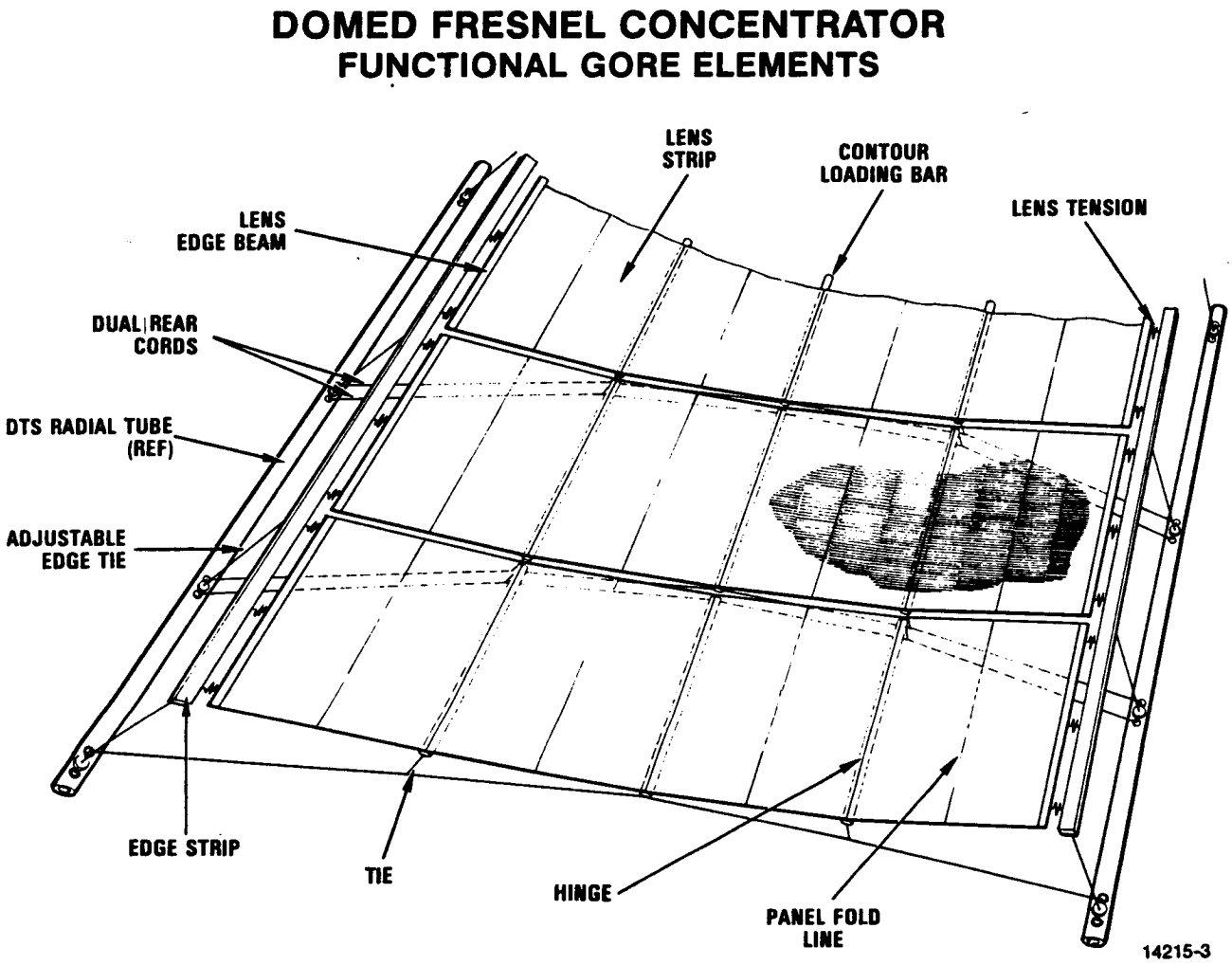

Figure 6.3-7. The Fresnel Lens Surface is Shaped by Catenary Rear Cords and Ties. The Dome is thus Approximated by a Series of Flat Panels.

The lens strips are tensioned between the edge strips by the spring devices shown in Figure 6.3-8. The springs are housed in lightweight composite sleeves and act on cables passing through low friction guides. These devices also provide thermal elastic isolation between the surface and DTS. The lens materials being considered for use on the domed Fresnel approach have high coefficients of thermal expansion (CTE), typically in the range of 36-108 m/m/°K. On orbit temperature fluctuations due to eclipse could lead to considerable expansion and contraction of the strip. The tension devices limit the load introduced into the structure thus acting as buffers between the high CTE stiff plastic surface and the low CTE DTS.

The hinges and panel fold lines required to fold the surface for transport are shown in Figures 6.3-7 and 6.3-9. The panel fold lines, integral with the surface, are formed during panel manufacture. The fold lines are areas where the panel thickness has been reduced to allow hinging without permanently creasing the plastic. The hinge assembly is constructed of plastic and bonded to the flat lens panels. The contour loading bars are slipped into the hinge tube at final assembly of the strip. Adequate clearance between the plastic hinge tube and the graphite composite load bar precludes inducing thermal stress at this interface during temperature excursions. The hinge wraps up on itself during folding, forming a tightly wrapped drum, providing a rigid restraint, Figure 6.3-10.

The lens strips are hinged along symmetric radial lines to allow for the compact packaging of the concentrator during transport, Figure 6.3-11. The lens strips are manually folded accordian style and interleaved as shown in Figure 6.3-12. Tapered, hollow fiberglass skewers are attached to the DTS structural members and telescope into adjoining skewers, Figure 6.3-13, forming continuous, concentric rings which contain the surface. Skewer rings, attached to the lens surface at the hinge points, slide onto the skewers. As the DTS deploys, the skewers separate and allow the rings to drop off, releasing the surface in a repeatable, controlled manner.

Figure 6.3-14 depicts the compact envelope of the stowed concentrator. The height of the stowed package, 2.0 m, is determined by the length of the individual DTS rib segments between the hinges. The diameter of the package, 1.8 m, is dictated by the spacing between the hinge and fold lines of the surface. Increasing the number of hinge lines within each lens strip can reduce the diameter of the stowed package at the expense of increased surface complexity and reduced efficiency caused by hinge shadows. These factors and the size limitations of the panel fabrication process were considered in the present surface attachment, shaping, and stowage designs.

The structural shading of the surface was calculated to verify compatibility with ENTECH's 5 percent shadow loss estimate used in sizing the concentrator. The results, presented in Table 6.3-3, verify that the 5 percent loss estimate has not been exceeded.

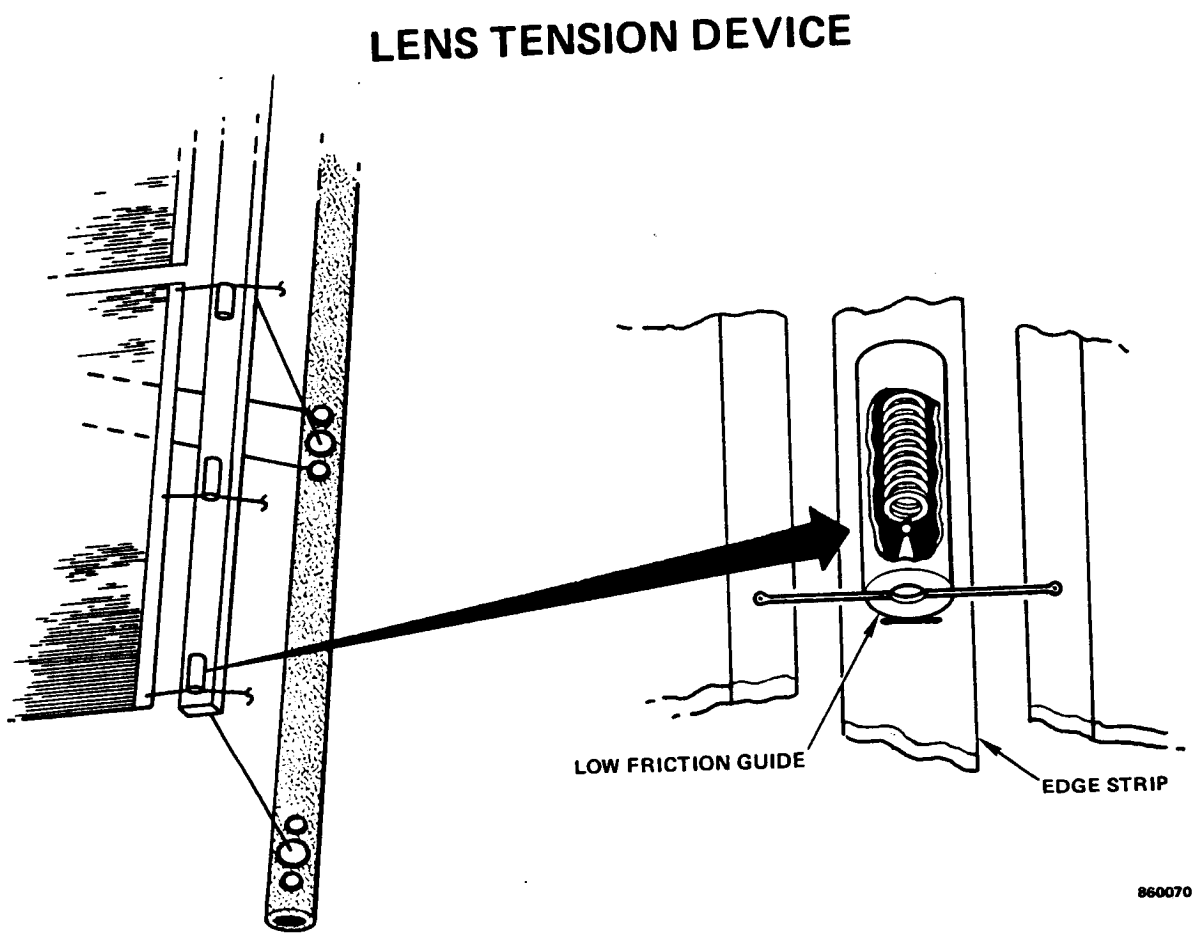

Figure 6.3-8. The Lens Strip is Tensioned Using Springs Housed in Composite Tubes. Cables Passing Through Low Friction Guides Connect the Surface to the Edge Strip.

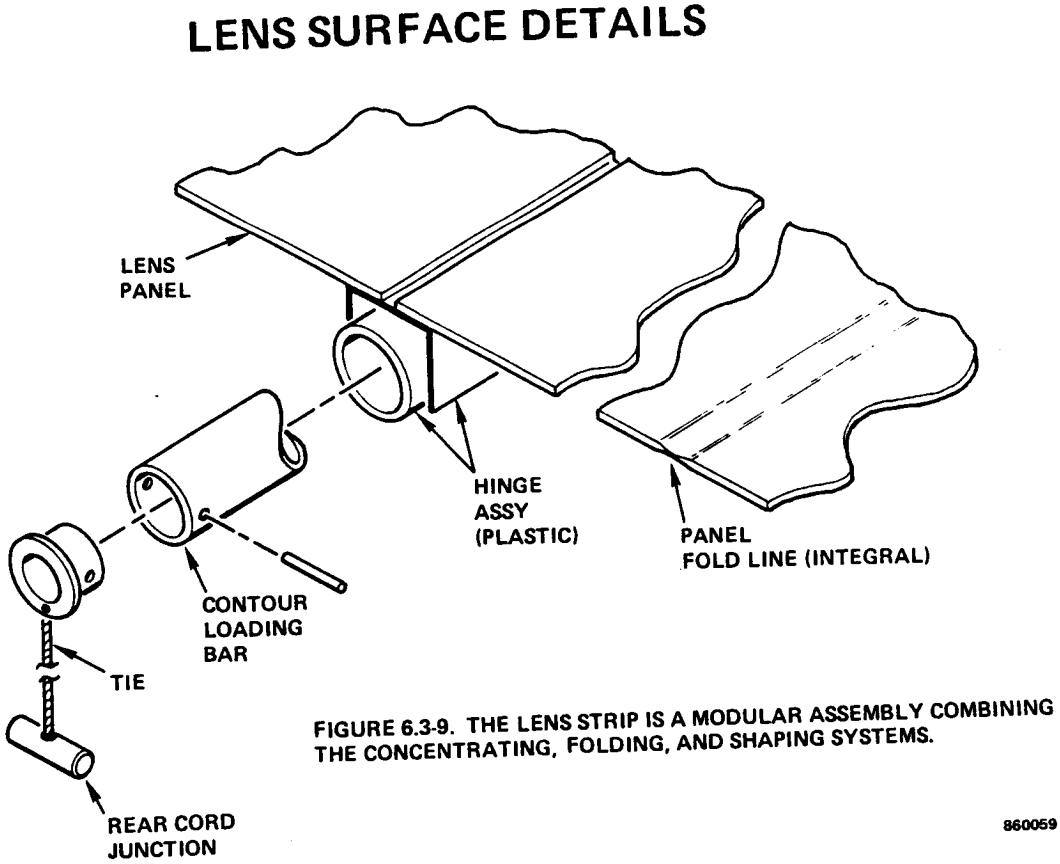

FIGURE 6.3-9. THE LENS STRIP IS A MODULAR ASSEMBLY COMBINING THE CONCENTRATING, FOLDING, AND SHAPING SYSTEMS.

Figure 6.3-9. The Lens Strip Modular Design Provides for Integrated Shaping and Folding of the Refractive Concentrating Surface.

DOMED FRESNEL CONCENTRATOR

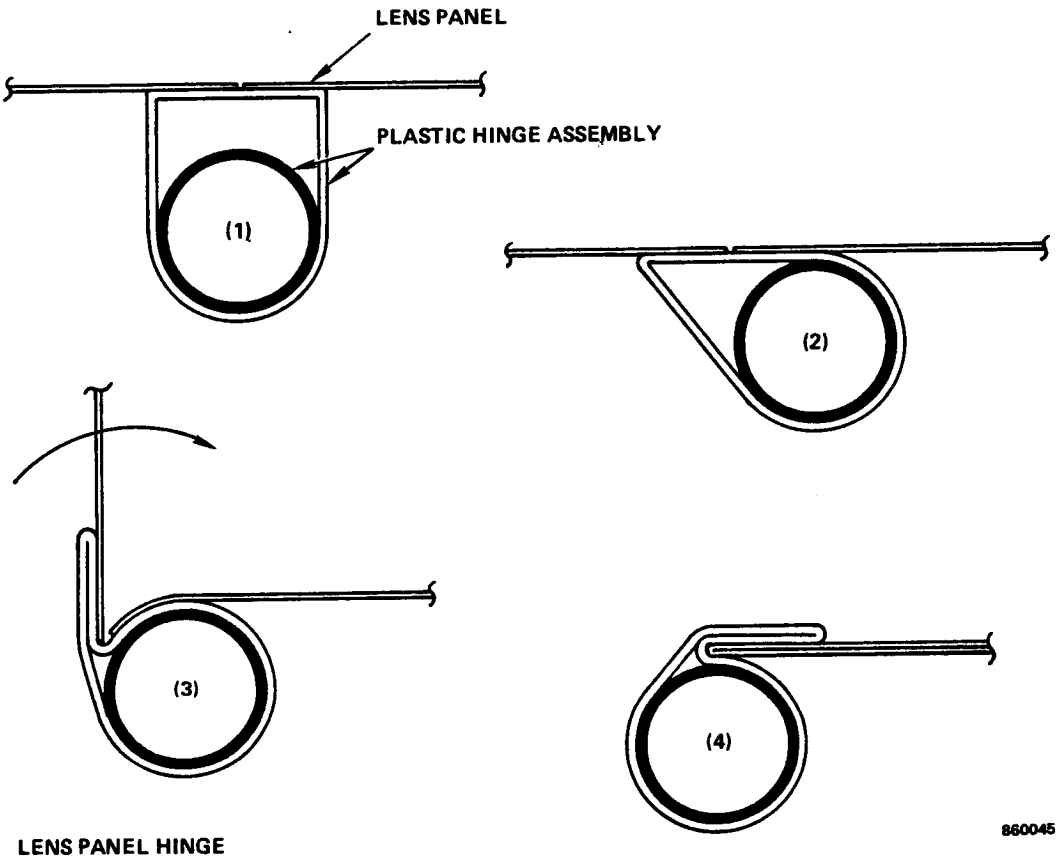

LENS PANEL HINGE

- CONTROLS PANEL FOLD LINE
- PROVIDES CONSTANT TENSION

Figure 6.3-10. Lens Strip Hinge Design Forms a Rigid Restraint When Folded and Constant Tension, Dimensional Stability When Unfolded.

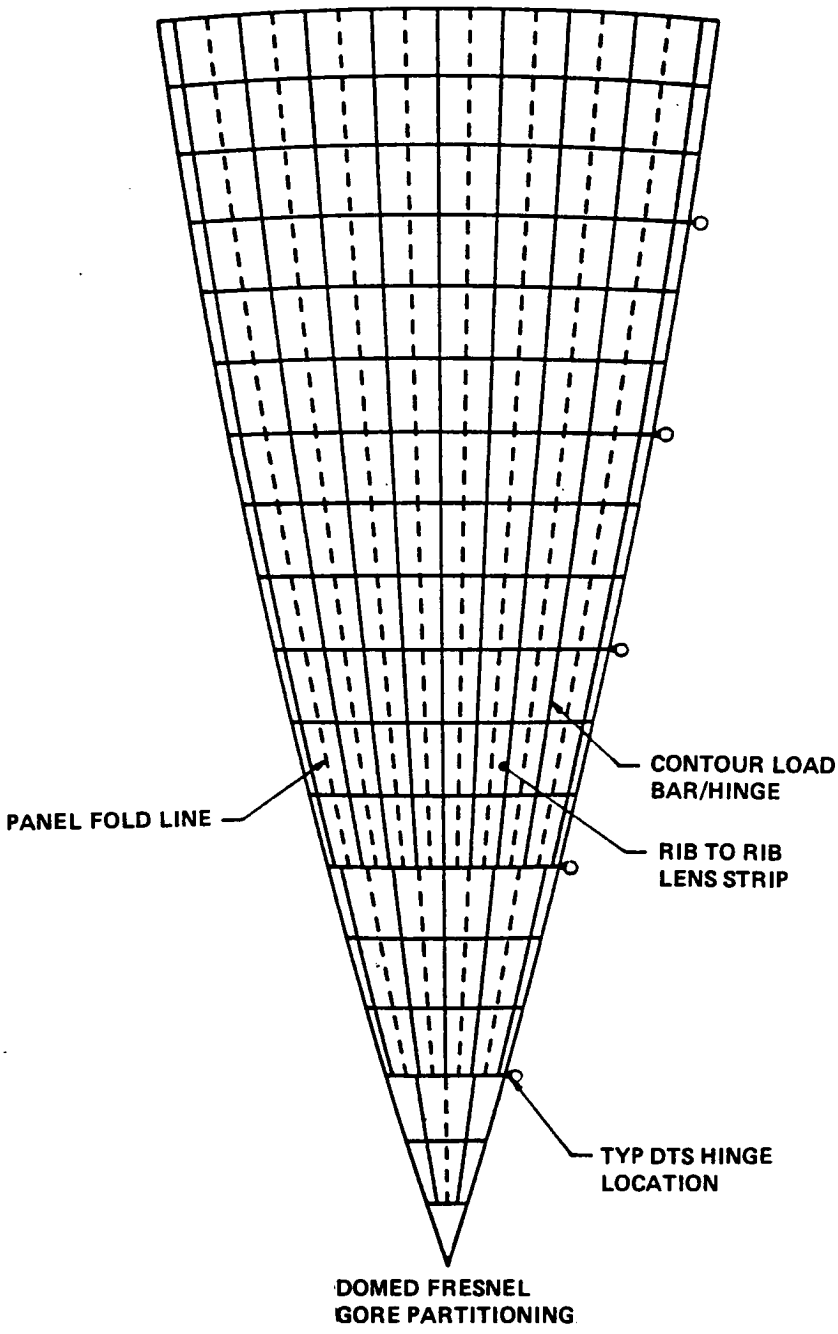

Figure 6.3-11. Radial Hinge and Fold Lines Enable Lens Strips to Fold Accordian Style for Compact Surface Packaging.

DOMED FRESNEL CONCENTRATOR
STOWED GORE AND RIB PAIR (END VIEW)

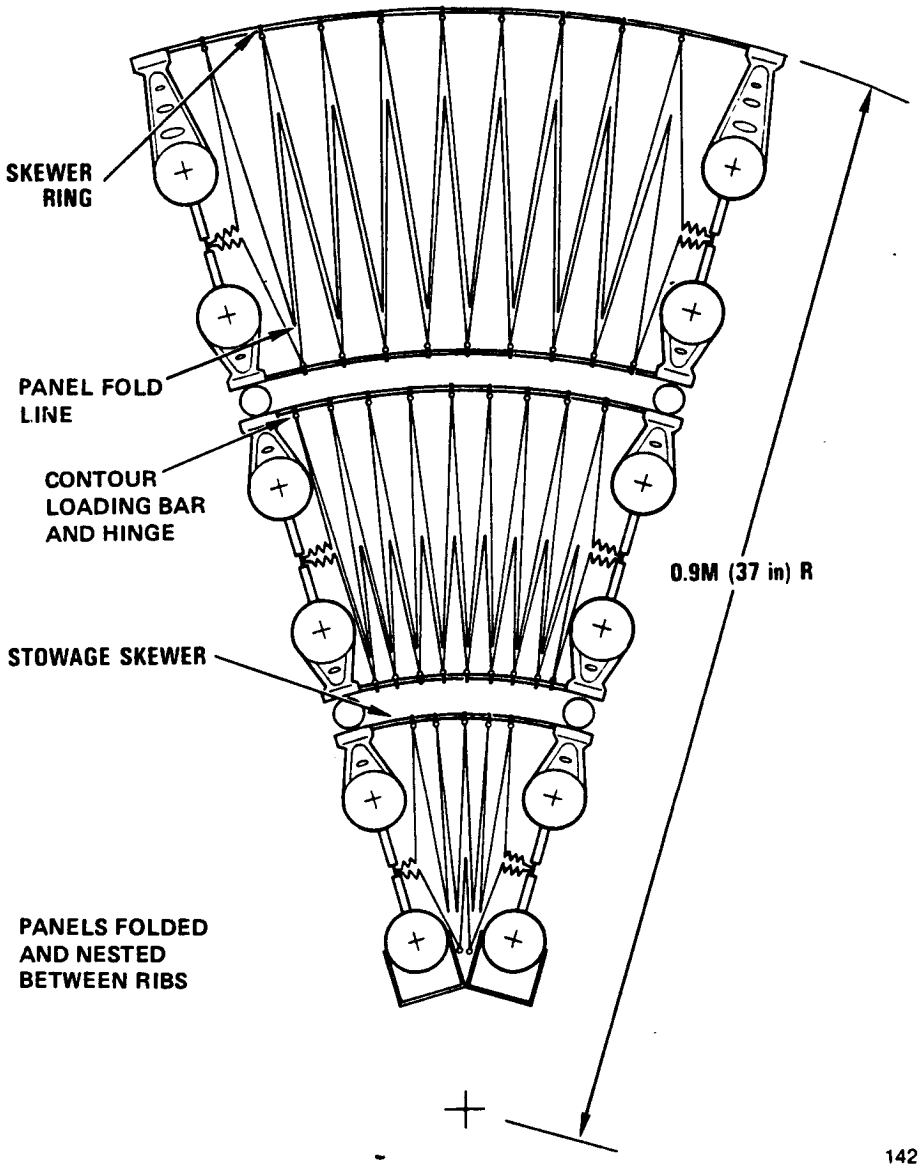

Figure 6.3-12. Accordian Fold Lens Surface Panels are Interleaved for Maximum Volume use.

DOMED FRESNEL CONCENTRATOR

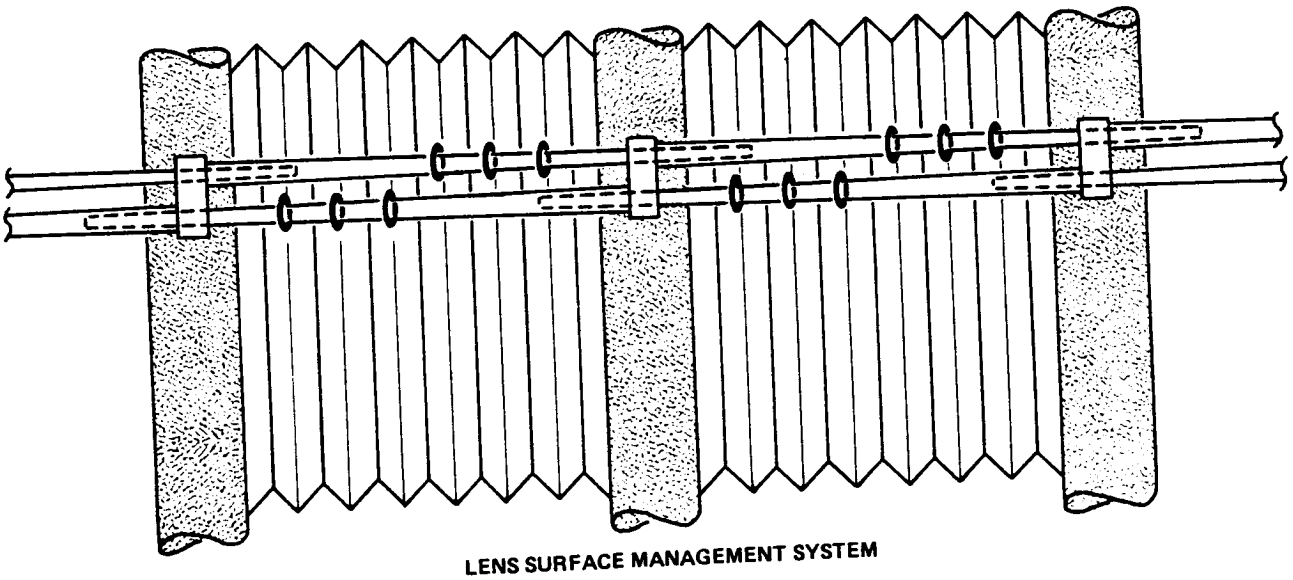

LENS SURFACE MANAGEMENT SYSTEM

SLIDING RINGS ATTACHED TO PANEL FOLD LINES ARE CAPTURED BY PAIRS OF TAPERED, HOLLOW SKEWERS:

- LOCATES THE SURFACE WHILE STOWED
- PROVIDES CONTROLLED RELEASE DURING DEPLOYMENT

860055

Figure 6.3-13. Telescoping Skewers Form Continuous, Concentric Rings Which Contain Surface During Launch and Provide Controlled Release During Deployment.

DOMED FRESNEL CONCENTRATOR STOWED ENVELOPE

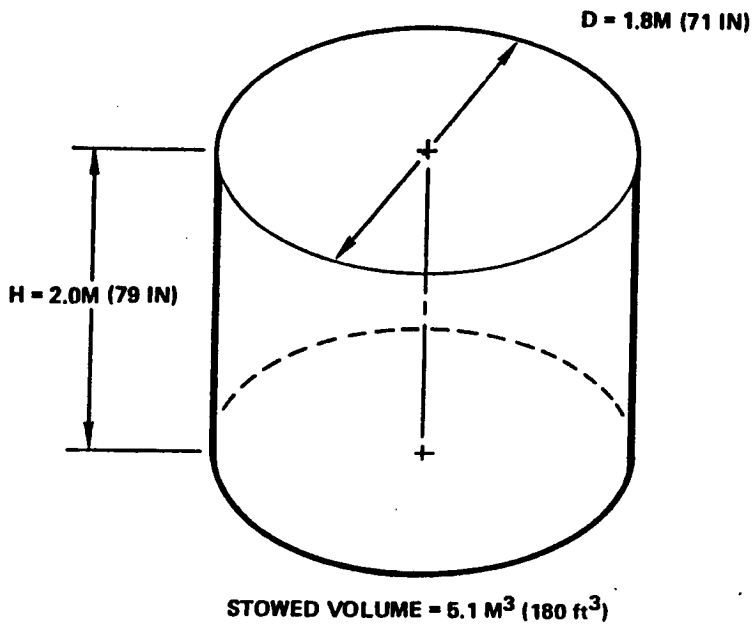

Figure 6.3-14. The Domed Fresnel Concentrator Folds Compactly into a Small Stowed Volume for Transport.

Table 6.3-3. Domed Fresnel Concentrator
Shadow Loss Estimate
One Gore Basis, Gore Area = 22.14 m^2 (34.320 in^2)

Item	Qty	Total Area cm^2	Total Area in^2
Load Bar/Hinge	127	4,710	730
Panel Fold Line	110	970	150
DTS Tube	1	4,060	630
Rear Cords	34	480	74
Gaps	16	210	33
Hub	1/12	52	8
Total Loss	---	10,580	1,627

$$\text{Area Loss} = 100\left[1 - \frac{(34,320 - 1,627)}{34,320}\right]\%$$

Area Loss = 4.7 percent

The following assumptions were made for Domed Fresnel concentrator mass calculations.

- The specific gravity of the lens material ranges from 1.2 - 2.2 and the lens thickness ranges from 0.15 - 0.25 mm (6-10 mils). These estimates cover the anticipated lens thickness and the densities of lens materials under consideration.
- The major structural members of the DTS, surface edge strips, cords, ties, and lens tension spring housings are of composite graphite construction.

For preliminary sizing Entech estimated a 5 percent loss due to structural blockage.

- Miscellaneous fittings and the DTS hinges are of aluminum alloy construction.
- The drive system and other miscellaneous mechanisms have some parts fabricated from steel alloys.
- Thermal control blankets are of multilayered kapton construction.

Table 6.3-4 presents an itemized mass estimate listing for the major surface and structural elements. As expected the lens is a major contributor to the total mass. Depending on material and thickness, the lens accounts for between 50 and 74 percent of the total surface mass and between 42 and 58 percent of the total concentrator mass. The mass moment of inertia and the center of gravity were not calculated. Final materials selections were not made for the Domed Fresnel concentrator and heavier but less costly materials could be considered for use. The materials assumptions reflect what might be achieved in weight reduction and are typical of flight type, low weight, precision space structures that must perform in extreme environments.

6.3.3 Analysis Results - Domed Fresnel

Optical analysis of the conceptually designed Domed Fresnel concentrator was performed by ENTECH. They provided preliminary estimates of allowable surface contour errors and concentrator pointing accuracy requirements. Key outputs of this analysis included quantitative data on the effects of the errors and receiver flux profiles for the recommended designs.

ENTECH used the flux profile for a lens optimized at a 500 GCR (which is not optimal for the 300 and 600 GCR designs) to obtain first-order, conservative values for allowable tracking error tolerances for the systems under study. For the 600 GCR CBC system, a 1 percent reduction in lens optical efficiency occurs for a tracking error of 0.25 degree. For the 300 GCR ORC system, a similar 1 percent reduction in optical efficiency occurs for a 0.5 degree tracking error. These allowable pointing errors are considerably higher than the design requirements of 0.025 degree (ORC) and 0.075 degree (CBC) for reflectors but are tighter than the alpha and beta joints provide. The design requirements for concentrator pointing accuracy can be relaxed considerably to take advantage of the lens' insensitivity to tracking errors but fine pointing is required. ENTECH recommends that these three-sigma, conservative values be used for specifying tracking error tolerance for the Domed Fresnel concentrator.

ENTECH generated a small computer program which models errors to consider the effect of surface displacement and rotational errors on lens performance, Figure 6.3-15. The model determines the movement of the solar image in the focal plane due to Δx, Δy, or Δz simple displacements, or due to $\omega x, \omega y, \omega z$ pure rotations of the prism under study. To generate first-order allowable error levels, ENTECH evaluated the 600 GCR CBC system with a recommended receiver aperture diameter of 64 cm (25 in.). If each of the six error sources (Δx, Δy, Δz, ωx, ωy, ωz) produces an individual image movement of 2.54 cm (1 in.), the RSS statistical combination of all six simultaneous errors is 6.2 cm (2.4 in.), more than an order of magnitude smaller than the selected 64 cm receiver aperture diameter. ENTECH computed the magnitude of each of the six errors required to produce a 2.54 cm (1 in.) image movement. The magnitude of these errors depends on the position of the prism within the

Table 6.3-4. Domed Fresnel Concentrator
Mass Estimate

Item	Qty	Mass (kg)	Weight (lbs)	Assembly
Lens	1	50-145	110-320	Surface
Load Bars	1,524	21	46	Surface
Edge Beams	408	5.0	11	Surface
Hinge	1,524	4.5	10	Surface
Cords, Rear	408	7.3	16	Surface
Ties		0.72	1.6	Surface
Springs	612	0.33	5.0	Surface
Case, Spring	612	0.38	0.83	Surface
Tie Junctions	3,048	1.3	2.8	Surface
Edge Strip	12	1.0	2.2	Surface
Surface Total	---	92-190	220-430	
Hinge	60	54	120	Structure
Strut	24	7.3	16	Structure
Rib Tube	72	35	78	Structure
DPSO	36	1.5	3.4	Structure
Tapes	60	5.0	11	Structure
Hub	1	23	50	Structure
Sync Rods	120	3.7	8.1	Structure
Skewers	408	0.54	1.2	Structure
Stowage	AR	0.41	0.90	Structure
Rib Blankets	12	2.0	4.3	Structure
Hub Blanket	1	0.34	0.75	Structure
FSM Tape	AR	0.68	1.5	Structure
Structural Total		130	300	
Surface Total		92-190	220-430	
Unit Total*		220-320	520-730	

*+/-20%
AR - As required

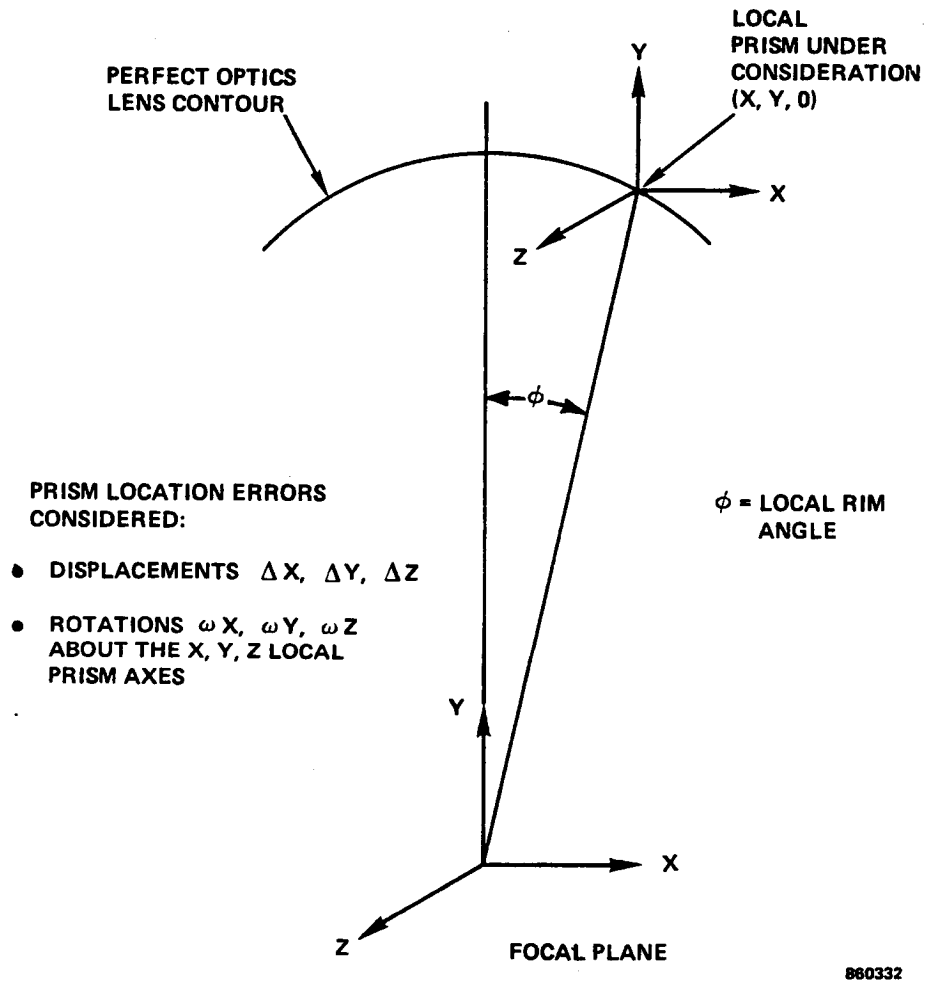

Figure 6.3-15. Coordinate System Used for Domed Fresnel Surface Error Tolerance Analysis.

lens (local rim angle), with greatest error tolerance at the vertex of the surface and least error tolerance at the rim of the lens. The table below summarizes the allowable error (corresponding to an individual 2.54 cm (1 in.) image movement) for each of the six error sources at three different locations within the lens surface.

Local Rim Angle ϕ (Degrees)	Δx	Δy (cm, (in))	Δz	ωx	ωy (Degrees)	ωz
0	2.54 (1)	*	2.54 (1)	*	*	*
30	2.54 (1)	4.6 (1.8)	2.54 (1)	0.9	0.25	3.0
45	2.54 (1)	2.54 (1)	2.54 (1)	0.45	0.2	1.9

*infinite error allowed

Conservatively applying the worst-case tolerance levels at the lens periphery for the full lens, ENTECH recommends that the following one-sigma tolerances be used.

$$\Delta x = \Delta y = \Delta z = \pm 2.54 \text{ cm (1 in.)}$$
$$\omega x = \pm 0.5 \text{ deg.}$$
$$\omega y = \mp 0.2 \text{ deg.}$$
$$\omega z = \pm 2.0 \text{ deg.}$$

ENTECH generated a computer model to provide the irradiance (flux) profiles over the receiver aperture and the receiver cavity side and back walls. Both the baseline ORC and CBC geometries were considered. The receiver aperture, cavity side wall, and back wall dimensions were normalized to the appropriate lens aperture radii, Figure 6.3-16. The analysis is based on the dispersion curve (refractive index versus wavelength) of silicone polymer as this material has been fully characterized. These results do not include the absorption losses within the lens material since this effect depends on lens material and thickness; parameters that have not been finalized. The analyses do not include the defocusing effect of the flat plane approximation to the perfect dome contour and therefore represent the highest possible internal receiver cavity flux profiles.

The flux profiles were determined using ENTECH's cone optics equations with an integration step size of 1 degree over the full 45 degree rim angle. 320 rays are traced for each small element of the lens surface. The solar energy spectrum is divided into ten equal energy flux bands to include effects of spectral dependencies of optical properties. Figure 6.3-17 summarize ENTECH's cone optics analysis approach. The receiver cavity focal plane aperture, side wall, and back wall were segmented into twenty annular rings, with the flux, in units of suns, tabulated for each region. Tables 6.3-5 through 6.3-8 present the completed flux distributions for the CBC and ORC preliminary lens designs.

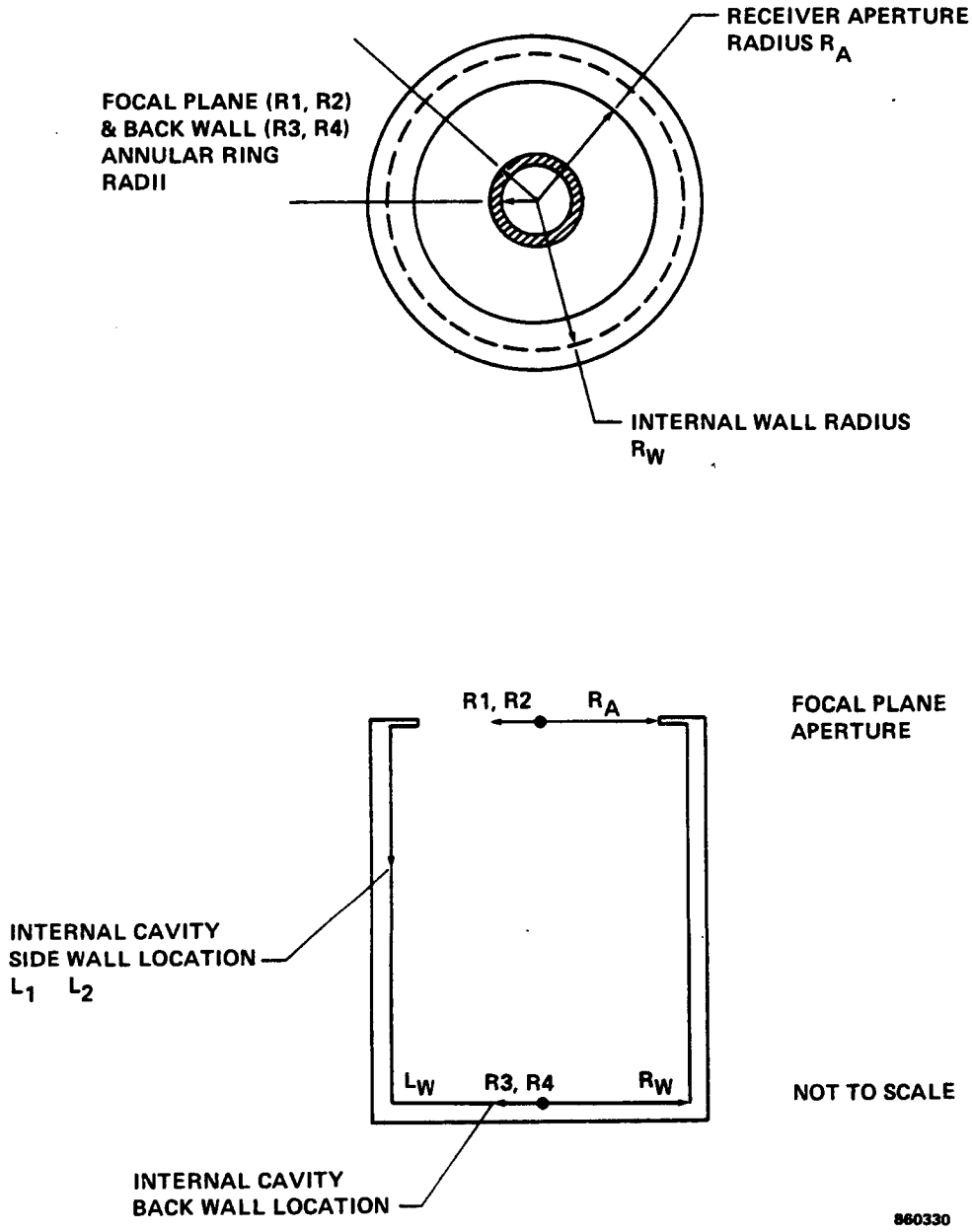

Figure 6.3-16. Domed Fresnel Concentrator Flux Profile Analysis was Performed Using Receiver Geometry Normalized to Lens Aperture Radius.

ENTECH CONE OPTICS APPROACH

SOLAR DISK IS SUBDIVIDED INTO 32 EQUAL ENERGY FLUX REGIONS TO TREAT FINITE SUN SIZE.

AMO SPECTRUM IS SUBDIVIDED INTO 10 EQUAL ENERGY FLUX BANDS TO TREAT SPECTRAL DEPENDENCIES OF OPTICAL PROPERTIES (N AND K), INCLUDING DISPERSION, REFLECTION, AND ABSORPTION EFFECTS.

DOME FRESNEL LENS IS SUBDIVIDED INTO 1 DEGREE ANGULAR APERTURE RADIAL SUBDIVISIONS.

PARQUET ELEMENT WIDTH IS SUBDIVIDED INTO 6 LENGTHWISE CIRCUMFERENTIAL SUBDIVISIONS.

INTERNAL FACET ANGLES ARE OPTIMIZED TO MAXIMIZE OPTICAL EFFICIENCY AND SMOOTH FLUX

FOR EACH SMALL ELEMENT OF LENS APERTURE, 320 RAYS ARE TRACED FROM THE SOLAR DISK TO THE FOCAL PLANE, WITH PROPER TREATMENT OF REFLECTION AND ABSORPTION LOSSES.

OUTPUTS ARE FLUX PROFILES OVER APERTURE PLANE AND INSIDE CAVITY RECEIVER.

Figure 6.3-17. ENTECH Cone Optics Analysis Approach has been Verified by Correlation with Solar Tests.

Table 6.3-5. Focal Plane Flux Profile for Domed Fresnel CBC System without Flux Smoothing

Dome Lens Optics Program

Space Silicone Dome Lens - 12/29/85 - Cavity Fluxes
Rim Angle (degrees) = 45
Integration step (degrees) = 1
Design Geometric Concentration Ratio (GCR) = 600
Receiver Cavity Radius/Lens Aperture Radius = .07 (R_A/R_L)
Receiver Cavity Length/Lens Aperture Radius = .17 (L_W/R_L)

Focal Plane Annular Ring (Unit of Aperture Radius) R_1		R_2	Flux (Suns)	Cumulative Optical Efficiency (Percent)
0	-	2e-03	2004	0.8
2e-03	-	4.1e-03	2249	3.6
4.1e-03	-	6.1e-03	2037	7.9
6.1e-03	-	8.2e-03	1472	12.2
8.2e-03	-	.0102	1084	16.2
.0102	-	.0122	880	20.3
.0122	-	.0143	751	24.3
.0143	-	.0163	676	28.6
.0163	-	.0184	656	33.2
.0184	-	.0204	615	38.1
.0204	-	.0225	608	43.4
.0225	-	.0245	546	48.6
.0245	-	.0265	575	54.6
.0265	-	.0286	562	61.0
.0286	-	.0306	471	66.6
.0306	-	.0327	452	72.5
.0327	-	.0347	298	76.6
.0347	-	.0367	201	79.5
.0367	-	.0388	164	82.0
.0388	-	.0408	80	83.3

Table 6.3-6. Cavity Side Wall and Back Wall Flux Profiles for Domed Fresnel CBC System without Flux Smoothing

Internal Cavity Side Wall Location (Unit of Aperture Radius) L_1		L_2	Flux (Suns)	Cumulative Optical Efficiency (Percent)
0	-	8.5e-03	0	0
8.5e-03	-	.017	0	0
.017	-	.0255	0	0
.0255	-	.034	2	.2
.034	-	.0425	6	.9
.0425	-	.051	10	2.1
.051	-	.0595	13	3.6
.0595	-	.068	15	5.3
.068	-	.0765	19	7.6
.0765	-	.085	21	10.1
.085	-	.0935	22	12.7
.0935	-	.102	26	15.9
.102	-	.1105	27	19.1
.1105	-	.119	27	22.4
.119	-	.1275	27	25.6
.1275	-	.136	25	28.5
.136	-	.1445	24	31.4
.1445	-	.153	23	34.2
.153	-	.1615	21	36.6
.1615	-	.17	20	39.0

Internal Cavity Back Wall Location (Unit of Aperture Radius) R_3		R_4	Flux (Suns)	Cumulative Optical Efficiency (Percent)
0	-	3.5e-03	970	1.2
3.5e-03	-	7e-03	767	4.0
7e-03	-	.0105	551	7.4
.0105	-	.014	326	10.2
.014	-	.0175	247	12.9
.0175	-	.021	182	15.4
.021	-	.0245	154	17.8
.0245	-	.028	128	20.2
.028	-	.0315	105	22.3
.0315	-	.035	92	24.5
.035	-	.0385	79	26.5
.0385	-	.042	71	28.5
.042	-	.0455	65	30.5
.0455	-	.049	60	32.5
.049	-	.0525	58	34.6
.0525	-	.056	53	36.6
.056	-	.0595	47	38.5
.0595	-	.063	48	40.5
.063	-	.0665	43	42.5
.0665	-	.07	39	44.3

Table 6.3-7. Focal Plane Flux Profile for Domed Fresnel ORC System without Flux Smoothing

Dome Lens Optics Program

Space Silicone Dome Lens - 12/29/85 - Cavity Fluxes
Rim Angle (degrees) = 45
Integration step (degrees) = 1
Design Geometric Concentration Ratio (GCR) = 300
Receiver Cavity Radius/Lens Aperture Radius = .07 (R_A/R_L)
Receiver Cavity Length/Lens Aperture Radius = .17 (L_W/R_L)

Focal Plane Annular Ring (Unit of Aperture Radius) R_1		R_2	Flux (Suns)	Cumulative Optical Efficiency (Percent)
0	-	2.9e-03	1182	1.0
2.9e-03	-	5.8e-03	1136	3.8
5.8e-03	-	8.7e-03	765	7.0
8.7e-03	-	.0115	500	9.9
.0115	-	.0144	390	12.9
.0144	-	.0173	337	15.9
.0173	-	.0202	305	19.3
.0202	-	.0231	283	22.8
.0231	-	.026	278	26.7
.026	-	.0289	268	31.0
.0289	-	.0318	267	35.6
.0318	-	.0346	280	41.0
.0346	-	.0375	296	47.2
.0375	-	.0404	303	54.0
.0404	-	.0433	318	61.7
.0433	-	.0462	328	70.1
.0462	-	.0491	294	78.2
.0491	-	.052	201	84.1
.052	-	.0548	115	87.6
.0548	-	.0577	45	89.1

Table 6.3-8. Cavity Side Wall and Back Wall Flux Profiles for Domed Fresnel ORC System without Flux Smoothing

Internal Cavity Side Wall Location (Unit of Aperture Radius) L_1		L_2	Flux (Suns)	Cumulative Optical Efficiency (Percent)
0	-	8.5e-03	0	0
8.5e-03	-	.017	1	.1
.017	-	.0255	5	.8
.0255	-	.034	7	1.6
.034	-	.0425	7	2.4
.0425	-	.051	9	3.5
.051	-	.0595	10	4.6
.0595	-	.068	10	5.8
.068	-	.0765	11	7.1
.0765	-	.085	13	8.6
.085	-	.0935	16	10.5
.0935	-	.102	18	12.6
.102	-	.1105	20	15.0
.1105	-	.119	22	17.6
.119	-	.1275	23	20.3
.1275	-	.136	25	23.3
.136	-	.1445	24	26.1
.1445	-	.153	23	28.9
.153	-	.1615	23	31.6
.1615	-	.17	21	34.1

Internal Cavity Back Wall Location (Unit of Aperture Radius) R_3		R_4	Flux (Suns)	Cumulative Optical Efficiency (Percent)
0	-	3.5e-03	1340	1.6
3.5e-03	-	7e-03	1023	5.4
7e-03	-	.0105	730	9.9
.0105	-	.014	430	13.6
.014	-	.0175	326	17.2
.0175	-	.021	258	20.6
.021	-	.0245	206	23.9
.0245	-	.028	176	27.1
.028	-	.0315	148	30.2
.0315	-	.035	124	33.1
.035	-	.0385	113	36.0
.0385	-	.042	95	38.7
.042	-	.0455	83	41.2
.0455	-	.049	72	43.6
.049	-	.0525	57	45.7
.0525	-	.056	50	47.5
.056	-	.0595	50	49.6
.0595	-	.063	43	51.4
.063	-	.0665	38	53.2
.0665	-	.07	38	55.0

The majority of the focused energy is concentrated on the cavity back walls with intensities at the center of this area exceeding 1300 suns in the ORC receiver. This situation is undesirable since the back wall is not a heat transfer surface. ENTECH redesigned the prism geometry for the two systems to tailor the flux profile to decrease the maximum flux peaks and increase the energy intercepted on the side walls. The tailored (smoothed) flux profiles are presented in Tables 6.3-9 through 6.3-12. Flux tailoring resulted in considerable improvement. Table 6.3-13 compares the flux profiles before and after flux tailoring. The peak back wall intensities have been reduced by almost an order of magnitude and the side wall energy fractions have been increased, both without lowering the overall optical efficiencies.

As discussed in Paragraph 6.2.3, the DTS used as an RF reflector is capable of achieving fundamental deployed frequencies ranging from 3.0 to 5.0 Hz depending on design configuration. The Domed Fresnel concentrator surface weight is almost an order of magnitude greater than typical RF surface weights and represents a large percentage of the total weight. Although no analysis has been performed to determine the deployed stiffness of the concept, it is believed that a fundamental frequency greater than 1.0 Hz can be achieved.

6.3.4 Evaluation of Significant Parameters - Domed Fresnel

The Domed Fresnel concentrator developed for this program combines two relatively mature technologies; lightweight, deployable, precision, space structures and solar dynamic power systems. Solar dynamic power systems have been thoroughly developed for terrestrial use. Precision space structures are well developed for radio frequency (RF) space applications.

As part of the Harris IR&D Program, we have designed and built a prototype 16 foot diameter DTS with a RF surface. This prototype verified the DTS design approach and deployment kinematics reducing the associated risk and cost for the Domed Fresnel concentrator concept. ENTECH has proven experience in the design, analysis, and integration of refractive Fresnel lens solar concentrators for terrestrial use. The Domed Fresnel concentrator lens surface is patterned after ENTECH's 14 m dome design being built under DOE contract and is fully compatible with existing lens panel manufacturing capabilities available to ENTECH.

The major remaining unkown in the domed Fresnel lens design is the selection of a material for the surface that will endure 7-10 years in the harsh LEO environment. The lens material issue is discussed in detail in Section 7.0.

The DTS support uses symmetry to reduce overall design complexity. Each deployable rib has five hinge mechanisms - three locking and two nonlocking. The hinge designs are similar; differing only in minor geometric detail. The composite rib tubes, synchronization rods, and other structural members vary in length only and all end fittings and attachments are identical.

Table 6.3-9. Focal Plane Flux Profile for Domed Fresnel CBC System with Flux Smoothing

Dome Lens Optics Program

Brayton Dome Lens with Cavity Flux Smoothing
Rim Angle (degrees) = 45
Integration step (degrees) = 1
Design Geometric Concentration Ratio (GCR) = 600
Receiver Cavity Radius/Lens Aperture Radius = .07 (R_A/R_L)
Receiver Cavity Length/Lens Aperture Radius = .17 (L_W/R_L)

Focal Plane Annular Ring (Unit of Aperture Radius) R_1		R_2	Flux (Suns)	Cumulative Optical Efficiency (Percent)
0	-	2e-03	3101	1.3
2e-03	-	4.1e-03	3459	5.6
4.1e-03	-	6.1e-03	3085	12.0
6.1e-03	-	8.2e-03	2261	18.6
8.2e-03	-	.0102	1578	24.6
.0102	-	.0122	1238	30.2
.0122	-	.0143	1016	35.7
.0143	-	.0163	850	41.0
.0163	-	.0184	755	46.4
.0184	-	.0204	660	51.6
.0204	-	.0225	557	56.5
.0225	-	.0245	424	60.6
.0245	-	.0265	397	64.7
.0265	-	.0286	360	68.7
.0286	-	.0306	271	72.0
.0306	-	.0327	293	75.8
.0327	-	.0347	195	78.5
.0347	-	.0367	105	80.0
.0367	-	.0388	135	82.1
.0388	-	.0408	76	83.3

Table 6.3-10. Cavity Side Wall and Back Wall Flux Profiles for Domed Fresnel CBC System with Flux Smoothing

Internal Cavity Side Wall Location (Unit of Aperture Radius) L_1		L_2	Flux (Suns)	Cumulative Optical Efficiency (Percent)
0	-	8.5e-03	0	0
8.5e-03	-	.017	0	0
.017	-	.0255	0	0
.0255	-	.034	2	.2
.034	-	.0425	6	.9
.0425	-	.051	10	2.1
.051	-	.0595	13	3.6
.0595	-	.068	15	5.4
.068	-	.0765	20	7.8
.0765	-	.085	23	10.6
.085	-	.0935	24	13.5
.0935	-	.102	28	16.8
.102	-	.1105	29	20.3
.1105	-	.119	30	23.8
.119	-	.1275	30	27.3
.1275	-	.136	28	30.6
.136	-	.1445	27	33.9
.1445	-	.153	27	37.1
.153	-	.1615	25	40.1
.1615	-	.17	24	42.9
Internal Cavity Back Wall Location (Unit of Aperture Radius) R_3		R_4	Flux (Suns)	Cumulative Optical Efficiency (Percent)
0	-	3.5e-03	0	0
3.5e-03	-	7e-03	0	0
7e-03	-	.0105	0	0
.0105	-	.014	0	0
.014	-	.0175	0	0
.0175	-	.021	0	0
.021	-	.0245	0	0
.0245	-	.028	1	0
.028	-	.0315	15	.3
.0315	-	.035	57	1.7
.035	-	.0385	106	4.4
.0385	-	.042	147	8.5
.042	-	.0455	165	13.6
.0455	-	.049	163	19.0
.049	-	.0525	132	23.7
.0525	-	.056	108	27.8
.056	-	.0595	89	31.4
.0595	-	.063	75	34.6
.063	-	.0665	64	37.5
.0665	-	.07	60	40.4

Table 6.3-11. Focal Plane Flux Profile for Domed Fresnel ORC System with Flux Smoothing

Dome Lens Optics Program

Ranking Dome Lens with Cavity Flux Smoothing
Rim Angle (degrees) = 45
Integration step (degrees) = 1
Design Geometric Concentration Ratio (GCR) = 300
Receiver Cavity Radius/Lens Aperture Radius = .07
Receiver Cavity Length/Lens Aperture Radius = .17

Focal Plane Annular Ring (Unit of Aperture Radius) R_1		R_2	Flux (Suns)	Cumulative Optical Efficiency (Percent)
0	-	2.9e-03	2681	2.2
2.9e-03	-	5.8e-03	2369	8.2
5.8e-03	-	8.7e-03	1643	15.0
8.7e-03	-	.0115	1004	20.9
.0115	-	.0144	748	26.5
.0144	-	.0173	608	32.0
.0173	-	.0202	510	37.6
.0202	-	.0231	455	43.3
.0231	-	.026	405	49.0
.026	-	.0289	350	54.5
.0289	-	.0318	301	59.8
.0318	-	.0346	249	64.6
.0346	-	.0375	209	68.9
.0375	-	.0404	159	72.5
.0404	-	.0433	144	76.0
.0433	-	.0462	145	79.7
.0462	-	.0491	129	83.3
.0491	-	.052	89	85.9
.052	-	.0548	67	87.9
.0548	-	.0577	34	89.1

Table 6.3-12. Cavity Side Wall and Back Wall Flux Profiles for Domed Fresnel ORC System with Flux Smoothing

Internal Cavity Side Wall Location (Unit of Aperture Radius) L_1		L_2	Flux (Suns)	Cumulative Optical Efficiency (Percent)
0	-	8.5e-03	0	0
8.5e-03	-	.017	1	.1
.017	-	.0255	7	1.0
.0255	-	.034	14	2.7
.034	-	.0425	16	4.5
.0425	-	.051	15	6.3
.051	-	.0595	13	7.9
.0595	-	.068	13	9.5
.068	-	.0765	19	11.8
.0765	-	.085	22	14.4
.085	-	.0935	23	17.1
.0935	-	.102	27	20.4
.102	-	.1105	30	24.0
.1105	-	.119	36	28.2
.119	-	.1275	37	32.6
.1275	-	.136	38	37.1
.136	-	.1445	38	41.5
.1445	-	.153	42	46.5
.153	-	.1615	46	52.0
.1615	-	.17	47	57.6

Internal Cavity Back Wall Location (Unit of Aperture Radius) R_3		R_4	Flux (Suns)	Cumulative Optical Efficiency (Percent)
0	-	3.5e-03	0	0
3.5e-03	-	7e-03	0	0
7e-03	-	.0105	0	0
.0105	-	.014	0	0
.014	-	.0175	0	0
.0175	-	.021	0	0
.021	-	.0245	0	0
.0245	-	.028	0	0
.028	-	.0315	0	0
.0315	-	.035	0	0
.035	-	.0385	0	0
.0385	-	.042	0	0
.042	-	.0455	1	0
.0455	-	.049	15	.5
.049	-	.0525	59	2.6
.0525	-	.056	108	6.7
.056	-	.0595	136	12.2
.0595	-	.063	149	18.6
.063	-	.0665	146	25.3
.0665	-	.07	129	31.4

Table 6.3-13. Comparison of Domed Fresnel Concentrator Flux Profiles Before and After Flux Tailoring

Case	Item	Without Flux Tailoring	With Flux Tailoring
Rankine 300 GCR	Side Wall Energy	34.1%	57.6%
	Back Wall Energy	55.0%	31.4%
	Total Energy	89.1%	89.1%
	Peak Side Wall Flux	25 suns	47 suns
	Peak Back Wall Flux	1340 suns	149 suns
Brayton 600 GCR	Side Wall Energy	39.0%	42.9%
	Back Wall Energy	44.3%	40.4%
	Total Energy*	83.3%	83.3%
	Peak Side Wall Flux	27 suns	30 suns
	Peak Back Wall Flux	970 suns	165 suns

* Total energy is higher than the optical efficiencies reported in Tables 6.3-1 and 6.3-2 since absorption losses were not included in the analysis.

The deployment mechanism in the central hub has a single motor similar to the proven TDRSS drive unit. Limit switches (redundant) stop the motor at the end of deployment and simultaneously provide telemetry. The reliability of these deployment mechanisms has been verified on the 16 foot DTS model and TDRSS flight hardware. The complexity of the surface was also reduced by symmetry. The twelve gores are identical and each lens strip is symmetric about its mid gore radial hinge line. The folding hinges and contour load bars have identical sections and differ only in length. Ties and cords also have common end fittings.

Scaling the Domed Fresnel concentrator to meet changing power requirements is straight forward. Increased collection area is provided by increasing the deployed diameter. Changes in diameter involve altering the length of the DTS rib tubes and tapes, with corresponding changes in section properties to maintain equivalent stiffness. The same principle applies to the surface lens strip/panel dimensions, within limits. The basic surface configuration can tolerate growth until the required lens strip widths exceeded the present capabilities of current manufacturing machinery or approximately twice the current diameter, 32 m (105 feet). A 32 m diameter Domed Fresnel concentrator is capable of delivering almost 100 kWe of continuous power. The design of the prismatic surface is unique to a given diameter, requiring the complete replacement of the prism forming tool set.

Deployment of the Domed Fresnel concentrator refractor assembly is completely automatic and does not require any astronaut assistance. Deployment time is estimated at 20 minutes. EVA/IVA time required to connect the six tripod legs between the concentrator and receiver was not estimated. Conceptual design of the tripod joints was not performed, but joints which operate in the same manner as those recently tested in flight on the Access program are the prime candidate. Access verified the ability of astronauts to assemble a modular tower structure in the shuttle bay using quick connect-disconnect jointed truss elements.

The complexity of assembly tooling required to fabricate the Domed Fresnel concentrator is similar to the tooling used to fabricate the 15 m diameter hoop-column reflector recently completed for NASA Langley Research Center (LaRC). Deployment testing of the concentrator in 1 g requires an off-loading fixture, since the DTS is not capable of deploying with the high surface weights. Fabrication of the raw lens panel material requires special tooling. Each of the seventeen lens strips requires a unique set of tools to produce the prismed plastic and to cut out the individual lens panels. Due to the symmetry of the surface design, these tools will, however, see extensive, repeated use. Assembly of the surface panels and hinges into completed lens strips involves repetition of a few simple steps.

The DTS structure is assembled by mating the twelve identical ribs to the hub. Prior to installation of the surface, repairs to these components are possible by replacing the affected assemblies. The surface is installed to the deployed structure one strip at a time. Complete lens strips can be replaced without disturbing other components. Removal of individual lens

panels within the strip would be difficult at best, due to the bonded construction, but could be attempted after removing the strip from the unit. Replacement of individual lens strips on orbit is very difficult and considering the nonrigid nature of the plastic lens surface, the cleaning or polishing of contaminated areas is not practical in flight.

Stowing the concentrator for transport requires "hands on" assistance to the surface and restraint mechanisms. As the DTS is closed, the deployment mechanism is stopped to allow manipulation of the surface onto the stowage skewers. Stowage continues in steps until the surface is fully under control and the restraint skewers have been connected. This level of activity would be prohibitive on orbit. The concentrator could, however, be closed without management of the surface and circumferential straps could be tightened around the DTS. The closed concentrator would then be placed into a shipping container for transport in the shuttle. The surface would certainly sustain some damage and it is possible that some structural elements of the DTS would be broken during landing. As an alternative to returning the concentrator from orbit, the stowed or deployed concentrator could be allowed to re-enter the earth's atmosphere and be consumed. This alternative may be desirable based on safety considerations.

The Domed Fresnel concentrator concept is compatible with either the ORC or CBC system thermal requirements. Receivers designed to accommodate the refractive optics may be needed to fully exploit the efficiency of the Domed Fresnel concentrator. The surface shaping and supporting DTS structure designs are easily fine tuned to accommodate the differences in optimal contours defined by the average refractive indexes of the materials being considered for the lens surface.

The optimal GCR's specified by ENTECH were 300 and 600 for the ORC and CBC systems, respectively. ENTECH's optimization included the thermal reradiation losses through the receiver apertures and resulted in minimum lens diameter that offered the maximum overall thermal efficiency possible for the Fresnel optics. The aperture diameters for the Boeing reference receivers are not commensurate with those recommended by ENTECH as optimal. The following table compares the aperture diameters.

Cycle	Receiver Aperture Diameters, m	
	ENTECH Recommendation	Boeing Reference
CBC	0.64	0.33
ORC	0.91	0.46

ENTECH performed calculations to determine the required lens diameter increase needed to compensate for the optical efficiency lost in accommodating the CBC reference receiver aperture. The concentrator diameter would have to grow from 14.8 to 16 m for the 45 degree AR coated case. Calculations were not performed for the ORC case, but would result in a similar diameter growth. Table 6.3-14 summarizes the significant design parameters and features of the Domed Fresnel concentrator concept.

Table 6.3-14. Domed Fresnel Concentrator

Summary of Concept Characteristics

Configuration	Baseline: Lens, ORC system Applicable to CBC systems		
Deployed Diameter	15.8 m (52 feet)		
Focal Length	13.1 m (43 feet)		
Stowed Package	Cylindrical: 1.8 m diameter x 2.0 m (71 inch x 79 inch) Volume: 5.1 m^3 (180 ft^3)		
Mass	Surface	190	(419)
	Support Structure	130	(287)
	Total	320 kg	(706 lbs)
Deployed Stiffness	>1 Hz		
Support Structure	12 rib, 6 segment DTS		
Surface Design	204 refractive lens strips 114 panels per gore in 17 strips 12 gores		
Deployment	Automatic with redundant drive motor (15 - 30 min) Manual override through drive mechanism only EVA for attachment of receiver support struts		
Maintainability	No replacement of lens panels or structure Insignificant degradation to surface from micrometeoroid/debris damage Slight system degradation from damage to tensioned members - low probability Lens adjustment on orbit is not possible		
Restow and Disposal	Structure can restow Structural lockup not practical Requires containment vessel for return		

Table 6.3-14. Domed Fresnel Concentrator (Continued)

Summary of Concept Characteristics

Complexity	High parts count in DTS structure Repeated assembly - 12 ribs
Reliability	Automatic deployment with single, central mechanism High tolerance for slope errors Deployment of surface has undetermined snag potential
Scalability/Growth	Cannot grow by addition of modules System design growth potential meets any projected Space Station requirement Design easily scalable to different sizes
Producibility	Surface material selection is uncertain Structural assembly and surface integration techniques well developed Surface manufacture and assembly techniques are defined but different from past experience More tooling required than Truss Hex
Receiver Compatibility	Must be fully integrated during surface design Flux tailoring by design No adjustment of completed assembly Optimized system has larger receiver aperture than current designs
Design Maturity	Conceptual design with demonstrated technology Domed Fresnel lens 15 m (50 ft) demonstration under construction DTS kinematic demonstration at Harris Needs development of lens material, surface shaping, and surface deployment control
Development Risk	Lens material not yet defined Deployment of lens surface is different from mesh antenna experience

6.4 Planar Fresnel - Conceptual Comparison

A conceptual comparison between a planar Fresnel and a domed Fresnel demonstrated the superiority of the domed Fresnel contour for the Space Station mission. The domed Fresnel concept uses a transmittance maximized prism geometry which also results in a smaller image size at the receiver aperture (higher concentration ratio) and greater tolerance to contour slope errors. Compared to a planar lens, the domed lens geometry reduces the spread in the image by 38 percent due to solar disk, 28 percent due to chromatic aberation and 62 percent due to prism manufacturing errors. For a 1° slope error the domed lens geometry produces a 0.01° exit ray angular deviation. The planar geometry produces a 1.75° deviation.

The planar Fresnel requires an f/D ratio of 1.0 or greater which is not compatible with proposed receiver designs. The longer focal length increases the percentage of flux intercepted on the receiver back wall, a nonheat transfer surface. The higher f/D results in a higher moment of inertia and reduced pointing error tolerance.

It appears that a planar Fresnel geometry could be easier to shape, support and possibly easier to package. However, no conceptual designs were developed for the planar concept since the domed concept has a very attractive shaping and support structure design provided by the DTS. The domed concept packages in a stowed volume 1.8 m in diameter and 2.0 m in length. There does not appear to be any advantages to further reduction from this stowed volume even if the planar concept could support the reduction. The cost, development and life cycle, of either concept, is unknown but both are driven by the development and performance of a transparent lens material capable of surviving the LEO environment.

The advantages and disadvantages of the planar and domed Fresnel concepts are summarized in Table 6.4-1. Reference 2 provides greater detail on performance of domed Fresnel geometry compared to other lens shapes and is the basis of this comparison.

Table 6.4-1. Summary of Fresnel Concepts

Evaluation Issue	Planar Fresnel	Domed Fresnel
Complexity	Possibly easier to shape and support	Attractive shaping and support provided by DTS
Stowed Volume	Possibly lowest stowed volume	Competitive stowed volume

Table 6.4-1. Summary of Fresnel Concepts (Continued)

Evaluation Issue	Planar Fresnel	Domed Fresnel
Optical Performance	Lower concentration ratio and transmittance, and lower tolerance to contour slope errors	Maximum transmittance, concentration ratio and greatest tolerance to slope errors
Receiver Compatibility	f/D $\geq$ 1.0 increases energy intercepted on back wall	f/D near 0.5 used for proposed receivers are achievable
System Moment of Inertia	Increased diameter, to accommodate lower efficiency, and high f/D results in large moment of inertia	Optimum efficiency and reduced f/D results in attractive moment of inertia
Pointing Error Tolerance	High f/D reduces tolerance	Low f/D and unique prism geometry provides greatest tolerance of any concept

7.0 MATERIALS EVALUATION

This section summarizes data from a series of tests performed to document the durability of solar concentrator materials in the low earth orbit environment. Primary emphasis was placed on identifying reflective and protective coatings for reflective concentrators and lens materials for a domed Fresnel refractive concentrator which would exhibit little or no degradation due to monoatomic oxygen exposure. Simulated atomic oxygen bombardment was accomplished in two ways. One set of samples was exposed at NASA Lewis Research Center in a Structure Probe Plasma Prep II plasma reactor. A second set of samples was exposed in the University of Toronto Institute for Aerospace Studies facility which utilizes an oxygen seeded carrier gas dissociated with microwave energy. Optical properties were characterized following exposure to determine the effect of exposure on total and specular reflectivity, total and specular transmittance, solar absorbance, and IR emissivity. Tests were also conducted to assess the impact of thermal cycling, micrometeoroid and debris impacts, and corrosive environments on sample integrity.

Paragraph 7.1 presents a brief overview of the low earth orbit (LEO) environment and identifies areas of concern relative to concentrator performance during its mission lifetime. Paragraphs 7.2 and 7.3 describe the areas addressed under Task 1, Subtask 2, and the test program, respectively. Representative test data are summarized in Paragraph 7.4; additional data can be found in Appendix B. Material concept selection trades are presented in Paragraph 7.5, and a task summary is presented in Paragraph 7.6.

7.1 Concentrator Environment

Materials used in solar dynamic power applications for the Space Station will require minimal degradation in the LEO environment during the defined 10 year system lifetime. Primary environmental concerns are summarized in Table 7.1-1, and consist of atomic oxygen impingement, thermal cycling, UV radiation, micrometeoroid and debris impacts, and vacuum outgassing of volatiles (reference 6). Each of these concerns is briefly discussed below.

7.1.1 Atomic Oxygen

Early STS flights (reference 7-9) experienced errosive degradation of thermal control blankets following short duration missions at low attitudes. The observed degradation was attributed to monoatomic oxygen which is the predominant atmospheric species at shuttle orbital altitudes. Figure 7.1-1 illustrates atmospheric composition as a function of altitude for several gaseous species. Although the number density is not high, being on the order of 10^9 cm^{-3}, the high velocity of the spacecraft (~8 km/sec) produces large fluxes on ram facing surfaces. Figure 7.1-2 shows atomic oxygen flux as a function of altitude and solar activity, assuming a nominal orbital velocity of 8 km/sec.

Table 7.1-1. LEO Environment Considerations for the Design of Solar Dynamic Power Systems

Environmental Parameter	Nominal Range of Parameter	Reason for Interest in Parameter
Vacuum	Pressure 10^{-11}-10^{-19}Pa	Vacuum outgassing results in loss of moisture and solvents resulting in dimensional and mechanical property changes
Ultraviolet	Wavelength 0.1-0.4 μm Intensity 1.4 kW/m^2	Degradation of coatings
Protons	Energy 0.1-4.0 MeV Flux 10^8 p+/cm^2 -sec	Degradation of coatings and surface plies of composites
Electrons	Energy 0.1-4.0 MeV Flux 10^8 e-/cm^2 -sec	Surface and bulk damage Spacecraft charging
Temperature Cycling	Material temperature 80K to 420K	Microcracking, thermal warping, deterioration of critical surfaces
Atomic Oxygen	Energy: 4-5 eV Flux: 10^{15}/cm^2 -sec	LEO degradation of thermal blankets and coatings
Micrometeoroid Debris	Size Range: 0.000006 cm to 2.0 cm	Concentrator surface damage Fluid line punctures

ATMOSPHERIC COMPOSITION AS A FUNCTION OF ALTITUDE IN LOW EARTH ORBIT

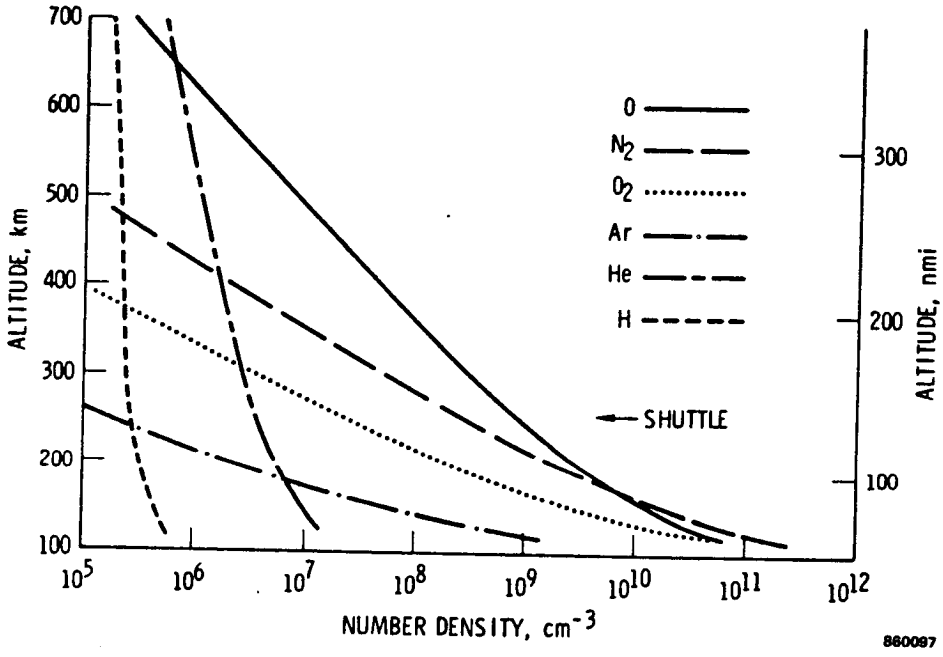

Figure 7.1-1. Atmospheric Composition as a Function of Orbital Altitude. Atomic Oxygen is the Dominant Species at Shuttle and Space Station Operational Altitudes.

ATMOSPHERIC ATOMIC OXYGEN DENSITY AS A
FUNCTION OF ALTITUDE IN LOW EARTH ORBIT

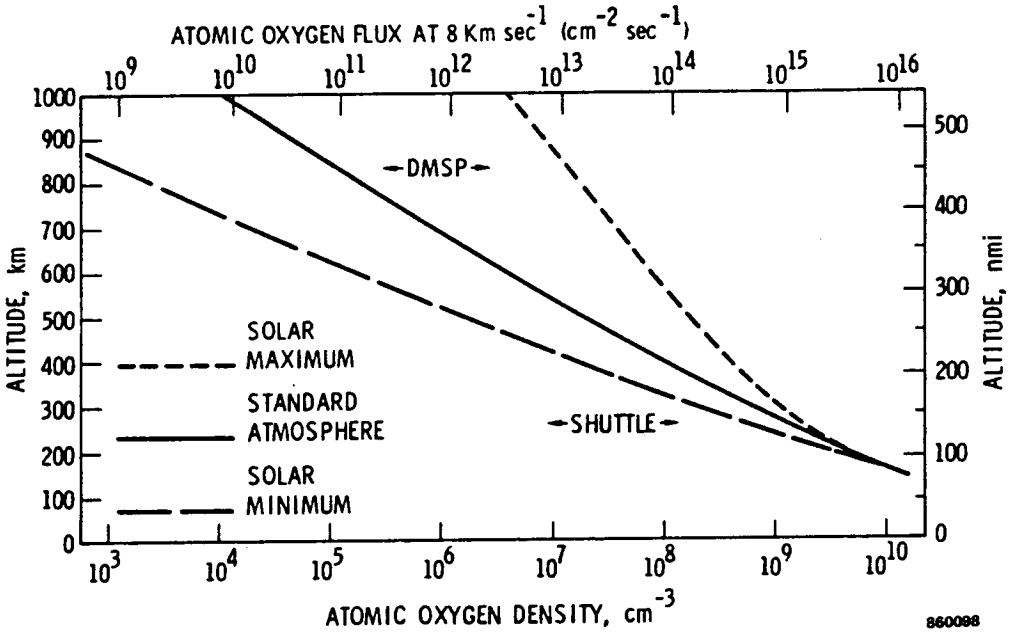

Figure 7.1-2. Atomic Oxygen Flux and Density as a Function of Altitude at Orbital Velocity of 8 km/sec

Dedicated atomic oxygen experiments were flow on STS-5 and STS-8 (reference 10-12) to document the effects of atomic oxygen flux on different materials. The primary effects noted were surface erosion and associated mass loss. In addition, changes in front surface optical properties occurred for many thermal control coatings and blankets. An increase in absorbance is generally observed with only a slight change, or no change, in emittance. Surface erosion of epoxy matrix composites was also noted indicating that structural members will also require protection.

Finally, it should be noted that the fluence (integrated flux) experienced by a given surface will be a strong function of several factors, including: a) orbital altitude and inclination, b) solar activity, c) impingement angle, and d) spacecraft geometry. Thus, a material may experience different mass loss rates depending on its location and orientation relative to the ram direction.

7.1.2 Thermal Cycling

Due to the relatively low orbit of the Space Station, the concentrator system will be exposed to the incident solar flux for only sixty minutes out of a total orbital period of slightly greater than ninety minutes. This exposure/eclipse cycling will result in a considerable number of thermal cycles for the structural components and optical surface during their operational lifetime. Preliminary analysis indicates that reflective concentrators can experience a temperature delta of 100° F or greater.

7.1.3 Ultra Violet Radiation

The ultra violet (UV) content of the air mass zero solar spectrum is much greater than that at the earth's surface due to the greatly reduced atmosphere. Figure 7.1-3 shows the solar spectrum at air mass zero. The UV portion of the incident solar flux is approximately six percent of the total flux, assuming the UV cut-off wavelength to be 375 nanometers. The enhanced UV flux presents a potential problem for graphite reinforced epoxy structures such as the concentrator facets and support structure. UV photons of certain wavelengths possess sufficient energy to cleave chemical bonds in epoxy materials, other organics, and some dielectric materials.

The enhanced solar UV flux also presents a potential problem for silver surface reflectors since silver is transparent to UV radiation. This could lead to decohesion at the silver/substrate interface or enhanced degradation of protective coatings. Aluminum coated reflectors are not as susceptible to this problem since aluminum is highly reflective in the UV portion of the spectrum.

7.1.4 Micrometeoroid and Debris Impacts

High velocity impacts from micrometeoroids and space debris could lead to severe degradation of optical surfaces or failure of structural components. Calculations based on NASA flux models indicate that damage will

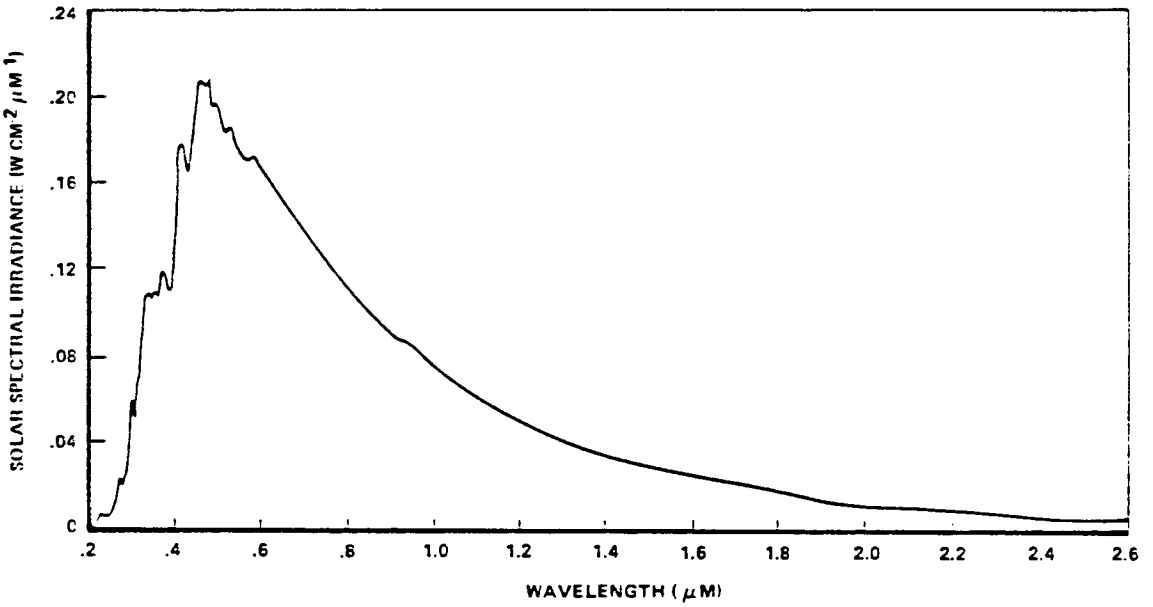

Figure 7.1-3. Air Mass Zero Solar Spectrum

be confined to a small percentage (< 0.01%) of the total concentrator surface area. Although this will have a negligible effect on the energy delivered to the receiver, the creation of pinholes in the surface may lead to an increase in the total damaged area due to other factors (e.g., atomic oxygen or contamination effects). Thus, the damage may not be limited to an area slightly larger than the diameter of the impinging particle. Similar calculations performed by LTV for Rocketdyne on the Phase B Work Package 4 program based on space debris profiles, indicate that the probability of impact from a large particle is very low.

7.1.5 Outgassed Species and Contaminants

The Space Station environment will also contain volatile species and contaminants originating from the orbiter and the station. Plumes produced by orbiter and station control thrusters could condense on the concentrator surface and lower performance. Should a pinhole be created by a particle impact, these contaminants could attack the surface in the presence of sufficient oxygen and increase the total damaged area. Although the volume of condensible species may be quite low, this area needs to be considered.

7.2 Areas of Investigation

The main objective of the materials evaluation task was to identify materials which would undergo minimal changes in optical properties due to LEO environmental effects. Efforts were thus focused in two general areas: reflective concepts and refractive concepts. For reflective surface concepts, the goal was to maximize end of life specular reflectance as this quantity directly determines the amount of energy delivered to the receiver. Three issues of concern were the reflector substrate, the reflective surface, and the protective overcoat. For the reflector substrate, several options were considered, including aluminum, glass, graphite reinforced glass, and graphite reinforced thermoset resins. Considerations included weight, fabrication methods, ease of fabrication, and cost. Also examined were various methods for depositing the reflective and protective coatings, including resistive heating evaporation, ion beam sputtering, electron beam sputtering for metals and dielectrics. Organic coatings, such as the silicones, were applied by brushing or spraying. Testing of substrates included mechanical and thermal properties, surface quality, and outgassing behavior. Coatings were evaluated for coverage, reflectivity, adhesion, and resistance to environmental degradation, both terrestrial and orbital.

For the Domed Fresnel refractive concept, the materials investigation focussed on three areas: 1) lens materials resistant to atomic oxygen degradation, 2) potential protective coatings, and 3) manufacturing methods. The initial part of the investigation concentrated on identifying materials with the necessary optical properties (e.g., index of refraction, chromatic dispersion) to function as a lens. The next step was to generate data on the degradation of these materials in the LEO environment. Because early test data indicated that single component lens elements might not function satisfactorily, protective coatings and hybrid lens systems were also examined.

7.3 Test Program

The main objective of the materials evaluation task was to identify materials for solar concentrator applications and then generate as much data as possible on the environmental effects of low earth orbit on the performance of these materials. A summary of the test program followed is presented in the following sections.

7.3.1 Atomic Oxygen Exposure

Samples were exposed to atomic oxygen by two different methods. At NASA Lewis Research Center, samples were placed inside the reaction chamber of a Structure Probe, Inc. Plasma Prep II plasma reactor. This device creates a simulated atomic oxygen environment by passing a carrier gas (air in this case) over the samples and then exiting the oxygen molecules with approximately 100 watts of continuous wave RF power at 13.56 MHz. The resulting environment contains a number of species including molecular oxygen, atomic oxygen, and oxygen radicals. The operating pressure for all tests was kept at 50 microns. While it is difficult to calculate or estimate the resultant flux accurately, estimates have been made based on kapton erosion data from the asher and STS experiments that 16 asher hours approximate one year in LEO in terms of total fluence.

Similar samples were exposed in the atomic oxygen test facility at the University of Toronto Institute for Aerospace Studies. This facility utilizes an oxygen seeded carrier gas (argon or helium) released into a quartz tuning cavity in which microwave energy partially dissociates the oxygen. The monoatomic oxygen is then passed into an evacuated sample chamber where it impinges on the sample at a normal angle of incidence. The microwave generator was run at 2450 MHz and 20-200 W which resulted in an approximate flux of 10^{15} atoms/cm^2-sec at an average velocity of 1.2 km/sec with oxygen atom translational energies on the order of 0.14 eV. While the flux is representative of that at an altitude of 200-220 nautical miles ($\sim$400 km) the energy is significantly lower than the 4.2 eV in actual LEO. The samples were positioned $\sim$3 cm from the nozzle source resulting in an exposed surface area of 0.78 cm^2.

7.3.2 Optical Property Characterization

Spectral transmittance and reflectance measurements were made using a Perkin Elmer Lambda 9 UV/VISIBLE/NEAR IR spectrophotometer equipped with a 60 mm diameter $BaSO_4$ coated integrating sphere. The wavelength range evaluated extended from 200 nm to 2500 nm. Specular reflectances were obtained by placing the sample over the sample port of the sphere and trapping out the specularly reflected light with a trap. The angle of incidence was 8° from the normal. Total reflectances were measured by replacing the light trap with a $BaSO_4$ coated blank to re-reflect the light back into the sphere. Solar reflectances (specular and total) were obtained by convoluting the air mass zero solar spectrum (reference 13) into the experimentally obtained reflectance spectrum (reference 14-15) according to the following expression:

$$\overline{\rho} = \frac{\int_{\lambda}^{\lambda 2} \rho(\lambda)\, Q(\lambda)\, d(\lambda)}{Q(\lambda)\, d(\lambda)} \qquad (1)$$

where $\overline{\rho}$ is the integrated solar reflectance (specular or total), $\rho(\lambda)$ is the reflectance at wavelength λ, and $Q(\lambda)$ is the air mass zero intensity at wavelength λ. The above calculations were performed automatically by computer which corrected for the reflectance of the $BaSO_4$ (reference 16).

Spectral transmittances were obtained in similar fashion, except that the samples were placed over the entrance port of the sphere for total transmittance measurement, and in the regular sample compartment of the spectrophotometer for specular transmittance measurement. Solar transmittances were obtained using equation (1) by replacing the reflectance with transmittance.

7.3.3 Thermal Cycling Tests

Two thermal cycling tests were conducted to document the behavior of the materials under extreme temperature conditions. The first test was done using a Delta thermal chamber with a nominal cycle time of ten minutes (five minutes hot, five minutes cold). The temperature range extended from -65° C (-85° F) to +100° C (+212° F). Samples were cycled for times ranging from 24 to 120 hours for a maximum of 720 cycles. The second test was a thermal shock in which samples were immersed in liquid nitrogen for five minutes, held at room temperature for ten minutes, placed in a preheated oven for five minutes, and then back to room temperature for ten minutes for a total cycle time of thirty minutes. Samples were cycled for a total of twenty-five cycles.

7.3.4 Micrometeoroid Impact Simulation

A series of samples were exposed to a grit blast using 27 micron alumina at a velocity of 1100 ft/sec to study the effects of micrometeoroid impacts on sample integrity. The impact energy of the incident particles was sufficient to break through the protective outer coatings on the solid surface reflector samples. Following the exposure to the grit blast, the samples were placed in the plasma asher to determine the effects of atomic oxygen impingement on areas of sample surface cracked by the grit blast exposure. Sample surface morphology was documented following atomic oxygen exposure using SEM.

7.3.5 Composite Testing

Sample composite laminates fabricated for substrate applications were tested in tension to determine strength and modulus. Coefficient of thermal expansion (CTE) for sample laminates was also measured using Differential Thermal Analysis (DTA).

7.3.6 Coating Adhesion Evaluation

The adherence of reflective coatings to the substrate and protective coatings to the reflective layers was tested in accordance with ASTM standard D-3359-83. This test involves cutting a grid pattern approximately 16 mm by 16 mm on the surface of the sample to be tested, firmly applying a high peel strength tape, and rapidly pulling back the tape at an angle of 180° to the surface. Adhesion is classified from 5B to 0B, where 5B indicates no decohesion and 0B indicates greater than 65% surface loss over the test area.

7.4 Material Test Results

Representative test data are summarized below for the experiments described in Section 7.3. A complete compilation of data generated during the materials evaluation task is provided as Appendix B under separate cover.

7.4.1 Atomic Oxygen Effects on Optical Properties

A number of reflective samples were fabricated and tested using various combinations of reflective and protective coatings. Table 7.4-1 summarizes reflective and protective coatings evaluated during subtask 2. Reflective surfaces were selected based on their reflectivity in the solar spectrum. Figure 7.4-1 shows the spectral reflectance of several metals superimposed on the air mass zero solar spectrum. As is evident, silver and aluminum provide the highest total reflectance in the wavelength range of interest (200 to 2500 nanometers). Copper is very reflective for wavelengths greater than 700 nanometers, but falls off sharply in the visible spectrum. This results in a lower integrated reflectance than silver or aluminum. Platinum and rhodium are also highly reflective but again are far below silver and aluminum in the high energy region of the solar spectrum. For the series of experiments conducted in this study, silver and aluminum were selected as the best candidate reflective materials.

Table 7.4-1. Candidate Reflective and Protective Materials for the Truss Hex and Splined Radial Panel Concepts

Reflective Surface	Protective Coatings
Silver	RTV Silicones
Aluminum	Magnesium Fluoride
Aluminum/Silver	SiO_x
Gold	ITO
Copper	Si_3N_4
Nickel	Al_2O_3
Chromium	SiO_x/PTFE
Platinum	MgF_2/PTFE
	PTFE

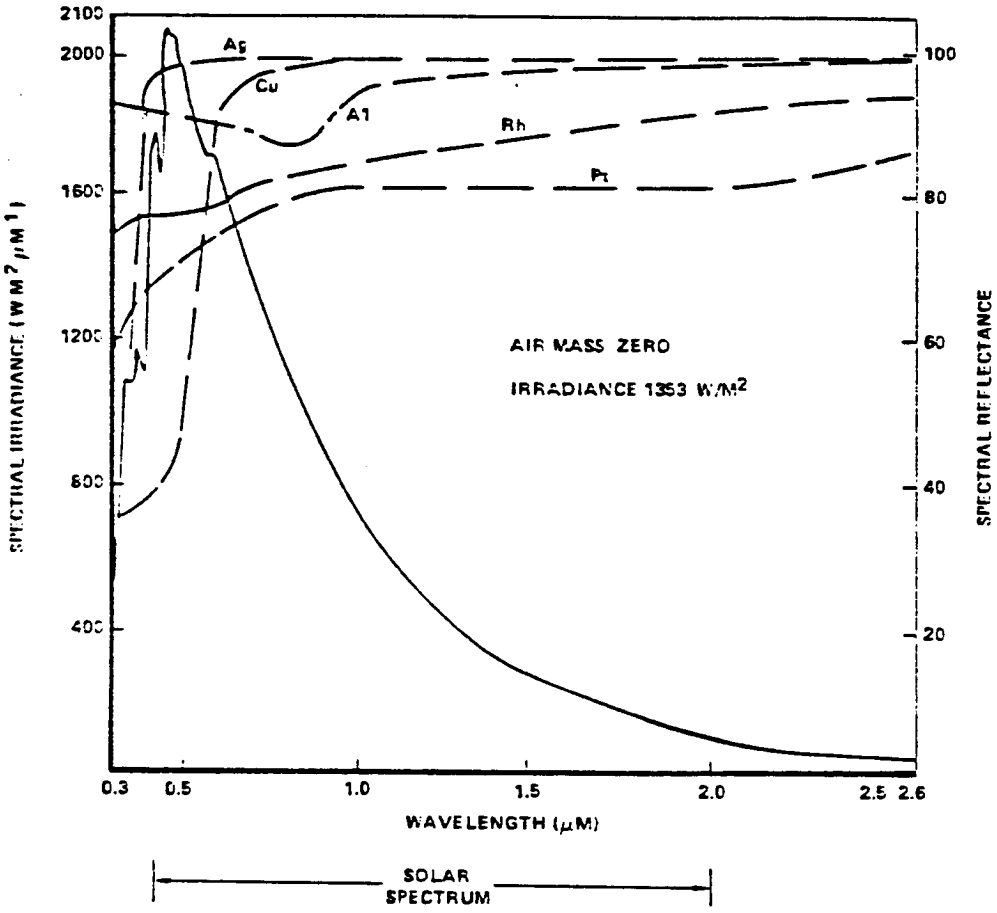

Figure 7.4-1. Spectral Reflectance of Various Metals Relative to Incident Solar Spectrum

Deposition of the reflective layer was initially done using both resistive heating vapor deposition and ion beam sputtering. Both methods result in highly reflective surfaces when glass substrates are used. Vapor deposited surfaces typically yield slightly higher reflectance values, however, the difference was less than 2 percent. When graphite reinforced epoxy substrates were used, it was difficult to effectively deposit the reflective layer using ion beam sputtering. Substrate heating during the deposition resulted in warping and degradation of the composite. This effect was not encountered with vapor deposition, which was used whenever possible. Compounds requiring sputtering, such as SiO_x and ITO, were done carefully at the lowest beam power level which produced reasonable films and kept substrate heating to a minimum.

Reflectance data for aluminum and silver samples exposed to atomic oxygen are summarized in Tables 7.4-2 and 7.4-3, respectively. The silver samples result in higher integrated reflectance values than aluminum samples with equivalent coatings. The data indicates that high specular reflectance values can be achieved and maintained despite the impinging oxygen atoms. For aluminum, measured specular reflectances ranged from a high of .910 for the MgF_2 coated sample to a low of .805 for the sample coated with RTV 655. Silver samples consistently yielded specular reflectance values above .90 following atomic oxygen exposure. As was the case with the aluminum, the RTV coated sample proved to be the poorest reflector following atomic oxygen exposure falling from an initial value of .940 to .840 following 151 asher hours. Samples coated with SiO_x, ITO, and/or MgF_2 showed excellent resistance to atomic oxygen degradation, even after 634 asher hours. Calculations indicate that 16 asher hours simulate the fluence experienced by a ram facing surface during one year in LEO, so that some samples were exposed to a fluence equivalent to over thirty years in LEO.

Typical reflectance curves showing specular and total reflectance as a function of exposure time are shown in Figure 7.4-2 through 7.4-8. Figures 7.4-2 and 7.4-3 compare silver samples protected with SiO_x on two different substrates, glass and graphite reinforced epoxy. In both cases, there is an initial decrease in the specular and total reflectance followed by a leveling out of the curves at a consistent value and little or no subsequent change. It was noted that samples fabricated using glass substrates typically yielded reflectance values higher than equivalent samples formed on graphite/epoxy substrates. With careful preparation of the substrate, however, similar reflectances could be obtained on composite structures indicating that the specular reflectance obtained from a given sample is a strong function of the initial surface morphology. This is an important fact considering the significant difference in density between glass (2.20 g/cc for ultra-low expansion glass) and graphite reinforced epoxy ($\sim$1.61 g/cc). The ability to fabricate optical quality composite substrates will result in a considerable savings in concentrator total weight. Substrate trades are discussed further in Section 7.5.

Table 7.4-2. Reflectance Data for Aluminum Samples with Various Protective Coatings Before and After Asher Exposure

				Reflectance*			
Substrate	R	P	Asher Hours	Start Total	Start Specular	Finish Total	Finish Specular
Glass	Al	SiO_x	634	0.912	0.891	0.904	0.879
Glass	Al	SiO_x/MgF_2	634	0.906	0.882	0.859	0.834
Glass	Al	ITO	225	0.858	0.850	0.852	0.844
Glass	Al	ITO/MgF_2	225	0.854	0.847	0.822	0.815
GFRP	Al	SiO_x	180	0.875	0.868	0.858	0.851
GFRP	Al	MgF_2	180	0.945	0.925	0.940	0.910
GFRP	Al	RTV655	151	0.935	0.905	0.850	0.805

*Measured over 200 nm to 2500 nm
R - Reflective Surface, P - Protective Surface, RTV655 - GE Silicone
GFRP - Graphite Fiber Reinforced Epoxy

Table 7.4-3. Reflectance Data for Silver Samples with Various Protective Coatings Before and After Asher Exposure

				Reflectance*			
Substrate	R	P	Asher Hours	Start Total	Start Specular	Finish Total	Finish Specular
Glass	Ag	SiO_x	634	0.978	0.972	0.958	0.937
Glass	Ag	SiO_x/MgF_2	634	0.978	0.970	0.943	0.927
Glass	Ag	ITO	225	0.905	0.899	0.914	0.908
Glass	Ag	ITO/MgF_2	225	0.932	0.925	0.909	0.902
G_R/E_P	Ag	SiO_x/MgF_2	180	0.955	0.940	0.930	0.915
GFRP	Ag	SiO_x	180	0.975	0.945	0.945	0.910
GFRP	Ag	MgF_2	180	0.955	0.930	0.955	0.925
GFRP	Ag	RTV655	151	0.965	0.940	0.905	0.840

*Measured over 200 nm to 2500 nm
R - Reflective Surface, P - Protective Surface, RTV655 - GE Silicone
GFRP - Graphite Fiber Reinforced Epoxy

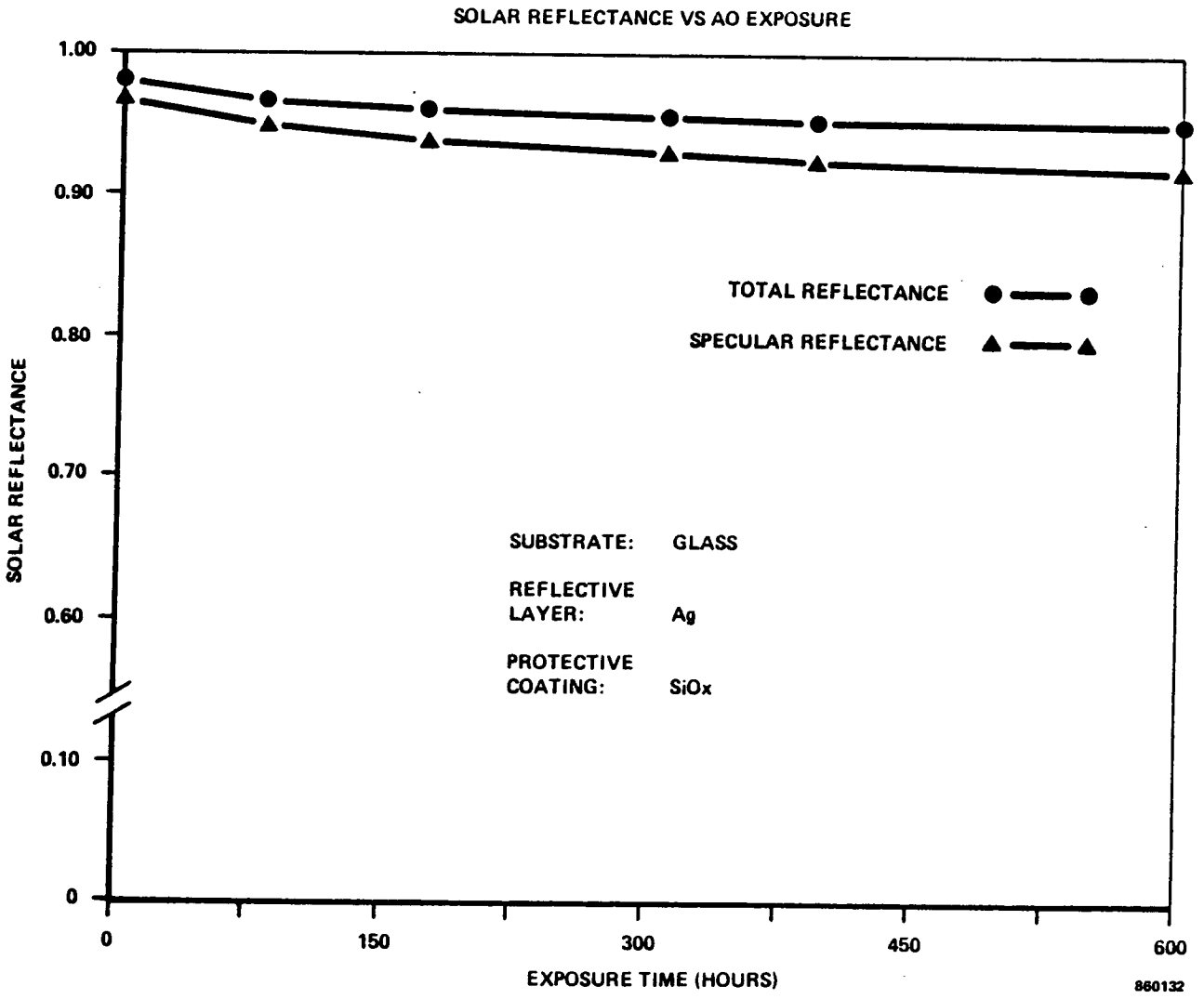

Figure 7.4-2. Total and Specular Reflectance as a Function of Atomic Oxygen Exposure Time for Silver Coated with SiO_x (Glass Substrate)

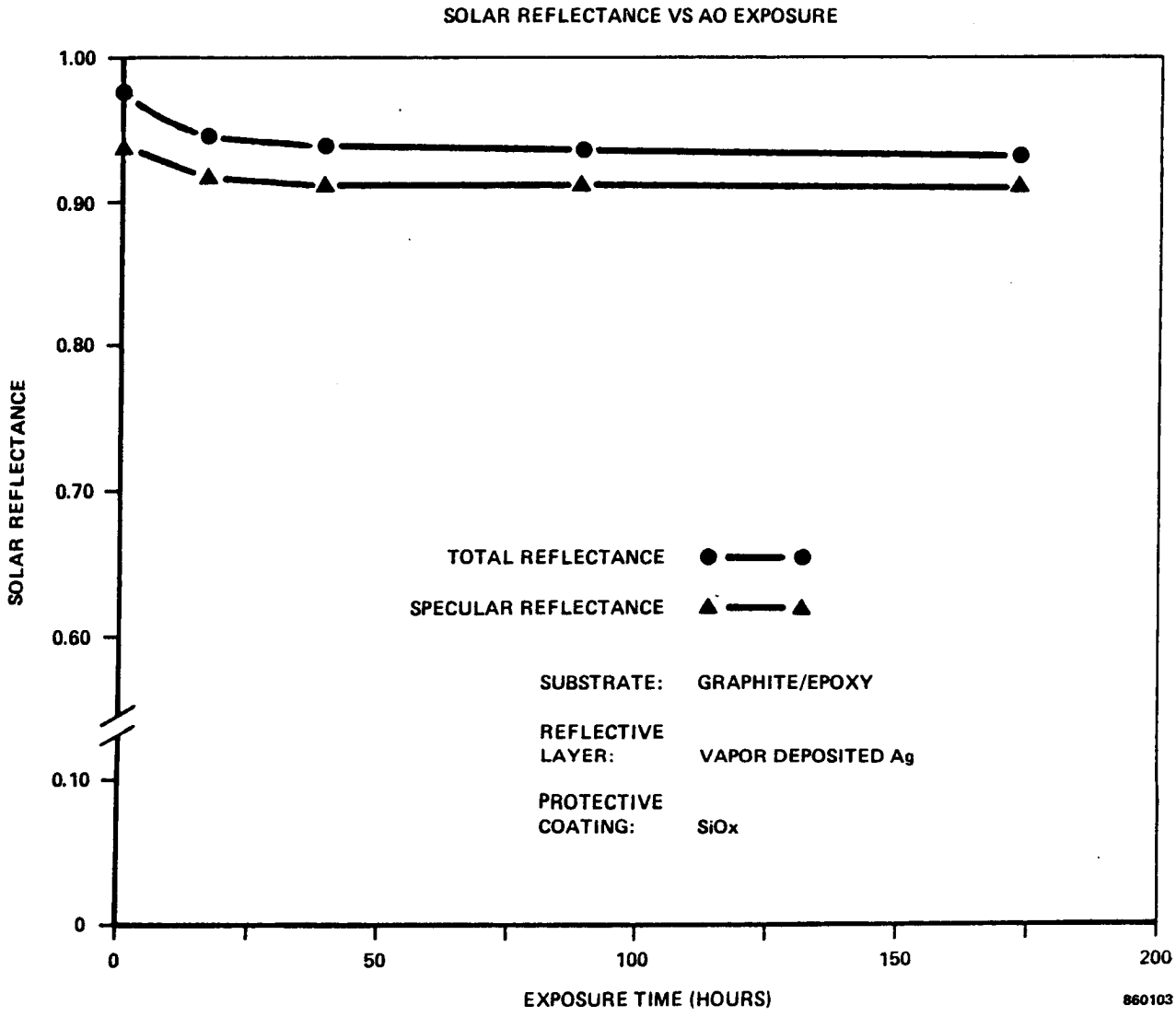

Figure 7.4-3. Total and Specular Reflectance as a Function of Atomic Oxygen Exposure Time for Silver Coated with SiO_x (GFRP Substrate)

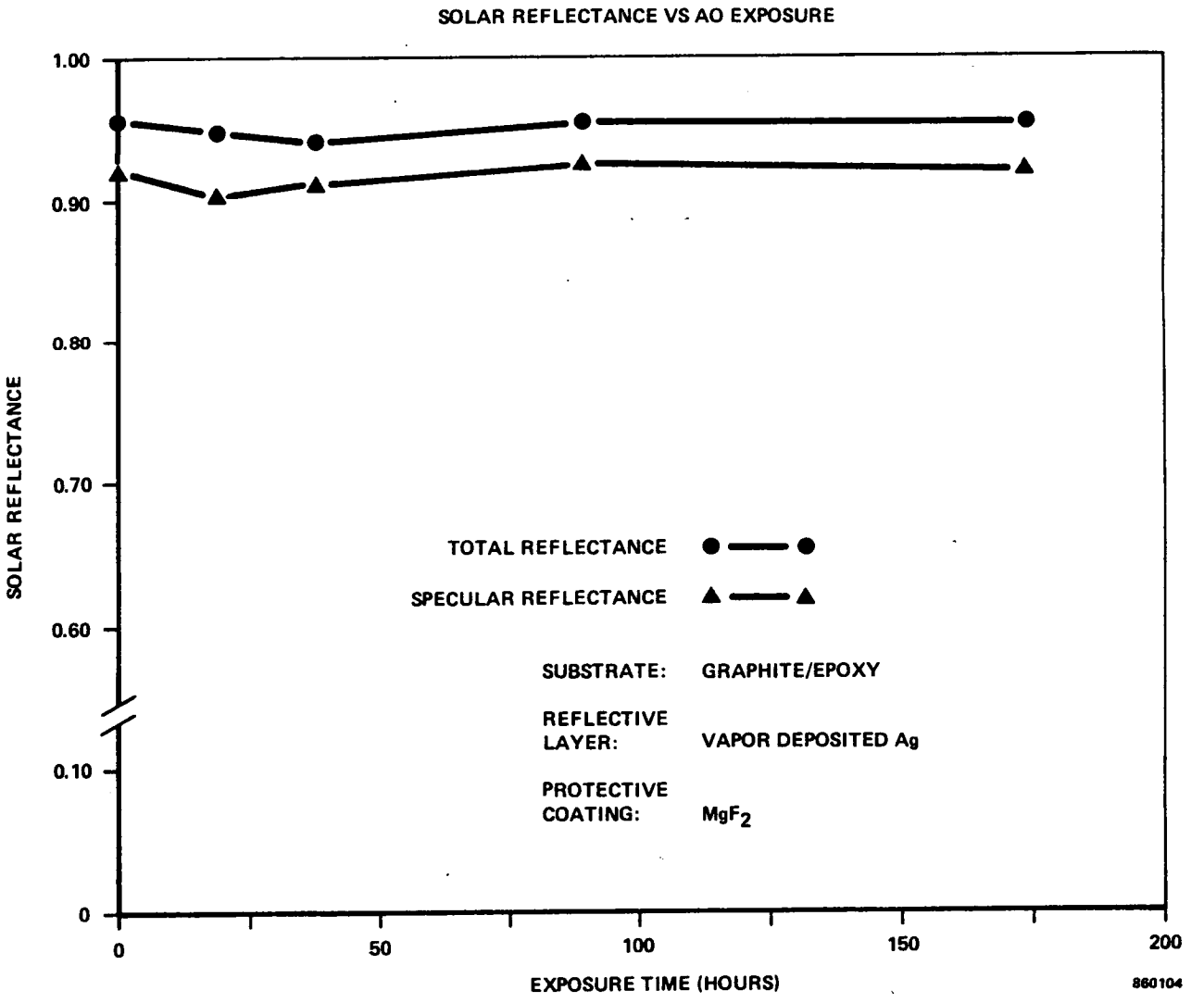

Figure 7.4-4. Total and Specular Reflectance as a Function of Atomic Oxygen Exposure Time for Silver Coated with MgF_2 (GFRP Substrate)

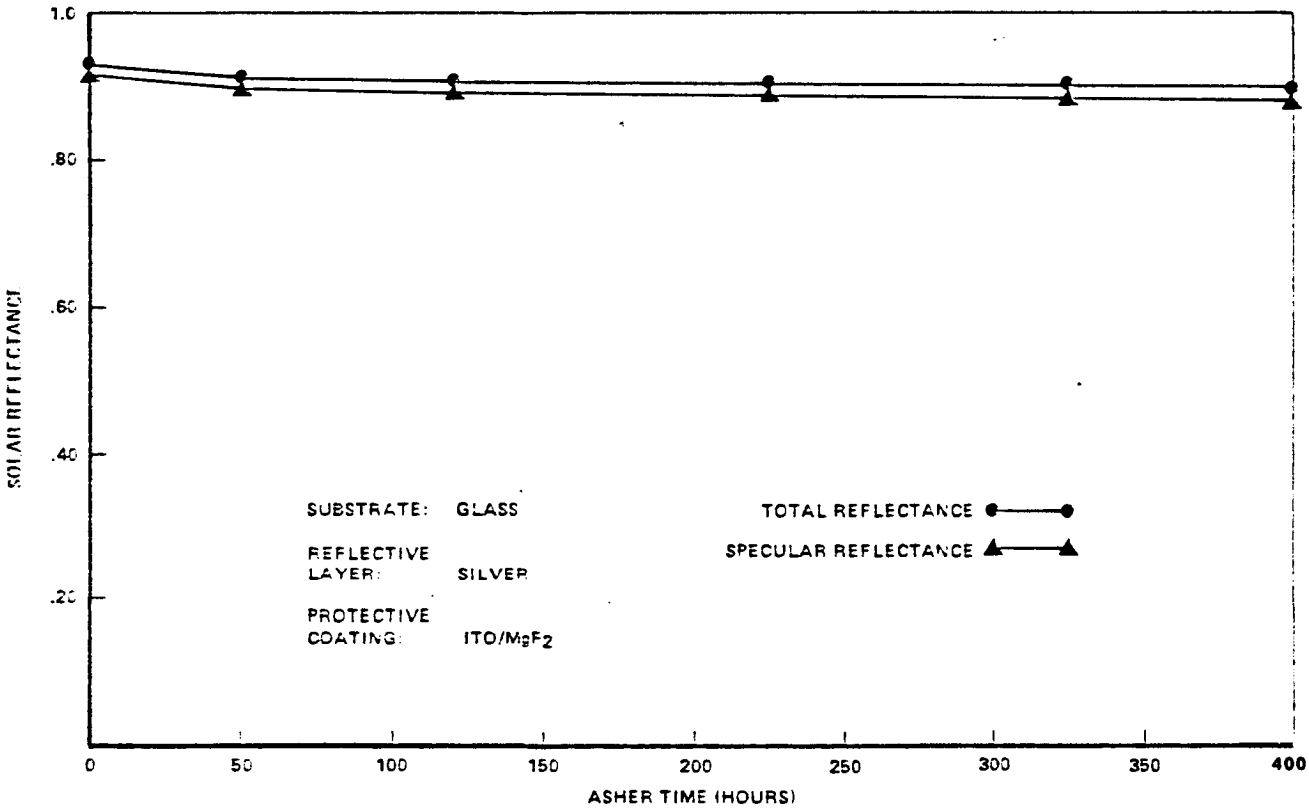

Figure 7.4-5. Total and Specular Reflectance as a Function of Atomic Oxygen Exposure Time for Silver Coated with ITO and MgF_2 (Glass Substrate)

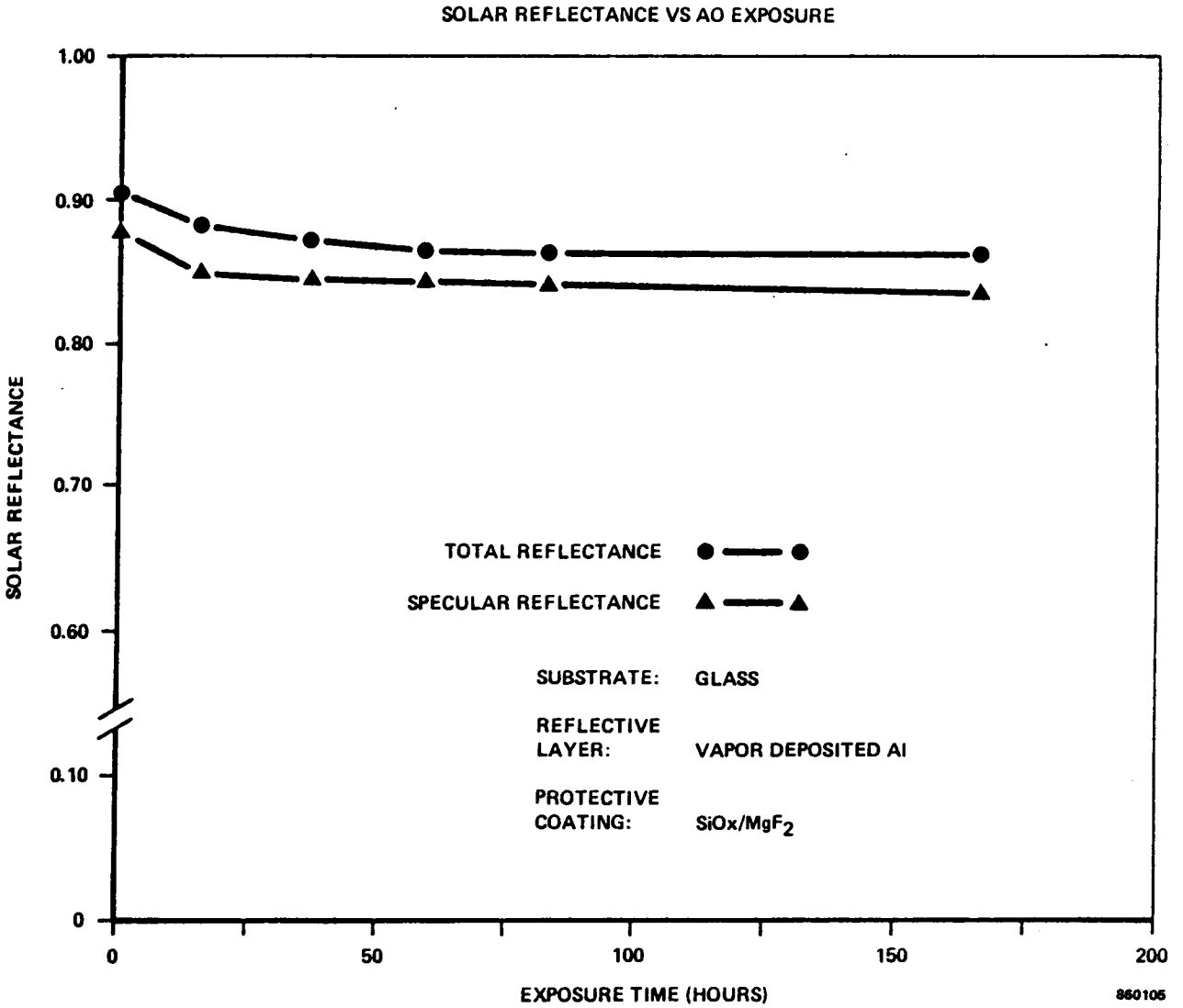

Figure 7.4-6. Total and Specular Reflectance as a Function of Atomic Oxygen Exposure Time for Aluminum Coated with SiO_x and MgF_2 (Glass Substrate)

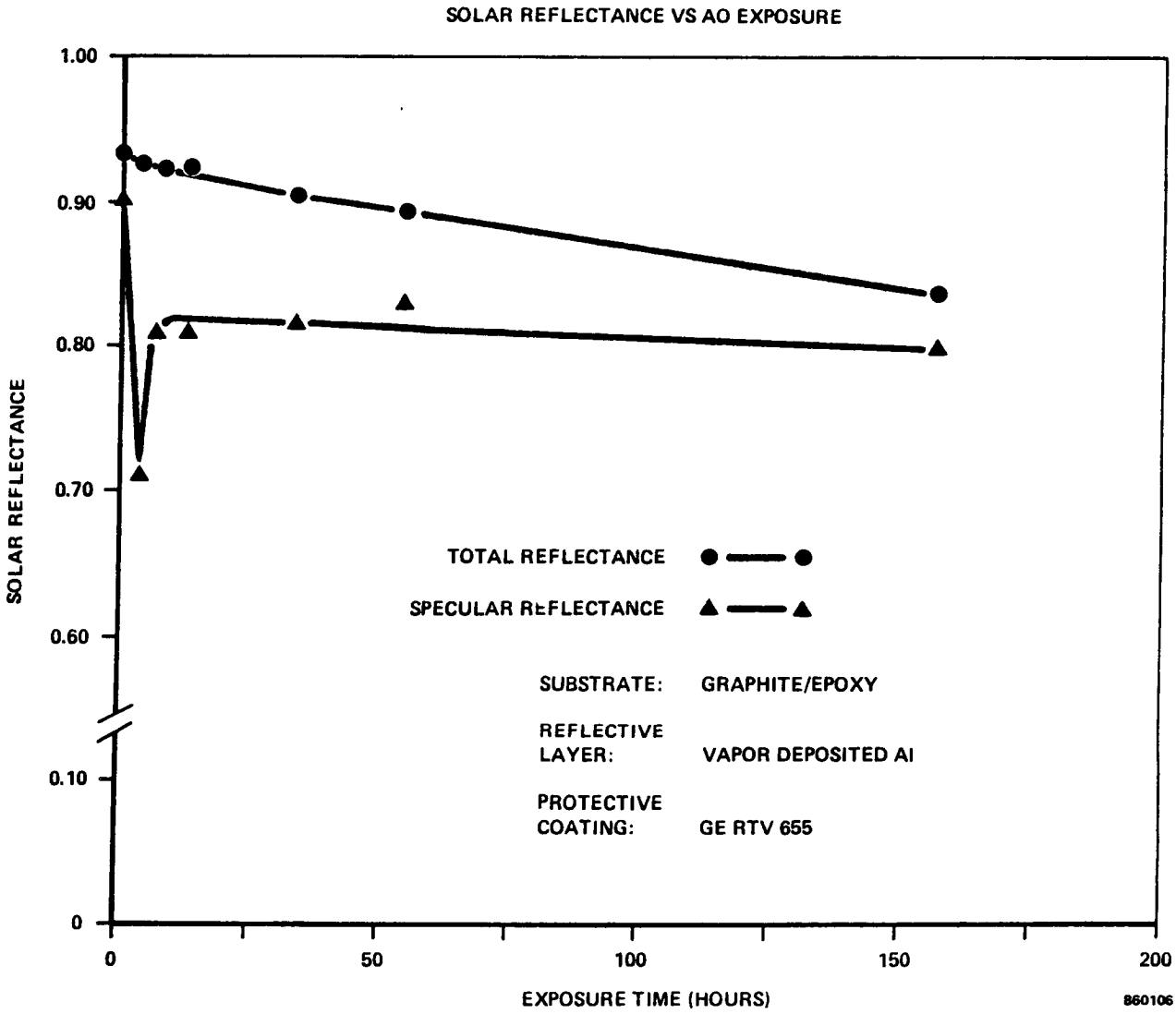

Figure 7.4-7. Total and Specular Reflectance as a Function of Atomic Oxygen Exposure Time for Aluminum Coated with ITO (Glass Substrate)

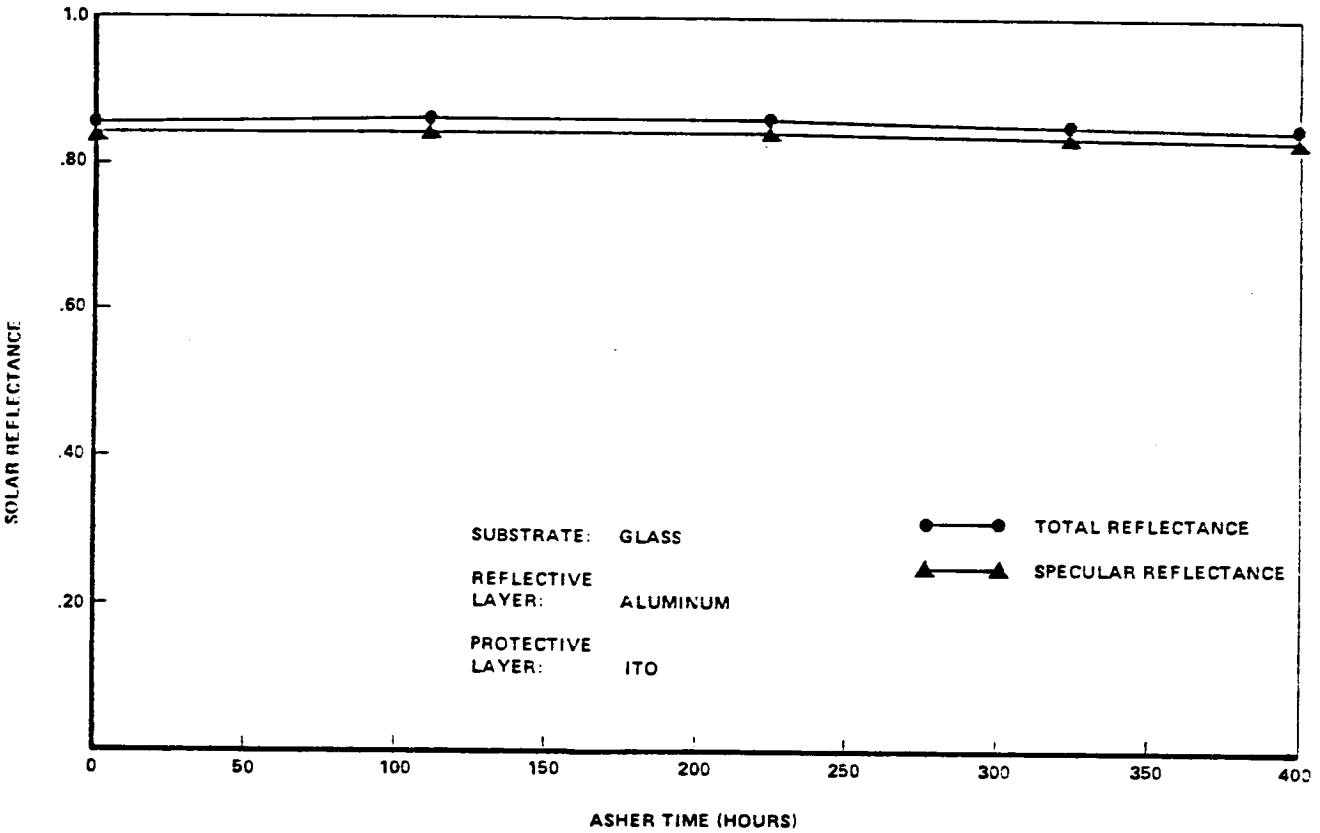

Figure 7.4-8. Total and Specular Reflectance as a Function of Atomic Oxygen Exposure Time for Aluminum Coated with RTV 655 (GFRP Substrate)

Figure 7.4-4 shows specular and total reflectance for a silver sample protected with magnesium fluoride. This material is used commercially for a number of optical applications, including an anti-reflection coating on binocular and camera lenses. The end of life specular reflectance, 0.925, was slightly higher than the SiO_x sample. An attractive aspect of MgF_2 is that is can be vapor deposited. This means that successive depositions can be done without breaking the chamber vacuum and creating the possibility of producing an oxide layer at the interface between the reflective layer and the protective coating. This is important for silver surfaces which exhibit poor bonding to metallic oxides.

Finally, Figure 7.4-5 shows the reflectance behavior of a silver sample coated with a combination of indium tin oxide and magnesium fluoride. The integrated end of life reflectance values were slightly lower than the other coatings, however, there was very little change in the reflectance after the first fifty hours of exposure. For this sample, the ITO was ion beam sputtered, however, it was difficult to identify precisely the stoichiometry of the deposited material. Analysis of the coating alone indicated the presence of tin, but no indium was found. Similar samples analyzed by Georgia Tech contained no evidence of indium or tin, but were found to have an SiOx layer instead. Both samples were produced using the same target, which could be poor. This discrepancy is still being addressed.

Figure 7.4-6 shows the behavior of an aluminum sample protected with SiO_x and MgF_2. Following 634 hours of asher exposure, the specular reflectance was measured to be .834, a decrease of 7.9 percent from the initial specular reflectance value. The comparable silver sample had a specular reflectance of .927 after the same exposure time which represents a decrease of 4.4 percent from its initial specular reflectance value. This trend was observed for all comparable aluminum and silver samples; the silver samples showed the highest reflectance independent of the coating type for similar samples.

The highest post atomic oxygen exposure specular reflectance for a sample with an aluminum reflective surface was obtained with a magnesium fluoride protective overcoat. Figure 7.4-7 shows total and specular reflectance for this sample as a function of exposure time. The sample showed a slight decrease in total and specular reflectance during the first fifty hours of exposure. During continued exposure, these values gradually increased to near their starting point. The specular reflectance following 180 hours of exposure was .910 and the total reflectance .940.

Two samples were fabricated on graphite/epoxy using RTV silicone 655 (GE) as the protective overcoat. Figure 7.4-8 shows the behavior of the aluminum sample during 151 hours of exposure; the silver sample resulted in a similar curve, although the reflectance values were slightly higher. The total reflectance curve decreases gradually from a starting value of .935 to .850 at the end of the experiment. The specular reflectance curve decreases drastically after just five hours of exposure, and then returned to above .800 where it remained. The sharp decrease in specular reflectance is due to mass loss and erosion of the RTV 655. Scanning electron micrographs of the surface

following exposure show considerable cracking and roughening of the silicone as a result of the atomic oxygen impingement.

Mass loss data for various reflective samples are summarized in Table 7.4-4. There was no discernible change in the mass of samples deposited on glass substrates with SiO_x, MgF_2, ITO, or combinations as the protective coating. Comparable samples on graphite/epoxy substrates did however show very small losses. This is due to the outgassing of volatiles from the epoxy in the sample chamber vacuum, and not the erosion of the protective coatings. This has been confirmed by independent outgas testing of the substrate material in accordance with ASTM 595-83.

Table 7.4-4. Mass Loss Data for Selected Reflective Samples Following Atomic Oxygen Exposure

SAMPLE	EXPOSED MATERIAL	EXPOSURE TIME (HRS)	INITIAL MASS LOSS (g)	FINAL* MASS LOSS (g)
GFRP/Ag/MgF_2	GFRP	168	1.781×10^{-3}	1.102×10^{-3}
GFRP/Ag/SiO_2	SiO_2	167	1.192×10^{-3}	4.51×10^{-4}
GFRP/Ag/MgF_2	MgF_2	168	7.62×10^{-4}	1.78×10^{-4}
GFRP/Ag/RTV655	RTV655	167	1.014×10^{-3}	9.47×10^{-4}
GFRP/Al/RTV655	RTV655	169	1.248×10^{-3}	$.738 \times 10^{-3}$
GFRP/Al/MgF_2	MgF_2	168	1.119×10^{-3}	$.57 \times 10^{-3}$
Peek	Peek	167	5.2×10^{-4}	2×10^{-4}
Glass/Al/SiO_2	SiO_2	167	6.0×10^{-5}	6.0×10^{-5}
Glass/Ag/ITO	ITO	166	0	0
Glass/Al/SiO_2/MgF_2	MgF_2	167	0	0
Glass/Ag/SiO_2/MgF_2	MgF_2	162	0	0
Glass/Ag/ITO/MgF_2	MgF_2	166	0	0

*After allowing sample to reabsorb moisture under ambient laboratory conditions

Table 7.4-5 summarizes total and specular transmittance data for candidate Fresnel lens materials exposed in the plasma asher. The asher was found to degrade organic materials more rapidly that the inorganic protective coatings evaluated for the reflective samples. All samples tested showed unacceptable mass loss and degradation of optical properties as a result of atomic oxygen impingement. Mass loss is summarized in Table 7.4-6. Sample curves are shown in Figures 7.4-9 through 7.4-11 for DC 93-500 silicone, Lexan UV stabilized polycarbonate, and FEP teflon, respectively. Four silicones were studied, each resulting in a transmittance curve similar to the one in Figure 7.4-9 for the DC 93-500. The total transmittance decreases gradually

Table 7.4-5. Total and Specular Transmittance Data for Lens Materials Coated with MgF_2

			TRANSMITTANCE			
MATERIAL	COATING*	ASHER HOURS	START TOTAL	START SPECULAR	FINISH TOTAL	FINISH SPECULAR
FEP	MgF_2	21.5	0.936	0.894	0.940	0.679
PFA	MgF_2	21.5	0.916	0.862	0.903	0.773
ETFE	MgF_2	21.5	0.897	0.858	0.889	0.119
LEXAN	MgF_2	21.5	0.858	0.859	0.798	0.056

*1000 Å on both sides of sample; transmittance measured from 200 nm to 2500 nm

Table 7.4-6. Mass Loss Data for Candidate Fresnel Lens Materials

	Polymer Mass Loss Data				
SAMPLE	INITIAL MASS	INITIAL THICKNESS	FINAL MASS	FINAL THICKNESS	ASHER HOURS
KEL-F	1.0100 g	0.86 mm	0.8488 g	0.76 mm	117
LEXAN PC	0.4077 g	0.25 mm	0.1098 g	0.11 mm	117
ETFE	0.2146 g		0.1374 g		46.5
PFA	0.2881 g		0.2267 g		46.5
FEP	0.2413 g		0.1820 g		46.5

Table 7.4-7. Total and Specular Transmission Data for Candidate Domed Fresnel Concentrator Lens Materials

Substrate	Asher Hours	Start Total*	Start Specular*	Finish Total*	Finish Specular*
SILICONES					
RTV615	214	0.910	0.845	0.830	0.640
RTV655	214	0.910	0.850	0.840	0.635
RTV670	214	0.880	0.810	0.840	0.725
DC 93-500	214	0.890	0.780	0.830	0.650

Table 7.4-7. Total and Specular Transmission Data for Candidate Domed Fresnel Concentrator Lens Materials (Continued)

Substrate	Asher Hours	Start Total*	Start Specular*	Finish Total*	Finish Specular*
FLUOROPOLYMERS					
ETFE	151	0.891	0.830	0.933	0.492
PFA	151	0.926	0.867	0.948	0.553
FEP (A)	151	0.937	0.900	0.952	0.602
KEL-F	168	0.918	0.885	0.947	0.430
OTHER ORGANICS					
LEXAN PC	117	0.825	0.825	0.842	0.728
UVA-11 Acrylic	21.5	0.845	0.838	0.872	0.393

*Transmittance Values measured over 200 nm to 2500 nm

with increased exposure time whereas the specular transmittance drops rapidly during the first 50 hours of exposure and then levels out at a roughly constant value.

Figure 7.4-10 shows transmittance as a function of exposure time for the UV stabilized polycarbonate. The total transmittance increases slightly during the exposure period whereas the specular component of the transmitted light decreases. Similar behavior is observed for the fluoropolymers tested. Figure 7.4-11 shows transmittance of FEP teflon as a function of exposure time. As with the Lexan sample, the total transmittance increases as the exposure time is increased. The specular transmittance decreases gradually with increasing exposure time. This behavior can be accounted for based on the primary effects of the oxygen plasma, namely surface erosion and subsequent mass loss. As the plasma interacts with the surface of the sample, mass is removed non-uniformly producing a rough surface. This causes the total transmission to increase for two reasons. First, the sample is becoming thinner decreasing the mass thickness which the light must transverse and thus increasing transmittance. Second, the increased surface roughness decreases the amount of light reflected by the sample surface thus making the sample appear cloudy and increasing total transmission. The surface roughening produced by the atomic oxygen also produces the decrease observed in the specular transmittance. This occurs due to the light being scattered more strongly as a result of the non-uniform surface structure.

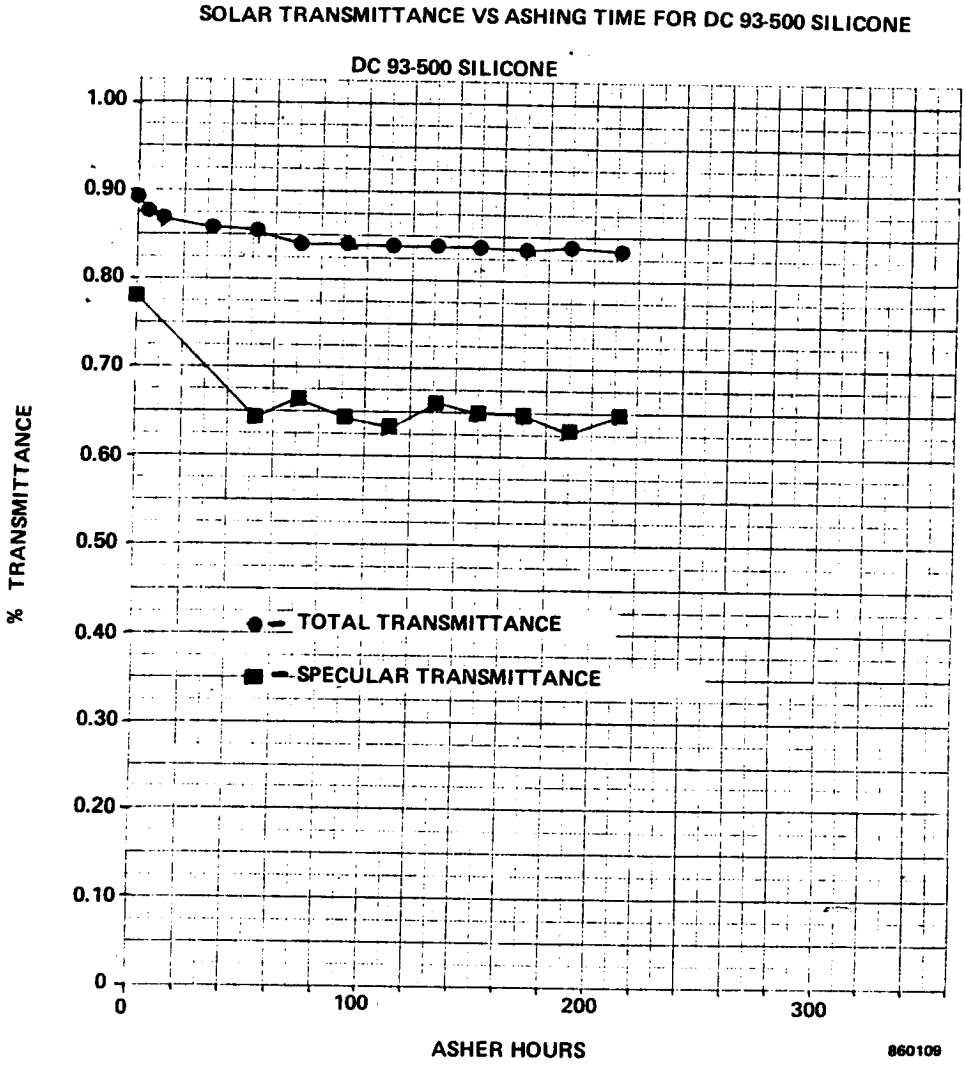

Figure 7.4-9. Total and Specular Transmittance as a Function of Atomic Oxygen Exposure Time for DC 93-500 Silicone

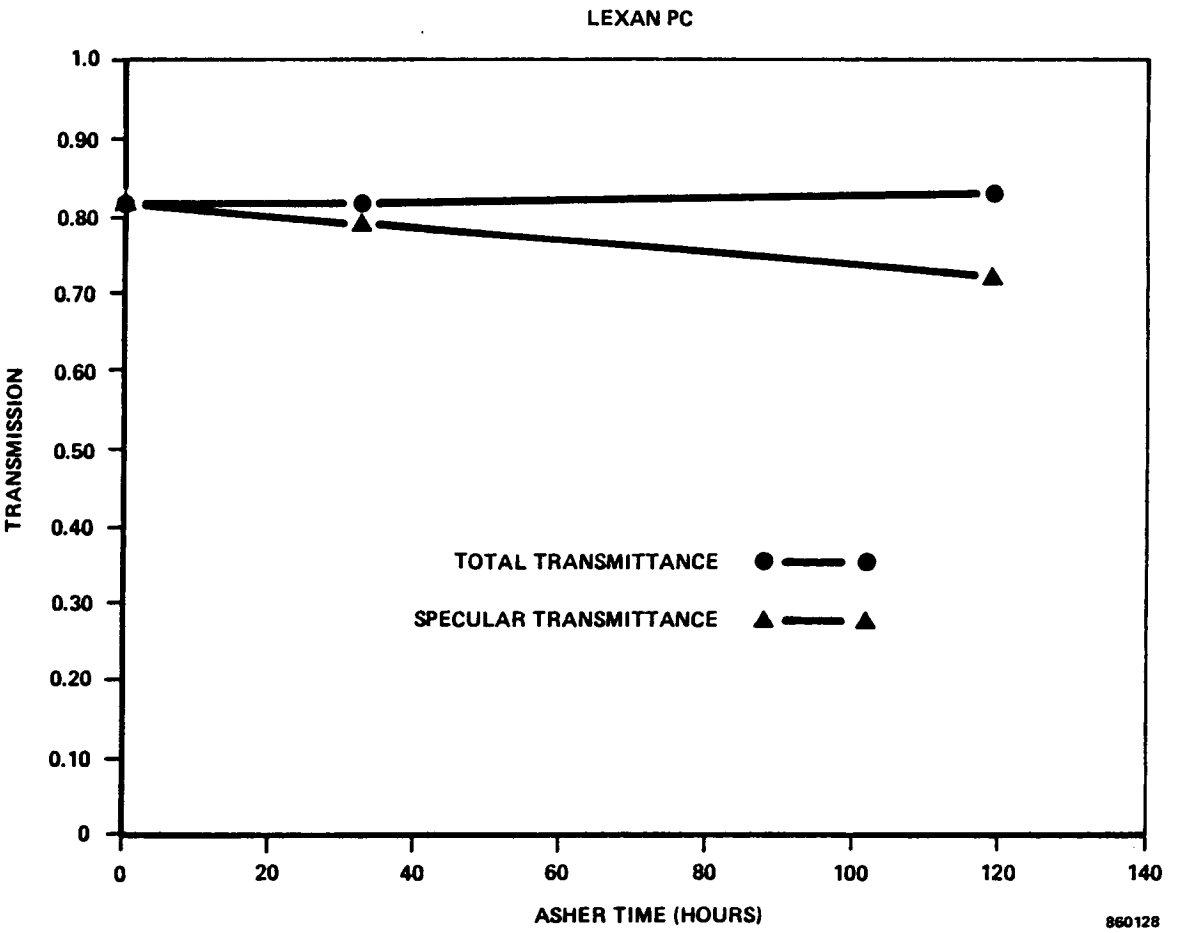

Figure 7.4-10. Total and Specular Transmittance as a Function of Atomic Oxygen Exposure Time for UV Stabilized Lexan Polycarbonate

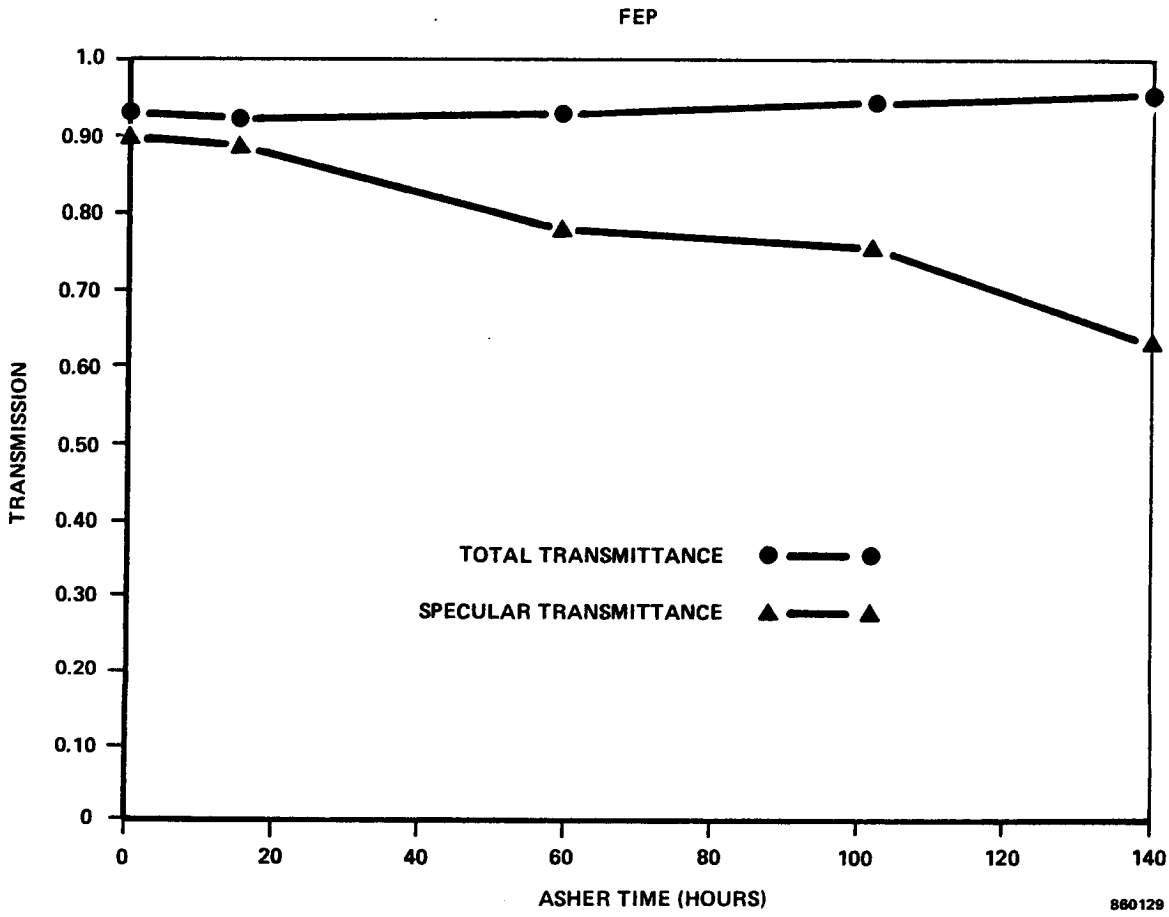

Figure 7.4-11. Total and Specular Transmittance as a Function of Atomic Oxygen Exposure Time for FEP Teflon

Figures 7.4-12 and 7.4-13 show representative scanning electron micrographs of a silicone (RTV 615) and Lexan following exposure to the oxygen plasma. The surface erosion and cracking are clearly evident. Comparable roughening of the surfaces exposed to the oxygen plasma were also observed for the other polymer samples tested.

Several samples were fabricated and tested with magnesium fluoride on both surfaces in order to eliminate the mass loss associated with atomic oxygen exposure. Transmittance data for these samples are summarized in Table 7.4-5. After 21.5 hours of exposure, each sample showed a considerable decrease in specular transmittance. Examination of the sample surfaces indicated that the MgF_2 did not uniformly coat the surface. Small beads of the material were observed randomly distributed across the sample. Deterioration of the surface was more pronounced than when uncoated samples were exposed.

Mass loss data for selected samples are given in Table 7.4-7. Thickness changes were also recorded for the Kel-F and Lexan polycarbonate samples. The Lexan sample showed the greatest changes, losing almost 75 percent of its initial mass and over 50 percent of its initial thickness.

7.4.2 Thermal Cycling

Silver and aluminum samples on GFRP substrates were coated with MgF_2, SIO_x, or a combination of the two and subjected to thermal cycling over two different temperature ranges. A total of 720 cycles from -65° C to +150° C produced no adverse effects on the sample surfaces. The primary effect noted concerned the silver samples which showed some evidence of moisture absorption and oxidation along the sample edges. This behavior is associated with the open nature of the sample edge and not with breakdown of the protective surface or delamination of the reflective surface as a result of induced thermal stresses. The affected area was < 0.5 mm wide and constituted approximately 2 percent of the total surface area.

A second set of samples was thermally shocked by immersing in liquid nitrogen and then heating to +150° C during a thirty minute period. This resulted in several very fine cracks in the surface of the samples on the order of 1-2 mm in length and 10-20 microns wide. These cracks did not affect the reflectance of the samples.

The thermal cycling tests were conducted at ambient pressure to document the effects of extreme temperature swings on the integrity of the coatings. Outgas testing of the composite substrate material has indicated that some volatiles are evolved at elevated temperature in a vacuum. Although the percentage of these species is small, they could create discontinuities in the coatings by diffusing and reacting with the metallic layers. It is recommended that thermal cycling of selected samples be considered for future testing.

SURFACE MORPHOLOGY OF GE RTV 615 SILICONE AS CAST (TOP) AND FOLLOWING 168 ASHER HOURS

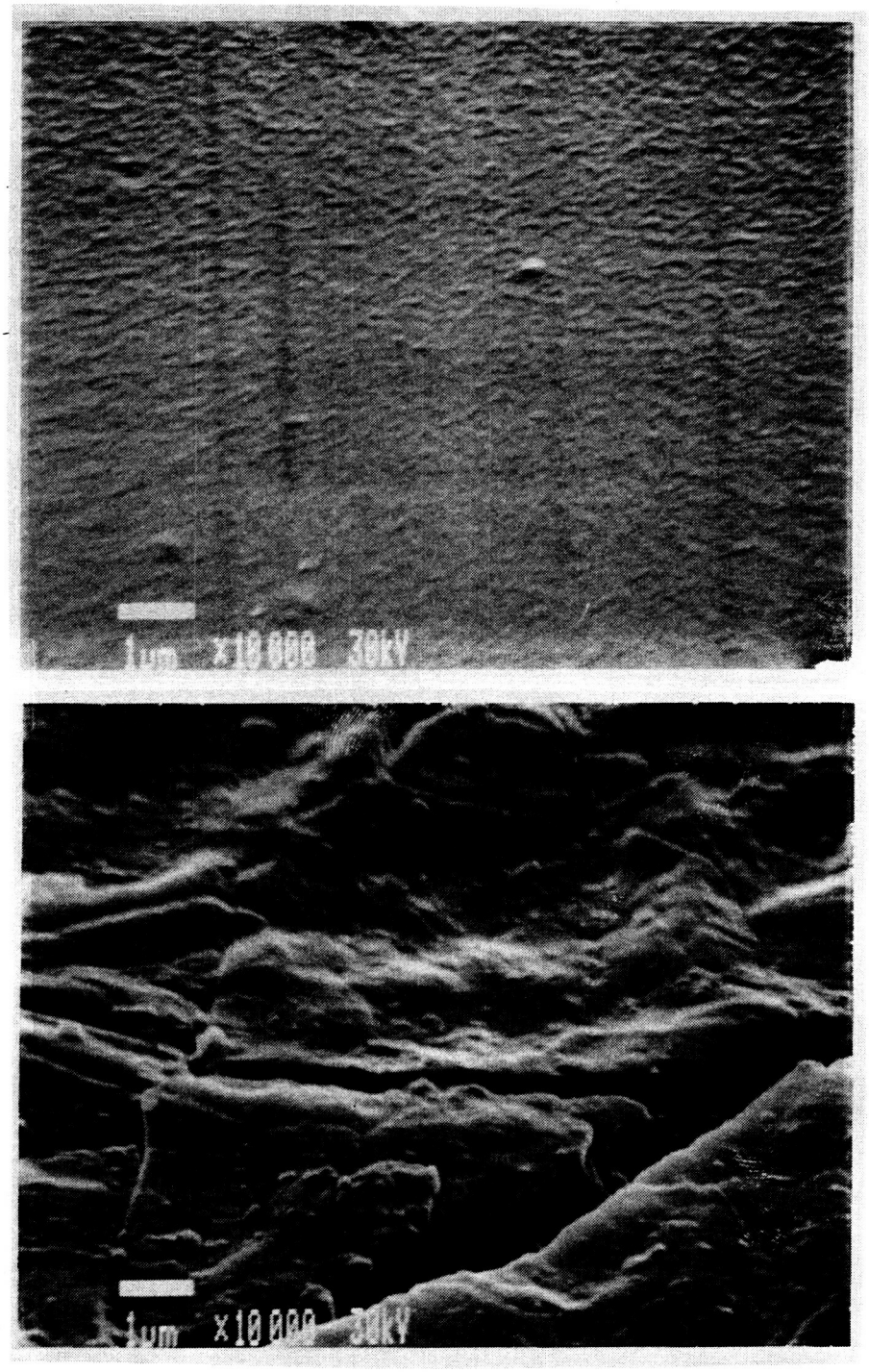

Figure 7.4-12. Before and After Atomic Oxygen Exposure Electron Micrographs of an RTV 615 Sample

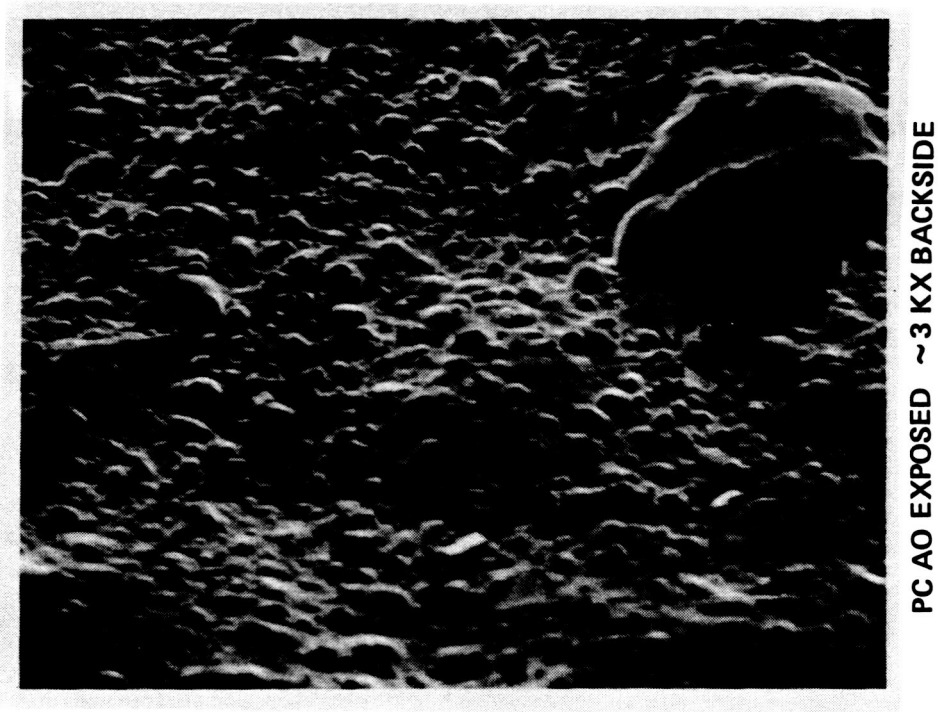

Figure 7.4-13. Electron Micrograph of a Lexan Sample After Atomic Oxygen Exposure

7.4.3 Micrometeoriod Impact Simulation

Aluminum and silver surfaced samples were exposed to a grit blast using 27 micron alumina particles to simulate micrometeoriod and debris impacts. The energy of the particles was enough to produce pinhole cracks in the surface of the samples thus exposing the reflective surface. Following the grit blast, the samples were placed in the plasma asher to examine the effects of oxygen exposure.

7.4.4 Composite Testing

Several materials were evaluated for use in reflective facets as indicated in Table 7.4-8. Considerations ranged from glass to aluminum to different composites. The large volume of material required for the facesheets (456 facets per concentrator with two facesheets per facet yield 912 total facesheets) requires that the facet material have a low density and as high a stiffness as possible. In addition, the coefficient of thermal expansion should be minimized in order to limit potential structural effects as a result of thermally induced stresses. Representative properties for selected facet materials are shown in Table 7.4-9.

7.4.5 Coating Adhesion Evaluation

The adhesive strength of vapor deposited and ion beam sputtered coatings was evaluated using ASTM test method D-3359-83. Results for different coating systems are summarized in Table 7.4-11.

Aluminum was found to adhere directly to the graphite epoxy material fairly well, however silver could easily be removed from the substrate using ordinary scotch tape. Thin layers of copper, titanium, and chromium (on the order of 500 angstroms thick) were deposited prior to the aluminum or silver layers in order to enhance adhesion. The adhesion of aluminum improved regardless of the special adhesion promoter, however silver adhesion was found to be strongly dependent on the chemical nature of the adhesion promoter's surface. Silver adhered well only to copper; when titanium or chromium was used as the promoter, oxide formation generally occurred even at vacuum levels of 10^{-5} torr. Energy dispersive spectroscopy of the interface between the adhesion promoter and silver layer confirmed the presence of titanium and chromium oxide in cases were adhesion was quite poor.

Figures 7.4-14 and 7.4-15 show two silver samples coated with magnesium fluoride. In Figure 7.4-14 no adhesion promoter was deposited prior to the silver layer. Following the tape test approximately 40 percent of the reflective surface was removed. In Figure 7.4-15, copper was deposited first followed by aluminum and then silver. The tape is completely void of any evidence of decohesion.

Table 7.4-8. Summary of Materials Evaluated for Reflective Substrate Application Including Representative Properties

Material	Density (g/cc)	Density (lb/in^3)	Facesheet* Mass (kg)	Facesheet* Weight (lb)	CTE (in/in/° F)	Modulus (GPa)	Modulus (Msi)
ULE Glass	2.20	0.079	263.15	580.25	-0.3×10^{-6}	66.0	9.57
Zerodur	2.55	0.092	306.46	675.74	0.8×10^{-6}	90.0	13.04
Aluminum	2.70	0.097	323.11	712.46	13.1×10^{-6}	71.0	10.3
Graphite/Glass	1.97	0.071	236.50	521.49	Tailorable -1×10^{-6}	Tailorable 58.6	8.5
Graphite/Polymer	1.61	0.058	193.20	426.01	-0.5×10^{-6}	87.0	12.6
Graphite/Aluminum	2.44	0.088	293.13	646.36	0.7×10^{-6}	160	23.19

*Assuming a nominal facesheet thickness of 0.010 inch excludes honeycomb and adhesive mass (weight).

Table 7.4-9. Summary of Fabric/Resin and Prepreg Composite Systems Tested

COMPOSITE SUBSTRATE EVALUATION

FABRIC	RESIN SYSTEM
MICROFIL 55	REN 195
FIBERITE 176	EPON 828/360L
A 193 P	EPON 828/V-140
	3501-6

PRE-PREG SYSTEMS

(FIBER/RESIN)

AS-4/3501-6	T-300/934
IM-6/3501-6	T-300/976
HMS-4/3501-6	T-300/966 (PMR-15)
	T-300/986 (BMI)

Table 7.4-10. Composite Test Data for Selected Substrate Materials

		FACET PROPERTIES						
FACET MATERIAL	NUMBER OF PLIES	FACET THICKNESS		MAX. USE TEMP.		MODULUS		CTE
		(MM)	(IN.)	(^{o}C)	(^{o}F)	(GPa)	(Msi)	(IN./IN./^{o}F)
MICROFIL 55 828/360L	1	0.15	0.006	121	250	87.0	12.6	2.0×10^{-6}
MICROFIL 55 828/360L	2	0.30	0.012	121	250	87.0	12.6	2.0×10^{-6}
FIBERITE 176 828/360L	2	0.30	0.012	121	250	43.0	6.2	2.0×10^{-6}
FIBERITE 176* 934 EPOXY	2	0.30	0.012	177	350	53.2	7.4	1.7×10^{-6}
AS-4/3501-6*	4	0.30	0.012	177	350	81.4	11.8	1.59×10^{-6}
IM-6/3501-6*	4	0.30	0.012	177	350	89.7	13.0	0.79×10^{-6}
HMS-4/3501-6*	4	0.30	0.012	177	350	107.6	15.6	0.30×10^{-6}
A193P/3501-6	1	0.18	0.007	177	350	69.0	10.0	2.0×10^{-6}
A193P/3501-6	2	0.36	0.014	177	350	69.0	10.0	2.0×10^{-6}
T300/966*	4	0.61	0.024	316	600	36.3	5.3	1.0×10^{-6}
T300/986*	4	0.61	0.024	232	450	48.3	7.0	1.0×10^{-6}

*DENOTES PREPREG SYSTEM

Table 7.4-11. Coating Adhesion Results

ADHESION TESTING

- COATING ADHESION TO SUBSTRATE EVALUATED USING ASTM METHOD D-3359-83
- Cr, Ti, AND Cu USED AS ADHESION PROMOTERS FOR A1 AND Ag
- ALUMINUM SAMPLES SHOWED NO DECOHESION OR FLAKING
- SILVER SAMPLES VERY SENSITIVE TO OXIDE FORMATION AT INTERFACE. NO DECOHESION WHEN Cr OR Cu IS USED TO PROMOTE ADHESION.

SUBSTRATE	PROMOTER	REFLECTIVE LAYER	PROTECTIVE SURFACE	CLASSIFICATION
MICROFIL 55 828/360L	Cr	Al	MgF_2	5B
MICROFIL 55 828/360L	Cr	Ag	MgF_2	OB
MICROFIL 55 828/360L	Cr	Al	SiO_x/MgF_2	5B
MICROFIL 55 828/360L	Cr	Ag	SiO_x/MgF_2	1B
MICROFIL 55 828/360L	Cr	Al/Ag	SiO_x/MgF_2	5B
MICROFIL 55 828/360L	Cu	Ag	$SiOx/MgF_2$	5B

- 5B DENOTES NO DECOHESION OCCURRED
- 0B INDICATES GREATER THAN 65% DECOHESION

Figure 7.4-14. Micrograph Showing Decohesion of Ag and MgF_2 Coating From Substrate Due to Lack of Adhesion

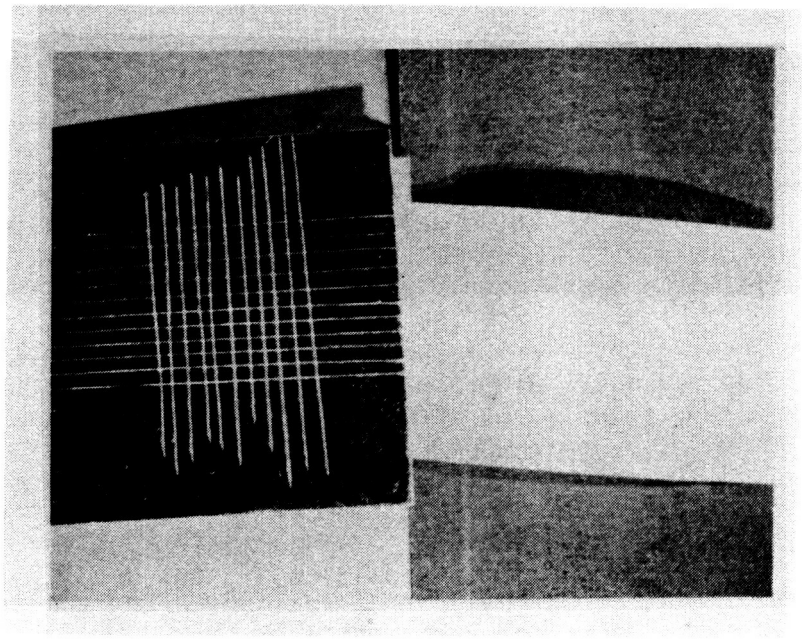

Figure 7.4-15. Micrograph Showing Improved Adhesion of Ag and MgF_2 Due to Adhesion Promoter

7.5 Materials Evaluation Summary

A number of tests have been conducted to assess the survivability of potential solar concentrator materials in the low earth orbit environment. The primary focus was on composite facet materials, reflective coatings, and protective coatings for the truss hex and splined radial panel concepts and on lens materials for the domed Fresnel concept. Data generated during these tests indicate that reflective facets can be fabricated with sufficient surface specularity to meet reflectance requirements over the ten year system lifetime. Domed Fresnel lens materials tested under went considerable surface erosion and mass loss due to the atomic oxygen flux, and thus showed a considerable decrease in specular transmittance.

Of the reflective surfaces evaluated, silver has the highest integrated reflectance over the wavelength range of interest followed by aluminum. The best optical surfaces were obtained from glass substrates, however, wet lay-up fabrication techniques have been demonstrated to yield surfaces of the desired quality. Graphite reinforced epoxy substrates will result in a considerable increase in overall performance while reducing weight considerably. Several protective coatings have been shown to provide excellent protection against atomic oxygen degradation. Two reflective surface designs are shown in Figures 7.5-1 and 7.5-2. Each utilizes a graphite epoxy composite substrate fabricated using a high modulus bidirectional woven cloth impregnated with a space qualified epoxy resin, EPON 828. An adhesion promoter is then deposited (500 Å thick) followed by the desired reflective surface. Aluminum was found to adhere well directly to the substrate, however, a titanium or chromium layer is still recommended. Silver adhered the best to copper; in some cases excellent adhesion was also found between silver and aluminum. The critical point in achieving sufficient adhesion with silver is to not allow oxide formation on the surface of the promotor prior to deposition of the silver. Thus the promotor layer and reflective coating should be put down during the same deposition without breaking vacuum. If possible, the protective coating(s) should also be deposited prior to breaking vacuum to ensure the best optical properties.

For the silver surface concept, a two layer protective overcoat is recommended. A coating of silica (t = 1000 Å) is first sputtered onto the surface followed immediately by a layer of magnesium fluoride (t = 750 Å). The key to the effectiveness of the protective coatings is the continuity. Coatings as thin as 500 A provide adequate protection, however, once the integrity of the overcoat is compromised oxidation occurs. This is especially important in the case of the silver reflective surface. Limited experimental evidence suggests that once a pinhole is formed in the surface, the oxidized portion of the reflective coating will continue to grow beneath the protective overcoat. Oxygen diffuses rapidly along silver grain boundaries and thus may affect a large portion of the surface.

The aluminum concept is protected using a 1000 Å thick layer of magnesium fluoride. Excellent results were obtained during the asher tests using this approach. Limited flight data also exist for aluminum coated with magnesium fluoride which indicate that the coating is very durable in LEO, although the exposure times were short (7 days).

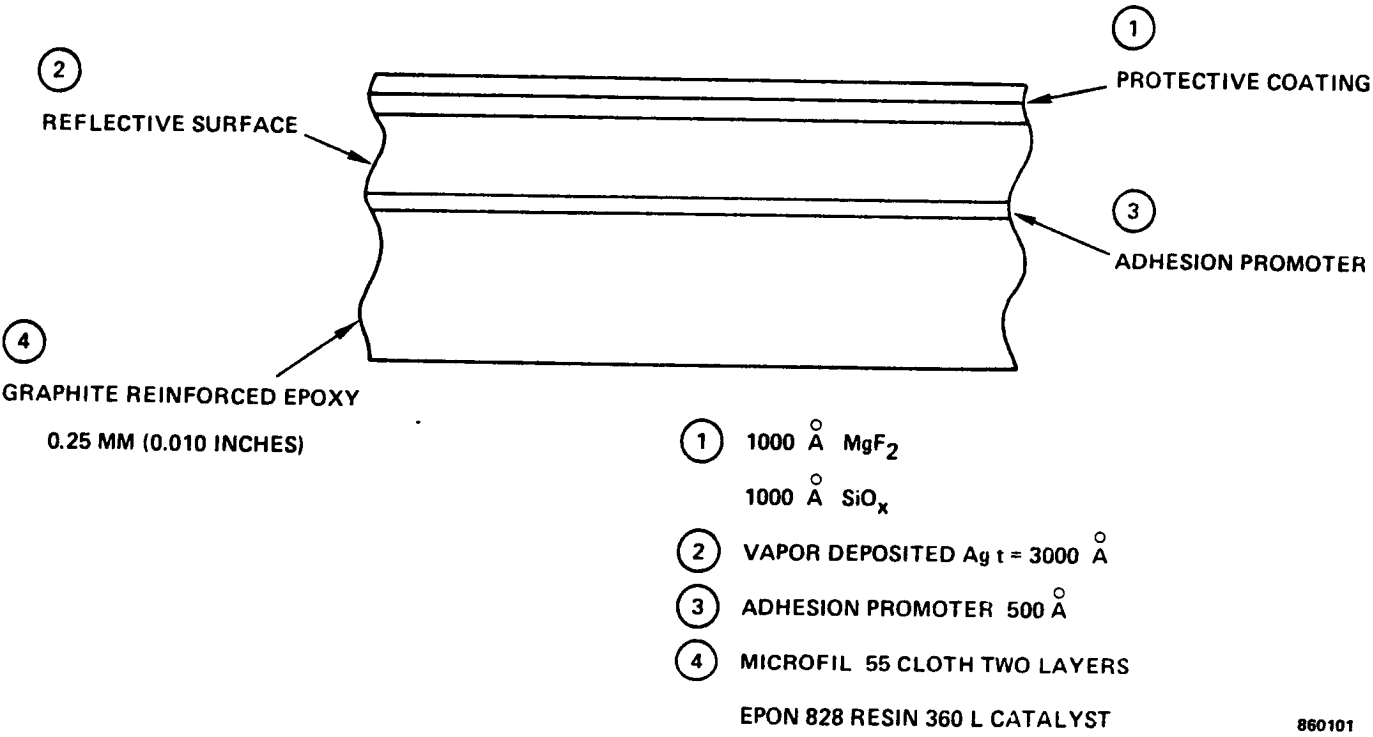

Figure 7.5-1. Cross Section View of Silver Surface Reflective Facet

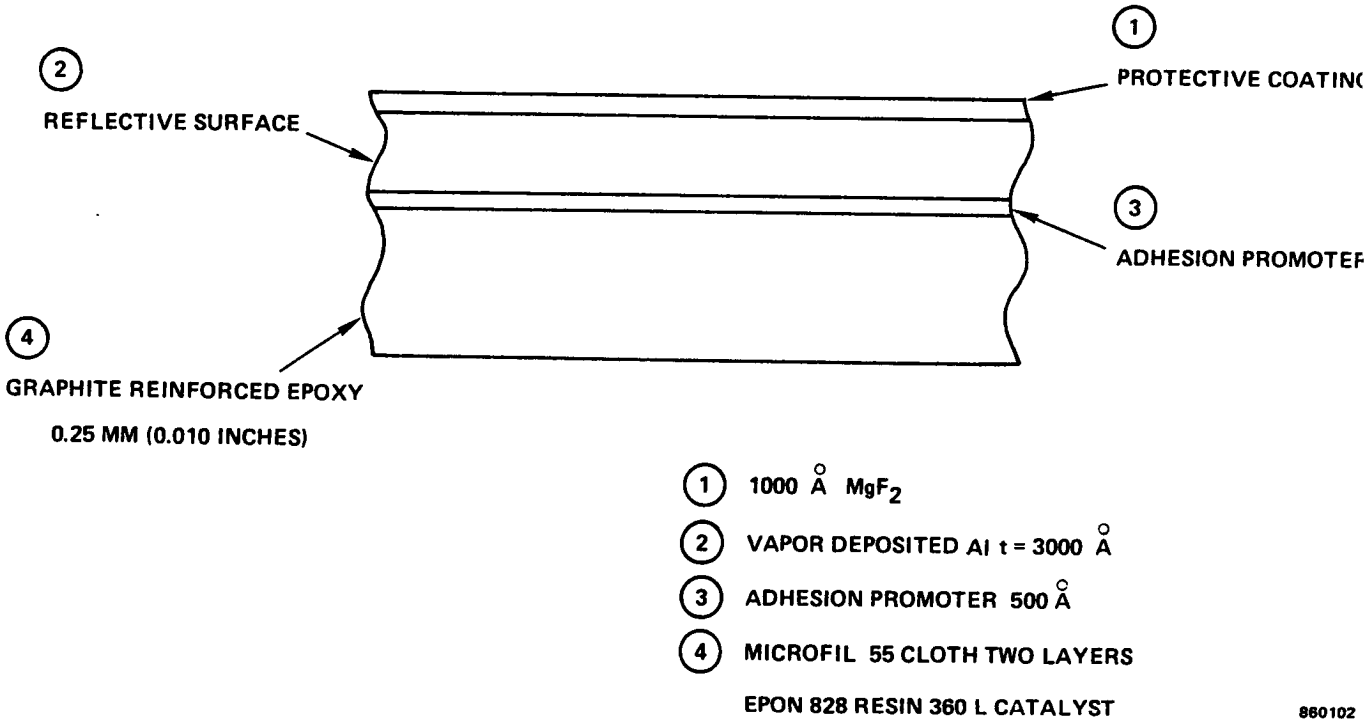

Figure 7.5-2. Cross Section View of Aluminum Surface Reflective Facet

Fresnel materials tested consisted of silicones, fluoropolymers, acrylic, and polycarbonate. In each case surface erosion and mass loss were observed, indicating that these materials will require some sort of protective coating also. Attempts to protect the polymer surfaces with vapor deposited magnesium fluoride were not successful. Scanning electron micrographs of the coated surfaces indicated that the coating did not wet the surface well. Of the polymeric materials tested, RTV 670 silicone and FEP teflon exhibited the greatest inherent resistance to degradation.

It is important to note that different materials degrade at different rates in the asher when compared with actual data from shuttle experiments. It is thus difficult to quantitatively interpret wear rates in the asher and correlated these with actual behavior in LEO. Additional data are therefore necessary to correlate behavior in the asher with LEO performance.

Future work on Fresnel concentrators should address hybrid concepts where the ram facing surface is a thin layer of an atomic oxygen resistant material bonded to a relatively flexible lens formed from a molded silicone, for example. The subject of transparent coatings for lens materials should also be further investigated.

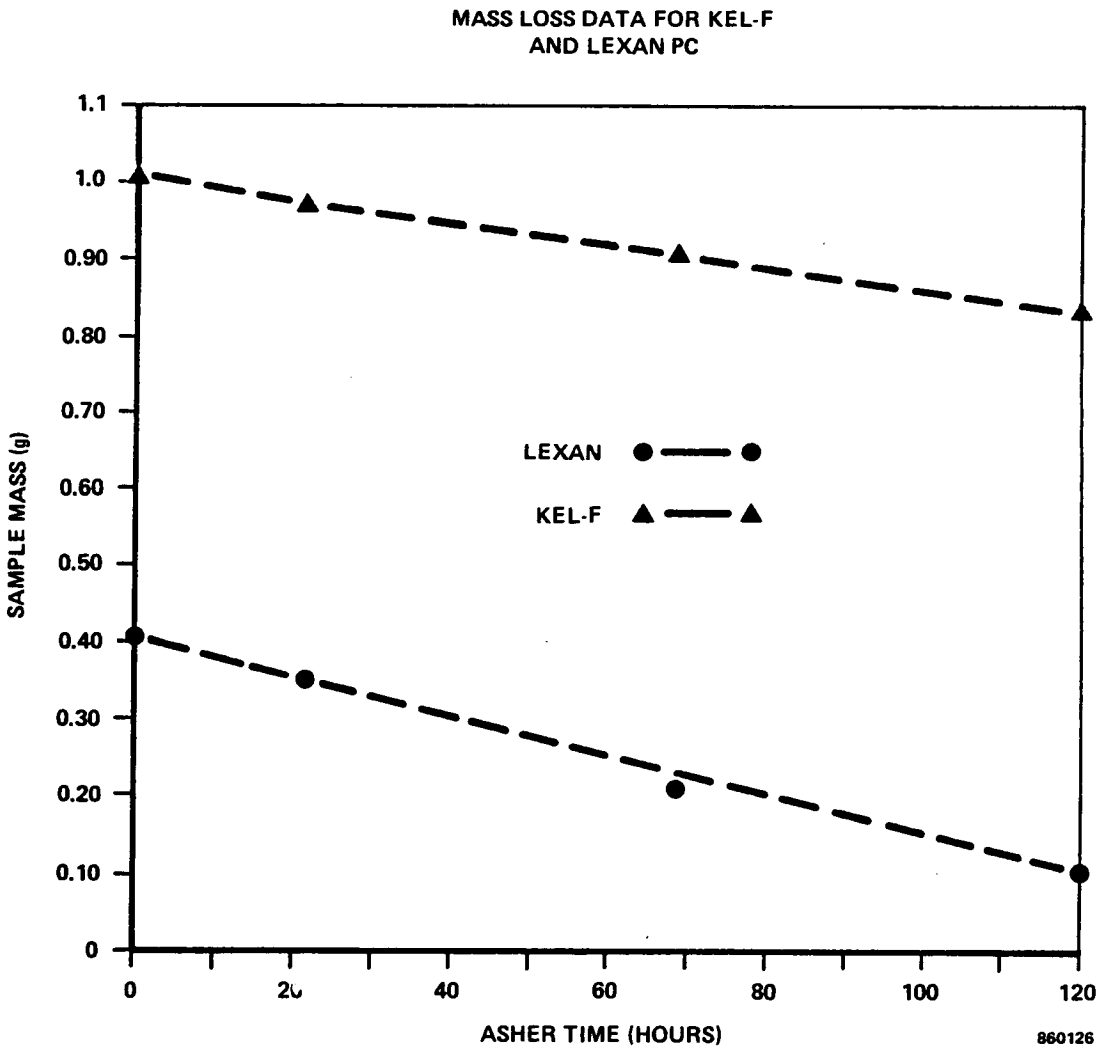

Figure 7.5-3. Plot Showing Decrease in Sample Mass as a Function of Atomic Oxygen Exposure for Two Fresnel Materials, Kel-F and Lexan

8.0 TRADE COMPARISON OF CONCENTRATOR CONCEPTS

Trade evaluation criteria and weighting factors were used to compare the concentrator concepts. The concepts were evaluated against the 16 criteria presented in Table 8.0-1. These criteria address to the technology issues Harris perceives as either key drivers or discriminators. Specific comments on each criteria are included in Table 8.0-1. Three weighting factors were used as given below:

1. Below average importance
2. Average importance
3. Above average importance

The three concentrator concepts; Truss Hex, Domed Fresnel and Splined Radial Panel, were evaluated against the trade criteria. Three ranking values were used as given below:

1. Significant disadvantage
2. Meets requirements
3. Significant advantage

The ranking values assigned to each concept for each criteria are given in Table 8.0-2. Comments on the scoring are presented in Table 8.0-3. The trade comparison rates the Truss Hex concept first. The Domed Fresnel and Splined Radial Panel concepts compare equally well against the criteria.

8.1 Concentrator Concept Selection

The Truss Hex concentration concept was selected as the best design for both the ORC and CBC Space Station power systems. The primary reasons for selecting the Truss Hex concept are that it is:

- Easiest to maintain
- Simplest
- Most reliable
- Most flexible
- Easiest to produce
- Lowest risk
- Lowest cost

The Domed Fresnel and Splined Radial Panel concentrator designs have proven to be sound concepts with unique features better suited for other applications.

Table 8.0-1. Evaluation Criteria and Weighting Factors for Concentrator Design Comparison

Parameter	Factor	Comments
Optical Performance	3	Impacts entire power system design requirements
Packaging Efficiency		
Stowed Volume	2	Primary shuttle constraint which
Stowed Length	2	determines payload integration
Mass Properties	2	Constraints total launch payload
Maintainability		
Surface Replacement	2	Better option than restow/return
Damage Susceptibility	2	Impacts system design performance
Restow and Disposal	1	Maintenance is better option than return
Design Complexity	2	Impact costs, reliability and maintainability
Reliability	3	Provides power for man-rated system
Design Flexibility		
Deployment Options	2	Provides flexibility in mission planning
Receiver Compatibility	2	Affects receiver performance and temperature margins
Scalability	2	Supports changing system requirements
Producibility	2	Needed for near term demonstration
Design Maturity	2	Needed for near term demonstration
Development Risk	3	Needed for near term demonstration
Relative Cost	1	Qualitative estimates limited

Weighting Factors: 1 - Below Average Importance
2 - Average Importance
3 - Above Average Importance

C-3

Table 8.0-2. Solar Concentrator Advanced Development Trade Study

Parameters	Weight Factor	Truss Hex	Domed Fresnel	Splined Radial
Optical Performance	3	2	2	2
Packaging Efficiency				
Stowed Volume	2	2	3	3
Stowed Length	2	2	3	3
Mass Properties	2	2	3	3
Maintainability				
Surface Replacement	2	3	1	1
Damage Susceptibility	2	3	2	1
Restow and Disposal	1	3	1	1
Design Complexity	2	3	2	1
Reliability	3	3	2	2
Design Flexibility				
Deployment Options	2	3	2	2
Receiver Compatibility	2	2	1	2
Scalability	2	3	2	2
Producibility	2	3	1	2
Design Maturity	2	3	2	2
Development Risk	3	3	1	2
Relative Cost	1	3	2	2
Total Score (Unweighted)		43	30	31
Total Score (Weighted)		88	62	65

* High Score is Best *

Values: 3 - Significant Advantage
2 - Meets Requirement
1 - Significant Disadvantage

Table 8.0-3. Comments on Scoring

• Optical Performance	• All concepts can tailor flux by design; only Truss Hex is adjustable in service
	• Domed Fresnel has very high tolerance for slope errors
• Packaging Efficiency	• Deployable Truss Structure (DTS) provides significant advantage to spline and Fresnel concepts
	• All three concepts package more efficiently than other generic concepts
• Mass Properties	• Same as packaging efficiency
• Maintainability	• Removal and replacement of individual mirror facets, or individual panel modules in unique advantage of Truss Hex
	• Impact of DTS damage more significant to radial spline than Domed Fresnel
	• Truss Hex restow and lock capability easily implemented
	• Restow and lock of DTS difficult to accomplish
• Design Complexity	• Repeated, modular design with assisted deployment is advantage of Truss Hex
	• Radial spline has highest part count; Truss Hex has lowest
• Reliability	• Truss Hex has manual deployment, lowest parts count, simple mechanisms, and lowest susceptibility to damage
• Design Flexibility	• Truss Hex deployment can be automated or manual; DTS deployment by drive mechanism only
	• Domed Fresnel performance must be more closely integrated with receiver design
	• Truss Hex is easily expandable with modular design

Table 8.0-3. Comments on Scoring (Continued)

• Producibility	• Low parts count, replicated structure and mechanisms is advantage of Truss Hex • Domed Fresnel lens material selection is uncertain
• Design Maturity	• Truss Hex is application of current technology • Domed Fresnel demonstration under way • Non-mesh surface design on DTS requires technology development and demonstration
• Development Risk	• Truss Hex is application of current technologies • Domed Fresnel lens material selection is uncertain
• Relative Cost	• Truss Hex had advantage of simplicity, maturity, producibility, and low risk

9.0 MANUFACTURING AND TEST PLANS

Manufacturing and assembly and test plans were addressed for the Truss Hex Concentrator after the concept was selected as the recommended design for the Space Station. Fabrication of the major components and assembly of the components into an operational concentrator are described in Section 9.1. The concentrator demonstration test plan is described in Section 9.2. The production and test activities have been defined on a conceptual basis and will be updated as the design, manufacturing processes and test procedures mature.

9.1 Manufacturing and Assembly Flow

The Truss Hex Concentrator manufacturing flow chart is presented in Figure 9.1-1. The modularity of the Truss Hex design supports parallel fabrication of the mirror facets, hexagonal panels, and hinge and latch mechanisms.

Facet Assembly

The facet, which is of sandwich construction, is assembled from pre-cured face sheets, honeycomb core and corner reinforcements. The front face sheet, high temperature cured to specularity and spherical requirements, is trimmed to shape and aligned on the mold. The corner reinforcements and honeycomb are placed on the rear surface of the front face sheet. The back face sheet is added to the assembly. The assembly is vacuum bagged and cured, Figure 9.1-2.

Mounting hardware is installed on the rear of the facet. The facet is positioned in an evaporation chamber and the reflective and protective coatings are applied, Figure 9.1-3. The completed facets are subjected to acceptance test procedure (ATP) and accepted articles are stored.

Panel Assembly

A panel consists of structural beam elements and shear fittings which are assembled, aligned and bonded using an assembly table, Figure 9.1-4. The bonded assembly undergoes ATP, as required, then the hinge and latch mechanisms and the facet attachment hardware are installed on the panel. The completed panel is dimensionally inspected.

Concentrator Assembly

Panels, without facets, are assembled and the structure is aligned by shimming the hinges and latches. Once stowed and deployed alignment is established, the concentrator is deployed.

The panels require an offloading device only during the 180 degree panel rotation. When the panels have engaged the latches, no supplemental support is necessary. The axis of rotation for panel rotation occurs at only

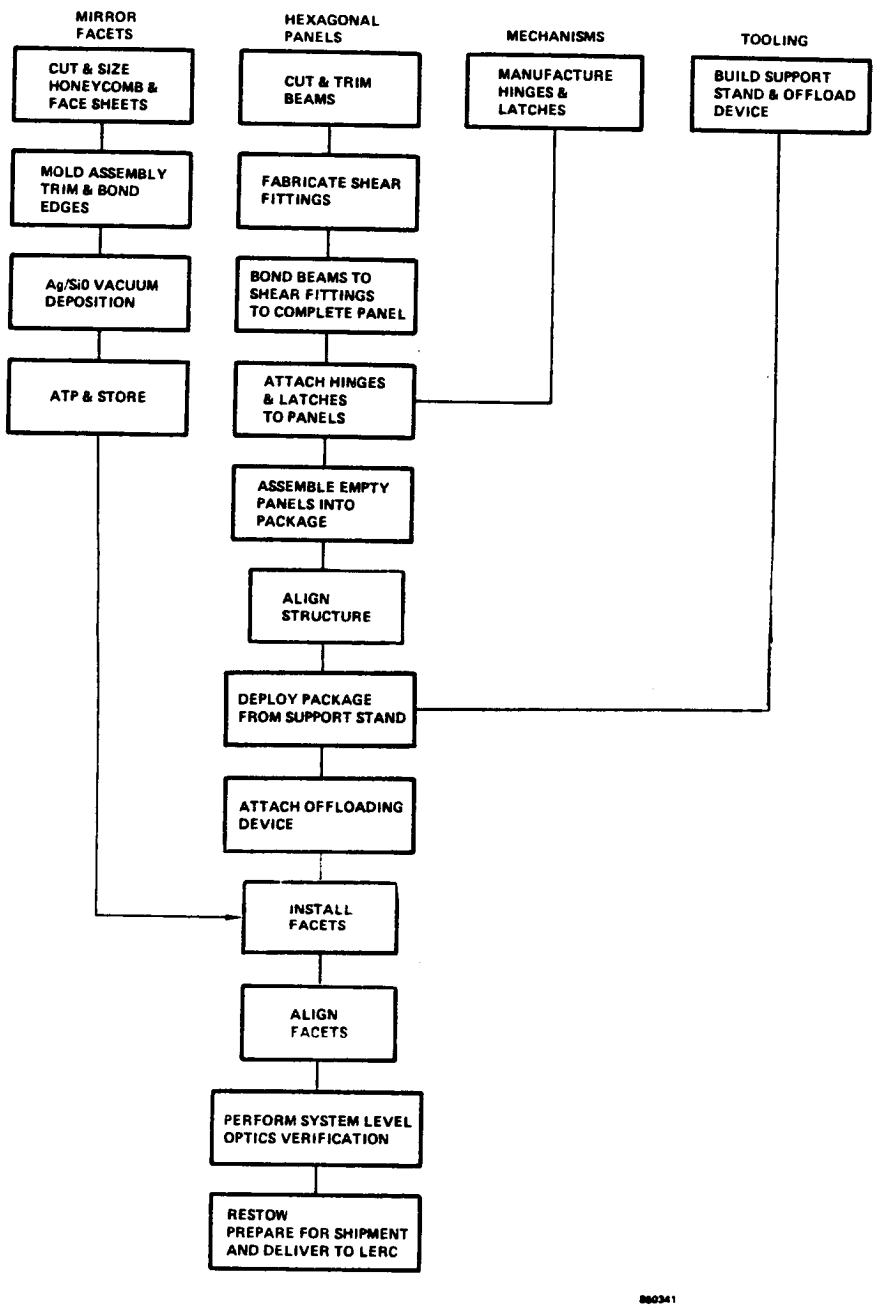

Figure 9.1-1. Parallel Component Fabrication Possible Due to Modularity of Truss Hex Design

MIRROR MOLD ASSEMBLY

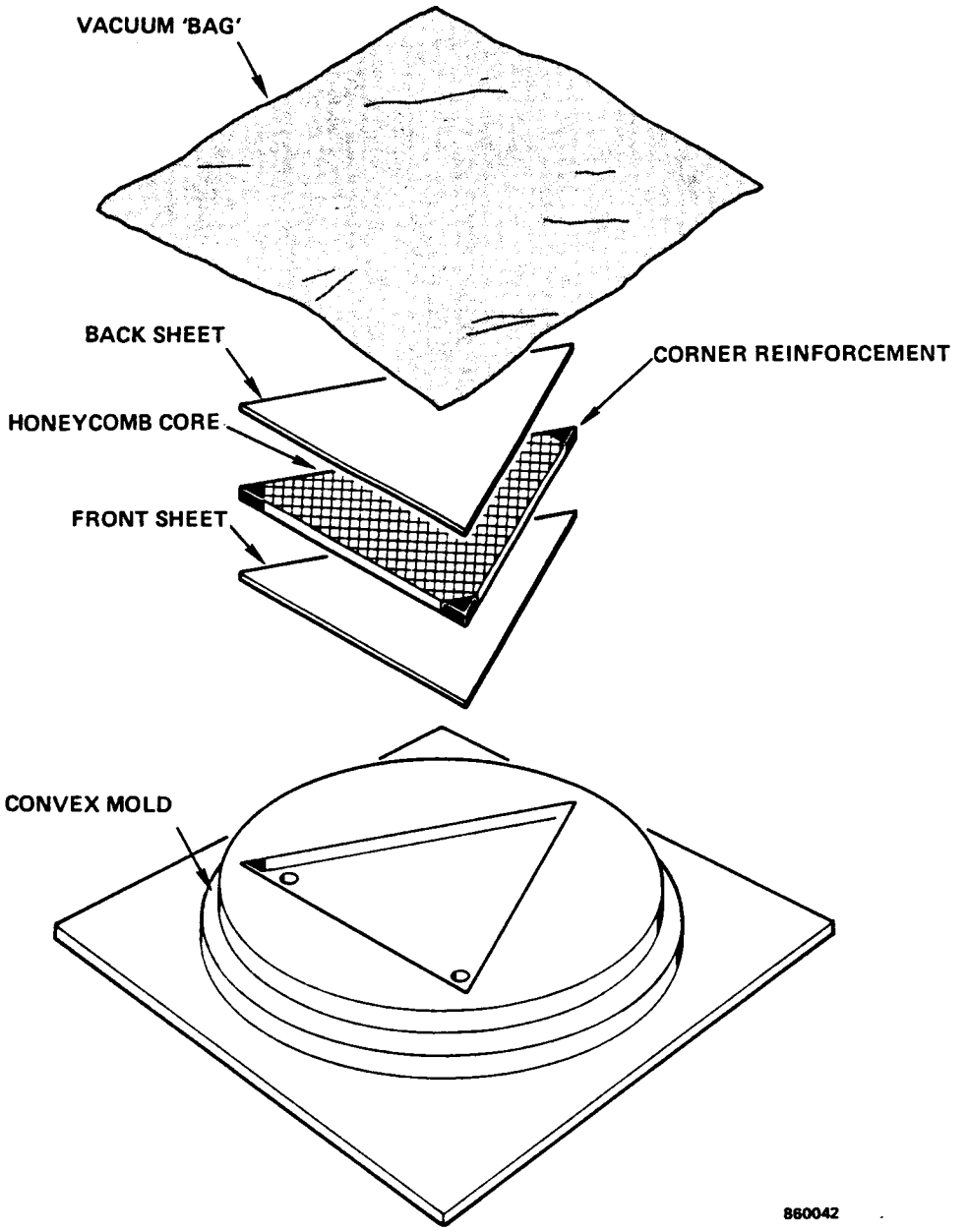

Figure 9.1-2. Precured Components are Assembled and Cocured on the Mold Producing High Quality Facets

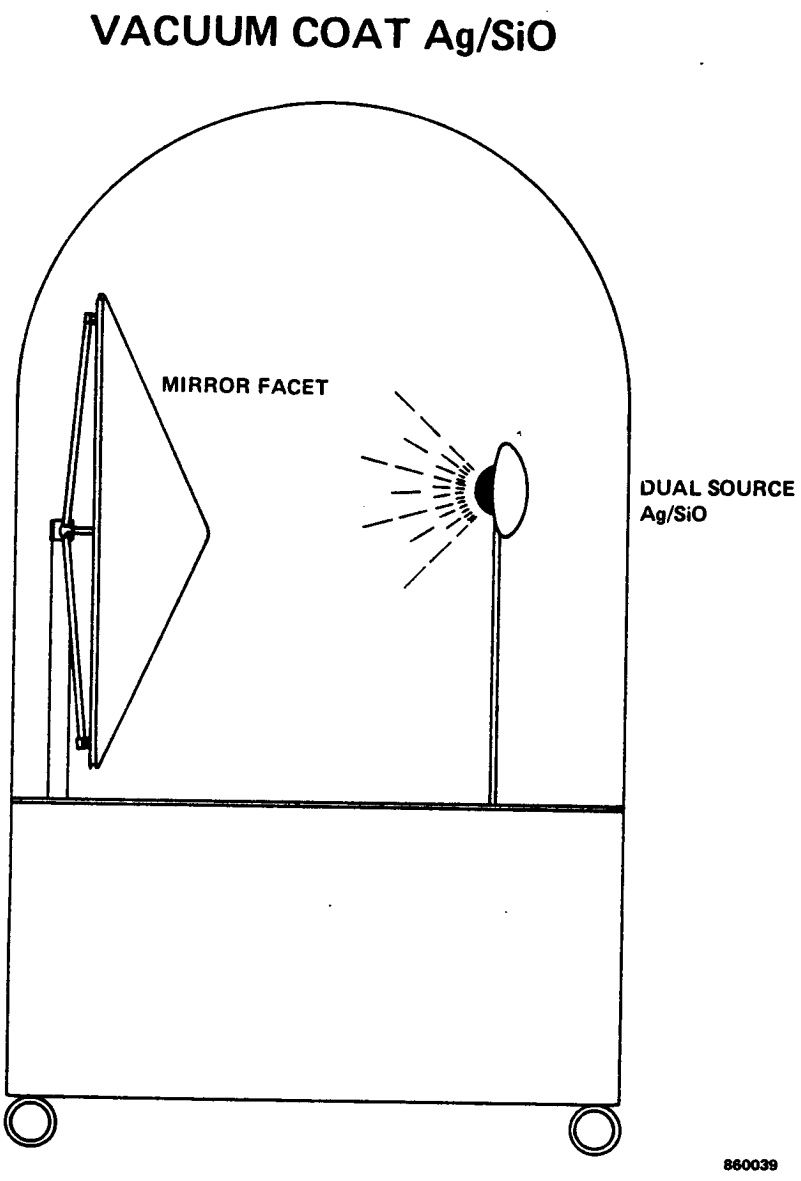

Figure 9.1-3. Vacuum Deposition of Coatings Provides Uniform, Controlled, Specular Mirror Surface

HEX FRAME ASSEMBLY TABLE

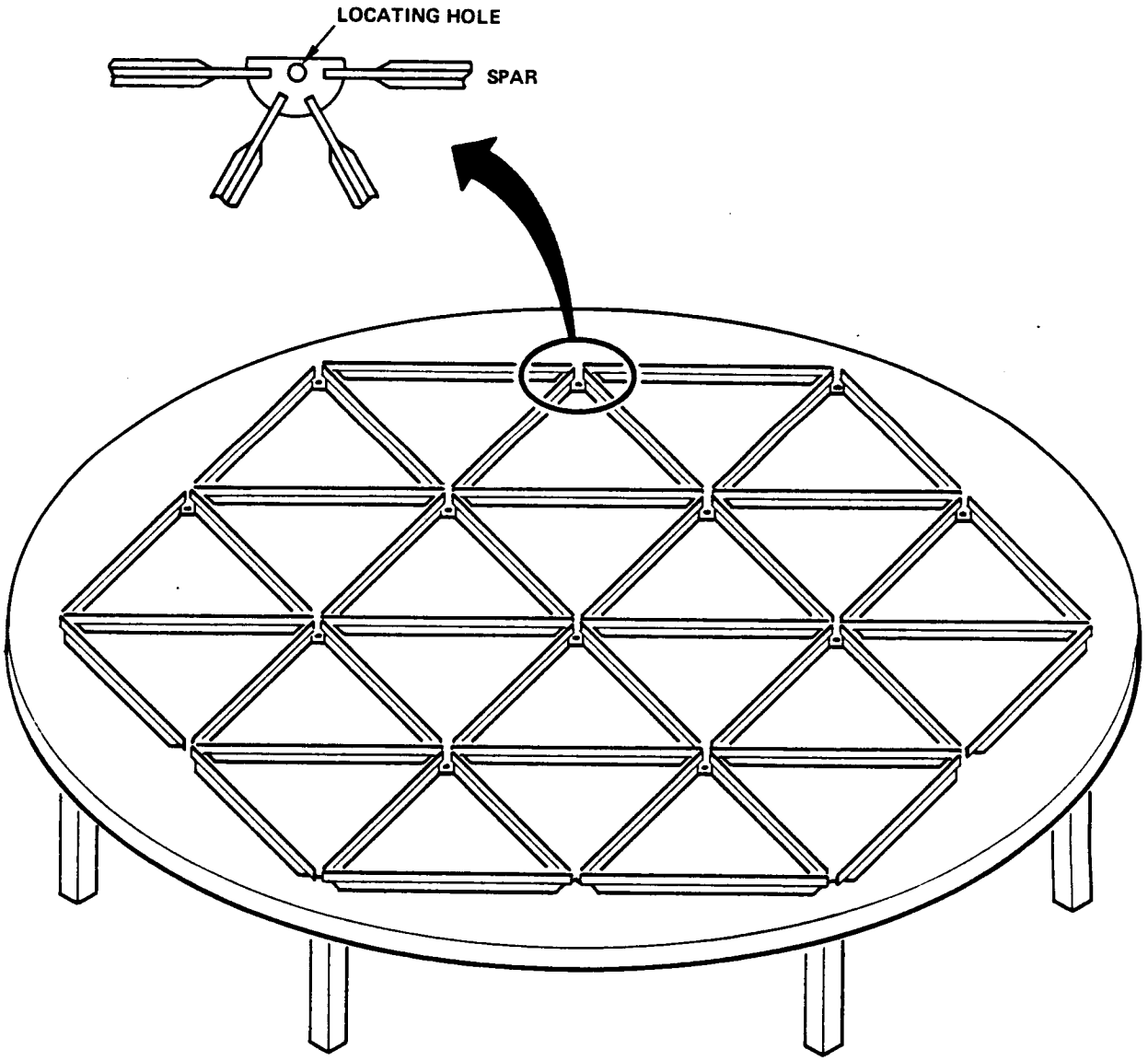

Figure 9.1-4. The Hex Frame Assembly Table is a Bonding and Alignment Tool

two locations: once at the left side of Panel No. 1 (first fold), and all others 60 degrees clockwise from that position, Figures 9.1-5 and 9.1-6. With the offloading device attached, Panels 2 through 8 are folded out away from Panel 1. The offloading device is detached and all panels rotate clockwise 60 degrees. The offloading device is reattached once the counterweight has been reduced to correspond to the five panel stack configuration. Panels 3 through 7 rotate and Panel 2 engages the appropriate latches. The previous steps are repeated until all 7 panels are deployed.

The facets are installed into the deployed panels from the rear of the concentrator using the maintenance probe, Figure 6.1-26. Working platforms are used as needed to access all facet locations. The facets are aligned using a translating laser beam. The beam is translated to illuminate a predetermined point(s) on each facet. A translucent cylindrical target grid with an aperture is placed at the focal plane and aligned to the proper tilt angle. The illuminated facet is adjusted, via adjustment screws at the corners, until the reflected ray intercepts the simulated receiver target at the correct grid point. This process is illustrated in Figure 9.1-7. The target point for each facet is determined by optical analysis. Once the facets have been aligned, jam nuts are tightened on the adjustment screw to lock in the alignment. The completed concentrator is ready for system level optics verification, Section 9.2.

9.2 Demonstration Concentrator Test Plan

The foremost objective of the SCAD concentrator demonstration test is to demonstrate that the optical characteristics support system requirements for; specular reflectance, effective slope error, optical boresight alignment, focal length and deployment repeatability. The preliminary optical test plan for meeting this objective is presented in Figure 9.2-1. The facet acceptance test is described pictorially in Figure 9.2-2. The facet alignment procedure was described in Section 9.1 and illustrated in Figure 9.1-7. The method for characterizing the concentrator, the system level focus verification, is described in Section 9.2.1.

9.2.1 System Level Focus Verification

The optical boresight of the concentrator is aligned, relative to the articulating periscope, by design since the periscope is used to align the facets, see Section 9.1. Counter weight supports are attached as required to maintain panel 1 g deflections within the linear elastic region. A digital photosensor is located at the aperture plane to record reflected ray strike locations. An articulating periscope directs a laser beam to a known location on the concentrator surface. This testing arrangement is shown in Figure 9.2-3.

The articulating periscope, Figure 9.2-4, folds the optical path thus changing the incident beam origin. The route traversed by the laser beam can be manually or computer controlled. A unique feature of the periscope

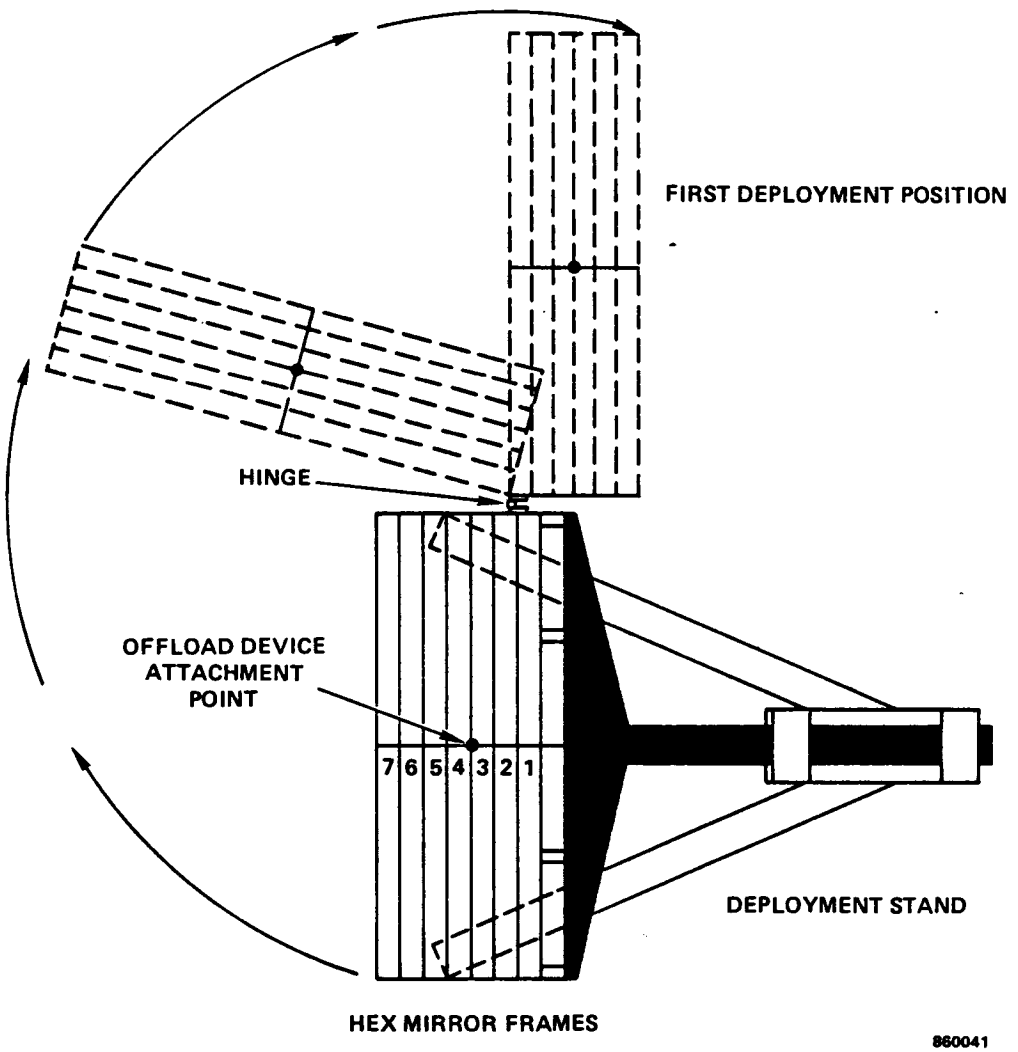

Figure 9.1-5. Each Panel Rotates 180° About a Vertical Hinge Line

DEPLOYMENT SEQUENCE

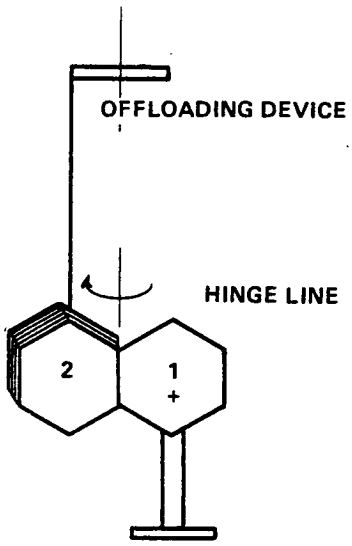

HEXES NO. 2 THRU 7 AWAY FROM 1, SUPPORTED BY OFFLOADING DEVICE

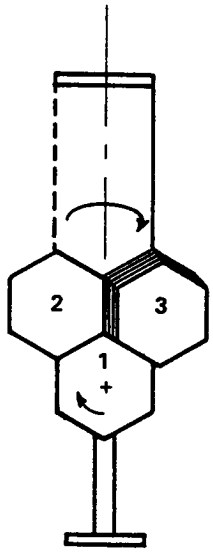

UNHOOK OFFLOADING DEVICE ROTATE ASSEMBLY CLOCKWISE 60°, REATTACH OFFLOADING DEVICE AND DEPLOY 3 THRU 7

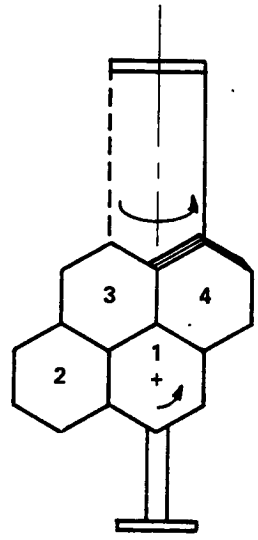

UNHOOK OFFLOADING DEVICE ROTATE COUNTER CLOCKWISE 60°, REATTACH OFFLOADING DEVICE AND DEPLOY 4 THRU 7

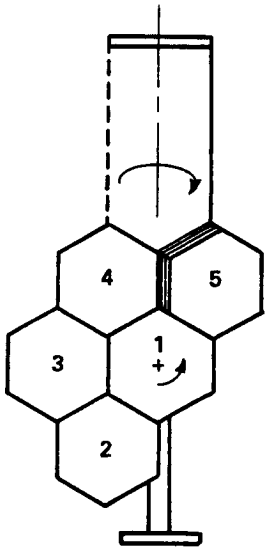

REPEAT PREVIOUS STEP.

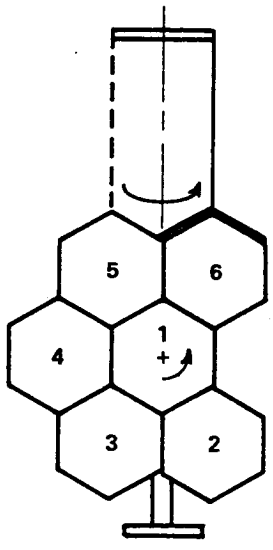

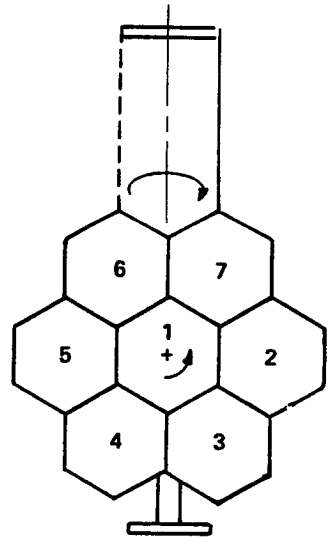

860060

Figure 9.1-6. Deployment Stand and Sequence Keep Hinge Lines Vertical During Panel Rotation

FACET ALIGNMENT PROCESS

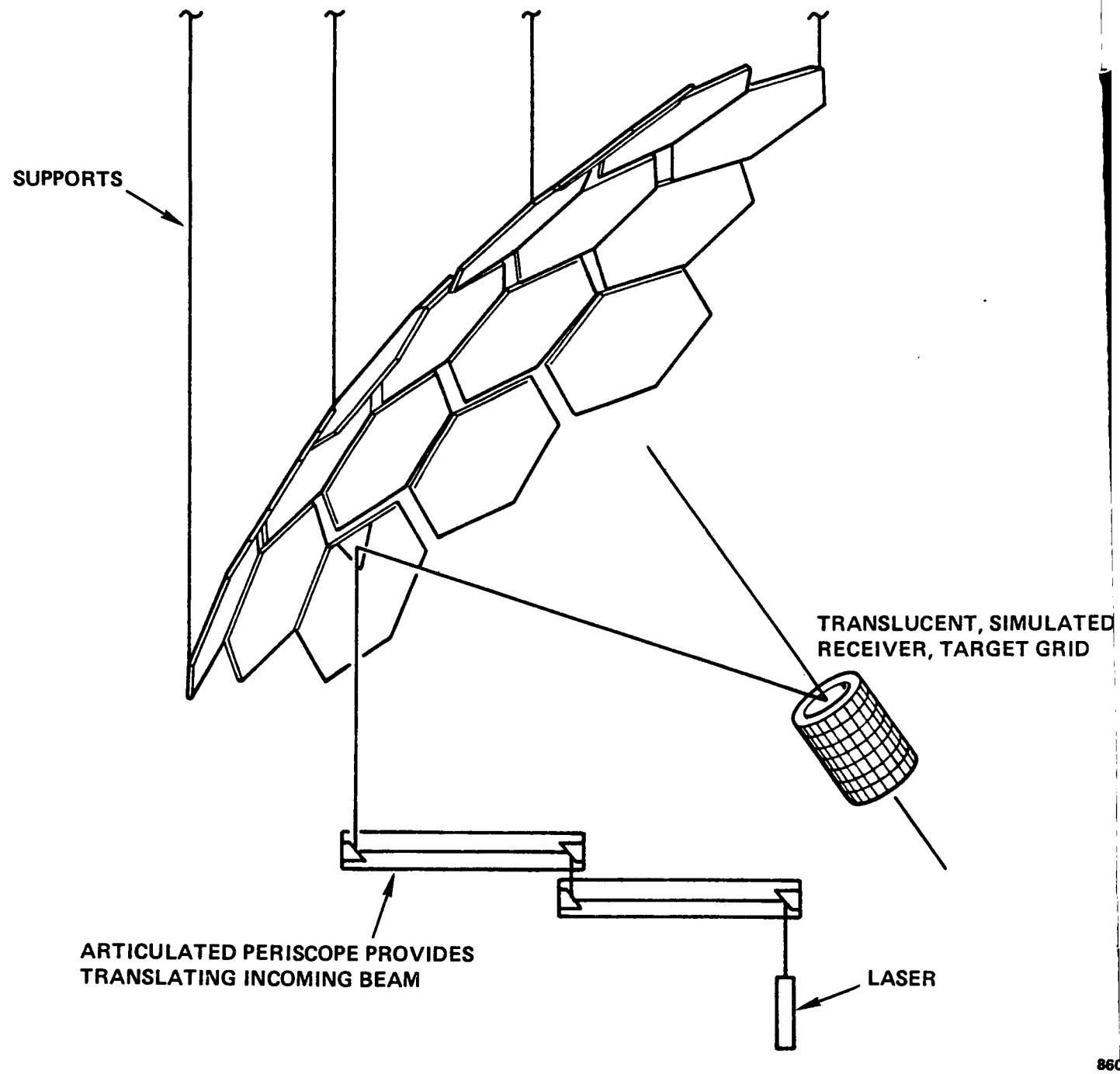

Figure 9.1-7. Translating Laser and Simulated Receiver Target Provides Visual and Direct Facet Alignment Method

PRELIMINARY OPTICAL TEST PLAN

OBJECTIVE	DEMONSTRATE BY
• DETERMINE SPECULAR REFLECTANCE OF COATINGS	• REFLECTANCE TESTS PERFORMED BY DEPOSITION VENDOR
• PERFORM DETAILED FIRST ARTICLE FACET CHARACTERIZATION (EACH MOLD)	• LASER SCAN
• PROVIDE LOW COST ACCEPTANCE TEST FOR EACH FACET	• GO-NO/GO AUTOFOCUS TEST
• PERFORM OPTICAL FACET ALIGNMENT AT ASSEMBLY LEVEL	• USE TRANSLATING VERTICAL LASER BEAM TO AIM FACETS AT PRE-DETERMINED CYLINDRICAL GRID POINTS
• DETERMINE GLOBAL CHARACTERISTICS - OPTICAL BORESIGHT - EFFECTIVE SLOPE ERROR - FOCAL LENGTH	• TRANSLATING VERTICAL LASER BEAM WITH DIGITIZED PHOTOSENSING SCAN IN THE APERTURE PLANE
• ASSESS EFFECTS OF 1 g DISTORTIONS	• PERFORM ABOVE WITH & WITHOUT COUNTER WEIGHTS
• DEMONSTRATE DEPLOYMENT REPEATABILITY	• APERTURE PLANE SCANS WITH INTERVENING STOW/DEPLOY
• CHARACTERIZE RECEIVER OPTICS	• MAINTAIN CORRESPONDENCE DATA FOR LASER BEAM LOCATION & INTERCEPT LOCATION AT APERTURE PLANE. DEFINE VECTOR INPUTS FOR OPTICAL ANALYSIS TO PREDICT FLUX

Figure 9.2-1. Preliminary Optical Test Plan meets Concentrator Demonstration Test Objectives

I. RADIUS OF CURVATURE CAN BE DETERMINED BY REMOVING THE FRESNEL LENS AND POSITIONING THE SLIDE UNTIL THE MINIMUM SIZE IMAGE IS FORMED ON A SCREEN ATTACHED TO THE FRONT OF IRIS 1.

II. SLOPE ERROR - WITH THE FOCUSING OPTICS SET AT INFINITY, THE BEAM IS AIMED AT THE CENTER OF THE FACET THROUGH A PIN HOLE (IRIS-2). THE IRIS IS OPENED AND THE LIGHT BEAM DIVERGED TO COVER THE ENTIRE FACET. IRIS 1 IS FULLY OPENED AND PHOTOCELL READING CHARACTERIZE MIRROR QUALITY.

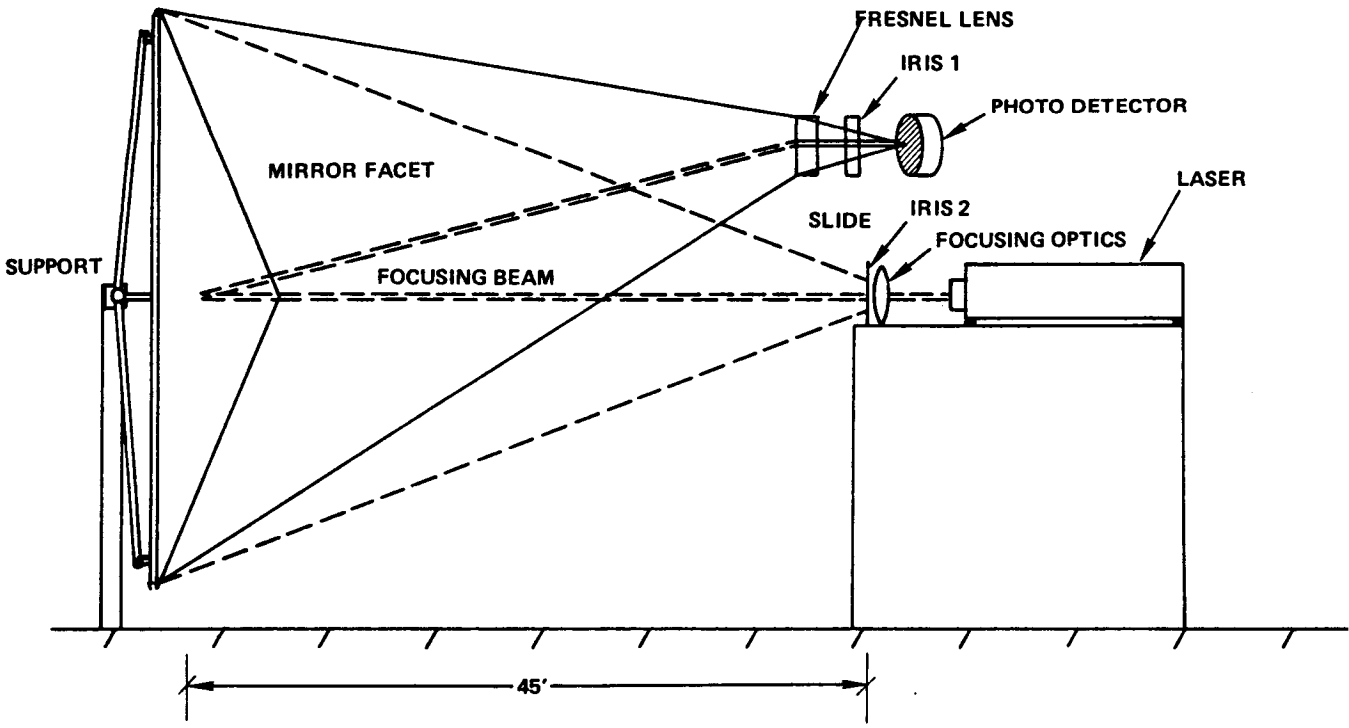

MIRROR FACET INSPECTION
FOR RADIUS OF CURVATURE AND SLOPE ERROR

86004

Figure 9.2-2. Facet Test Characterizes Radius of Curvature and Effective Slope Error Prior to Article Acceptance

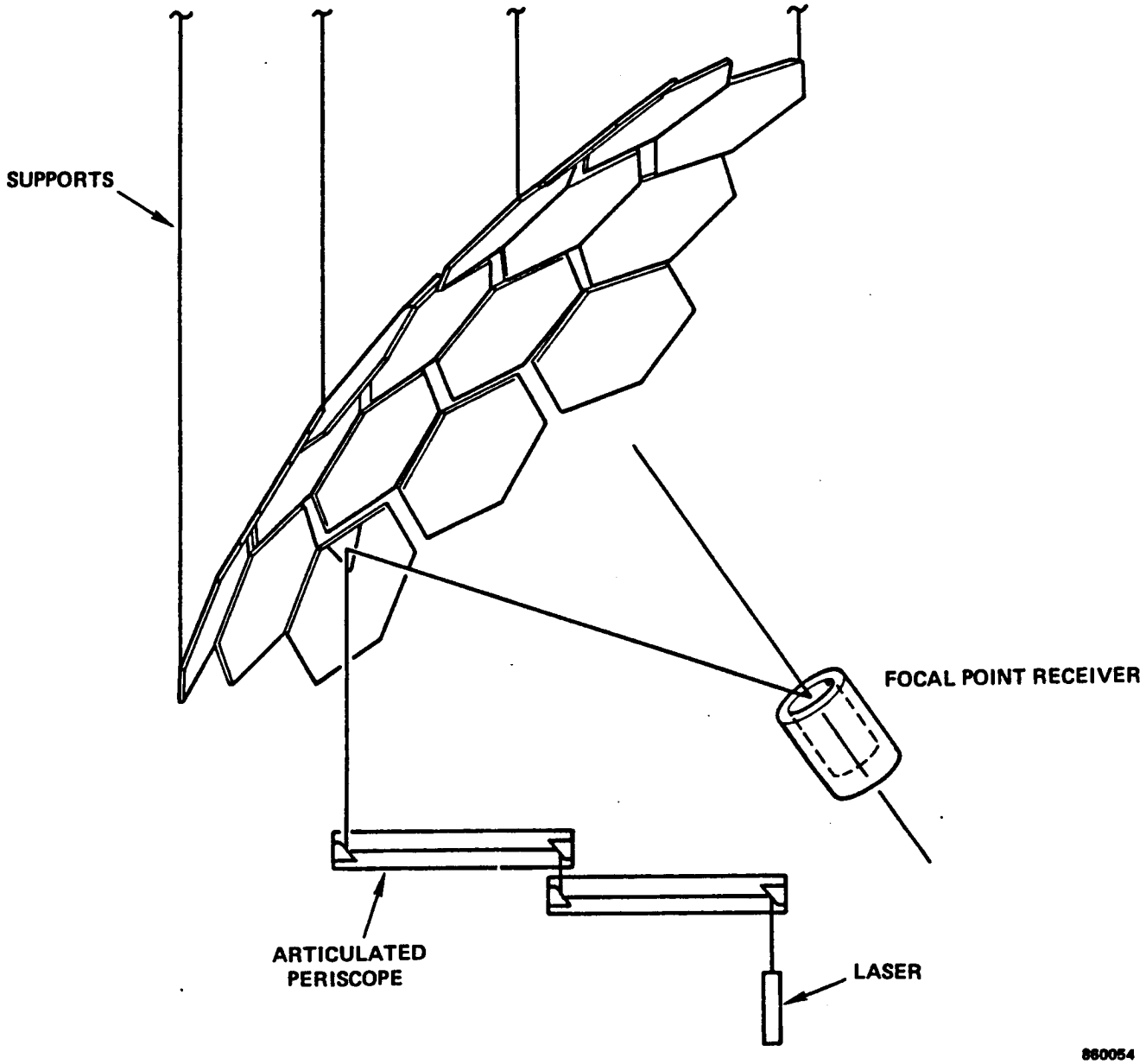

Figure 9.2-3. Focus Verification Test Determines Concentrator Optical Boresight, Effective Slope Error, Focal Length and Ray Traces

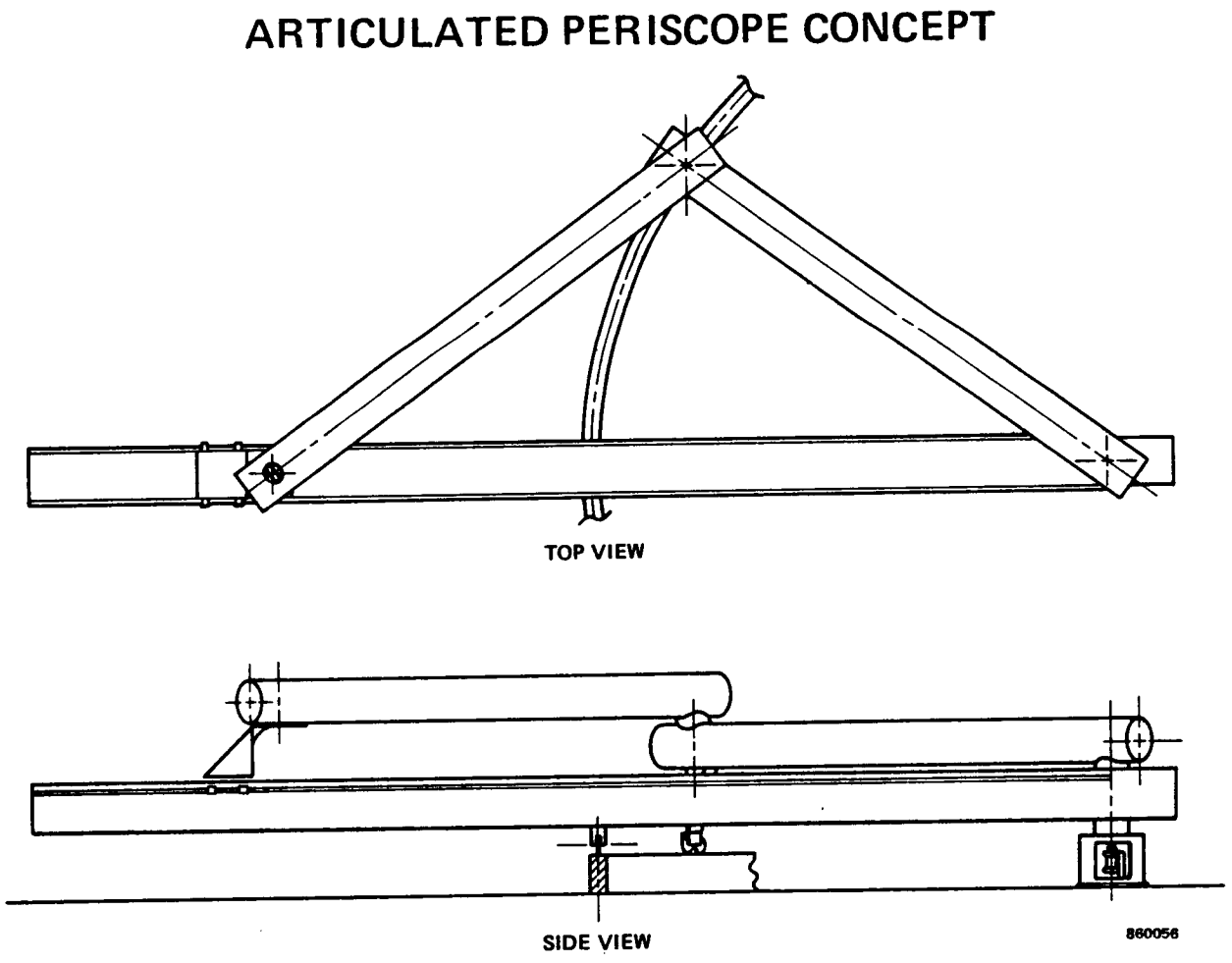

Figure 9.2-4. Articulating Periscope Maintains Laser Beam Vertical and Changes Incident Beam Location for Scanning by Folding Optical Path

design is that the exit ray and entrance ray are always parallel if the periscope is not bent by thermal or other forces. The periscope is aligned using a liquid mirror.

The test measurement process includes:

1. Align articulating periscope.
2. Position periscope exit beam, concentrator incident ray, to illuminate desired location on surface (manually or automatically).
3. Intercept reflected ray on digital photosensor.
4. Record incident ray and reflected ray intercept locations.
5. Repeat Steps 2 through 4 for all desired measurement points.

The incident ray and reflected ray intercept locations are the as built ray traces, optical paths, of the concentrator. The summation of all reflected ray intercepts directly provides the contour of the as built receiver aperture flux profile. Analytically comparing the measured intercept location to the ideal intercept, predicted by optical analysis, yields the as built slope error at the point in question. The measured slope errors can be input to the optical analysis to produce aperture and receiver cavity flux profiles, operational and as tested, for the manufactured concentrator.

The effects of 1 g distortions and deployment repeatability can be addressed by performing the focus verification tests on the concentrator in before and after configurations. 1 g distortions are addressed by:

1. Scan concentrator with counterweight supports
2. Add or subtract weight; remaining in linear deflection region
3. Attach new counterweight supports
4. Scan concentrator
5. Compare ray traces resulting from Steps 1 and 4.

Deployment repeatability is demonstrated by:

1. Scan concentrator
2. Stow panels
3. Deploy panels
4. Scan concentrator
5. Compare ray traces from Steps 1 and 4

10.0 CONCLUSIONS AND RECOMMENDATIONS

Several conclusions have been made as a result of the Task 1 engineering effort.

- The Truss Hex Concentrator ranks as the best design for the Space Station application.
- The Domed Fresnel and Splined Radial Panel Concentrators are viable, sound concepts.
- Material investigations have demonstrated a service life greater than 10 years on small reflective surface samples.
- An adequate refractive lens material has not been found.
- Facilities and test equipment are defined for the manufacture and verification of the Truss Hex Concentrator.

Harris recommends the Truss Hex Concentrator for Space Station and further development by continuing with Tasks 2 and 3 of the Solar Concentrator Advanced Development program.

11.0 REFERENCES

1. "Space Station Work Package 4 Power System Final Draft, Conceptual Design Final Study Report", Harris Government Aerospace Systems Division, 19 December 1985, Rockwell International Contract No. R50PAB85560973, NASA Contract No. NAS3-24666.

2. O'Neill, Mark J., E-Systems Inc., "A Unique New Fresnel Lens Solar Concentrator", Silver Jubilee Congress of the International Solar Energy Society, Atlanta, GA, May 1979.

3. "Remotely-Controlled Docking System", NASA JSC Houston, NASA MSC-18969, 1984.

4. Solar Concentrator Advanced Development Technical/Management Proposal, Volume 1, Harris Government Aerospace Systems Division, 2 May 1985, Response to NASA LeRC RFP2-171017, pp. 5-97 to 5-113.

5. O'Neill, M. J., "Solar Concentrator and Energy Collection System", U. S. Patent No. 4,069,812, 24 January 1978.

6. JSC 30000 Space Station Program Definition and Requirements, Section 3, Space Station System Requirements, Appendix 3.1, Natural Environment Design Requirements, January 1986.

7. L. J. Leger, "Oxygen Atom Reaction with Shuttle Materials at Orbital Altitudes," NASA TM-58246, May 1982.

8. L. J. Leger, J. T. Visentine, and J. F. Kuminecz, "Low Earth Orbit Atomic Oxygen Effects on Surfaces", AIAA 22nd Aerospace Sciences Meeting, 1984, Paper No. 84-0548.

9. L. J. Leger, I. K. Spiker, J. F. Kuminecz, T. J. Ballantine, and J. T. Visentine, "STS Flight LEO Effects Experiment-Background Description and Thin Film Experiments", AIAA Shuttle Environment and Operations Meeting, October 1983.

10. W. S. Slemp, B. Santos-Mason, G. F. Sykes, Jr., and W. G. Witte, Jr., "Effects of STS-8 Atomic Oxygen Exposure on Composites, Polymeric Films, and Coatings", AIAA 23rd Aerospace Sciences Meeting, 1985, Paper 85-0421.

11. J. T. Visentine, L. J. Leger, J. F. Kuminecz, and I. K. Spiker, "STS-8 Atomic Oxygen Effects Experiment", AIAA 23rd Aerospace Sciences Meeting, 1985, Paper 85-0415.

12. A. F. Whitaker, S. A. Little, R. J. Harwell, D. B. Griner, and R. F. DeHaye, "Orbital Atomic Oxygen Effects on Thermal Control and Optical Coatings", AIAA 23rd Aerospace Sciences Meeting, 1985, Paper No. 85-0416.

13. H. S. Rauschenbach, "Solar Cell Array Design Handbook", van Nostrand Rheinhold, New York, NY, 1980, p. 411.

14. W. R. Hudson, et. al., NASA TM X-73598, 1977.

15. M. J. Mirtich and H. Mark, NASA TN D-3187, 1966.

16. F. Grum and G. W. Luckey, Applied Optics, 7, 2289 (1968).

APPENDIX A
DEPLOYABLE TRUSS STRUCTURE DEPLOYMENT SEQUENCE

Figure A-1 illustrates the folded or stowed configuration of a three hinge deployable truss structure (DTS) structure. The surface has been omitted for clarity. The central hub assembly is the primary structural member in the stowed configuration. The mechanical deployment system (MDS) is housed in the hub structure. The folded ribs are restrained in the stowed configuration by a series of restraint spokes which secure the ribs to the center hub structure. These restraint spokes are released from the restraint mechanism as the first event of the deployment action. The rib deployment is actuated by the MDS, shown in detail in Figure A-2.

As the drive motor turns the drive screw, the carrier moves from the lower (stowed) position shown in Figure A-2 to the upper (deployed) position. The drive links (or push rods) connect the carrier to each of the ribs, and the linear motion of the carrier is translated to each of the ribs, causing them to rotate about their respective pivot axes on the hub from the stowed to the deployed position. The carrier is driven overcenter with respect to the pivot points to provide for deployed latching.

Deployment actuation of the hinges or articulating joints in the ribs is accomplished by the synchronization of drive rods shown in Figure A-1. As shown, these drive rods are attached between the pivot joint where the rib is attached to the hub and the articulating joint. As the MDS actuates rotation of the rib at the pivot joint on the hub, the drive rod translates this action to the first articulating joint. Thus, the kinematic motion of the rib pivot joint at the hub is used to actuate deployment of the first articulating joint. Similarly, deployment of the second articulating joint is actuated by the first joint through a drive rod attached between these two joints. Finally, in a similar manner, the third outboard articulating joint is actuated by the kinematic motion of the second joint. This deployment approach allows a controlled, synchronized deployment of all the ribs as shown in Figure A-4.

Since the articulating joints are a critical element in the rib deployment, a considerable amount of development work has been expended on these areas. The joint mechanism design, Figures A-5 and A-6, is similar to a compass divider where the drive link roller slides inside tracks. This results in symmetric deployment of the joint. The joint has a small number of parts but is redundant with dual drive link rollers. It is lightweight and has a high deployed stiffness when fully preloaded. Latching is accomplished by the overcenter travel of the drive link roller.

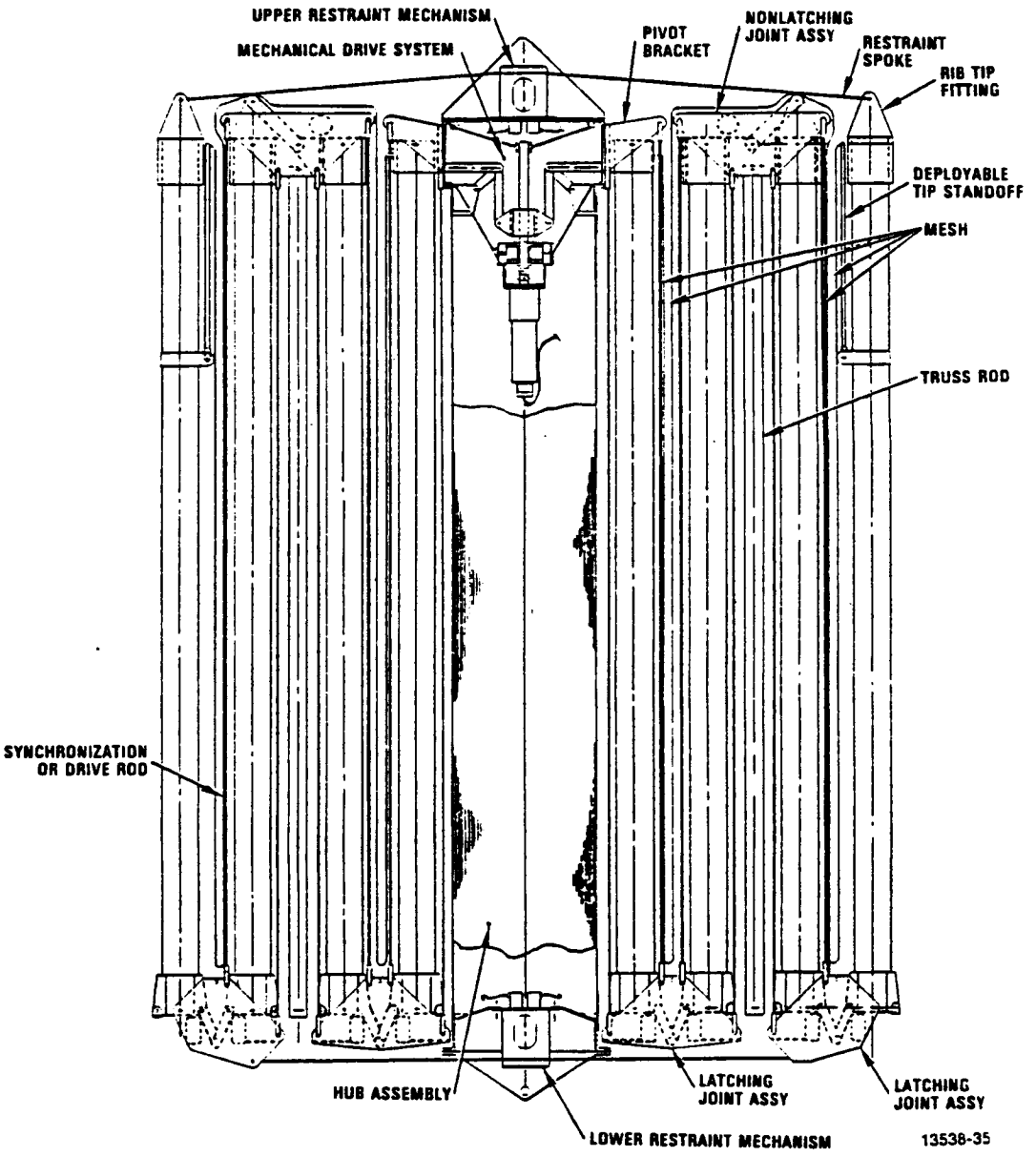

Figure A-1. The Ribs of the DTS Structure Fold Compactly Against the Central Hub

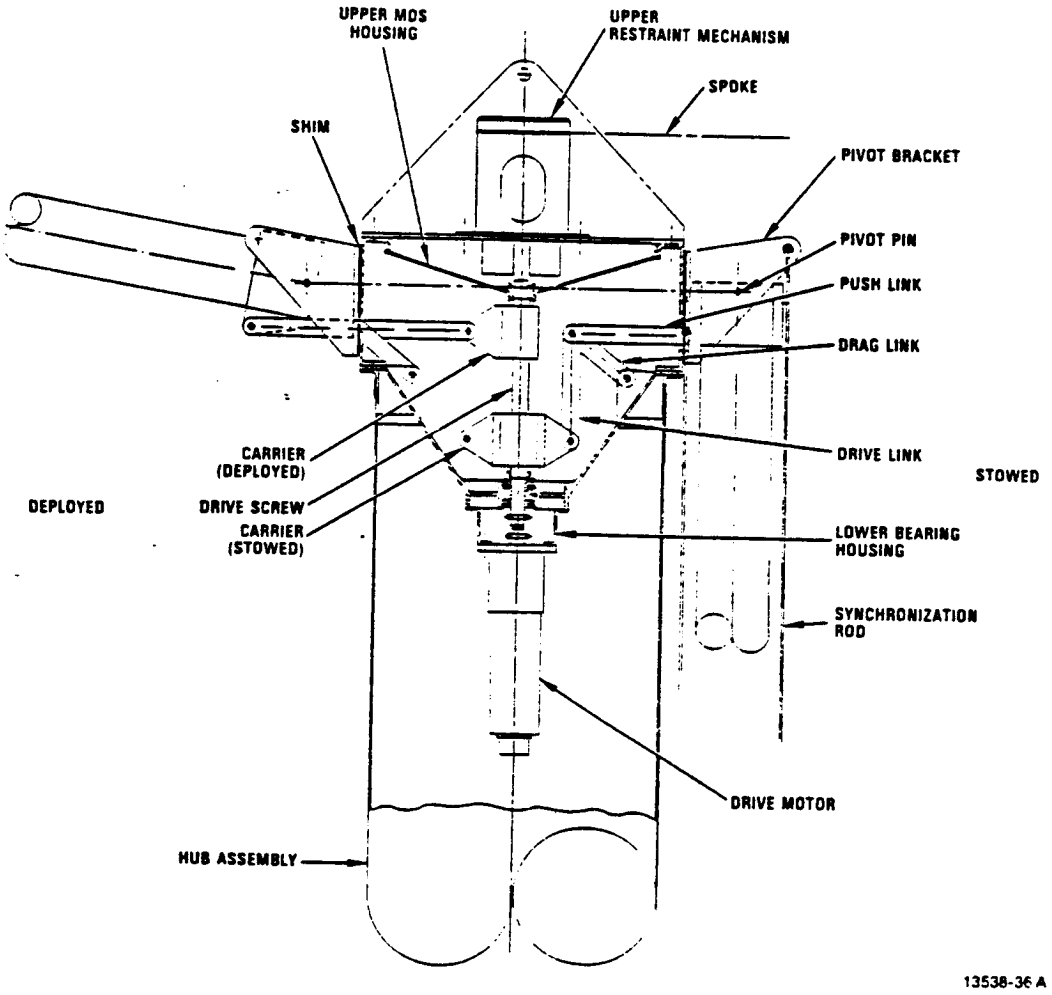

Figure A-2. Rotational Motion of the Drive Screw Deploys the Ribs Using a Push Link Mechanism

HARRIS DEPLOYABLE TRUSS STRUCTURE (DTS)
RIB DEPLOYMENT SEQUENCE

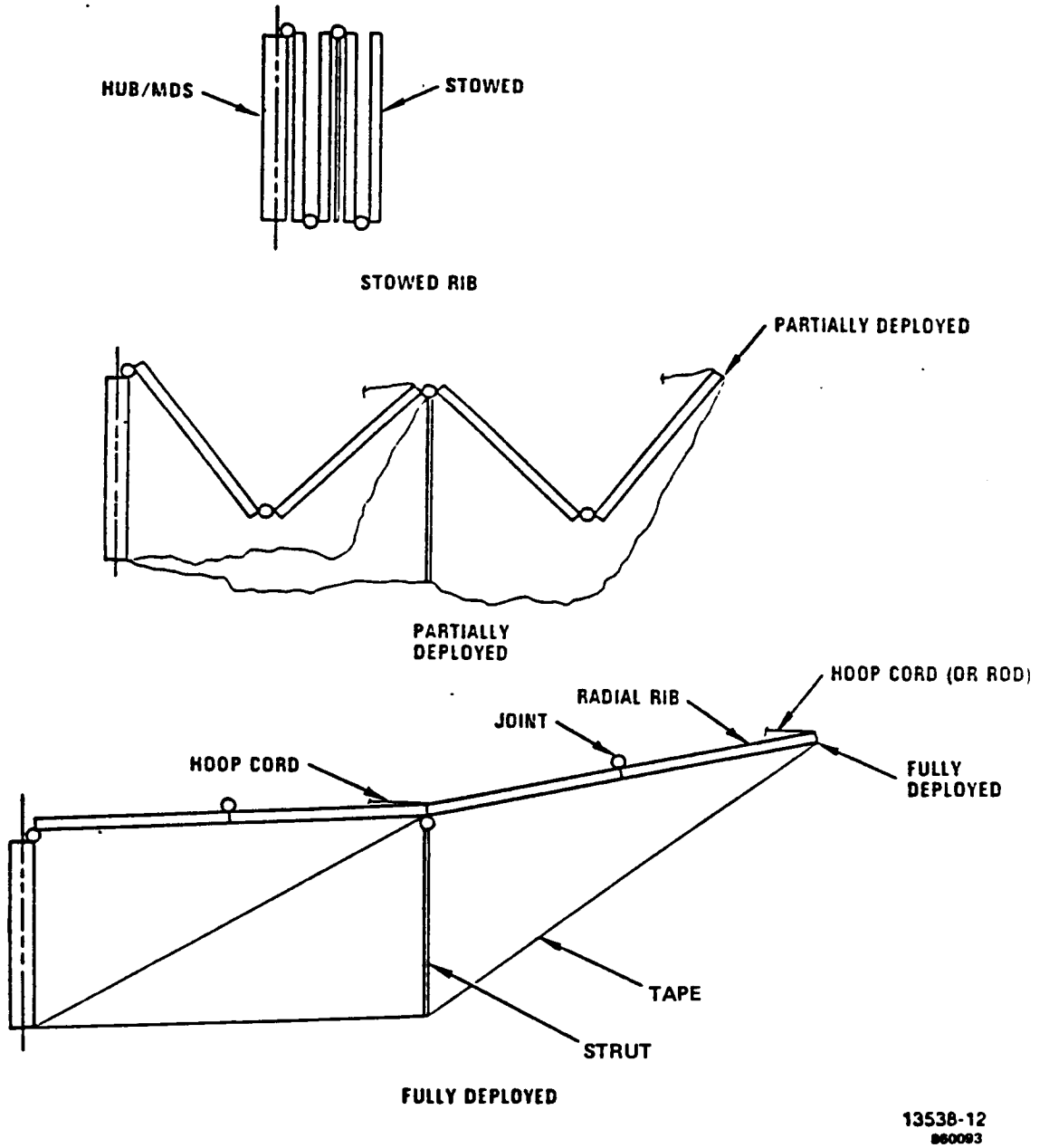

Figure A-4. The Rib Packages Compactly and Deploys in a Controlled Manner

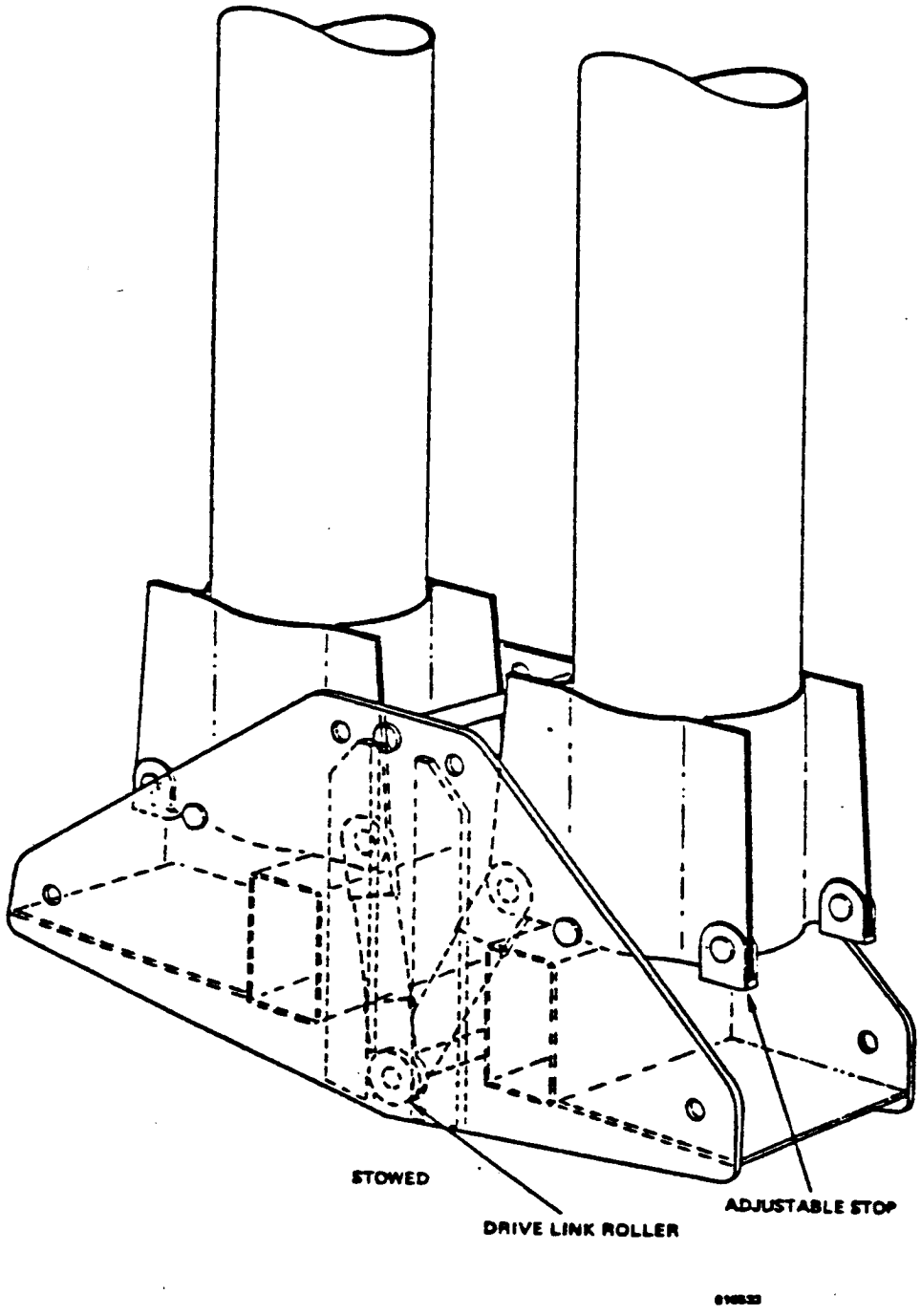

Figure A-5. Latching Joint, Stowed Position, Provides Symmetric Deployment

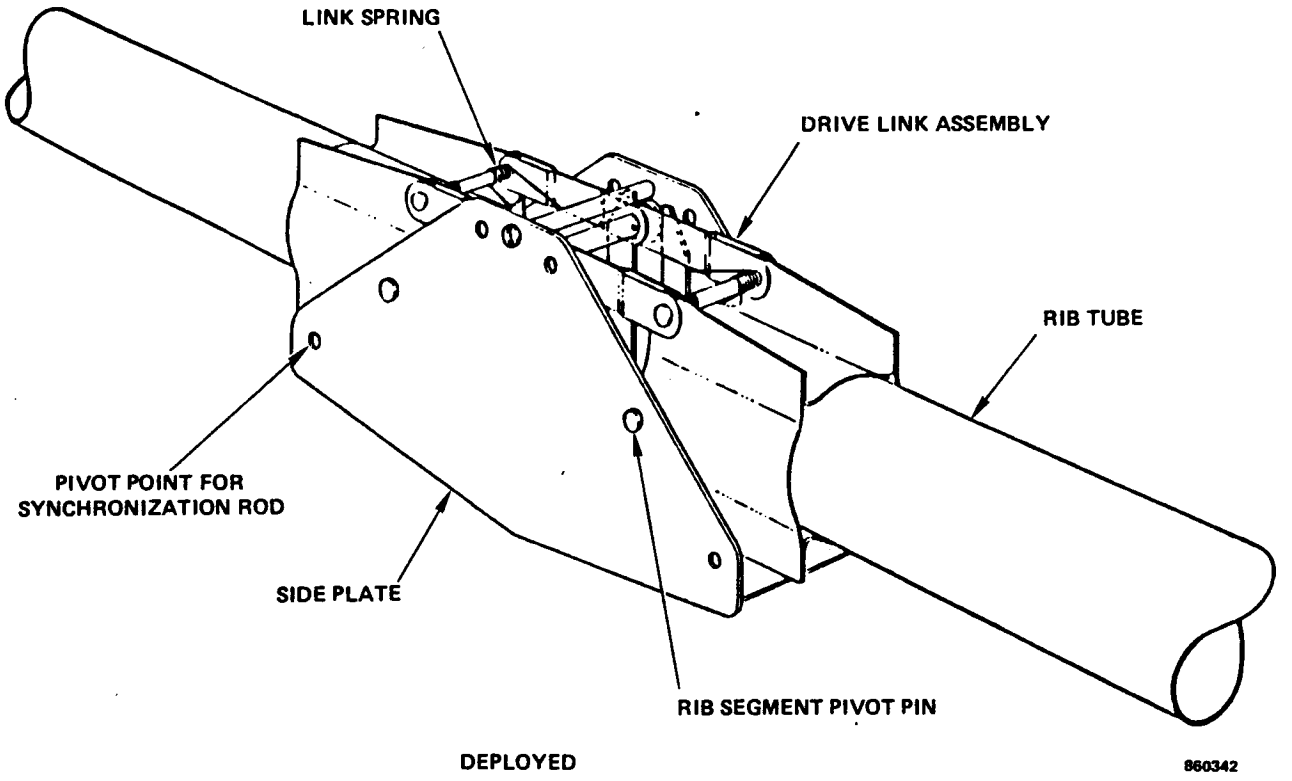

Figure A-6. Latching Joint, Deployed Position has a High Stiffness when Fully Preloaded

APPENDIX B

MATERIALS TESTING RESULTS

To Be Supplied Under Separate Cover